Synthesis and Characterisation of Polynuclear Complexes with Macrocyclic and Related Ligands

---

A thesis

submitted for the degree

of

Doctor of Philosophy in Chemistry

at the

University of Canterbury

by

Sally Anne Brooker

University of Canterbury 1989

To my Family and Friends

Acknowledgements

I would like to thank Dr. Vickie McKee for her considerate supervision, advice and constant enthusiasm throughout this period of study. My thanks are also due to Dr. Peter Steel, Dr. Santokh Tandon, Dr. Ward Robinson, Dr. Alison Downard and Dr. Alan Happer for many helpful discussions.

I am grateful to Professor S.P. Cramer for the XANES and EXAFS results, Dr. J-M. Latour and Dr. J-P. Tuchagues for the magnetic susceptibility data, and Dr. L.K. Pannell for the ^{252}Cf PDMS results.

The assistance provided by the technical staff of the Department of Chemistry, especially Mr. R. Thompson, is gratefully acknowledged.

I wish to thank Wendy Marsh for typing the text and Robyn Caygill for typing the references. Finally, my thanks go to my family and friends for all their help, encouragement and support.

Contents

Abstract

This thesis is in two distinct but related parts. The first deals mainly with manganese complexes of multinucleating Schiff-base macrocycles derived by condensation of 2,6-diacetylpyridine (DAP) and 1,3-diamino-2-hydroxypropane (H_2L1, H_4L1'), or 1,3-diaminopropane (L13). Six tetramanganese(II) complexes of H_2L1 and H_4L1', three pentamanganese(II) complexes of H_2L1 and one mixed-valence manganese(II)$_2$manganese(III)$_2$ complex of L13 were synthesised and characterised by single crystal X-ray structure analysis. A mechanism for the observed ring expansion reaction from the (2+2) macrocycle (H_2L1) to the (4+4) macrocycle (H_4L1') is proposed and supported by the results of ^{252}Cf PDMS, conductivity and EPR measurements. Possible reasons for the isolation of three pentamanganese(II) complexes as well as a tetramanganese(II) complex of H_2L1 in the presence of acetate ions are discussed. The mixed-valence complex of L13 has led to the proposal of a new mechanism for water oxidation by the OEC (oxygen evolving complex) of photosystem II in green plants. The complexes are discussed in terms of their relevance as models for the OEC. This includes discussion of the results of EXAFS (Extended X-ray Absorption Fine Structure), XANES (X-ray Absorption Near Edge Spectroscopy), cyclic voltammetric and magnetic susceptibility studies. An unusual eight-coordinate manganese(II) complex of DAP was prepared and structurally characterised, as was a macrocyclic dilead complex with unusual single atom bridging *via* the nitrogen atom of a thiocyanate ligand.

Less constrained noncyclic ligands are described in the second Section. These are related to the macrocyclic systems, and are derived from the condensation of formyl- or acetylpyridine derivatives with 1,n-aminoalcohols. Particular emphasis was given to manganese complexes because of their potential relevance to the OEC. Two ligand rearrangement reactions, involving the pyridine nitrogen and resulting in the formation of five-membered rings, were observed and possible mechanisms are proposed. Sixteen single crystal X-ray structure determinations were performed including those of eight manganese(II) complexes.

Chapter 1

REVIEW

1.1 Introduction

One of the major aims of the work described in this thesis was to prepare model compounds for the manganese-containing oxygen evolving complex (OEC) in photosystem II (PSII). Hence Section 1.2 outlines what is currently known about the OEC and demonstrates how well characterised model compounds could make a valuable contribution to interpreting data obtained on the OEC. Some of the manganese model compounds prepared to date are discussed in Section 1.3, and finally, as most of the model compounds prepared during the course of this work were complexes of macrocyclic (or closely related noncyclic) ligands, the synthesis and properties of macrocycles are reviewed in Section 1.4. In this Section particular emphasis is given to the discussion of the chemistry of polynucleating Schiff-base macrocycles of the type employed in this work.

1.2 Role of Manganese in Photosystem II

Green plants carry out the fundamental life process of photosynthesis:

$$H_2O + CO_2 + \text{light} \rightarrow O_2 + \text{carbohydrate} \quad (1)$$

This transformation involves interactions between many different complex molecules and metalloproteins which absorb light energy, transfer electrons, bind substrates and so on. A brief outline of these reactions is shown in Figure 1.[1] A manganese-containing metalloprotein in photosystem II (indicated by the red circle in Figure 1) is responsible for binding and subsequently oxidising water to release oxygen; there have been several recent reviews of this general area by Govindjee[2], Dismukes[3], Renger[4], Pecoraro[5] and Volkov[6]. In this Section current understanding of this manganese-containing oxygen evolving centre (OEC) is reviewed.

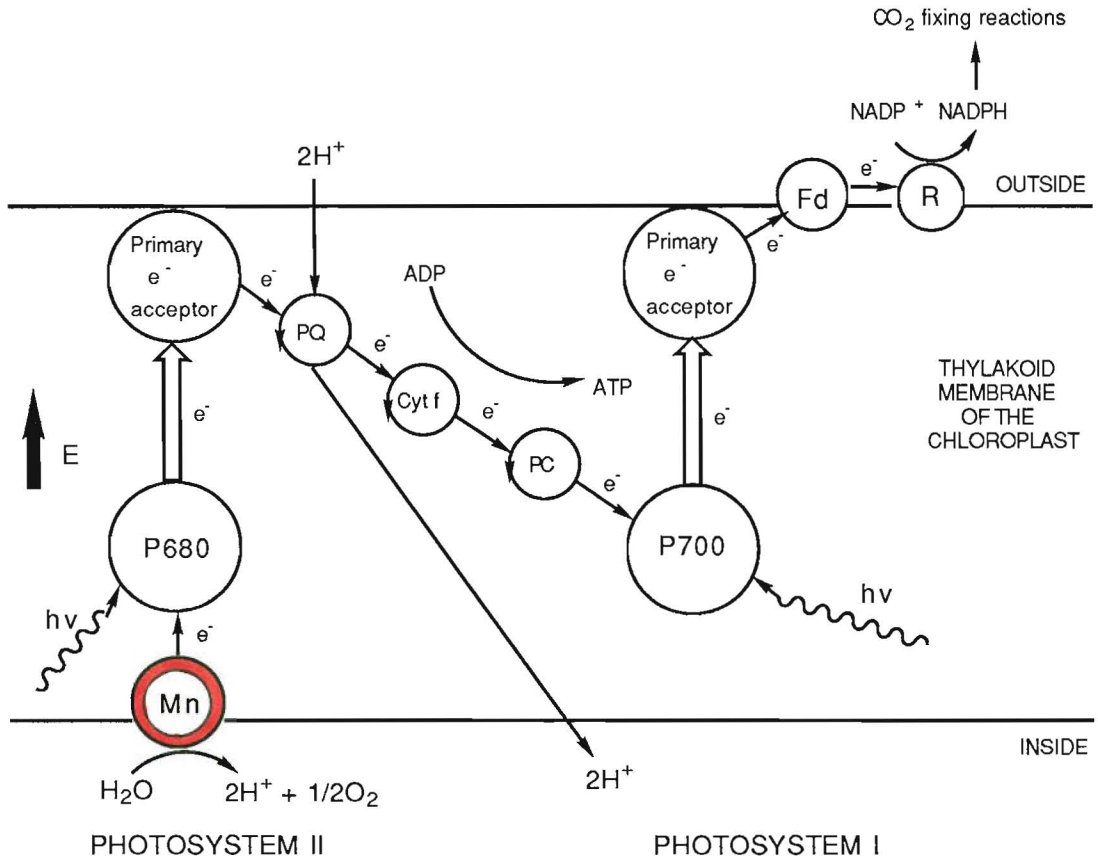

Figure 1: An outline of the reactions of PSI and PSII. Mn=Mn cluster (OEC), P680 and P700=chlorophylls, PQ=plastoquinone, cyt f=cytochrome f, PC=plastocyanin, Fd=ferrodoxin, R=reductase.

A major advance in understanding the action of the OEC was provided by Joliot *et al*[7,8] and Kok *et al*[9] who studied isolated whole spinach chloroplasts maintained in buffered solutions. When dark-adapted chloroplasts were exposed to a series of flashes of light the oxygen evolution varied as shown in Figure 2.[8]

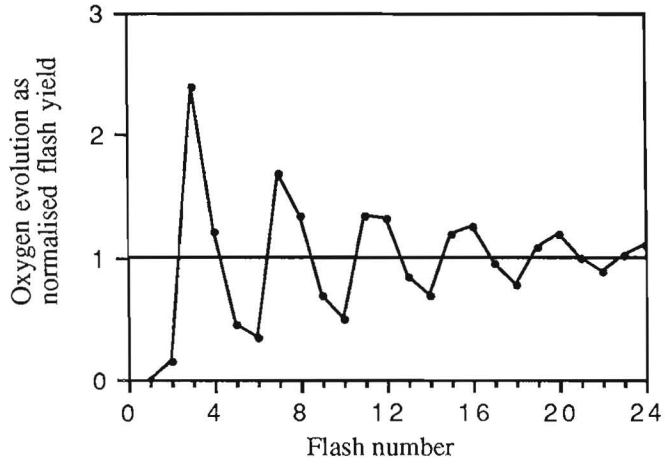

Figure 2: Variation in oxygen evolution of dark-adapted chloroplasts with flash number. Normalised flash yield= yield/steady state yield.

To explain this cyclic variation with periodicity four Kok[9] proposed that there were five oxidation levels S_0, S_1, S_2, S_3 and S_4 (S-states) organised as follows:

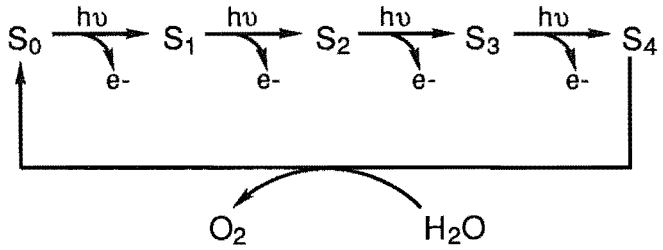

Figure 3: The functional organisation of the S-states.

Dark adaptation causes S_2 and S_3 to return predominantly to S_1 (S_0 is stable in the dark and remains at an approximately constant level). This results in the first maximum of oxygen evolution being observed on the third flash as S_4 returns to S_0 (Figure 2). Damping to a steady state oxygen evolution rate occurs quite rapidly because the S-states get out of phase due to "misses" (some centres not oxidised by the flash) and "double hits" (some centres oxidised twice in one flash).

Manganese-deficient chloroplasts show inhibited oxygen evolution which can be reactivated by the addition of Mn^{2+}, demonstrating that manganese is involved in the oxidation of water.[10,11] The first direct spectroscopic evidence for the involvement of manganese was the observation of a manganese multiline EPR (Electron Paramagnetic Resonance) spectrum of the S_2 state by Dismukes and Siderer in 1981.[12] Extraction experiments have shown that there are four manganese atoms per active centre and this is now generally accepted as correct.[11,13] However, there is some question as to whether all four form a single tetranuclear cluster[14] or whether there are smaller tri or bi and/or mononuclear clusters present.[5,15] There is also some debate over whether or not two of the four manganese atoms can be replaced by other divalent metal ions such as Mg^{2+}.[11]

These uncertainties are due to the many difficulties associated with the study of large and complex biomolecules. Attempts to isolate the manganese metalloprotein intact from the chloroplast have been unsuccessful to date, ruling out a definitive single crystal X-ray structure determination and limiting investigations to the study of various chloroplast preparations. Techniques which can overcome the problem of high dilution of the manganese active centre within the surrounding protein[16] by focusing on the manganese active centre itself are particularly useful. Examples of such techniques are EPR, magnetic susceptibility, EXAFS (Extended X-ray Absorption Fine Structure)[17,18] and XANES (X-ray Absorption Near Edge Spectroscopy)[18]; the results of these investigations are presented in this Section. One difficulty with all of these techniques is that the results can be ambiguous, leading to a need for well characterised model compounds of similar structure and oxidation levels to aid in the interpretation of the results.

XANES, EPR and electronic spectral studies have shown that the oxidation states of the manganese ions vary as the active centre cycles through the S-states but the specific oxidation levels are still unknown. XANES should provide information on the manganese oxidation states because the manganese K- and L-

edge positions are sensitive to the electron density about the manganese. Because of experimental limitations only K-edges have been reported to date. The problem with K-edges is that other factors, including the number and type of donors and their coordination geometry, also affect the electron density about the manganese and therefore the position is not a direct indication of the manganese oxidation state. The observed K-edge for dark adapted (S_1) samples falls in the range expected for Mn(III) complexes.[19] There appears to be Mn(IV) present in S_2 (by comparison with model compounds) and there is some structural rearrangement occurring on going to S_3 which causes the K-edge position to fall between that of S_1 and S_2.[19,20] An alternative, and indistinguishable (due to the sensitivity of K-edge XANES to both oxidation state and geometry) reason for the latter result would be that there is no oxidation level change occurring as $S_2 \rightarrow S_3$.

Cramer has used polarised synchrotron radiation to study the K-edges of oriented chloroplasts in the S_1 state (Figure 4).[21]

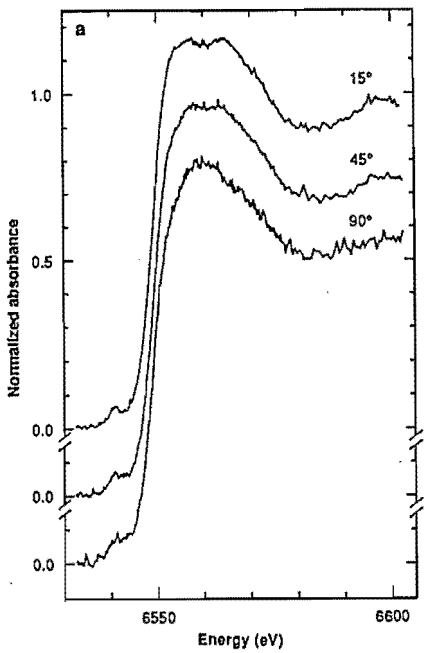

Figure 4: Manganese K-edge XANES of oriented chloroplasts in the S_1 state.

The small, formally dipole-forbidden 1s→3d transition observed at about 6540.8eV suggests that the manganese sites do not approach tetrahedral geometry (tetrahedral complexes have extensive p d orbital mixing which causes this transition to be intense). When the X-ray electric field vector is at an angle of 15° (θ) to the membrane normal, features at 6567eV and 6564eV are observed. These merge to a single broad feature at 6560eV when θ=90°. This implies that the manganese cluster is highly oriented in the membrane but is not a highly symmetric structure (see later). This group is generating a database of model compound L-edge spectra using new more sensitive detectors. It appears that oxidation states can be assigned with much more confidence than for the K-edge studies because of

the sharper line widths and different selection rules for L-edge data. More model compounds are needed so that further comparisons can be made and hence more accurate information obtained from the data on the S-states.

Detailed EPR studies led Brudvig and Crabtree to conclude that the four manganese ions in S_2 are probably arranged as a dimer of dimers with one of the three EPR-consistent sets of oxidation levels shown in Table 1.[22]

Table 1. Possible manganese oxidation levels in the OEC.

State	A	B	C
S_0	$(III)_3(IV)$	$(II)(III)_3$	$(II)_3(III)$
S_1	$(III)_2(IV)_2$	$(III)_4$	$(II)_2(III)_2$
S_2	$(III)(IV)_3$	$(III)_3(IV)$	$(II)(III)_3$
S_3	$(IV)_4$	$(III)_2(IV)_2$	$(III)_4$
S_4	$(IV)_3(V)$	$(III)(IV)_3$	$(III)_3(IV)$

To explain the observed EPR data Brudvig has concluded that there must be large antiferromagnetic exchange coupling within each dimer and ferromagnetic exchange coupling between dimers. Exchange coupling of this sort has also been observed in the Fe_4S_4 and Cu_4O_4 clusters.[14] The temperature dependence of the EPR signals was explained in terms of a temperature dependent conformational change.[23]

Hansson *et al* have interpreted their EPR data as being consistent with the S_2 state comprising a binuclear Mn(III)Mn(IV) complex in redox equilibrium with an almost axial Mn(III) ion from a separate mononuclear centre.[15] The possibility of a trinuclear cluster has not been excluded either.[5,23]

One concern about these EPR studies is that they are run at low temperatures and the electron density distribution between the manganese and the ligands may well be temperature dependent.[4] Hence Dismukes has measured the changes in room temperature magnetic susceptibility as a function of S-state.[24] These results are inconsistent with a sequential one-electron oxidation of water and indicate that no oxidation of water occurs until S_4. This supports the often stated concept that the manganese cluster acts to store oxidising equivalents.[2,5,14,19]

Difference ultraviolet spectra appear to indicate that the $S_0 \rightarrow S_1$ transition may be a Mn(II) $\rightarrow$ Mn(III) oxidation, whereas $S_1 \rightarrow S_2$ and $S_2 \rightarrow S_3$ are probably Mn(III) $\rightarrow$ Mn(IV) oxidations.[25] This favours set B oxidation states (Table 1)but is not definitive because other factors, such as the type of donor atoms and the overall charge of the complex, may also affect the electronic spectrum.[4] Changes in the visible absorption spectrum have been tentatively assigned to electrochromic shifts which arise from a net change in the overall charge of the OEC. The observed pattern indicates that there is a positive surplus of charge in states S_2 and S_3

relative to S_0 and S_1.[26] This pattern is in agreement with that found by the study of P_{680} re-reduction kinetics.[27]

EXAFS studies on the manganese in chloroplast preparations give information on the type (atomic weight) and number of donor atoms, and their distance from manganese. Interpretation of the EXAFS data is ambiguous and therefore (as for XANES) structurally characterised model compounds are very important as they allow valuable comparisons to be made. Nitrogen and oxygen atoms can not be distinguished by this method because of their very similar atomic weights. EXAFS indicates that there is no major structural change on $S_1 \rightarrow S_2$.[19] Klein and co-workers conclude from their data that for both the S_1 and S_2 states there are 2±1 oxygen and/or nitrogen donors bridging the manganese atoms at *ca.* 1.75Å and 3±1 oxygen and/or nitrogen atoms bound terminally to the manganese at *ca.* 2.00Å.[19,28] These donor atoms are thought to be from protein amino acids (e.g. nitrogen from histidine[29] or oxygen from tyrosine[30,31]). A second manganese atom at *ca.* 2.70Å and further manganese centres at 3-4Å can be accommodated by this EXAFS data.

Cramer and co-workers have used polarised synchrotron radiation in their oriented EXAFS study of S_1 (Figure 5).[21] In contrast to previous results, they find no evidence for a short 1.75Å interaction. These results indicate 2±1 oxygen and/or nitrogen atoms at an average of 1.9Å from each manganese atom. The low coordination number is thought to result from a broad range of contributing bond lengths (e.g. caused by Jahn-Teller distortion about Mn^{3+}) rather than being a true low coordination number. Little angular dependence was found for the manganese-oxygen/nitrogen interactions. The data indicate 2.1±1 and 0.8±0.3 other manganese atoms at distances of 2.7 and 3.3Å respectively and these interactions show significant angular variation. These results, along with the XANES results outlined earlier, led Cramer to conclude that both the symmetrical regular cubane (see later, Figures 9 and 10) and "butterfly" (see later, Figure 9) structures are ruled out by this data but similar, less symmetrical versions are still possible.

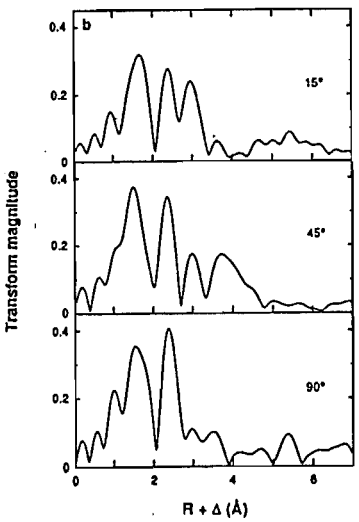

Figure 5: EXAFS Fourier transforms of oriented chloroplasts in the S_1 state.

The question of whether or not chloride ions bind directly to manganese in the S_1 and S_2 states is not resolved by these studies but it is thought that a maximum of one chloride per manganese could be accommodated by the EXAFS data.[19,32] The reason for the difficulty in determining chloride ion content is that the Mn-Cl bonds (particularly for bridging chloride, Section 1.3) may occur at about the same distance as the Mn-Mn interactions i.e. 2.7Å.

After some initial disagreement,[33] chloride depletion studies have shown that about 4 chloride ions per PSII are essential to oxygen evolution.[3] Oxygen evolution from chloride-deficient chloroplasts can be reactivated by adding Cl^- or an ion with a similar volume, such as Br^-, as shown in Figure 6.[33]

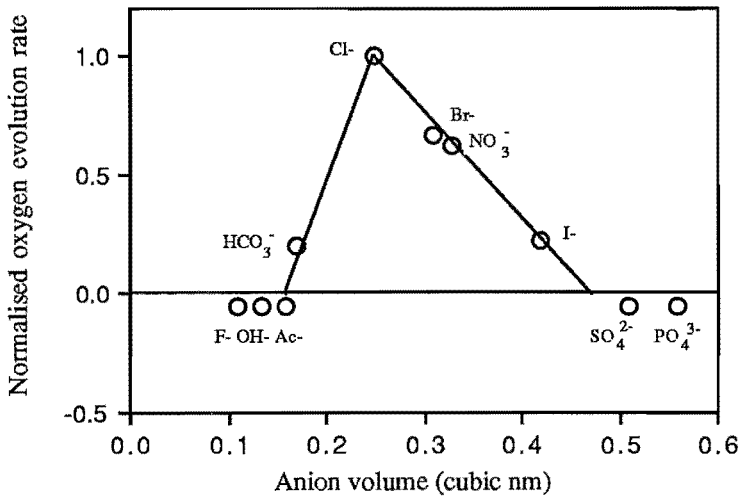

Figure 6: Effect on oxygen evolution of the treatment of chloride-deficient chloroplasts with X^{n-}. Normalised oxygen evolution rate=rate-rate of control.

This indicates that there is some steric hindrance or access restriction around the chloride ion binding site which blocks the binding of larger anions. Smaller anions may inhibit oxygen evolution by binding at the water (substrate) binding site.

Evidence for the existence of different binding sites for water and chloride ions comes from EPR-probed experiments. No differences have been observed between the S_2 multiline EPR spectra of chloride- and bromide-treated chloride-deficient chloroplasts implying that these ions do not bind directly to the manganese cluster.[34] However, recent work indicates that tightly bound chloride may not have been removed in this experiment and that when all of the chloride is removed bromide inhibits the formation of the multiline signal.[35] It is generally agreed that in the native OEC chloride is necessary for the production of an EPR detectable S_2 state.[34,35] The addition of $^{17}OH_2$ or NH_3 causes changes in the multiline EPR spectrum of S_2 indicating that these molecules bind directly to manganese.[36] EPR-probed amine binding studies suggest that only NH_3 can bind directly to manganese, thus inhibiting oxygen evolution by competing with H_2O (poorer base/nucleophile)

for the substrate binding site on the manganese cluster.[37] The other bulkier amines (NRR'OH; R,R'=H,Me) do not bind directly to manganese but delay the S_2 multiline EPR signal formation by two light flashes, probably by competing with chloride at the chloride binding site and reducing the manganese cluster by two electrons (S_{-1}).[38] Thus it appears that the manganese substrate binding site is selective for the coordination of small Lewis bases.

The interpretation of these EPR-probed ligand binding studies is difficult and there is still some uncertainty over the proposed binding sites and their properties. Hence the role of chloride (reviewed by Critchley in 1985[33]) is still the subject of much debate.[39] Chloride may be bound directly to the manganese cluster, stabilising the higher S-states,[35,39(b)] and controlling the binding of water and the oxidation potential of the S_2 state.[3] Bound chloride may also facilitate electron transfer by bridging the manganese ions (see later, Figure 8).[33] Alternatively, the chloride may not be bound directly to the manganese cluster but to another site in close proximity. In this case the chloride could serve to balance charge, or to maintain the structure around the manganese cluster.

The proton release pattern observed as the OEC cycles through the S-states has been determined by monitoring the changes in pH using highly sensitive glass electrodes[4] or suitable pH indicators (e.g. neutral red)[40]. However all other proton movements have to be subtracted out, and in the case of pH indicators, changes in absorbance due to other factors must also be taken into account. The generally accepted pattern is 1, 0, 1, 2 for $S_0 \rightarrow S_1$, $S_1 \rightarrow S_2$, $S_2 \rightarrow S_3$, $S_3 \rightarrow S_0$; although these protons do not necessarily result directly from deprotonation of the bound water molecules. Which S-state first binds the substrate water is still unclear. Hansson[41] showed by EPR of $^{17}OH_2$-treated PSII particles that there is ^{17}O bound in the S_2 state. However, if the manganese atoms are bridged by exchangeable oxo/hydroxo ions then this study tells us nothing about the binding of the substrate.[36] Radmer and Ollinger have used mass spectroscopic methods to detect $^{18}O_2$ *vs* $^{18}O^{16}O$ *vs* $^{16}O_2$ evolution from $^{18}OH_2$ treated OEC.[42] This study indicates that water is not unexchangeably bound before S_3. Beck and Brudvig have proposed, by analogy with their observation that NH_3 binds directly to manganese only after the formation of the S_2 state, that H_2O binding may be triggered by the formation of an especially electron deficient S_3 state.[36]

Interpretation of the available biochemical data has led to a large number of proposals for the structure of the active site as it cycles through the S-states to produce oxygen.[6] Four of the more recent suggestions are described below.

A binuclear active site is still favoured by some workers. An example is the scheme outlined in Figure 7 proposed by Saygin and Witt in 1987.[43] Two water molecules are bound as S_4' returns to S_0 with concomitant loss of two protons. One of the remaining protons is stabilised by H-bonding to the oxygen atom of the second

hydroxide. This is proposed to account for the lack of proton release accompanying $S_1 \rightarrow S_2$. The resulting overall positive charge on S_2 is balanced by outer sphere coordination of chloride. Some redox active group D is oxidised in the $S_3 \rightarrow S_4$ step. Oxidation of the bound oxo atoms then occurs as $S_4 \rightarrow S_4'$, possibly *via* a 2Mn(III) peroxo intermediate. No suggestions were made as to the rest of the bridging or terminal donors of the manganese coordination sphere, other than that they would be from polypeptides. The oxidation states are consistent with the current electronic spectral and XANES data; also the proton release pattern (1, 0, 1, 2) and positive surpluses of charge on S_2 and S_3 are as observed for the OEC.

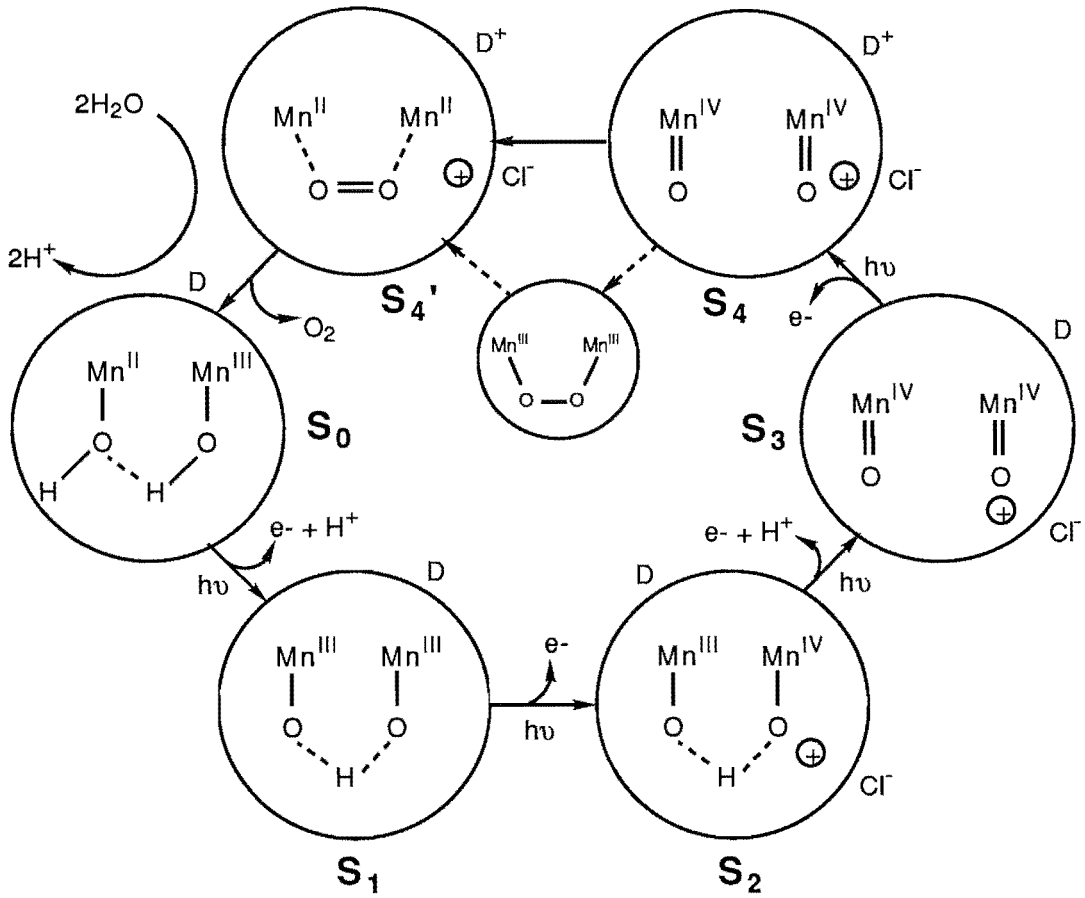

Figure 7: The possible states and configurations of water and manganese in the OEC cycle proposed by Saygin and Witt. D=electron carrier between P680 and the OEC.

In 1984 Critchley and Sargeson[44] proposed a tetramanganese cluster with chloride bridging as shown in Figure 8. The manganese cycles through quite low oxidation states which are inconsistent with current XANES data. The proton release pattern 1, 0, 1, 2 is as for the model proposed by Saygin and Witt. In this model chloride bridging is proposed to facilitate the necessary electron transfers and to stabilise the cluster. It is known that bridging chloride can lead to antiferromagnetic coupling of metal ions and EPR silent systems.[44] This could explain the lack of EPR signal from the S_0 state. Two two-electron oxidation steps

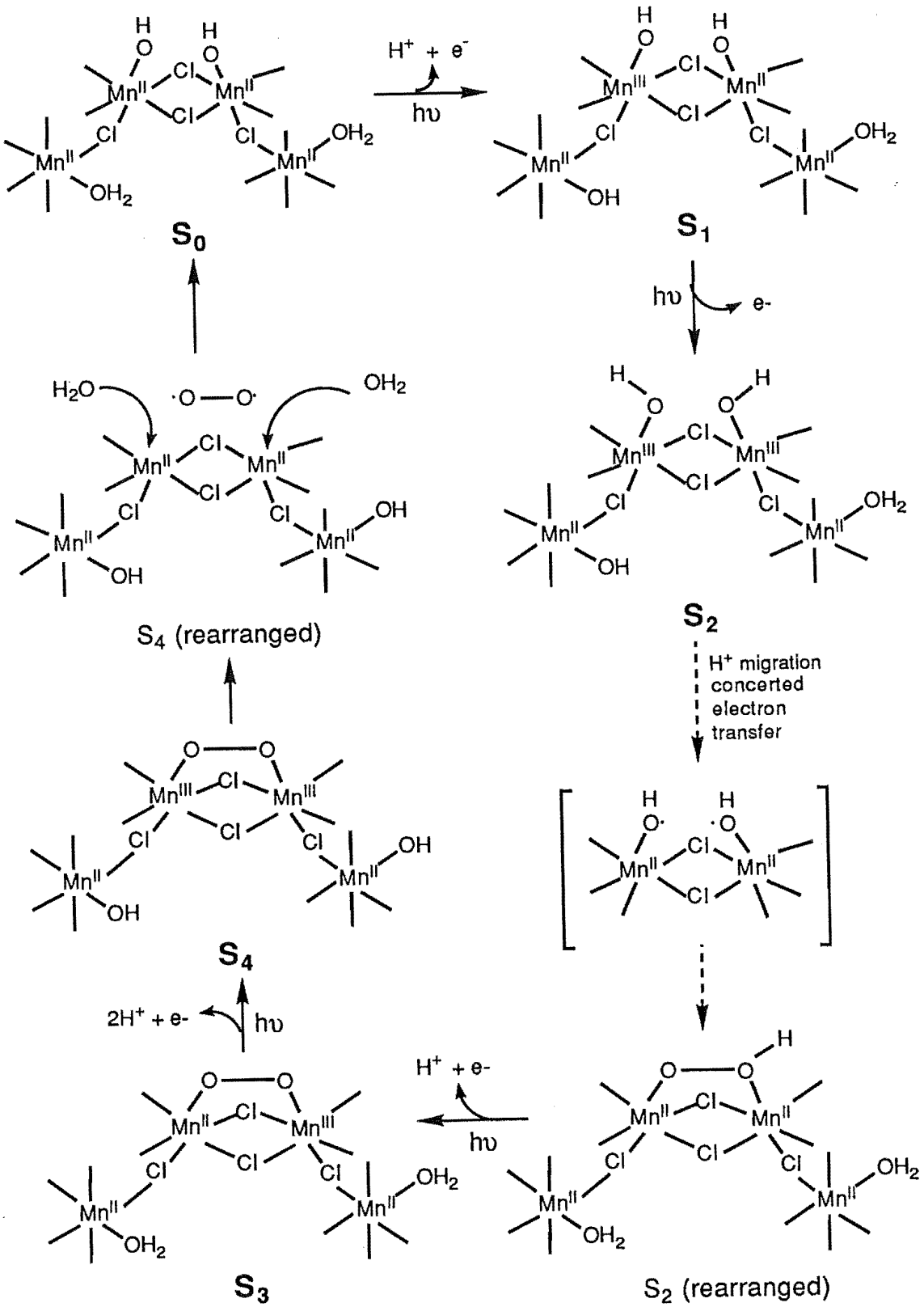

Figure 8: The possible states and configurations of water and manganese in the OEC cycle proposed by Critchley and Sargeson.

are a feature of this model. The first oxidation of water occurs during $S_2 \rightarrow S_3$ which contradicts results which indicate that no water oxidation occurs prior to S_3.[24,42]

Vincent and Christou[29] have proposed a similar "butterfly" shaped structure for the S_0, S_1 and S_2 states of their suggested mechanism of water oxidation (Figure 9); substituting bridging oxygen for the bridging chlorine atoms in the above proposal.

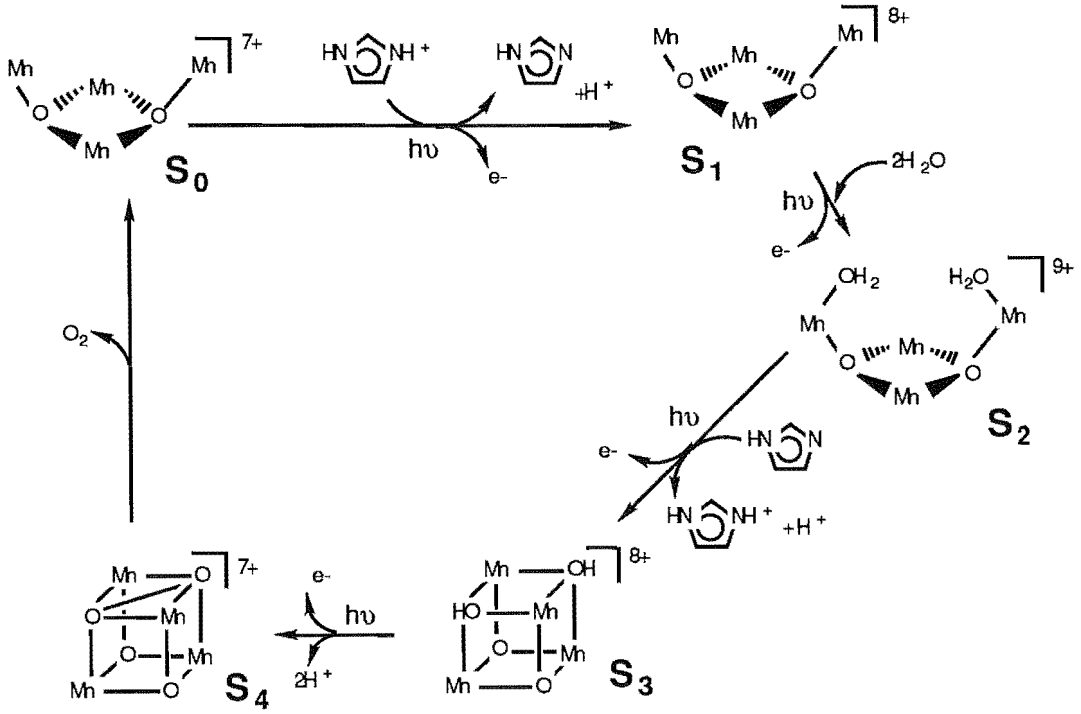

Figure 9: The possible states and configurations of water and manganese in the OEC cycle proposed by Vincent and Christou.

The proton release pattern is again 1, 0, 1, 2 but this is where the similarities end. To rationalise the H^+ release pattern, they have invoked the protonation and deprotonation of a histidine residue.[29] Higher oxidation states (Table 1, set B) are suggested for S_3 ($Mn(III)_2Mn(IV)_2$) and S_4 ($Mn(III)Mn(IV)_3$) and the structural rearrangement on oxidation of $S_2 \rightarrow S_3$ suggested by XANES studies[20] is proposed to involve pivoting of the two "wingtip" Mn-O vectors about the μ_3-O atoms to create a Mn_4O_4 cubane. The Mn_2O_2 base is not required to move during this manoeuvre but the wing-tips do shift, bringing the H_2O molecules much closer together. Subsequent deprotonation allows cubane formation. Oxidation to S_4 causes the transfer of two electrons from oxygen to manganese and O-O bond formation (bound peroxide). Continued approach of the O atoms causes the manganese atoms to pivot further apart, two further electrons to be transferred to manganese, and oxygen to be evolved as the assembly returns to the S_0 butterfly conformation. One feature of this mechanism is that it allows two two-electron oxidation steps to occur after S_3 formation rather than one four-electron step.

An Mn_4O_4 cluster also forms the active centre in Brudvig and Crabtree's proposal (Figure 10).[22]

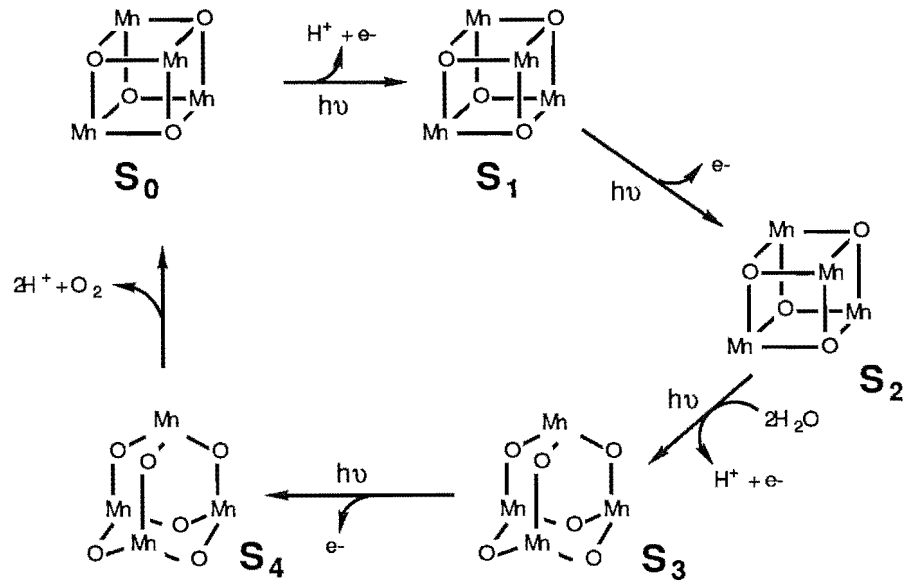

Figure 10: The possible configurations of water and manganese in the OEC cycle proposed by Brudvig and Crabtree.

To account for the EPR signals from the S_2 state, and the EXAFS and XANES of the S_1 state, the Mn_4O_4 cubane would have to be elongated along one of its axes. None of the three sets of EPR-consistent oxidation states (Table 1) can be conclusively ruled out. An argument against set A is that an S_1 state of $Mn(III)_2(IV)_2$ may be too oxidised to be consistent with K-edge XANES studies - although K-edge XANES interpretation is difficult. The favoured set is set B due to factors already outlined above. An attractive feature of this scheme is that the manganese atoms do not need to move very much in converting from cubane to adamantane forms. This is an advantage as the manganese atoms are expected to be anchored to the surrounding protein and hence may not be very mobile. This model incorporates a structural change $S_2 \rightarrow S_3$ cubane $\rightarrow$ adamantane, to fit the XANES data, due to the Mn_4O_4 cluster becoming sufficiently electron deficient to bind H_2O with subsequent rearrangement. Further electron loss causes the high valent manganese to pull electrons away from the oxygen, triggering formation of an O-O bond. Reduction of manganese and nucleophilic attack by the bridging oxygen atoms then causes oxygen release. The observation that ^{17}O is bound to S_2 (as shown by EPR) is explained by assuming that there are exchangeable μ-oxo groups bound to the manganese cluster.

1.3 Model Complexes for the OEC

Much recent research effort has been directed towards producing compounds which will mimic the oxygen evolving complex (OEC). Several approaches have been taken in the development of functional water-splitting model compounds. Some involve non-manganese complexes which will not be discussed further here.[45] The manganese model compounds presented in this Section are divided into two groups, firstly structural models in order of increasing nuclearity, then functional models.

Manganese complexes of various nuclearities and oxidation states with oxygen and/or nitrogen donors (with and without chloride present) all aid our understanding of the OEC by expanding the basic manganese chemistry, showing which structures are feasible, and by providing data for comparison with the OEC.

Numerous binuclear complexes have been characterised; a few of these will be presented next. An elegant series of complexes of the ligands 1,4,7-triazocyclononane (tacn) and N,N',N"-trimethyl-1,4,7-triazocyclononane (Metacn) have been prepared by Wieghardt and co-workers.[46] These are particularly informative because all of the oxidation levels $Mn(II)_2$, Mn(II)Mn(III), $Mn(III)_2$, Mn(III)Mn(IV) and $Mn(IV)_2$ have been well characterised. In fact, single crystal X-ray structures have been reported (two examples in Figure 11) for all but the Mn(II)Mn(III) case.

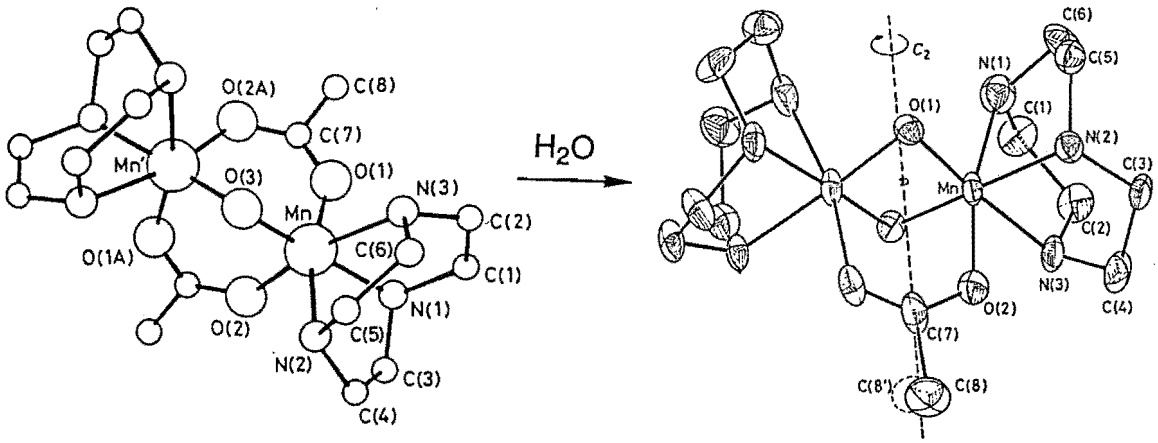

11A 11B

Figure 11

Electrochemical studies indicate that it is possible to generate these dimeric model compounds in various oxidation states without dramatically altering the structure. This parallels the conservation of the OEC structure upon the $S_0 \rightarrow S_1$ and $S_1 \rightarrow S_2$ oxidations. However, Wieghardt has observed that the acetate bridges are quite labile (Figure 11);[46(b),46(c)] this is consistent with the observed reversible inhibition of the OEC by acetate being due to the replacement of two water molecules by an acetate group (Figure 12).

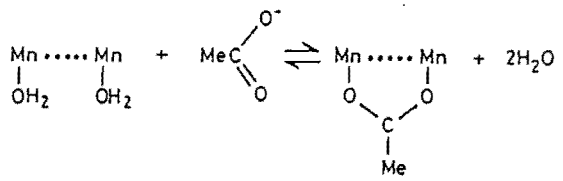

Figure 12

By analogy with this acetate bridging, the H-bonding proposed in the S_1 and S_2 states of Saygin and Witt's scheme (Figure 7) could occur in the native OEC. The bis oxo-bridged product (Figure 11B) has Mn-μ_2O distances (1.817(5) and 1.808(4)Å) which are similar to the 1.75Å distance predicted by Klein and the Mn-Mn separation of 2.588(2)Å is close to the OEC distance of 2.7Å. In comparison, the mono oxo-bridged complex (Figure 11A) has a larger Mn-Mn separation of 3.084(3)Å. Dismukes, Lippard and co-workers and Girerd and co-workers have reported very similar $Mn(III)_2$ compounds with the hydrotris(1-pyrazolyl)borate ligand[47] and bipyridine.[48] respectively.

Acetate bridges are not necessary to hold the dimeric structures together. Many bis μ-oxo only bridged structures have also been reported.[46(c),49] One example is the Mn(III)Mn(IV) complex made by Hodgson (Figure 13A).[50]

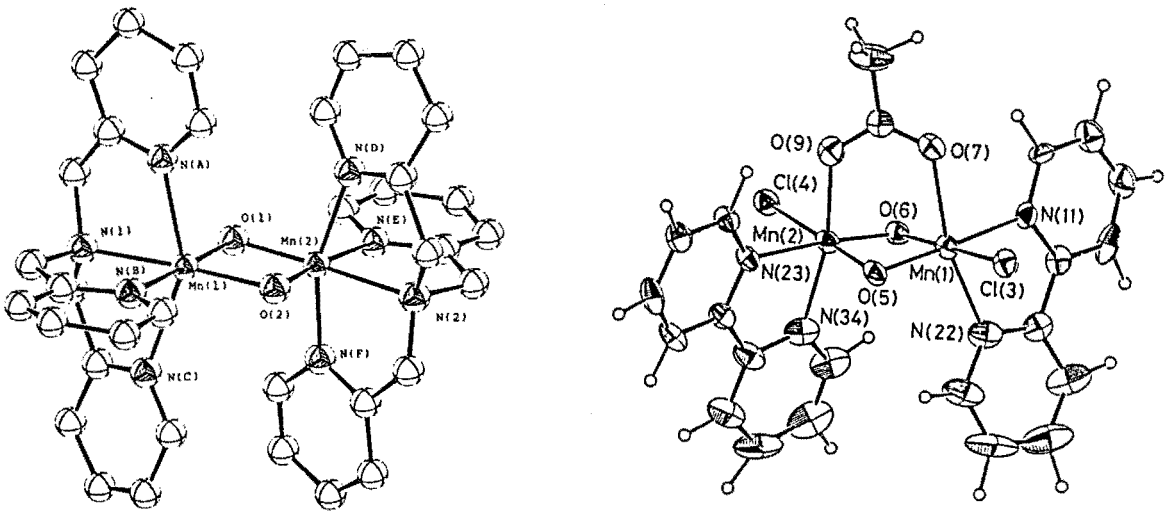

13A 13B

Figure 13

The Mn-Mn separation of 2.643(1)Å is again comparable to that of the OEC. Christou, Hendrickson and co-workers have also characterised binuclear oxo- and acetato-bridged mixed-valence complexes.[51] In the bis μ_2-oxo mono-acetato bridged Mn(III)Mn(IV) complex (Figure 13B) the Mn-Mn separation is 2.667(2)Å, again very similar to that reported for the OEC. Chloride is bound terminally at 2.327 and 2.341Å, Mn1-Cl3 and Mn2-Cl4 respectively.

As seen in the complexes described above, Mn-Mn distances of 2.6-2.8Å are characteristic of bis μ_2-oxo-bridged dimanganese complexes.[29(c)] This indicates that a similar structural unit may occur in the OEC. Mono oxo-bridging usually leads

to longer Mn-Mn separations of 3.1-3.2 Å similar to the 3.3Å long Mn-Mn distance predicted for the OEC by Cramer.

A tri μ_2-oxo-bridged Mn(IV) dimer has been characterised.[46(c)] It has an unprecedented short manganese-manganese separation of 2.296(2)Å which makes it a borderline case as to the question of whether or not this represents a metal-metal bond.

Chloride-containing polymanganese complexes are important as they allow investigation of the properties imparted by terminal and/or bridging chloride ions. Hendrickson has made the binuclear chloride-containing compounds shown in Figure 14.[52]

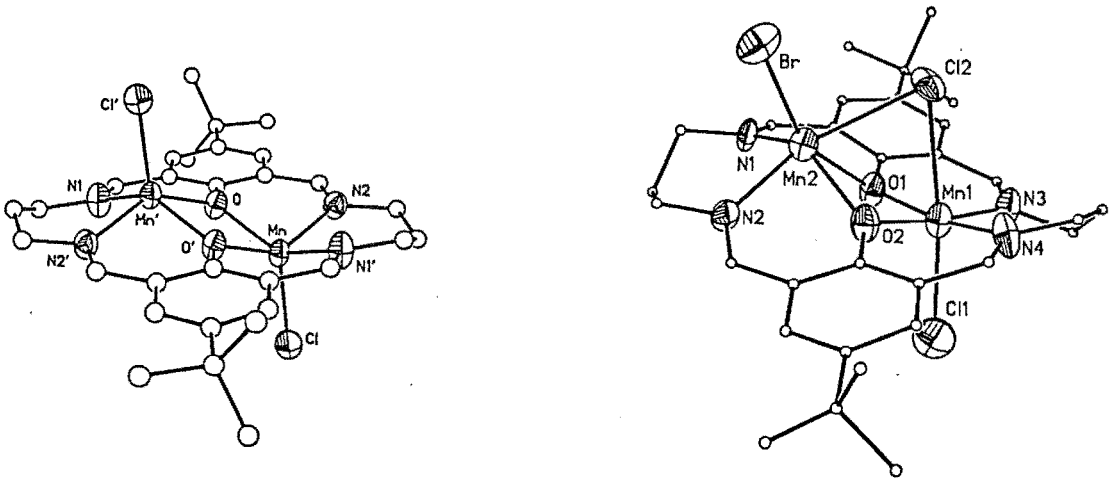

14A 14B

Figure 14

In the first structure (Figure 14A) the chlorine atoms are terminally bound to the Mn(II) atoms which are bridged by the macrocyclic phenolate oxygens. The product of bromine oxidation of this compound (Figure 14B) is mixed-valence Mn(II)Mn(III) with chloride bound both terminally (2.491(5)Å)and in bridging mode (2.766(6)Å). In this example a change from terminal to bridging mode is seen to result in a large increase in bond length. This long 2.766(6)Å Mn-Cl bond is close to the 2.7Å Mn-Mn interaction of the OEC predicted by EXAFS, and could conceivably be hidden in the Mn-Mn envelope. Both of these complexes have longer Mn-Mn separations (3.324(4) and 3.168(3)Å respectively) than the bis μ_2-oxo bridged dimers.

Some of the advantages of using large macrocycles to bind more than one manganese atom have been exploited in the above examples. Firstly, the macrocycle can provide bridging atoms; secondly, the complex is more likely to stay intact in solution studies than an aggregate; and thirdly, the macrocycle can be used to impose an unusual geometry on the metal ions.

Nelson and McKee have also employed a binucleating Schiff-base macrocycle to bind two Mn(II) atoms (Figure 15).[53]

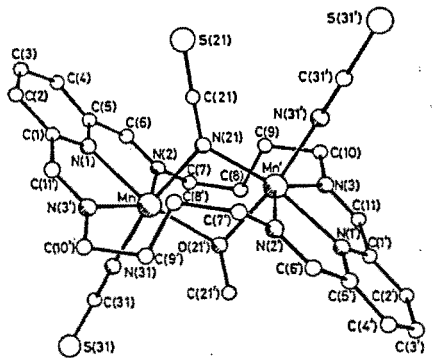

Figure 15

In this case the macrocycle holds the two manganese ions at a distance of 3.418(6)Å. Two single-atom bridges (-NCS, -OMe) also link the manganese atoms. Air oxidation of MeOH/MeCN solutions of this compound yields dark brown Mn(III) products. Binuclear Mn(III) products are also formed when manganese(III) acetate is used as the manganese source. A macrocycle closely related to this one has been used to form an interesting mixed-valence $Mn(II)_2Mn(III)_2$ dimer (later, Section 2.2, Figure 48).

Wieghardt and co-workers have produced a trimeric tri μ-oxo-bridged Mn(IV) complex (Figure 16A) by treating an aqueous solution of $[(tacn)_2\ Mn(III)_2\ (\mu\text{-}O)(\mu\text{-}MeCO_2)_2](ClO_4)_2$ (Figure 11A) with Na_2HPO_4/NaBr in the presence of air.[54]

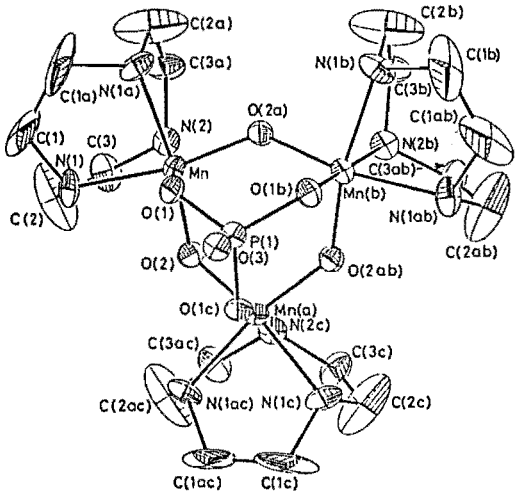

16A

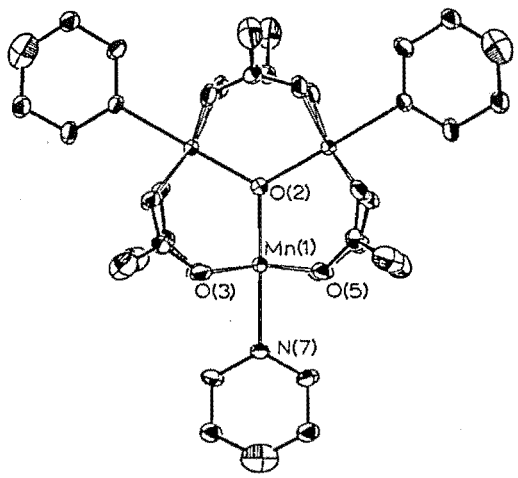

16B

Figure 16

The Mn-μ_2O distance of 1.785(6)Å is similar to the 1.75Å predicted by Klein. The manganese atoms are 3.226(1)Å apart as seen in the mono oxo-bridged dimers. Christou, Hendrickson and co-workers have also made some trimeric complexes.[55] Figure 16B shows a delocalised Mn(II)$Mn(III)_2$ mixed-valence complex held together by acetate bridges and a central μ_3-O. Difference electronic spectra of this and the isostructural $Mn(III)_3$ complex give a very similar profile to that obtained for S_0 and S_1 in the OEC.[25(a)] A similar μ_3-O trimeric core is found in the Mn(III)

complex of diethylenetriamine (Figure 17A) prepared by Weatherburn and co-workers.[56] This complex is the first peroxo-bridged manganese compound to be structurally characterised (O4-O4' 1.6(1)Å). Addition of a little concentrated HCl causes loss of the peroxo signal in the Raman spectrum. This complex is a valuable model for the peroxy intermediate in oxygen evolution (Figures 7, 8 and 9). Two structurally isomeric (linear *vs* bent) trinuclear $Mn(II)Mn(III)_2$ complexes have been synthesised by Pecoraro and co-workers.[57] The bent complex is shown in Figure 17B. This complex has a $g \approx 2$ multiline signal as do other mixed-valence bi-[52(b)] and tetranuclear[58] species. As bi-, tri- and tetramanganese complexes exhibit $g = 2$ multiline signals, care must be taken in the derivation of nuclearity and oxidation states of the OEC manganese from the $g = 2$ multiline EPR signal (which also varies according to data collection conditions).[59]

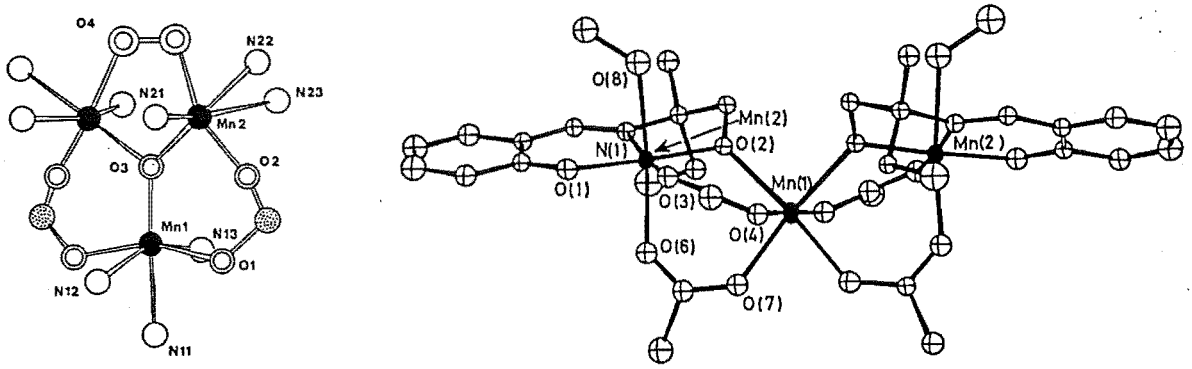

17A 17B

Figure 17

The $[Mn_4O_6]$ adamantane structure proposed by Brudvig and Crabtree (Figure 10) in their OEC cycle had been observed previously by Wieghardt (Figure 18A).[60]

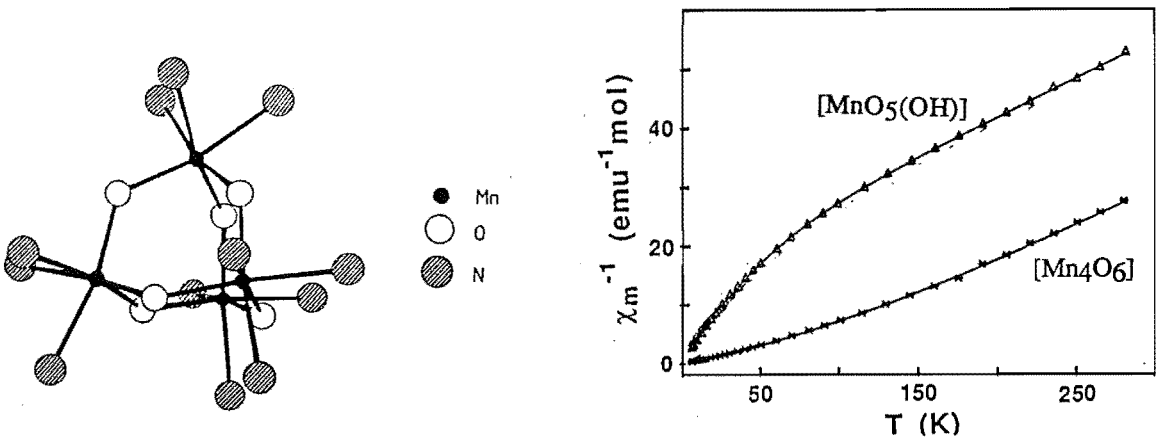

18A 18B

Figure 18

The Mn-Mn distance of 3.21Å is similar to the long Mn-Mn interaction (3.3Å) predicted by Cramer for the OEC, and the Mn-μ_2-O distance of 1.79Å matches well

with Klein's EXAFS interpretation. This Mn(IV) complex is very stable in water indicating that perhaps Mn(V) is necessary to trigger oxidation of water (Table 1, set A). An alternative view is that the adamantane core itself is too stable a configuration. The latter interpretation would invalidate Brudvig and Crabtree's proposed OEC scheme. Recently Armstrong and co-workers have studied the effect of protonating the adamantane skeleton at one oxygen giving a $[Mn_4O_5(OH)]$ core.[61] Protonation of the bridging oxygen significantly increased the Mn-O bond length from an average Mn-O of 1.79Å to an Mn-OH of 1.95Å. They also found that protonation caused a dramatic change from ferromagnetic to antiferromagnetic coupling (Figure 18B). It was concluded that attempts to interpret the magnetic properties of the OEC must take into account changes in the protonation of any water derived ligands.

The first structurally characterised discrete $[Mn(II)_4O_4]$ cubane was synthesised by McKee (Figure 19A).[62]

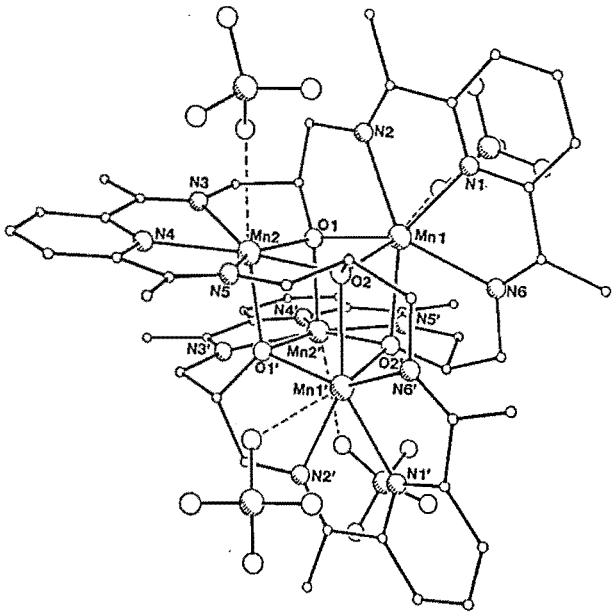

19A

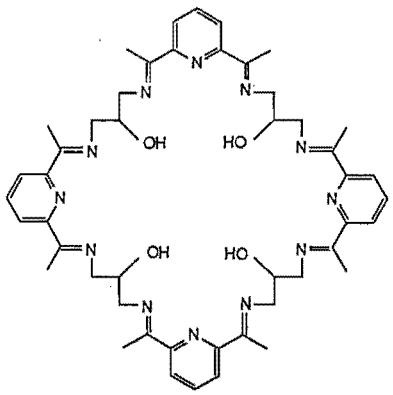

19B

Figure 19

Each manganese atom is seven coordinate; six donors come from the large Schiff-base macrocycle (Figure 19B) and the seventh donor is an oxygen atom of a semi-coordinated perchlorate anion. Both Vincent and Christou (Figure 9) and Brudvig and Crabtree (Figure 10) have suggested such a structure in the early S-states of the OEC. However this particular complex is not oxidised enough to match the proposed oxidation states of the OEC. Recent EXAFS of this Mn(II) complex by Cramer has shown that although a cubane structure is more symmetrical than the OEC (Figure 5), the first shells of scatters occur at similar distances to those of the OEC (later Section 2.2).[63] Tuchagues and co-workers have calculated the theoretical magnetic susceptibility of a four $S = {}^5/_2$ spin system and successfully applied this to data on this compound.[64] Understanding the magnetic exchange

properties of multinuclear manganese clusters is important as it will aid interpretation of the data available on the OEC.

Two mixed-valence $[Mn(III)_3Mn(IV)O_3Cl]$ cubanes have since been characterised by Christou, Hendrickson and co-workers.[58,65] The multiline EPR and magnetic data on $[Mn_4O_3Cl_4(OAc)_3(py)_3]$ (Figure 20A) fit an $S = {}^9/_2$ ground state.

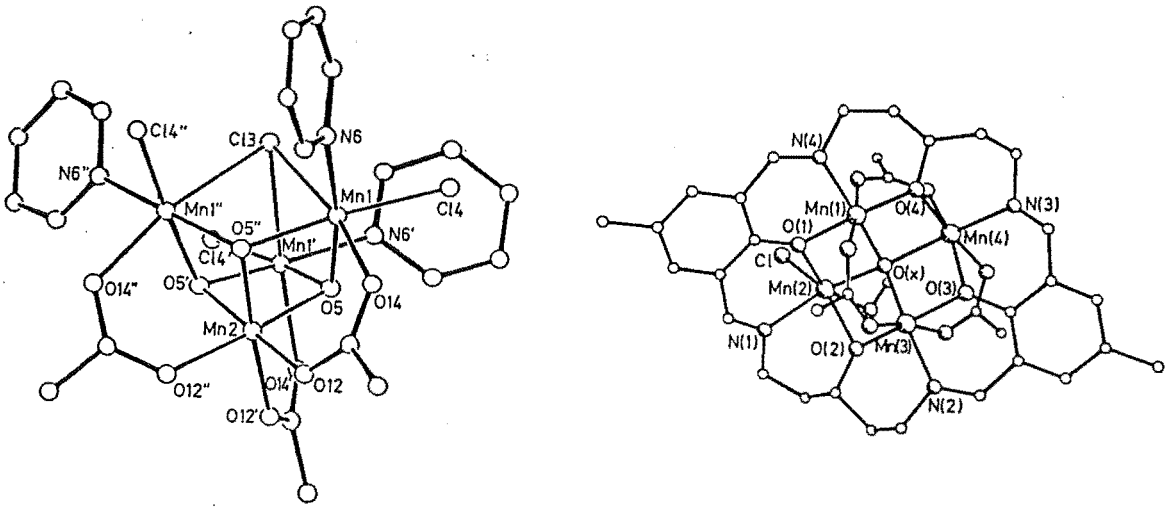

20A 20B

Figure 20

This work shows that the OEC S_2 state EPR spectrum could arise from such a large-spin ground state. The Mn1-Cl3 bond of 2.672(2)Å is long by comparison with terminally bound Cl (e.g. Mn1-Cl4 2.237(2)Å). Models like this, which incorporate chloride bridging and Mn-Mn separations of 2.815(2) and 3.272(2)Å, should provide very useful EXAFS data because they will help determine whether or not a Mn-Cl interaction at ≈ 2.7Å can be hidden in the Mn-Mn envelope.

McKee and Tandon have produced a mixed-valence $Mn(II)_2Mn(III)_2$ complex of a tetranucleating macrocycle (Figure 20B).[66] This complex adopts a "butterfly" conformation like that proposed by Christou and Vincent (Figure 9) for the later S-states of the OEC. Christou and Vincent have also proposed a similar $Mn(II)_2Mn(III)_2$ mixed-valence configuration for the S_{-1} state.[67(b)] Each manganese has two relatively short interactions with other metal ions and one longer separation. A central oxo ion (probably derived from oxygen) binds to all four manganese with bond distances ranging from 1.901(4) to 2.249(4)Å and bond angles varying from 96.1(2) to 141.9(2)°. A single chloride is bound to Mn2(II) at 2.463(3)Å. Therefore this is an important compound to obtain EXAFS and XANES data for to compare with the OEC.

Christou and Hendrickson have also characterised a $[Mn_4O_2]^{6+,7+,8+}$ series.[29(a),67] The crystal structures of $[Mn(II)_2Mn(III)_2(O)_2(O_2CMe)_6(bipy)_2]$ (bipy = bipyridine) and $[Mn(III)_4(O)_2(O_2CMe)_7(bipy)_2](ClO_4)$ are shown in Figures 21A and 21B. The "butterfly" structure of the latter complex led them to

propose their "double-pivot" OEC mechanism (Figure 9). The two central manganese atoms are in the +III oxidation state in both cases. Surprisingly, an additional acetate bridging these central manganese atoms is found in the latter case (octahedral coordination) but not in the former, which leads to unusual five-coordinate (trigonal bipyramidal) geometry. Ligand substitution reactions show that the acetate groups are labile.

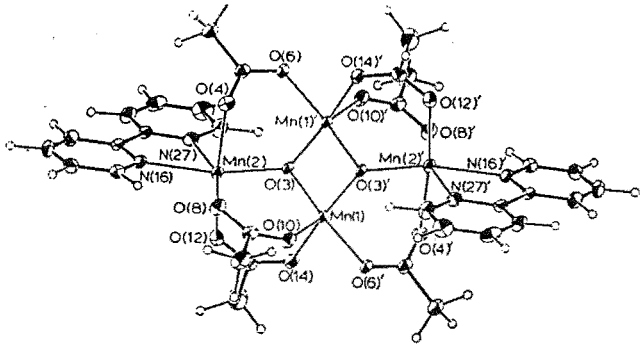

21A

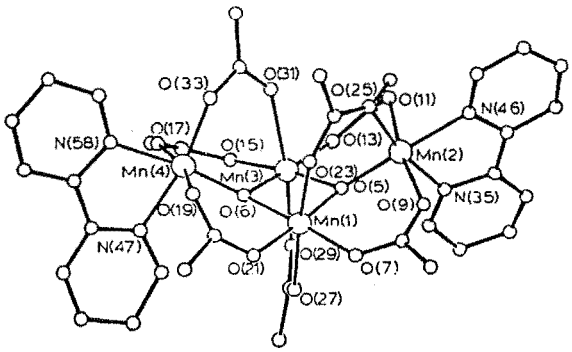

21B

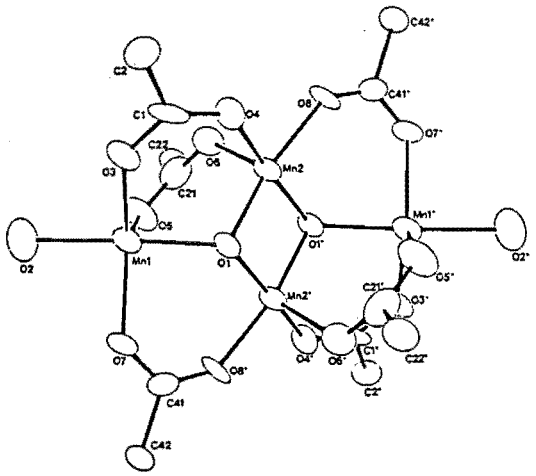

21C

Figure 21

Brudvig, Crabtree and co-workers have synthesised a mixed-valence $Mn(II)_2Mn(III)_2$ compound (Figure 21C) where all the donors are oxygen atoms.[30] Mn1 is in the +II oxidation state and Mn2 is +III. They both have unusual coordination geometries, distorted trigonal bipyramidal and distorted five-coordinate square pyramidal respectively. Another unusual feature of this complex is the coordination of diethylether (02) to Mn1. The open structure and coordinative unsaturation will allow investigation of ligand binding and substitution reactions. The Mn-Mn distances, Mn1-Mn2 = 3.265, Mn2-Mn2' = 2.770(4)Å, match very well with the 2.7 and 3.3Å seen by EXAFS of the OEC.

Clusters of more than four manganese ions have also been formed,[68] only two of which are shown in Figure 22A. The first (22A) is a nonanuclear $Mn(II)Mn(III)_8$ species characterised by Christou and co-workers.[69,31] The central eight-coordinate

manganese atom is assigned the +II oxidation state. The remaining eight Mn(III) atoms are in the form of two $[Mn_4(\mu_3\text{-}O)_2]$ "butterfly" units as seen before in the tetramanganese complex depicted in Figure 21B.

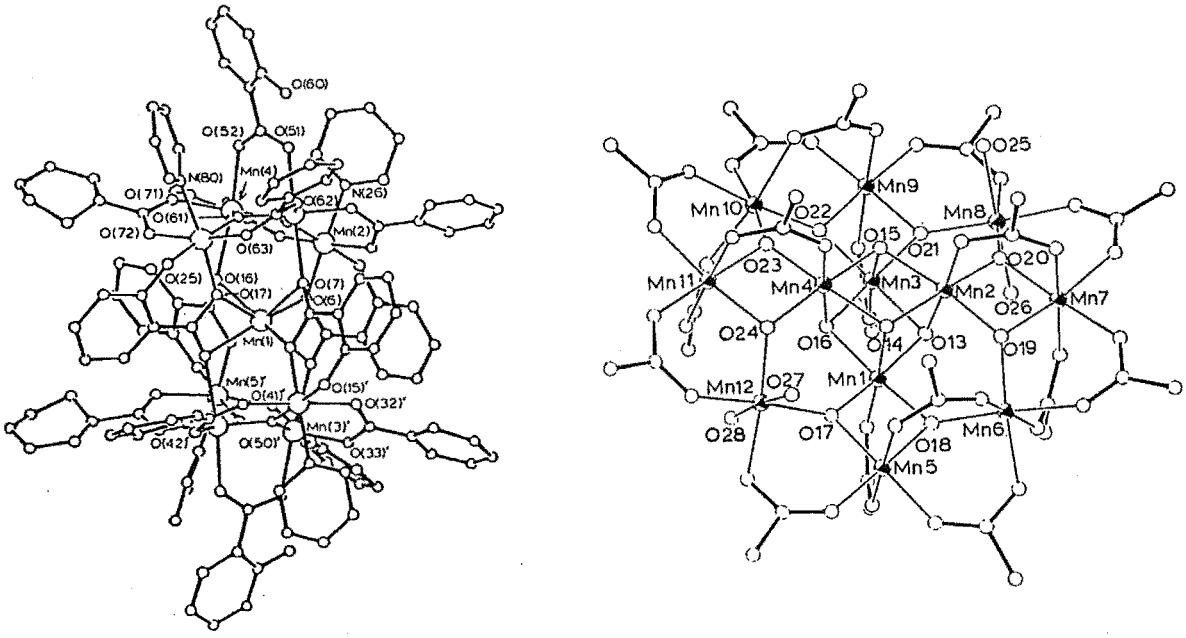

22A 22B

Figure 22

The second example in Figure 22, $[Mn(III)_8Mn(IV)_4O_{12}(O_2CPh)_{16}(H_2O)_4]$, was also reported by Christou and co-workers,[70] however, an almost identical structure, $[Mn(III)_8Mn(IV)_4O_{12}(O_2CCH_3)_{16}(H_2O)_4].2CH_3COOH.4H_2O$, had been previously reported by Lis.[71] The latter molecule differs in that it has higher (S_4) symmetry, presumably allowed by the smaller acetate group. In both cases there is a central $Mn(IV)_4O_4$ cubane as is proposed by Christou and Vincent (Figure 9) and Brudvig and Crabtree (Figure 10) in their OEC cycles. The short Mn-Mn distances in the acetate structure are 2.767(3), 2.820(3) and 2.943(3)Å, and another group occurs at 3.329(3) to 3.455(3)Å; these match the OEC distances quite well. In this case, even at this highly oxidised level, the Mn(IV)-μ_3O distances (1.854(7) - 1.916(7)Å) are longer than the 1.75Å bridging distances predicted for the OEC by Klein. As these large clusters contain fragments of the types of structures proposed to occur in the OEC they are useful models.

In 1984 McAuliffe and co-workers reported the first manganese complexes observed to oxidise water.[72] The general formula was $[Mn(III)L(H_2O)]ClO_4$ where L is salen, salpd or salbd or salpn (shown in Figure 23A). In the solid state, FAB mass spectroscopy, infrared data and magnetic interactions indicate a dimeric structure (I, Figure 23B); however in aqueous solution conductivity measurements imply that an equilibrium exists between monomeric (II, Figure 23B) and dimeric species.

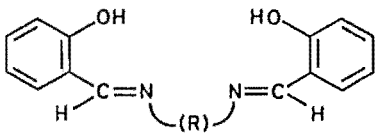

H_2L

	R
H_2salen	$(CH_2)_2$
H_2salpd	$(CH_2)_3$
H_2salbd	$(CH_2)_4$
H_2salpn	(CH_2CHMe)

23A

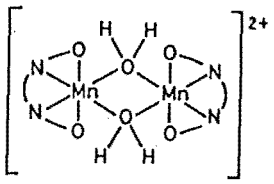

I

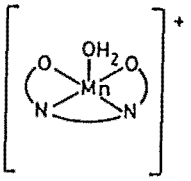

II

23B

Figure 23

Oxygen evolution from aqueous solutions of the manganese complex and p-benzoquinone (H-acceptor, λ_{max} = 247 nm), occurred when they were irradiated with visible light (specifically the green region, 450-600 nm). p-Benzoquinone was converted to p-benzohydroquinone (λ_{max} = 290 nm) during the reaction. All of the photolytically active manganese species absorbed at 590 nm in their electronic spectrum; the more intense this peak was, the more active the complex. Irradiation also caused a black precipitate of $[(Mn(III)L)_2O]$ to deposit. Thus the overall reaction is:

$$[\{Mn(salpd)(H_2O)\}_2][ClO_4]_2 \xrightarrow{h\nu} \tfrac{1}{2}O_2 + 2[H] + 2H^+ + 2ClO_4^- + [\{Mn(salpd)\}_2O] \qquad (2)$$

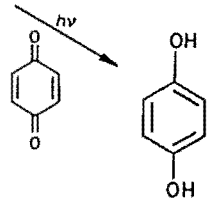

The rate increased as the pH was increased from 4.5 to 6.9. The water photolysed is almost certainly the coordinated water as a similar rate and quantity of oxygen was observed when the complexes were irradiated in anhydrous ethanol. The activity of the complex was very sensitive to the nature of the ligand. The complex of salpd (3C chain) was about eight times more active than the complexes of salen (2C chain) or salbd (4C chain). Methylene blue (MB) was also effective as a proton acceptor although not as effective as p-benzoquinone. This is potentially important as it has been shown that reduced MB plus hydrogenase gives H_2 and MB. Thus it is possible that photolysing water could allow separate production of H_2 and O_2 :

$$2H_2O \xrightarrow[\text{MB, hydrogenase}]{\text{Mn(III) complex, h}\upsilon} 2H_2\uparrow + 2O_2\uparrow \qquad (3)$$

As the manganese oxidation state is unchanged this system may be able to be modified (to stop precipitation) and made catalytic, thus harnessing the light energy provided by the sun.

Two other manganese complexes which apparently oxidise water, $[(bpy)_2Mn(III)(\mu\text{-}O)_2Mn(IV)(bpy)_2]^{3+}$ bipy = 2,2'-bipyridyl[49(c)] and

$[(phen)_2Mn(III)(\mu\text{-}O)_2Mn(IV)(phen)_2]^{3+}$ phen = 1,10-phenanthroline were reported by Ramaraj in 1986.[73] Visible oxygen bubbles were produced when either of these complexes was suspended in water, as a heterogeneous catalyst, in the presence of Ce(IV) (consumed). The pH of the solution did not affect the water oxidation process, indicating that water, and not OH^-, was the substrate. The redox potentials of these complexes showed that they could only act as one-electron transfer agents. Four electrons are required per oxygen molecule so these one-electron steps have to be efficiently coupled. These complexes were only catalytically active in the solid form indicating that a group of four Mn(IV) dimers may act in concert to oxidise two molecules of water at the surface by four electrons.

More recently Mn(IV) incorporated in vesicles has been shown to be able to oxidise water in the presence of an oxidant such as $[Ru(bpy)_3]^{3+}$ or $[Fe(bpy)_3]^{3+}$.[74] In this case the nature of the Mn(IV) catalyst is not known but it is assumed to be a polynuclear species.

1.4 Bi- and Poly-nucleating Macrocycles

To prepare informative manganese model compounds for the OEC it is necessary to design suitable ligands. The ligand must provide nitrogen and/or oxygen donors and encourage the formation of clusters of 2-4 manganese atoms. The latter requirement can be fulfilled in several ways; a large ligand can provide binding sites for 2-4 manganese atoms (Figures 14, 15 and 19), or a bridging anion such as acetate or oxo can be used to hold mono- or dimanganese fragments together (Figures 11, 13, 16-18 and 20-21) or finally, the ligand itself can provide a group which bridges between macrocyclic units (e.g. alkoxy group, later, Section 2.2).

The formation of transition metal clusters is of intrinsic interest in addition to providing structural and/or functional models of metalloproteins (e.g. OEC). These clusters allow the study of metal-metal interactions such as redox reactions and magnetic exchange. Binding of small substrate molecules can also be investigated with the aim of developing useful catalysts. Only multinucleating macrocycles will be considered in this Section as mononuclear complexes are not good models for the OEC or other polynuclear metalloproteins.

Macrocyclic complexes are usually more stable than their open chain analogues due to the macrocyclic effect.[75] This added stability is because of a balance of entropic and enthalpic effects. Linking the terminal donors of a multidentate ligand will only produce complexes of enhanced stability (macrocyclic effect) if the macrocyclic "hole" size matches well with the metal ion radius and the donor atoms can adopt a preferred coordination number and geometry for the metal ion.

The formation of macrocycles is achieved either by direct synthesis or by template methods.[75,76,77] Examples of the direct preparation of a free macrocycle are shown in Figure 24.[78]

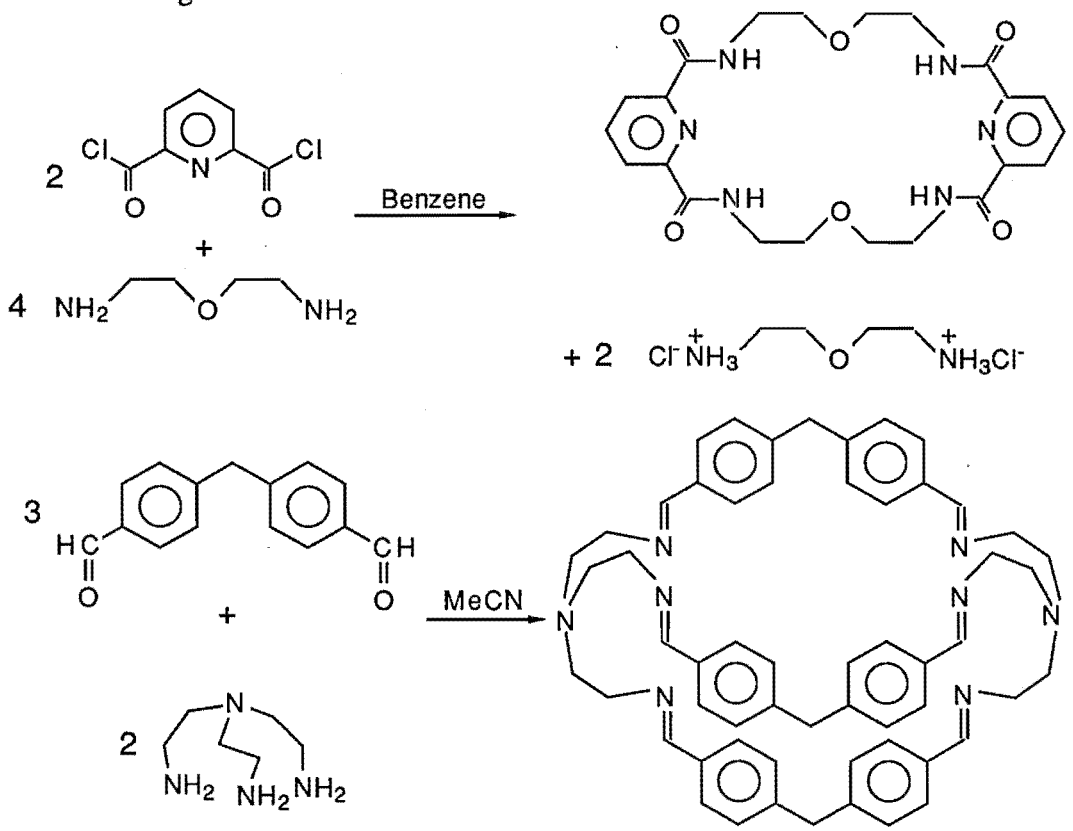

Figure 24

Often this method is low yielding due to the formation of noncyclic and polymeric species as well as the desired macrocyclic product. High dilution techniques are usually employed to reduce this problem. The main advantage of the method is that the free macrocycle is obtained and this is often more easily purified and characterised than the macrocyclic complex resulting from a template synthesis, as it is generally more soluble.

Template methods use a metal ion to promote cyclisation by coordination to the starting materials (kinetic template effect), and coordination by the metal ion also stabilises the macrocyclic product (thermodynamic template effect). Both kinetic and thermodynamic template effects are usually in operation. Examples of macrocycles which could not be isolated metal-free are shown in Figure 25.[79,80]

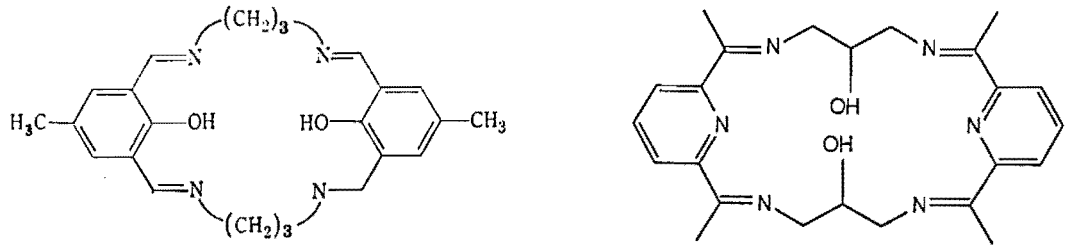

25A 25B

Figure 25

Both macrocycles are of the (2+2) type, that is they are formed by the condensation of two carbonyl and two amine moieties. Attempts to synthesise these ligands under various metal-free, high dilution conditions led only to the formation of polymeric gums. However, the use of appropriate metal ion templates (25A Mn(II), Ni(II), Cu(II), Fe(II) ; 25B Ba(II), Fe(II) [81]) has led to the successful isolation of many complexes of these macrocycles. The yields of these template reactions are frequently very good. The template ions for large macrocycles are usually non-transition metal ions such as Pb(II), Ba(II), Sr(II), Ca(II) or Ag(I) because these are large ions and therefore they match the large macrocyclic cavity. Some transition metal ions may also act as template ions for particular macrocycles (e.g. Figure 25) but in other cases they may be less effective, or fail entirely, due to their stereochemical and spatial preferences. The template ion must be of an appropriate size for the macrocycle to form around. In the examples shown in Figure 25 the transition metal ions are good template ions for the (2+2) rings because a (1+1) macrocycle can not form (the alkyl chains are not long enough) whereas (2+2) formation is promoted by the binding of two transition metal ions. The ability of $Mn^{II}(d^5)$ to promote the formation of the tetranucleating H_4L1' macrocycle (Figure 19B) will be discussed in Section 2.2.

As the macrocycles employed in the work described in this thesis are all single-ring Schiff-bases[76,77] the remainder of this Section will focus on the properties of these macrocycles. The general mechanism for the template formation of a Schiff-base macrocycle is outlined in Figure 26.

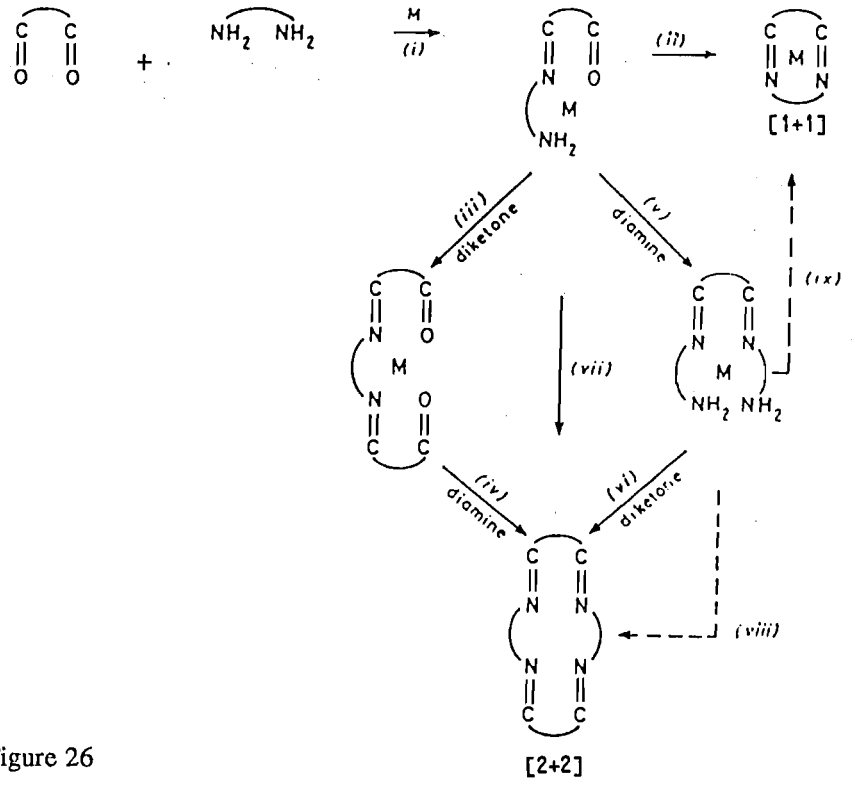

Figure 26

Whether a (1+1) or (2+2) macrocycle will be formed depends on the size and stereochemical preferences of the template ion, and the length of the diamine. For example in the system illustrated in Figure 27, Mn(II), Fe(II), Co(II), Ni(II), Cu(II), and Zn(II) templates yield a (1+1) macrocyclic complex whereas Ag(I), Pb(II), Ca(II), and Sr(II) promote (2+2) formation.[82]

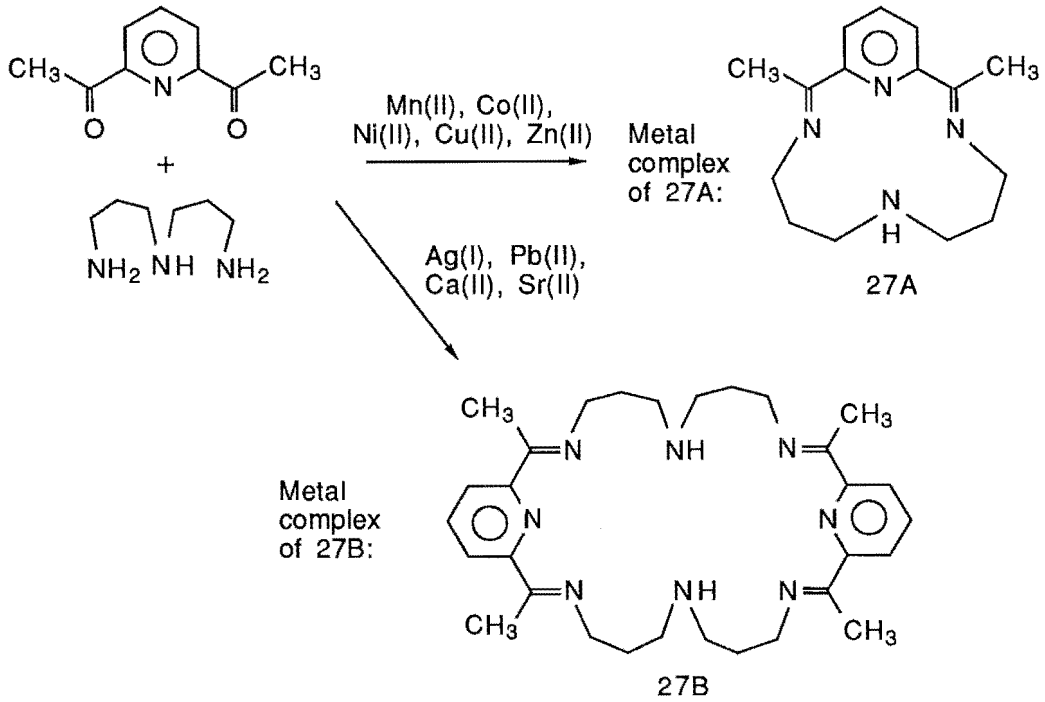

Figure 27

In fact the possibilities are not limited to the formation of (1+1) or (2+2) macrocycles. The first known (4+4) Schiff-base macrocycle (Figure 19B) was revealed by the single crystal X-ray structure of a tetramanganese complex prepared by McKee (Figure 19A).[62] This reaction has been investigated further, indicating that the Mn_4O_4 cubane acted as a template for the formation of the (4+4) macrocycle, and the results are presented Section 2.2. Fenton has reported the isolation of a trinuclear lanthanide (3+3) Schiff-base complex, evidence for which comes from NMR and FAB mass spectrometry.[83]

Once the macrocycle has formed on a non-transition metal template ion this ion may be replaced by the transition metal ion of interest in a transmetallation reaction. This is possible because the template ion complex is generally labile and allows a concerted replacement reaction to occur. The driving force for this metal ion replacement is the formation of a more stable transition metal complex.

Ring expansion and contraction reactions can occur readily and reversibly as observed by Nelson (Figure 28A)[84] and Fenton and Bailey (Figure 28B).[85] Ring contraction occurs by intramolecular nucleophilic attack on an imine linkage by a secondary amine or alcohol group respectively. The driving force is the mismatch in the metal ion *vs* the macrocyclic ring sizes. In both cases transmetallation by an ion of suitable size for the larger macrocycle causes ring expansion.[84,86]

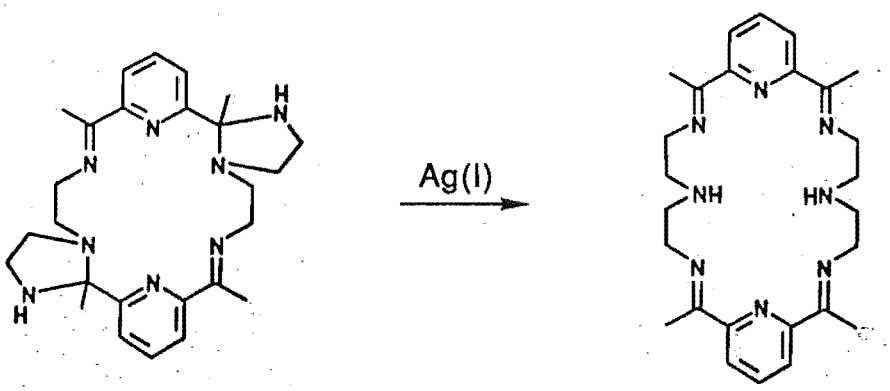

I II

28A

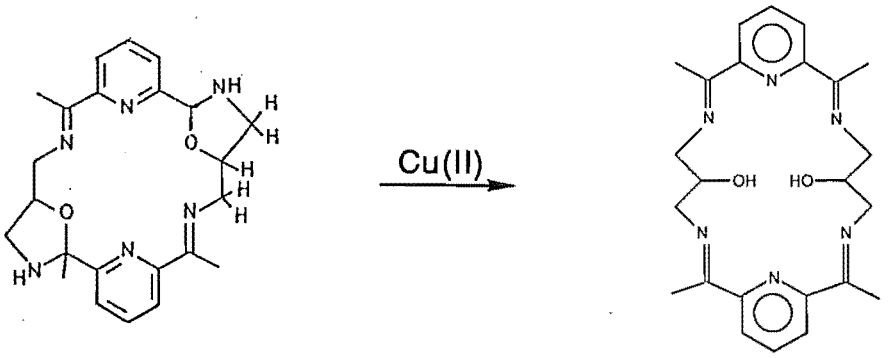

I II

28B

Figure 28

In some cases noncyclic complexes like 29A (Figure 29A) can be isolated.[76]

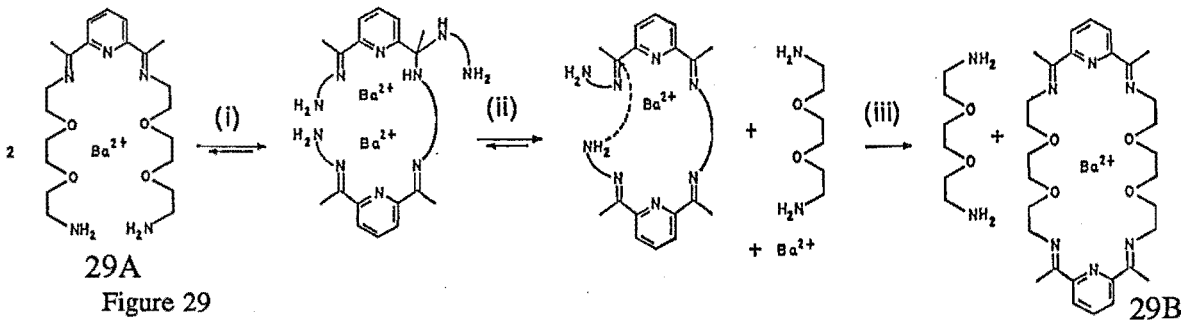

29A 29B

Figure 29

Warming complex 29A in dry methanol causes cyclisation to form 29B, even in the absence of added carbonyl (step iii in Figure 29). It is proposed that this occurs *via* nucleophilic attack of the free amine of one molecule on the imine of a second molecule (intermolecular transamination). Loss of an amine molecule then regenerates the imine linkage. The intramolecular nucleophilic attack of a second, uncoordinated amine group on the adjacent imine bond (intramolecular transamination), followed by loss of a second amine molecule, generates 29B.

Macrocyclic ligands may be designed to contain particular donor atoms and to encourage specific geometries. Potential bridging groups can also be incorporated in

the ring. The distance between the metal ions is also restricted by the choice of an appropriate macrocyclic ring size. Examples of the variations caused by a series of slight changes in the macrocycle are seen in the dicopper complexes (Figure 30).[86,87]

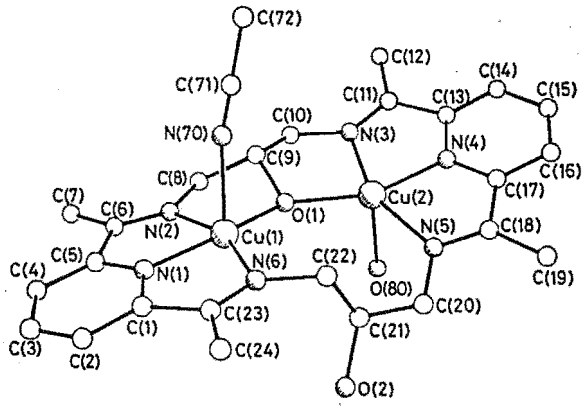

30A

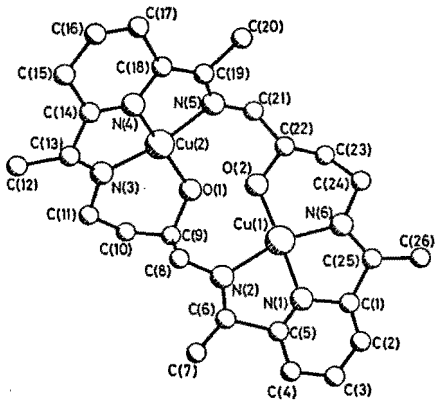

30B

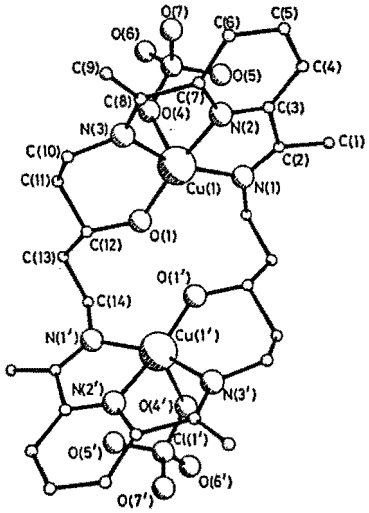

30C

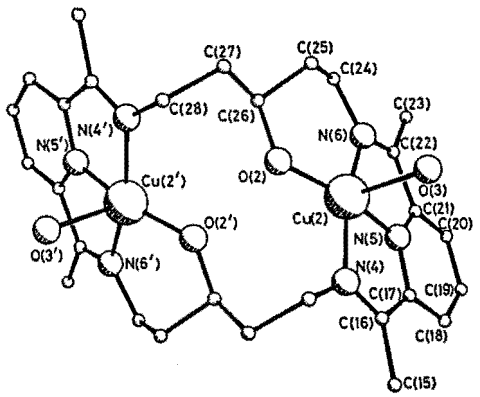

30D

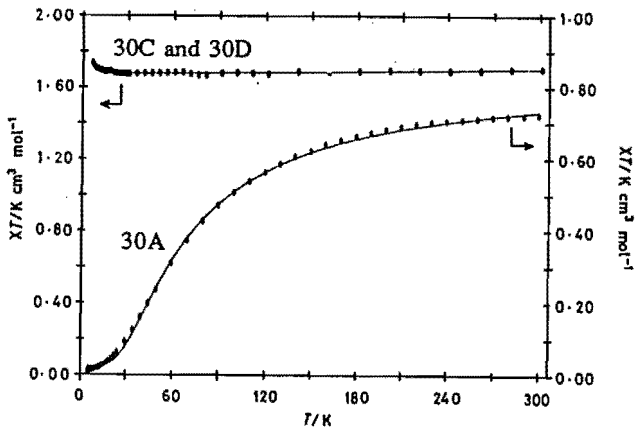

30E

Figure 30

The 20-membered macrocycle produces a fairly planar dicopper complex 30A, with an alkoxy bridge provided by the macrocycle. The Cu-Cu separation of 3.638(8)Å is

close to the values of 3.8 and 3.5Å obtained by EXAFS of oxyhaemocyanin and methaemocyanin respectively. Haemocyanin is thought to have an endogenous phenoxide, alkoxide, or hydroxide bridge so this complex is a good model from this aspect as well as it incorporates an alkoxide bridge. Increasing the ring size to 22 atoms results in the dicopper complex 30B. Again one of the pendant alcohol groups is deprotonated but this time it binds to only one copper atom. The second alcohol group binds to the other copper atom and hydrogen bonds to the deprotonated alcohol group. The macrocycle is folded. The copper atoms, no longer bridged by the pendant alcohol functions, are now 4.706(7)Å apart. This separation increases to 4.820(3) and 4.903(2)Å in 30C and 30D, the two molecules in the asymmetric unit when the macrocycle is 24-membered. The change from the bridged 20- to the non-bridged 22-membered macrocycle affects the observed magnetic exchange coupling as shown in Figure 30E. Antiferromagnetic coupling ($2J=-84cm^{-1}$) is observed in 30A, while only a small ferromagnetic interaction at low temperatures is apparent in 30C and 30D.

Complexes of multinucleating macrocycles allow several transition metal ions to be held together in a controlled manner allowing the study of binding and activation of small substrate ions or molecules. For example the macrocycle 31A (Figure 31A) binds four copper(II) ions producing a planar structure (Figure 31C).[88] Likewise macrocycle 31B (Figure 31B) binds four nickel(II) ions producing a domed structure (Figure 31D)[89]. In both examples all four alcohol/phenol groups are deprotonated and bridge two metal atoms, and a central μ_4-OH binds to all four metal atoms. These bridges provide pathways for magnetic exchange between the metal atoms resulting in antiferromagnetic coupling in the copper complex. The axial sites are open and therefore these and related tetrametallic complexes have potential as catalysts by promoting reaction between axially coordinated groups. Another catalytic possibilty would be the replacement of the central μ_4-OH group with other guest molecules which might be activated towards further reaction.

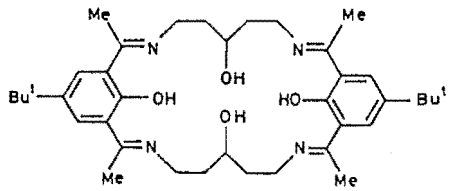

31A

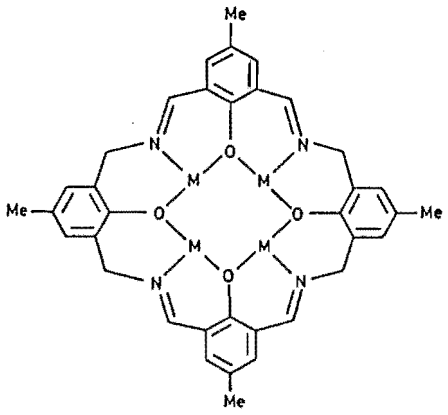

31B

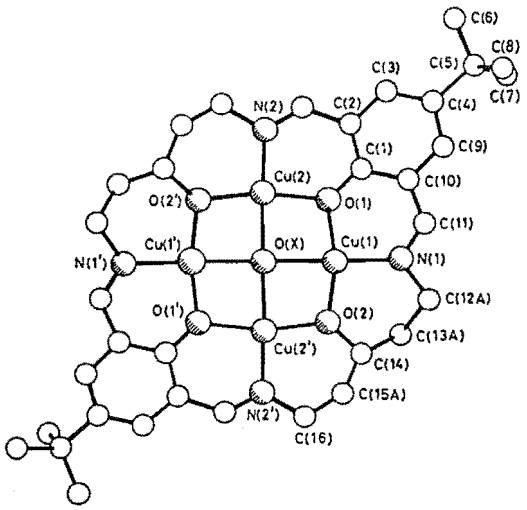

31C

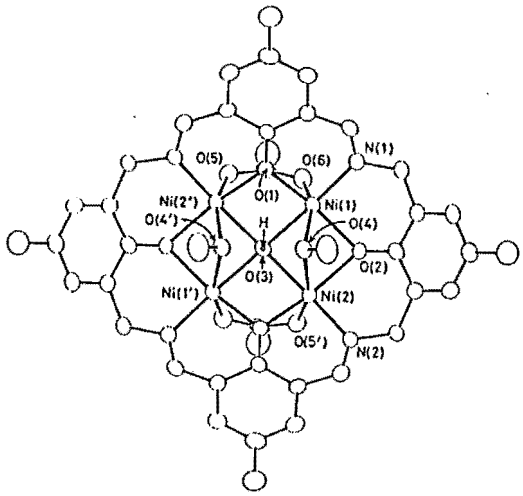

31D

Figure 31

Large macrocycles need not provide any bridging groups; they can be used just to hold metal ions at an appropriate distance for various exogenous bridging anionic groups to be incorporated. Many anions, including oxo (e.g. Figure 20B) hydroxo (e.g. Figure 31), alkoxo (e.g. Figure 15), acetato (e.g. Figure 20B), halide (e.g. Figure 14), azido (e.g. later, Figure 34E), thiocyanate (e.g. Figure 15), pyrazolate (e.g. later, Figure 35C) and imidazolate (e.g. later, Figure 34D) have been bound as one, two or three atom bridges in this way. The binding of these substrates can serve to activate them, producing unusual chemistry. The macrocycle shown in Figure 27B can bind two copper(II) atoms.[90] The complex isolated when thiocyanate ions are present has an infrared absorption at 1992 cm^{-1} which is characteristic of N-bridging thiocyanate.[53] However the internuclear distance is large and therefore a one atom bridge seemed unlikely. A single crystal X-ray structure determination revealed that there was no bridging group (Figure 32A shows one of the two cations in the asymmetric unit, the other is very similar) but that the nitrogen of the thiocyanate (N20) was protonated and sharing a hydrogen bond with N1' from a second macrocycle (3.49Å, Figure 32B shows the packing of these macrocycles). HNCS is not expected to coordinate to metal ions but in this case it appears that the normal relative acidities of NH and HNCS are reversed, due to coordination to the copper and the non-polar environment.

Unusual chemical transformations can also be carried out by multinucleating macrocycles capable of binding substrates. Nelson and co-workers have shown that in the presence of water and oxygen the dicopper(II) complex (Figure 33A) is converted to the pentacopper(I) complex (Figure 33B) with simultaneous (unprecedented) N-N coupling of the bound acetonitrile to form bound 1,2,4-triazolate ions *via* the scheme outlined in Figure 33C.[91]

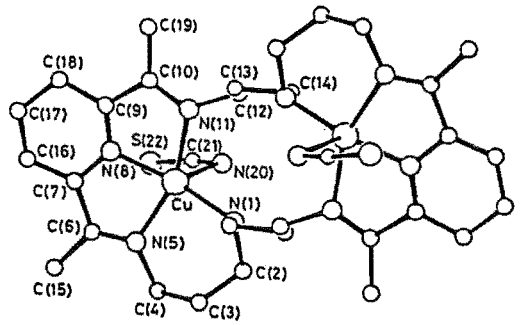

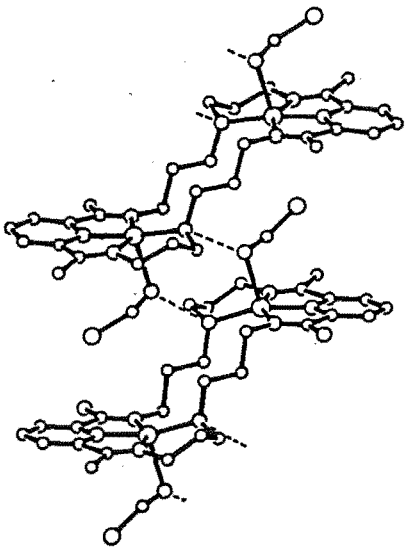

32A 32B

Figure 32

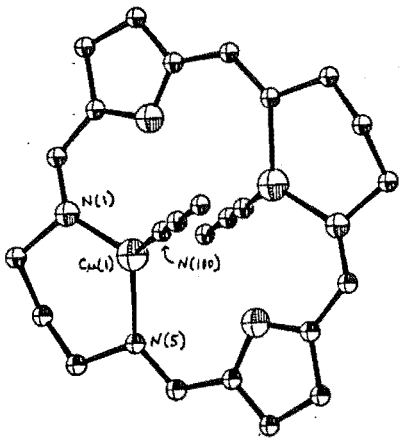

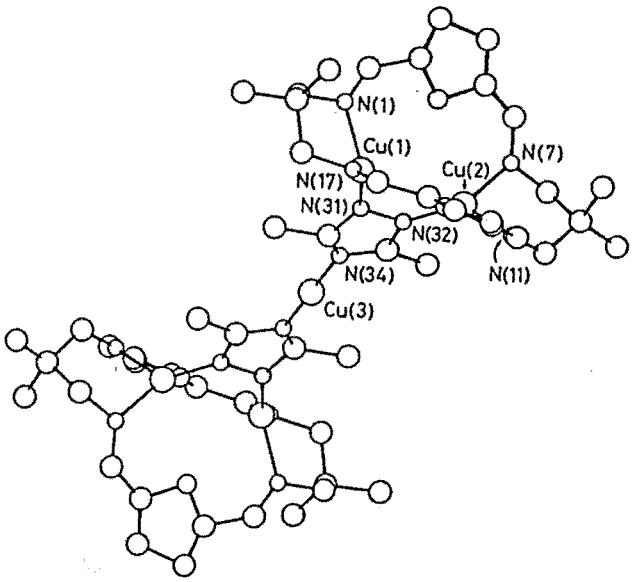

33A 33B

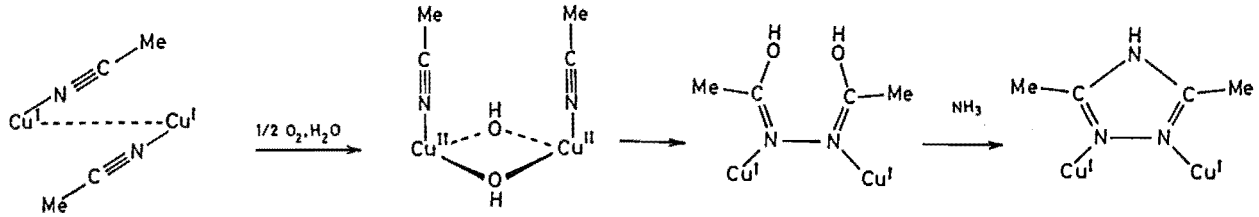

33C

Figure 33

Many macrocycles can fold to some extent producing different conformations (at the expense of added strain), thus varying the metal-metal separation and allowing bridges of different lengths to form between the metal centres. Two sets of examples of this feature are shown in Figures 34[92] and 35.[93]

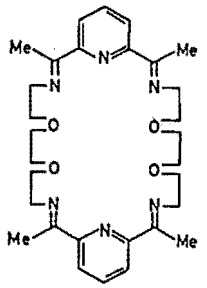

34A

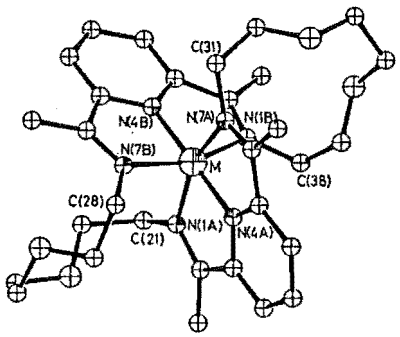

34B

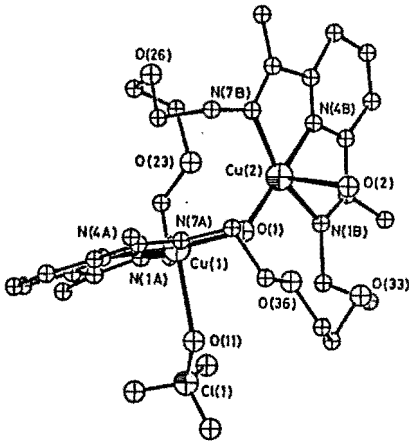

34C

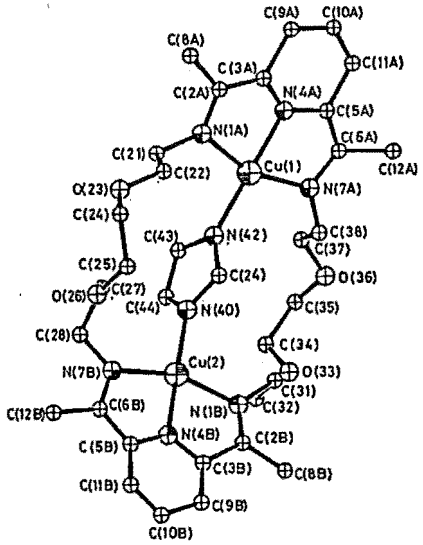

34D

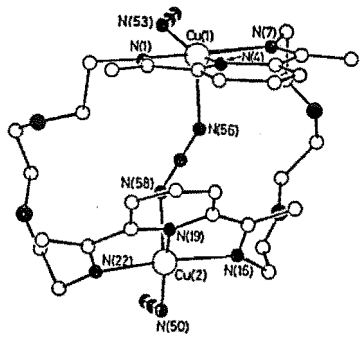

34E

Figure 34

Macrocycle 34A binds to Mn(II), Fe(II), Co(II) and Ni(II) *via* the six imine nitrogen donors producing very stable complexes due to the large LFSE (general structure shown in 34B); the iron and cobalt complexes are low spin. On treatment of the silver complex of 34A with one mole of copper(II), a mononuclear copper complex is formed. Further addition of copper ions followed by the addition of base, imidazole or azide led to the formation of the bicopper 1,1-μ_2-hydroxo (34C), 1,3-μ_2-imidazolato (34D) and 1,3-μ_2-azido (34E) complexes respectively (Figure 34). As can be seen from these structures the macrocycle is quite flexible and allows metal-metal separations to vary from mononuclear through 3.57Å (one atom hydroxo bridge), and 5.99Å (1,3-imidazolato bridge) to 6.02Å (1,3-azido bridge). In the second example, the macrocycle 35A binds two copper(II) ions *via* the imine nitrogen donors (furan oxygens do not generally coordinate to transition metal ions). In the presence of NCS^- the copper ions have approximate trigonal bipyramidal geometry (35B); the copper atoms are bridged by two ethoxy groups (mediating large antiferromagnetic exchange $2J = -332\ cm^{-1}$)and each one also has one terminally bound NCS^-. When

pyrazolate is bound it provides two two-atom bridges to give square planar copper(II) atoms (35C). The Cu-Cu separation increases from 3.003Å in 35B to 3.396Å in 35C, and the magnetic coupling drops to $2J = -135\ cm^{-1}$ in 35C.

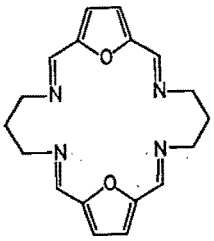

35A

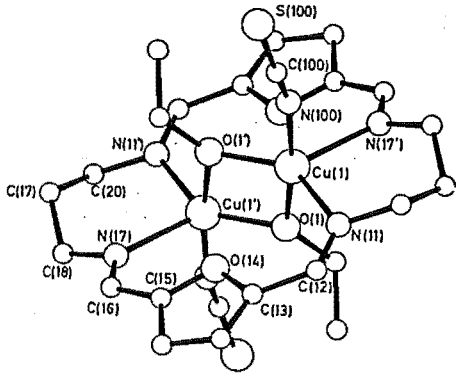

35B

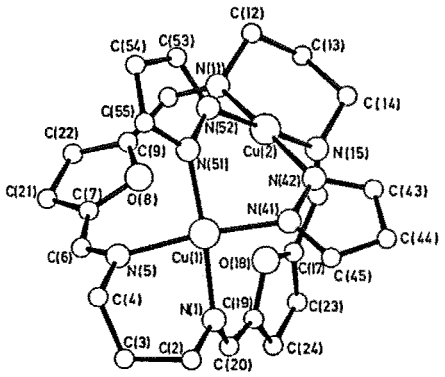

35C

Figure 35

The ability of macrocycles to help stabilise bridging by holding the metal ions in an appropriate configuration was used to model a metalloprotein in the following example. Bovine erythrocyte superoxide dismutase (SOD)[94] catalyses the reaction:

$$2O_2^- + 2H^+ \rightarrow O_2 + H_2O_2 \qquad (4)$$

SOD has been crystallised and its structure determined to 2Å resolution (Figure 36A). This metalloprotein consists of two identical subunits each containing one zinc and one copper atom bridged by imidazolate. Full catalytic activity is also observed when the zinc is replaced by copper. This is a useful feature as it simplifies the synthetic problem of making models. At the time the structure was published no binuclear copper complexes with a bridging imidazolate were known, and hence little was known about what properties such a bridge would give to the complex. Therefore, in order to test aspects of the mechanism by which the SOD was proposed to function model compounds were needed which reproduced the imidazolate bridge, known magnetic exchange properties ($J=-26cm^{-1}$) and pH stability (4.5-11) of Cu_2Cu_2SOD.

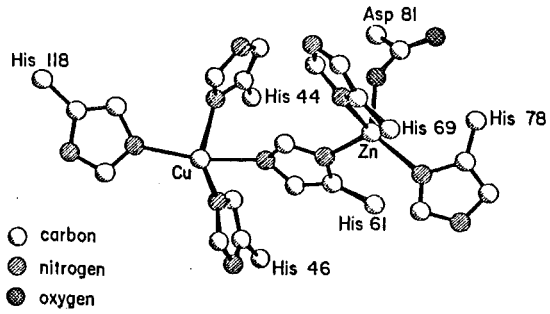

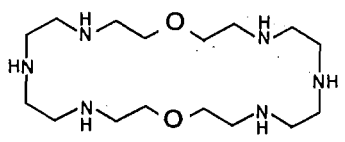

36A 36B

Figure 36

Various nonmacrocyclic dicopper complexes with imidazolate bridges were structurally characterised and were found to have similar J values to Cu_2Cu_2SOD. However, the imidazolate bridges were found to be stable only over a very narrow pH range (8.5-9.5) restricting their usefulness for solution studies. To overcome this problem macrocycles were employed to hold the copper atoms at the right separation for the imidazolate bridge.[95] This was successful and in the case of the dicopper complex of the macrocycle shown in Figure 36B resulted in an extension of the stable pH range to 6-10.

Chapter 2

COMPLEXES OF MACROCYCLIC LIGANDS

2.1 Experimental

Preparation of 2,6-Diacetylpyridine (DAP)

This compound was prepared in 41% overall yield from 2,6-dimethylpyridine *via* the three-step procedure outlined below.

Step 1 : 2,6-dimethylpyridine → 2,6-pyridinedicarboxylic acid

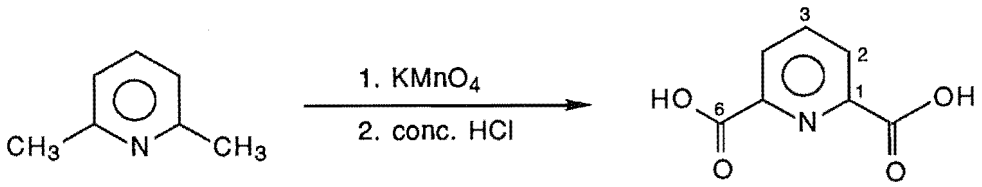

This oxidation is a slight modification of the method used by Black *et al* .[96] A mechanically stirred mixture of 2,6-dimethylpyridine (53.5 g, 0.5 mol) and water (1.25 l) was maintained at 75-85°C while potassium permanganate (377 g, 2.4 mol) was added in nine portions over approximately twelve hours. The initial portions were decolourised quickly but the reaction rate dropped substantially as the final portions were added. If the final portion was not decolourised in a reasonable time (1-2 hr) more 2,6-dimethylpyridine was added. The decolourised solution was then filtered through celite to remove the manganese dioxide (MnO_2) byproduct and the MnO_2 cake washed with 2x100 ml of water. The yellowish filtrate was concentrated to 1 l and 250 ml of conc. HCl was added, precipitating 2,6-pyridinedicarboxylic acid as a white solid. The solution was heated to boiling to redissolve the precipitate and then allowed to cool slowly. Overnight refrigeration at *ca.* 4°C yielded white needles of 2,6-pyridinedicarboxylic acid (50 g, 0.3 mol, 60%) which were collected by filtration, washed with 25 ml of cold water and air dried.

Infrared spectrum *inter alia* 3500(m), 1710(s,b), 1580(m) cm^{-1}

Melting point 243-244°C

NMR spectra (CD_3OD):

^{1}H H2 8.34(d); H3 8.19(m) ppm

^{13}C C1 149.11; C2 129.35; C3 141.10; C6 167.50 ppm

Step 2 : 2,6-pyridinedicarboxylic acid → 2,6-dimethylpyridinedicarboxylate

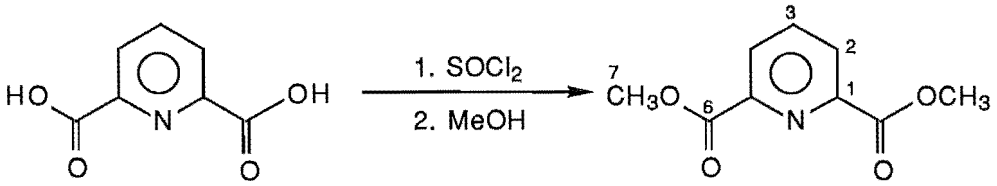

This esterification was performed according to the method of Cram and co-workers.[97] 2,6-Pyridinedicarboxylic acid (31 g, 0.186 mol) was refluxed in 200ml of thionyl chloride ($SOCl_2$) for 10 hr. Most of the $SOCl_2$ was then removed by evaporation under reduced pressure leaving a colourless liquid (2,6-pyridinedicarboxylic acid chloride) which solidified when cooled in an ice bath. Methanol (250 ml), which had been dried over Na_2SO_4 for a week, was added dropwise to the cooled solid and the resulting solution was refluxed for 30 min. This was followed by the removal of 150 ml of methanol under reduced pressure, initiating precipitation which was completed by cooling in an ice bath. The white, crystalline 2,6-dimethylpyridinedicarboxylate (34.44 g,0.18 mol, 95%) was filtered off, washed with a small amount of ice-cold methanol, and dried *in vacuo*.

Infrared spectrum *inter alia* 1720(s,b), 1550(m) cm^{-1}

Melting point 122-124°C

NMR spectra ($CDCl_3$) :

^{1}H H2 8.33(d); H3 8.06(t); H7 4.04(s) ppm

^{13}C C1 148.04; C2 127.86; C3 138.24; C6 164.85; C7 53.00 ppm

Step 3 : 2,6-dimethylpyridinedicarboxylate → 2,6-diacetylpyridine (DAP)

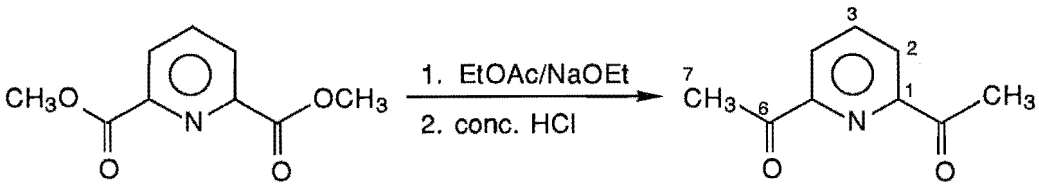

This step is a modification of the Claisen condensation method used by Lukes and Pergál.[98] Sodium ethoxide (made from 8 g, 0.35 mol sodium and dried *in vacuo*) was placed in a 1 l round-bottomed flask and xylene (50 ml), 2,6-dimethylpyridinedicarboxylate (19.67 g, 0.100 mol), and ethyl acetate (32.5 g, 0.37 mol) were added. A yellow colour developed upon mixing these components. A further 110 ml of xylene was added and the creamy yellow suspension refluxed on an oil bath at 140-150°C for 19 hr. This high temperature appeared to be important as

the yield dropped if lower temperatures were employed. The resulting thick suspension was cooled and ketonic fission initiated by the slow addition of distilled water (75 ml) followed by conc. HCl (140 ml). Refluxing for 30 min at 150°C completed the reaction. The xylene/water azeotrope was then distilled off over *ca.* 2 hr using a Dean-Stark collector to return the aqueous phase to the reaction vessel. Once all of the xylene was removed the golden aqueous phase was allowed to cool slowly over *ca.* 2 hr to room temperature. Neutralisation, by slow addition of solid $NaHCO_3$, was followed by addition of 100 ml of diethylether and filtration to remove a small amount of solid material which would have prevented the use of a separating funnel. The aqueous phase was extracted a further four times with 4 x 100 ml of diethylether. Evaporation of the ethereal extracts yielded off-white needles of DAP (11.78 g, 0.072 mol, 72%), which were used without further purification.
Infrared spectrum *inter alia* 1700(s,b), 1585(m) cm^{-1}
Melting point 79-80°C
NMR spectra ($CDCl_3$) :
^1H H2 8.22(d); H3 8.01(m); H7 2.80(s) ppm
^{13}C C1 152.59; C2 124.60; C3 137.85; C6 199.21; C7 25.41 ppm

Preparation of 2,5-Diformylpyrrole (DFP)

The four step method described by Miller *et al*[99] was used to transform pyrrole into 2,5-diformylpyrrole (DFP) in 38% overall yield. The reaction sequence is described below.

Step 1: pyrrole → pyrrole-2-carboxaldehyde

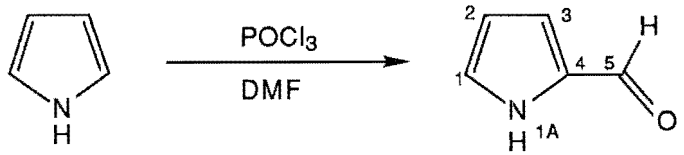

This Vilsmeir formylation was performed according to the method of Silverstein *et al.*[100] Dimethylformamide, (36 g, 0.50 mol) maintained at 10-20°C, was mechanically stirred while phosphorous oxychloride (76 g, 0.50 mol) was added over *ca.* 15 min. Discolouration occurred if this exothermic reaction was not cooled. When the addition was complete the mixture was stirred at room temperature for a further 15 min. The ice bath was replaced and 1,2-dichloroethane (112 ml) added. Once the temperature had dropped to 5°C a solution of pyrrole (30 g, 0.45 mol) in 1,2-dichloroethane (112 ml) was added to the stirred, cooled mixture over 1 hr. The mixture was then refluxed for 15 min (HCl evolved). After cooling to 25-30°C, sodium acetate (336 g, 2.46 mol) in 490 ml of H_2O was added, cautiously at first, then as quickly as possible. The two phases were stirred vigorously and refluxed for

15 min. After cooling, the 1,2-dichloroethane layer was separated from the aqueous phase which was then extracted with 3 x 230 ml of diethylether. Saturated aqueous sodium carbonate solution(45 ml) was added carefully (CO_2 evolved) to the combined 1,2-dichloroethane and diethylether solutions. The organic phase was separated, washed twice more as before, and finally left to dry over anhydrous Na_2CO_3 overnight. The solvents were removed under reduced pressure and the resulting oil cooled in an ice bath and scratched to initiate crystallisation of the golden-brown pyrrole-2-carboxaldehyde (28.76 g, 0.41 mol, 92%).
NMR spectrum ($CDCl_3$) recorded on a Varian T60 NMR spectrometer:
^1H H1 7.2(m); H2 6.4(m); H3 7.0(m); H5 9.5(s) ppm

Step 2: pyrrole-2-carboxaldehyde → ethyl α-cyano-2-pyrrole-acrylate

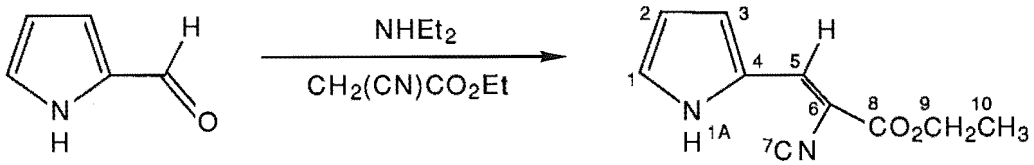

Before the second formylation (Step 3) can be performed the first aldehyde group must be protected. Here the method of Olsson and Pernemalm[101] was employed. A solution of pyrrole-2-carboxaldehyde (63 g, 0.66 mol), ethyl cyanoacetate (106.1 g, 0.93 mol) and diethylamine (4.7 g, 0.07 mol) in 830 ml of toluene was refluxed for an hour using a Dean-Stark water separator. After cooling, ethyl α-cyano-2-pyrroleacrylate (92 g, 0.48 mol, 73%), a tan powder, was filtered off, washed with 50-70 petroleum ether and air dried.
Infrared spectrum *inter alia* 3320(s), 2220(m), 1690(s,b), 1580(s,b) cm^{-1}
NMR spectra ($CDCl_3$):
^1H H1A 9.92(b); H1 6.95(s); H2 6.43(m); H3 7.25(m); H5 8.02(s); H9 4.34(q); H10 1.37(t) ppm
^{13}C C1 124.25; C2 112.41; C3 128.43; C4 126.70; C5 142.51; C6 91.73; C7 118.40; C8 163.46; C9 61.99; C10 14.20 ppm

Step 3: ethyl α-cyano-2-pyrroleacrylate → ethyl α-cyano-5-formyl-2-pyrroleacrylate

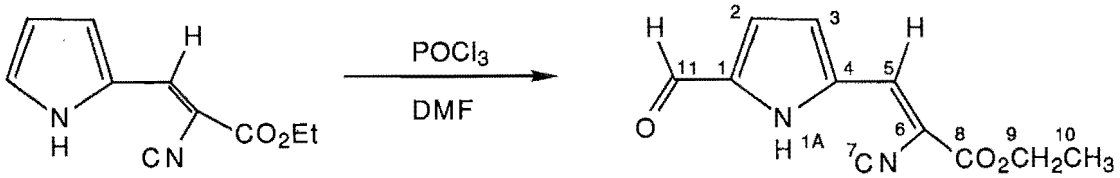

This formylation was basically a repeat of Step 1.[99] Dimethylformamide (34.1 g, 0.46 mol) and phosphorous oxychloride (70.8 g, 0.46 mol) were combined as in Step 1, stirred a further 15 min without cooling, and then 1,2-dichloroethane

(215 ml) was added. A suspension of ethyl α-cyano-2-pyrroleacrylate (72.7 g, 0.38 mol) in 320 ml of 1,2-dichloroethane was added over 30 min to the stirred solution at *ca.* 5°C. The resulting suspension was refluxed for 15 min (HCl evolved) and cooled to 25-30°C. Aqueous 4 M sodium acetate (590 ml, 2.36 mol) was added over *ca.* 5 min to the vigorously stirred mixture which was then refluxed for another 15 min. The resulting brown emulsion was left overnight and the brown ethyl α-cyano-5-formyl-2-pyrroleacrylate was collected by filtration the following day. Yield 57 g, 0.29 mol, 76%.

Infrared spectrum *inter alia* 3320(s), 2230(w), 1695(s), 1675(s), 1610(s) cm^{-1}

NMR spectrum ($CDCl_3$):

^1H H1A 10.37(b); H2 7.07(m); H3 7.22(m); H5 8.16(s); H9 4.41(q); H10 1.40(t); H11 9.73(s) ppm

^{13}C C2, C3 120.19, 121.04; C5 141.94; C9 62.98; C10 14.17; C11 180.03 ppm

Step 4: ethyl α-cyano-5-formyl-2-pyrroleacrylate → 2,5-diformylpyrrole (DFP)

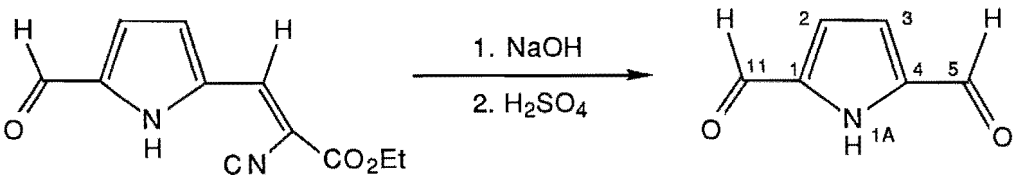

In this final step the protecting group was removed as described by Miller *et al.*[99] Ethyl α-cyano-5-formyl-2-pyrroleacrylate (42.5 g, 0.21 mol) was refluxed in 3 M aqueous sodium hydroxide (780 ml) for 2 hr. The brown solution was allowed to cool to below 20°C and then slowly acidified with *ca.* 2 M sulphuric acid to pH 4.5. Extraction with 650 + 130 ml of ethyl acetate gave an orange solution with a small amount of brown-black material floating on top which was removed by decantation. The ethyl acetate was evaporated under reduced pressure to leave orange-brown 2,5-diformylpyrrole (19.4 g, 0.16 g, 75%). Purification by decolourising with charcoal followed by recrystallisation from toluene was preferred to sublimation *in vacuo*.

Infrared spectrum *inter alia* 3190(s,b), 1660(s,b) cm^{-1}

NMR spectra ($CDCl_3$):

^1H H1A 10.5(b); H2 7.03 (d); H5 9.81(s) ppm

^{13}C C1 135.70; C2 119.47; C5 181.36 ppm

Preparation of 2,5-Diformylfuran (DFF)

Initially DFF was synthesised according to the methods of Haworth *et al*[102] and Papadopoulos *et al*,[103] in two steps from sucrose in 25-35% yield as outlined below. Later 2,5-furandimethanol was purchased and oxidised as in Step 2 in 91% yield.

Step 1: sucrose → 5-hydroxymethylfurfuraldehyde

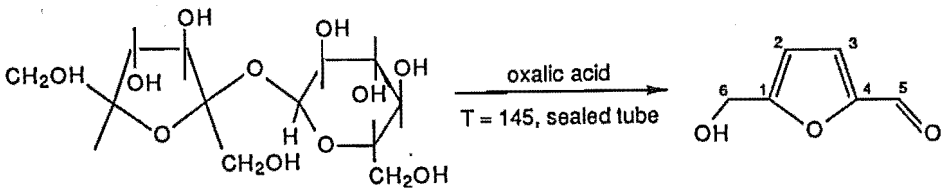

The method of Haworth and Jones[102] was modified slightly due to the unavailability of an autoclave. Sucrose (200 g, 0.58 mol) and oxalic acid (1.4 g, 0.02 mol) were dissolved in 600 ml of water. Glass tubes were half filled with this solution, sealed, and placed in an oven at 145°C. This temperature was maintained for 25 min, allowed to drop to 125°C over the next *ca.* 40 min, and maintained at 125°C for a further 2 hr. Once cool, the solution was neutralised with calcium carbonate. Lead acetate (10 g, 0.03 mol) was then added and the solution stirred for an hour before filtering through celite. The brownish filtrate was extracted into ethyl acetate over several days using a liquid-liquid extractor. The ethyl acetate solvent was removed from this extract by evaporation under reduced pressure yielding a brown oil, 5-hydroxymethylfurfuraldehyde. Yields were variable due to the lack of accurate control over temperature and pressure but were in the range 35-50%.
Infrared spectrum inter alia 3380(s,b), 1660(s,b) cm-1
NMR spectrum ($CDCl_3$) recorded on a Varian T60 NMR spectrometer:
^1H H2 6.6(d); H3 7.3(d); H5 9.6(s); H6 4.8(s) ppm

Step 2: 5-hydroxymethylfurfuraldehyde → 2,5-diformylfuran (DFF)

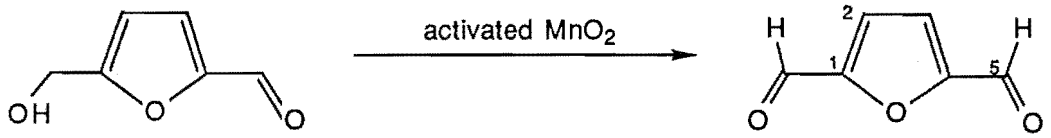

This oxidation was performed by the method of Papadopoulos *et al.*[103] Activated manganese dioxide was prepared by a modification of the method published by Mancera *et al.*[104] In a 5 l conical flask *ca.* 200 g of manganese(II) sulphate was dissolved in 250 ml of boiling water. A cold saturated solution of $KMnO_4$ (*ca.* 180 g in 5 l) was added dropwise to the boiling solution over 4-5 hr. The resulting black suspension was filtered off and washed thoroughly (stirred in a large beaker) with *ca.* 4 l of boiling water. The MnO_2 was filtered off again and dried at 110-120°C for 48 hr. Yield *ca.* 200 g. To a mechanically stirred suspension of freshly prepared manganese dioxide (90 g, 1.05 mol) in 1.5 l of chloroform was added 5-hydroxymethylfurfuraldehyde (17 g, 0.13 mol). The mixture was stirred

under reflux for 5 hr before filtering. The MnO_2 cake was washed with 5 x 300 ml of diethylether. The bright yellow combined filtrate and washings (stains hands) were evaporated to dryness under reduced pressure to give 2,5-diformylfuran (14.4 g, 0.12 mol, 89%) as a fluffy yellow solid. This product was recrystallised from 60:40 petroleum ether:benzene.

Infrared spectrum *inter alia* 1680(s) cm^{-1}

NMR spectra ($CDCl_3$):

^1H H2 7.34(s); H5 9.87(s) ppm

^{13}C C1 154.09; C2 119.10; C5 178.99 ppm

Preparation of 1,5-Diaminopentan-3-ol Dihydrochloride

1,5-diaminopentan-3-ol was prepared in 16% overall yield from 3-chloropropionyl chloride in four steps by the methods of Owen *et al*[105] and Murase *et al.*.[106]

Step 1: 3-chloropropionyl chloride → 1,5-dichloropentan-3-one

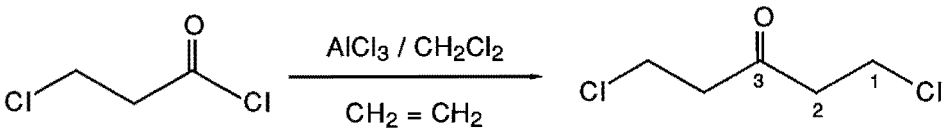

This Friedel-Crafts alkylation was carried out as reported by Owen *et al.*[105] 3-Chloropropionyl chloride (100 g, 0.79 g) was added slowly to a mechanically stirred, cooled (ice bath) suspension of dry $AlCl_3$ (147 g, 1.10 mol) in 110 ml of dichloromethane (which had been dried over molecular sieves); HCl was evolved during the addition. The solution was then allowed to warm to room temperature and ethylene gas (dried over KOH and $CaSO_4$) was bubbled through for *ca.* 5 hr. The dark brown solution was then tested for starting material by taking about 0.1 ml, treating it with about 0.1 ml of water, separating the CH_2Cl_2 layer, and after evaporating the CH_2Cl_2, examining the infrared spectrum of the remaining oil. An absorption at 1715 cm^{-1} showed that product had formed, while the disappearance of the initial carbonyl band at 1790 cm^{-1} indicated that the reaction had gone to completion. The reaction vessel was stoppered and the solution left to stir overnight. The resulting solution was added cautiously to a mixture of dichloromethane (100 ml), conc. HCl (40 ml) and ice (400 ml aqueous layer) in a high sided beaker, maintaining the temperature below 20°C. The organic phase was separated, washed with 3 x 400 ml of water, and dried over $MgSO_4$ for two hours. Evaporation of the dichloromethane under reduced pressure left 1,5-dichloropentan-3-one as a brown oil (67 g, 0.43 mol, 55%).

Step 2: 1,5-dichloropentan-3-one → 1,5-diphthalimidopentan-3-one

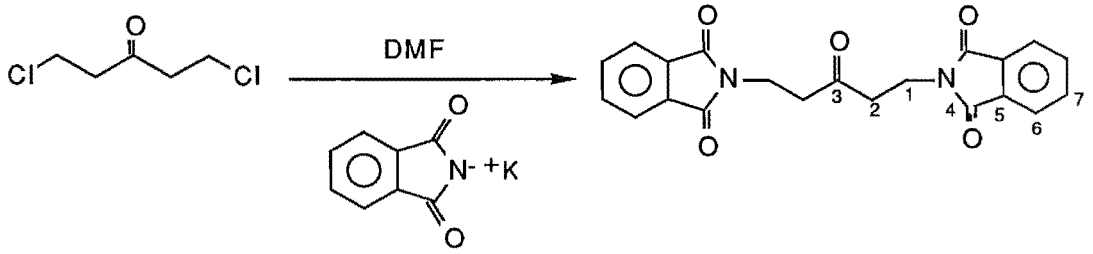

In this step phthalimide groups were substituted for chloride by the method of Murase *et al.*[106] To a vigorously stirred suspension of potassium phthalimide (103.3 g, 0.56 mol) in dimethylformamide (363 ml, dried over molecular sieves), crude 1,5-dichloropentan-3-one (67 g, 0.43 mol) was added dropwise over one hour. During the addition the suspension warmed up and changed colour from white to brown. The resulting mixture was heated at 80-85°C for 6 hr and allowed to stand at room temperature overnight. The 1,5-diphthalimidopentan-3-one was then collected by filtration and successive washings with chloroform, water and acetone resulted in a white product. Yield 78.4 g, 0.21 mol, 48%.

Infrared spectrum *inter alia* 1770(s), 1710(s,b) cm^{-1}

NMR spectrum (DMF):

^{13}C C1 33.37; C2 40.87; C3 206.92; C4 168.51; C5 132.73; C6 123.55; C7 134.97 ppm

Step 3: 1,5-diphthalimidopentan-3-one → 1,5-diaminopentan-3-one dihydrochloride

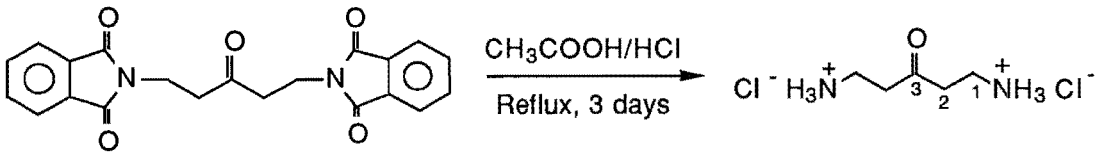

The harsh reaction conditions outlined by Murase *et al*[106] were used to break open the five-membered phthalimide ring thus releasing phthalic acid and 1,5-diaminopentan-3-one dihydrochloride. 1,5-Diphthalimidopentan-3-one (70 g, 0.19 mol) was boiled in a mixture of acetic acid (175 ml) and conc. HCl (113 ml), with an additional 63 ml of conc. HCl added in ten approximately evenly spaced aliquots over 3 days. On cooling, the fawn precipitate of phthalic acid was filtered off and washed with water. The combined filtrate and washings were evaporated nearly to dryness under reduced pressure, *ca.* 400 ml of water was added and the undissolved material filtered off. Again the solution was concentrated to approximately 50 ml, then *ca.* 700 ml of ethanol was added and the resulting white solid (1,5-diamino-pentan-3-one dihydrochloride, 41.5 g, 0.22 mol, 117% - contaminated with phthalic acid) was collected by filtration.

Infrared spectrum *inter alia* 3030(s,b), 1715(s), 1590(s), 1570(s) cm^{-1}

NMR spectra (D_2O):

^1H H1 3.14(t); H2 2.91(t) ppm

^{13}C C1 39.52; C2 34.94; C3 209.29 ppm

Step 4: 1,5-diaminopentan-3-one dihydrochloride → 1,5-diaminopentan-3-ol dihydrochloride

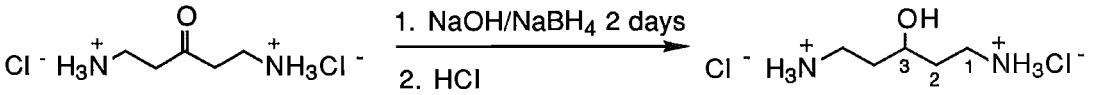

Reduction of the carbonyl function to an alcohol group was carried out by the method of Murase *et al.*[106] A solution of NaOH (17.64 g, 0.44 mol) and sodium borohydride (8.3 g, 0.22 mol) in 310 ml of water was maintained below 20°C while crude 1,5-diaminopentan-3-one dihydrochloride (41.5 g, 0.22 mol) was added in several portions. The resulting mixture was stirred at room temperature for 48 hr. Dilute HCl was added slowly and carefully to the cold solution until the pH was *ca.* 1. The solution appeared black during this neutralisation step but reverted to colourless on standing. After evaporating the solution to dryness under reduced pressure, excess boric acid was removed as its methyl ester by adding methanol to the remaining white solid followed by evaporation of the ester. The addition of methanol and evaporation under reduced pressure were repeated three times. A further 100 ml of methanol was added to the final residue, the mixture refluxed for 30 min, cooled, and filtered to remove NaCl. After concentrating the filtrate to approximately 90 ml, diethylether (450 ml) was added resulting in immediate separation of a white oil. Refrigeration overnight at *ca.* 4°C was followed by collection of the white powder, 1,5-diaminopentan-3-ol dihydrochloride (21 g, 0.11 mol, 51%), by filtration.

Infrared spectrum *inter alia* 3380(s,b), 3030(s,b), 1600(s), 1570(s) cm^{-1}

NMR spectra (CD_3OD):

^1H H1A,H1B 3.09(m); H2A, H2B 1.84(m); H3 3.86(m) ppm

^{13}C C1 68.58; C2 35.66; C3 38.60 ppm

Preparation of Complexes of H_2L1 and H_4L1'

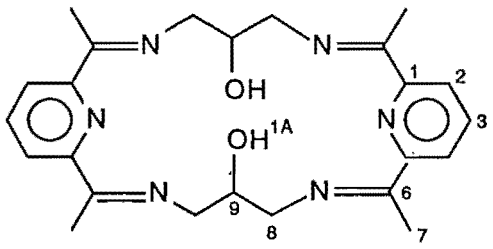

H_2L1

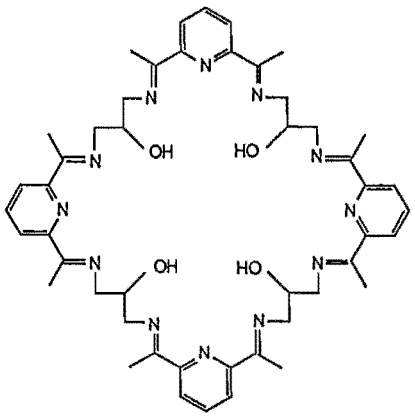

H_4L1'

$[Ba(H_2L1)(H_2O)_2](ClO_4)_2$

DAP (4.08 g, 25 mmol) and barium perchlorate (5.86 g, 15 mmol) were dissolved in methanol (200 ml) and heated to reflux. 1,3-Diamino-2-hydroxy-propane (2.25 g, 25 mmol) in methanol (20 ml) was added and the refluxing continued for 2.5 hr. The solution was evaporated under reduced pressure to a volume of about 100 ml and allowed to stand at room temperature for several hours before the white product was filtered off. Further crops were obtained after more solvent was evaporated.[80,86] Yield 7.6 g, 9.4 mmol, 75%.

Infrared spectrum *inter alia* 3400 (s,b), 1650 (m), 1590 (m), 1100 (s,b) cm^{-1}

^{252}Cf PDMS $[Ba(H_2L1)(ClO_4)]^+$ m/e = 671 a.m.u.

NMR spectra ($(D_3C)_2SO$):

^1H H2 7.78(d); H3 7.97(t); H7 2.328(s); H8 3.907(dd); H9 4.53(b); H1A 6.69(b) ppm.

^{13}C C1 165.83; C2 124.11; C3 139.87; C6 155.20; C7 16.24; C8 57.62; C9 68.77 ppm.

These assignments were confirmed by ^1H-^{13}C heteronuclear two-dimensional correlation spectroscopy.

$[Mn_2(HL1)(Cl)_2]_2(ClO_4)_2.2DMF.H_2O$

$MnCl_2.4H_2O$ (1 g, 5.1 mmol) in 50 ml of methanol was added to a refluxing methanolic (300 ml) suspension of $[Ba(H_2L1)(H_2O)_2](ClO_4)_2$ (2 g, 2.4 mmol), and refluxing continued for 2 hr. The orange product was collected by filtration of the cooled solution. Yield 1.17 g, 0.82 mmol, 68%. Crystallisation by diethylether diffusion into a DMF solution yielded crystals suitable for a single crystal X-ray structure determination.

Infrared spectrum *inter alia* 3430(m,b), 1645(m), 1590(m), 1095(s) cm^{-1}

Analysis Calculated for $[Mn_2(HL1)(Cl)_2]_2(ClO_4)_2(H_2O)_2$:
C 39.4; H 4.2; N 11.5%
Found: C 39.3; H 4.2; N 11.6%

$[Mn_2(HL1)(N_3)_2]_2(ClO_4)_2.3MeCN$

$[Ba(H_2L1)(H_2O)_2](ClO_4)_2$ (2 g, 2.4 mmol) was suspended in 600 ml of methanol and brought to reflux. $Mn(ClO_4)_2.6H_2O$ (1.80 g, 5 mmol, in 50 ml of methanol) was added, followed quickly by NaN_3 (1.30 g, 20 mmol, in 50 ml of methanol). The clear orange solution was refluxed for 3 hr over which time an orange solid began to precipitate. After cooling, the product was collected by filtration. Yield 1.3 g, 0.89 mmol, 75%. Crystals were obtained by vapour diffusion of diethylether into MeCN or DMF solutions; a crystal of $[Mn_2(HL1)(N_3)_2]_2(ClO_4)_2.3MeCN$ suitable for a single crystal X-ray structure determination was chosen from the former solvent.
Infrared spectrum *inter alia* 3410(m,b), 2045(s), 1645(m), 1590(m), 1090(s) cm^{-1}.
Analysis Calculated for $[Mn_2(HL1)(N_3)_2]_2(ClO_4)_2.DMF$:
C 40.1; H 4.3; N 22.9%
Found: C 38.8-39.8; H 4.1-4.9; N 21.1-22.0%

$[Mn_4(HL1)(L1)(NCS)_4]NCS.2H_2O$

$[Ba(H_2L1)(H_2O)_2](ClO_4)_2$ (2 g, 2.4 mmol) was suspended in refluxing methanol (200 ml). $Mn(ClO_4)_2.6H_2O$ (1.80 g, 5 mmol) in methanol (60 ml) was added, followed quickly by NaNCS (1.62 g, 20 mmol) in methanol (100 ml). The resulting orange solution was refluxed overnight, during which time an orange crystalline solid precipitated. More product precipitated as a powder on cooling. The precipitates were collected by filtration.[62(b)] Yield 0.86 g, 0.6 mmol, 50%. Crystals suitable for a single crystal X-ray structure determination were grown by slow evaporation of an acetonitrile:ethanol (5:1) solution containing NaNCS.
Infrared spectrum *inter alia* 3470(s,b), 2085(s), 2065(s), 2045(s), 2025(s), 1650(m), 1595(m) cm^{-1}
^{252}Cf PDMS $[Mn_4(L1)_2(NCS)_3]^+$ m/e = 1259 a.m.u.
Analysis Calculated: C 45.0; H 4.3; N 16.8%
Found: C 44.8; H 4.2; N 16.3%

$[Mn_2(L1)(HCOO)]_2(ClO_4)_2.2DMF.H_2O$

A suspension of $Mn(HCOO)_2.2H_2O$ (0.56 g, 3.1 mmol) in 40 ml of methanol was added to a refluxing methanol (150 ml) solution of $[Ba(H_2L1)(H_2O)_2](ClO_4)_2$ (1g, 1.2 mmol). The resulting cloudy orange solution was refluxed a further 3 hr then filtered hot to remove the white precipitate of $Ba(HCOO)_2$. The pinkish-orange powder which precipitated was collected by filtration the following day. Yield 0.4 g,

0.27 mmol, 44% (contaminated with further $Ba(HCOO)_2$). Crystals of $[Mn_2(L1)(HCOO)]_2(ClO_4)_2.2DMF.H_2O$ were grown by repeated recrystallisation from DMF by vapour diffusion of diethylether.
Infrared spectrum *inter alia* 3450(m,b), 1645(m), 1595(s,b), 1380(m), 1360(m), 1090(s,b) cm^{-1}

$[Mn_2(L1)(CH_3COO)]_2(ClO_4)_2.2DMF.5H_2O$

Manganese acetate (0.88 g, 3.6 mmol) dissolved in methanol (20 ml) was added to a refluxing methanol suspension (*ca.* 50 ml) of $[Ba(H_2L1)(H_2O)_2](ClO_4)_2$ (2 g, 2.5 mmol), and refluxing of the resulting thick orange suspension continued for 2 hr. After cooling, the orange powder was collected by filtration. Yield 1.15 g, 0.8 mmol, 66%. Crystallisation from DMF by vapour diffusion of diethylether gave crystals suitable for an X-ray structure determination.
Infrared spectrum *inter alia* 3450(b), 1660(m), 1560(m,b), 1100(s,b) cm^{-1}.

$[Mn_4(L1')(H_2O)_{1.6}(DMF)_3(ClO_4)_2](ClO_4)_2$

Crystals of this compound were obtained by recrystallising crude $[Mn_4(L1')](ClO_4)_4.2H_2O$ (Figure 19)[62] from DMF by vapour diffusion of diethylether.
Infrared spectrum *inter alia* 3400(w,b), 1650(m), 1585(m), 1085(s) cm^{-1}

$[Mn_5(L1)_2(CH_3COO)_2X_2]^{y+}$ series of complexes

$Ba(H_2L1)(H_2O)_2](ClO_4)_2$ (1 g, 1.2 mmol) was dissolved in 50 ml of refluxing methanol and $Mn(CH_3COO)_2.4H_2O$ (0.76 g, 3.1 mmol in 20 ml of methanol) was added causing an immediate deep orange colouration. The clear solution was refluxed for 1 hr and cooled slowly, allowing orange crystals to form. These crystals were unsuitable for single crystal X-ray structural analysis but recrystallisation from MeCN by vapour diffusion of diethylether gave good quality crystals of $[Mn_5(L1)_2(CH_3COO)_2(ClO_4)_2](ClO_4)_2.2H_2O$. Crystals of $[Mn_5(L1)_2(CH_3COO)_2(DMF)_2](ClO_4)_4.2DMF$ were obtained from DMF by vapour diffusion of diethylether. Crystals of $[Mn_5(L1)_2(CH_3COO)_2(H_2O)_4(ClO_4)_2](ClO_4)_2.6MeCN$ were obtained by vapour diffusion of diethylether into a slightly wet acetonitrile solution.
Infrared spectrum *inter alia* 3450(m,b), 1645(m), 1580(s,b), 1090(s,b) cm^{-1}

Preparation of Complexes of H_2L4

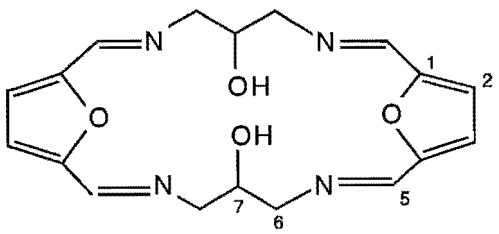

H_2L4

[Ba(H_2L4)(ClO_4)$_2$]

The preparation of this complex has been described by Fenton and co-workers[80] but attempts to repeat this procedure were unsuccessful. Instead the reaction was carried out at room temperature. Barium perchlorate (0.40g, 1 mmol) dissolved in ethanol (20 ml) was poured into a stirred gold coloured ethanolic solution (25 ml) of DFF (0.25 g, 2 mmol). 1,3-Diamino-2-hydroxypropane (0.18 g, 2 mmol) in ethanol (25 ml) was added dropwise causing the clear solution to become cloudy. After stirring at room temperature for 3 hr the thick cream precipitate was collected by filtration and dried *in vacuo*. Chunky colourless crystals grew in the filtrate. Yield 0.50 g, 0.72 mmol, 72%.

Infrared spectrum *inter alia* 3450(s,b), 1630(s), 1100(s,b) cm^{-1}

NMR spectra (CD_3CN):

^1H H2 6.79(s); H5 8.04(d); H6A, H6B 3.70(d), 4.08(ddd); H7 4.50(t) ppm

^{13}C C1 153.89; C2 116.91; C5 151.31; C6 64.61; C7 69.86 ppm

These assignments were confirmed by ^1H-^{13}C heteronuclear two-dimensional correlation spectroscopy.

Preparation of Complexes of DAP and H_2L5

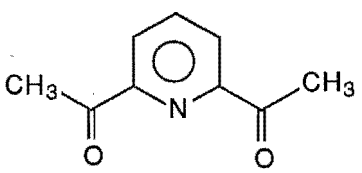

DAP

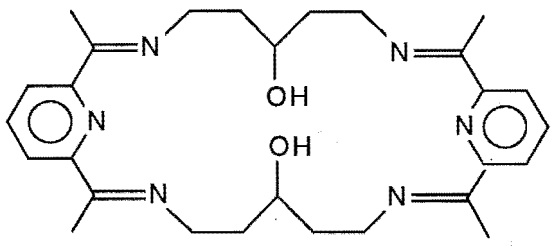

H_2L5

[Mn(DAP)$_2$(H_2O)$_2$](ClO_4)$_2$

1,5-diaminopentan-3-ol dihydrochloride (0.5 g, 2.6 mmol) in *ca.* 20 ml of methanol was added to a refluxing methanol solution (*ca.* 100 ml) of DAP (0.69 g, 4.2 mmol) and $Mn(ClO_4)_2$. $6H_2O$ (1.54 g, 4.3 mmol). The resulting yellowish

solution was refluxed 21 hr. On slow evaporation of the reaction solvent yellowish crystals suitable for an X-ray structure analysis grew. Yield 0.4 g, 0.65 mmol, 31%. Infrared spectrum *inter alia* 3430 (s,b), 1705 (s), 1680 (s), 1590 (m), 1100 (s,b)cm^{-1}

$[Pb_2(H_2L5)(NCS)_3]NCS$

This complex was prepared from $Pb_2(H_2L5)(OH)(ClO_4)_3$ which was made by the method of Fenton and co-workers.[80] DAP (0.65 g, 4 mmol) and lead perchlorate (1.84 g, 4 mmol) were dissolved in refluxing dry ethanol (50 ml). 1,5-Diamino-pentan-3-ol dihydrochloride (0.76 g, 4 mmol) was dissolved in a minimum volume of mixed 1:1 dry methanol:dry ethanol solvent, KOH (0.45 g, 8 mmol) in mixed alcohol solvent was added, and the KCl precipitate filtered off. The resulting 1,5-diamino-pentan-3-ol (4 mmol) solution was added to the refluxing Pb^{2+}/DAP solution causing an immediate white precipitate. The mixture was refluxed for 3 hr, cooled, and the fawn precipitate collected by filtration and dried *in vacuo*. The filtrate was concentrated to *ca.* 10 ml and a further crop collected. These crops were identified as $Pb_2(H_2L5)(OH)(ClO_4)_3$ by comparison of the infrared spectra with that reported by Fenton and co-workers. Yield 2.18 g, 1.8 mmol, 89%.
Infrared spectrum *inter alia* 3420(m,b), 1650(m), 1590(m), 1085(s,b) cm^{-1}

A suspension of $Pb_2(H_2L5)(OH)(ClO_4)_3$ (0.4 g, 0.33 mmol) and NaNCS (0.44 g, 5.43 mmol) in 125 ml of dry methanol was refluxed for two weeks, then filtered whilst still at reflux temperature. As the filtrate cooled slowly the product crystallised as small pale yellow blocks suitable for single crystal X-ray structural analysis. The yield (0.025 g, 0.002 mmol, 0.6%) was low as most of the starting material did not dissolve and was recovered before crystallisation.
Infrared spectrum *inter alia* 3450(b), 2083(s)†, 2060(s)†, 1983(s)†, 1650(m), 1595(m) cm^{-1}

† Measured on a Digilab FTS-7 Fourier Transform infrared spectrometer with a TGS detector

Preparation of Complexes of L13

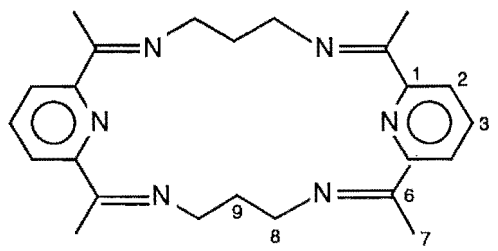

L13

[Ba(L13)](ClO$_4$)$_2$

Barium perchlorate (5.86 g, 15 mmol) dissolved in 100 ml of methanol was added to a methanol solution (90 ml) of DAP (4.08 g, 25 mmol), and the resulting solution brought to reflux. 1,3-Diaminopropane (2.25 g, 30 mmol) in 30 ml of methanol was added, the brownish solution refluxed for 1 hr and filtered hot to remove a small amount of undissolved material. White needles were filtered from the cold solution and further crops were obtained on reducing the volume of the solvent to *ca.* 40 ml and allowing to stand.[107] Yield 5.33 g, 7.2 mmol, 58%.
Infrared spectrum *inter alia* 3440 (w,b), 1640 (m), 1590 (m), 1100 (s,b).
NMR spectra (CD_3CN):

^{1}H H2 7.99(d); H3 8.18(t); H7 2.46(s);
H8 3.84(t); H9 2.33(m) ppm

^{13}C C1 170.59; C2 125.97; C3 141.25;
C6 156.88; C7 51.07; C8 29.37;
C9 17.26 ppm

These assignments were confirmed using ^{1}H-^{13}C heteronuclear two-dimensional correlation spectroscopy.

[Mn^{II}Mn^{III}(L13)(O)(OH)(DMF)]$_2$(ClO$_4$)$_4$.2H$_2$O

Mn(CH_3COO)$_2$.4H$_2$O (0.67g, 2.7 mmol) freshly dissolved in methanol (20 ml) was added to an oxygenated refluxing methanol (130 ml) suspension of [Ba(L13)](ClO$_4$)$_2$ (1g, 1.35 mmol), causing an immediate deep orange colour to develop. The resulting clear orange solution was refluxed for 7 hr with oxygen bubbling through it for the first 3.5 hr. After only 30 min the solution was brown in colour. A very small amount of material was removed by filtration of the hot solution and slow evaporation allowed a brown solid to precipitate. Yield 0.59g, 0.35 mmol, 54%. Production of single crystals suitable for X-ray structure analysis proved to be very difficult. Poor quality brown crystals were obtained on two occasions by vapour diffusion of diethylether into DMF solutions of the complex.
Infrared spectrum *inter alia* 3420 (m,b), 1650 (m,b), 1590 (w), 1090 (s,b) cm^{-1}

Crystallography

General Data

Crystals suitable for single crystal X-ray structural analysis were obtained as described in the Experimental Section. X-ray crystallographic data were collected on a Nicolet R3m four-circle diffractometer using graphite-monochromated Mo-K$_\alpha$ radiation (λ=0.71069). The cell parameters were determined by least squares refinement of 16 to 24 accurately centered reflections in the range $5 < 2\theta < 36$ °. The crystals generally lost solvate molecules on isolation from the mother liquor and

rapidly (5 min) crumbled to powder. Therefore crystals suitable for X-ray crystallography were coated with a hydrocarbon oil immediately on isolation and rapidly transferred into the low temperature gas stream of the diffractometer. The crystal stability was monitored by recording three check reflections every 97 reflections and no significant variations were observed for any data sets. The data sets were corrected for Lorentz and polarisation effects, and unless otherwise stated, an empirical absorption correction was applied, based on ψ-scan data. Hydrogen atoms were inserted at calculated positions using a riding model with thermal parameters equal to 1.2U of their carrier atoms unless otherwise stated. The function minimised in the refinement was $\Sigma w(|F_o| - |F_c|)^2$ where $w = [\sigma^2 (F_o) + gF_o^2]^{-1}$. Final atom coordinates and numbering schemes are given in Appendix A, and tables of selected interatomic distances and angles are given in Section 2.2. All programs used in data reduction and final refinement were contained in the SHELXTL (version 4.0) package.[108] SHELXTL or SHELXS[109] programs were employed to solve the structures, and in some cases the intermediate refinement was performed using SHELX76.[110]

$[Mn_2(HL1)(Cl)_2]_2(ClO_4)_2.2DMF.H_2O$

$C_{54}H_{74}Cl_6Mn_4N_{14}O_{15}$, regular golden-yellow block, crystal dimensions 0.25 x 0.25 x 0.34 mm^3, orthorhombic, a = 14.776(4), b = 21.358(5), c = 22.784(5) Å, U = 7190(3)Å^3, space group Pbcn , Z = 4, F(000) = 3272. Using 1.4° ω-scans at a scan rate of 6° min^{-1} , and a background to scan ratio of 0.5, 6969 reflections were collected with $4 < 2\theta < 50°$, index range: h 0/18, k 0/26, l 0/28, at 173K. Of these, 6329 were unique, and the 2671 having $I > 3\sigma(I)$ were used in the structural analysis. The data were corrected for extinction effects.

A Patterson calculation[108] revealed the position of the manganese atoms and the remaining non-hydrogen atoms were located from difference Fourier maps. Hydrogen atoms were not inserted on the two quarter occupancy water molecules, O80 and O90. Anisotropic thermal parameters were assigned to all non-hydrogen atoms except O80 and O90, and the refinement on 423 least-squares parameters converged with R = 0.0706, wR = 0.1044, g=0.003788 and a maximum least-squares shift/error of 0.052. The final difference map showed no features greater than $\pm$ 1.12 eÅ^{-3}.

$[Mn_2(HL1)(N_3)_2]_2(ClO_4)_2.3MeCN$

$C_{54}H_{67}Cl_2Mn_4N_{27}O_{12}$, regular orange block, crystal dimensions 0.20 x 0.32 x 0.34 mm^3, triclinic, a = 13.891(3), b = 15.369(3), c = 16.190(3) Å, α = 87.60(2)°, β = 82.18(2)°, γ = 85.20(2)°, U = 3411(1) Å^3, space group $P\bar{1}$, Z = 2, F(000) = 1615. Using 1.6° ω-scans at a scan rate of 4.88° min^{-1} , and a background to scan ratio of 0.1, 10471 reflections were collected with $4 < 2\theta < 47$ °, index

range: h 0/16, k -18/18, l -19/19, at 138 K. Of these, 9988 were unique, and the 6990 having I >3 σ (I) were ultimately used in the structure refinement. The data were corrected for extinction effects.

Direct methods[108] revealed the position of the four manganese atoms, the four alkoxide oxygens, and the bridging atoms N20 and N30. The remaining non-hydrogen atoms were located from difference Fourier maps. Hydrogen atoms were not inserted on the half occupancy acetonitrile molecules, C82 and C92. Anisotropic thermal parameters were assigned to all non-hydrogen atoms, except the two half occupancy acetonitrile molecules, and the refinement on 890 least-squares parameters converged with R = 0.0667, wR = 0.0927, g = 0.000549 and a maximum least-squares shift/error of 0.11. The final difference map showed no features greater than ± 1.5 eÅ^{-3}.

[Mn_4(HL1)(L1)$(NCS)_4$]NCS

$C_{53}H_{57}Mn_4N_{17}O_4S_5$, yellow, crystal dimensions 0.15 x 0.19 x 0.35 mm^3, monoclinic, *a* = 44.193(10), *b* = 13.082(4), *c* = 22.621(4) Å, β = 105.73(2)°, U = 12588(5)Å^3, space group C2/c , Z = 8, F(000) = 5647. Using 2° ω-scans at a variable scan rate of 3-29° min^{-1} , and a background to scan ratio of 0.5, 8991 reflections were collected with 3 < 2θ < 45 °, index range: h -48/48, k 0/15, l 0/25, at 130K. Of these, 8144 were unique, and the 3435 having I >3 σ (I) were ultimately used in the structure refinement.

The structure was solved by direct methods[108] and the remaining non-hydrogen atoms were located from difference Fourier maps. The hydrogen atom (H1) on the hydrogen bond between O1 and O3 was located from difference Fourier maps and not further refined. Anisotropic thermal parameters were assigned to all manganese, oxygen and sulphur atoms, and the refinement on 398 least-squares parameters converged with R = 0.074, wR = 0.094, g = 0.0013 and a maximum least-squares shift/error of 0.04. The final difference map showed no features greater than ± 1.3 eÅ^{-3} .

[Mn_2(L1)(HCOO)]$_2$(ClO_4)$_2$.2DMF.H_2O

$C_{56}H_{72}Cl_2Mn_4N_{14}O_{19}$, orange block, crystal dimensions 0.10 x 0.17 x 0.25 mm^3, monoclinic, *a* = 27.057(8), *b* = 14.793(5), *c* = 16.126(4) Å, β = 97.56(2)°, U = 6398(3) Å^3, space group C2/c , Z = 4, F(000) = 3175. Using 1.4° ω-scans at a scan rate of 3.66° min^{-1} , and a background to scan ratio of 0.1, 4470 reflections were collected with 4 < 2θ < 45 °, index range: h 0/30, k 0/16, l -18/18, at 170K. Of these, 4180 were unique, and the 1971 having I >3 σ (I) were ultimately used in the structure refinement.

Direct methods[108] revealed the structure and the remaining non-hydrogen atoms were located from difference Fourier maps. Hydrogen atoms were not

inserted on the half occupancy water molecule, O50. Anisotropic thermal parameters were assigned to all non-hydrogen atoms except the pyridine ring carbons and O50, and the refinement on 396 least-squares parameters converged with R = 0.0527, wR = 0.0485, g = 0.000188 and a maximum least-squares shift/error of 0.07. The final difference map showed no features greater than $\pm$ 0.4 eÅ^{-3} .

$[Mn_2(L1)(CH_3COO)]_2(ClO_4)_2.2DMF.5H_2O$

$C_{58}H_{84}Cl_2Mn_4N_{14}O_{23}$, orange, crystal dimensions 0.06 x 0.64 x 0.74 mm^3, monoclinic, *a* = 32.026(7), *b* = 14.623(6), *c* = 16.464(5) Å, β = 118.11(2)°, U = 6801(4) Å^3, space group C2/c , Z = 4, F(000) = 3391. Using 1.4° ω-scans at a scan rate of 4.88° min^{-1} , and a background to scan ratio of 0.5, 6351 reflections were collected with 4 < 2θ < 50 °, index range: h 0/39, k 0/18, l -20/20, at 173K. Of these, 5569 were unique, and the 3696 having I >3 σ (I) were ultimately used in the structure refinement. An empirical absorption correction was applied, based on ψ-scan data and face indexing.

Direct methods[108] revealed the structure and the remaining atoms were located from difference Fourier maps. Hydrogen atoms were not inserted on the half occupancy water molecule, O70. Hydrogen atoms on O50 (H50B) and O60 (H60B) were fixed to lie on the hydrogen bond interactions between O40 and O50, and O40 and O60 respectively. Anisotropic thermal parameters were assigned to all non-hydrogen atoms except the DMF molecule and O70, and the refinement on 430 least-squares parameters converged with R = 0.0683, wR = 0.0932, g = 0.001266 and a maximum least-squares shift/error of 0.1. The final difference map showed no features greater than $\pm$ 1.3 eÅ^{-3} .

$[Mn_4(L1')(H_2O)_{1.6}(DMF)_3(ClO_4)_2](ClO_4)_2$

$C_{57}H_{77}Cl_4Mn_4N_{15}O_{24.6}$, well formed orange block, crystal dimensions 0.40 x 0.44 x 0.56 mm^3, monoclinic, *a* = 28.049(9), *b* = 14.127(4), *c* = 20.473(4) Å, U = 7779(4)Å^3, space group C2/c , Z = 4, F(000) = 3779. Using 1.4° ω-scans at a scan rate of 4.88° min^{-1} , and a background to scan ratio of 0.1, 6500 reflections were collected with 4 < 2θ < 48°, index range: h 0/33, k 0/17, l -24/24, at 170K. Of these, 6091 were unique, and the 3709 having I >3 σ (I) were used in the structural analysis. A numerical absorption correction was applied, based on face indexing.

Previous Mn_4L1' structural coordinates (same space group) were used as a starting point for the refinement and the remaining non-hydrogen atoms were located from difference Fourier maps. Hydrogen atoms were not inserted on the three partial occupancy DMF molecules, O50-C52 (0.2 occupancy), O40-C42 (0.5 occupancy) and O30-C32 (0.8 occupancy). Atom O50 of the 0.2 occupancy DMF molecule coincides with a 0.8 occupancy H_2O molecule. The O50-C50 bond was constrained to be trigonal planar and *ca.* 1.15Å long. Anisotropic thermal parameters were

assigned to all non-hydrogen atoms except the three DMF molecules, and the refinement on 423 least-squares parameters converged with R = 0.0706, wR = 0.1044, g = 0.003788 and a maximum least-squares shift/error of 0.052 . The final difference map showed no features greater than ± 1.12 eÅ^{-3} .

$[Mn_5L1_2(CH_3COO)_2(ClO_4)_2]\ (ClO_4)_2\ .2H_2O$

$C_{52}H_{67}Cl_4Mn_5N_{12}O_{26}$, orange, crystal dimensions 0.25 x 0.31 x 0.34 mm^3, monoclinic, *a* = 13.032(4), *b* = 20.677(5), *c* = 14.113(5) Å, β = 108.13(2)°, U = 3614(2) Å^3, space group $P2_1/c$, Z = 2, F(000) = 1728. Using 2° ω-scans at a scan rate of 5.4° min^{-1} , and a background to scan ratio of 0.5, 5124 reflections were collected with 4 < 2θ < 45 °, index range: h 0/15, k 0/23, l -16/16, at 153K . Of these, 4720 were unique, and the 2788 having I >3 σ (I) were ultimately used in the structure refinement. The data were corrected for extinction effects.

Direct methods[108] revealed the position of the three manganese atoms and the remaining non-hydrogen atoms were located from difference Fourier maps. Hydrogen atoms were not inserted on the two half occupancy water molecules, O60 and O70. Anisotropic thermal parameters were assigned to all non-hydrogen atoms except O60 and O70, and the refinement on 448 least-squares parameters converged with R = 0.0816, wR = 0.1245, g = 0.006384 and a maximum least-squares shift/error of 0.2 . The final difference map showed no features greater than ± 1.2 eÅ^{-3} .

$[Mn_5(L1)_2(CH_3COO)_2(H_2O)_4(ClO_4)_2](ClO_4)_2.6MeCN$

$C_{64}H_{88}Cl_4Mn_5N_{18}O_{28}$, well formed orange block, crystal dimensions 0.16 x 0.25 x 0.66 mm^3, triclinic, *a* = 11.504(6), *b* = 13.860(7), *c* = 13.892(8) Å, α = 82.61(4), β = 80.46(4), γ = 72.41(4)°, U = 2075(2) Å^3, space group $P\bar{1}$, Z = 1, F(000) = 1015. Using 2° ω-scans at a scan rate of 5.33° min^{-1} , and a background to scan ratio of 0.3, 5739 reflections were collected with 4 < 2θ < 45 °, index range: h 0/13, k -15/15, l -15/15, at 150K. Of these, 5413 were unique, and the 3505 having I >3 σ (I) were ultimately used in the structure refinement.

A Patterson calculation and partial structure expansion[109] revealed the structure and the remaining non-hydrogen atoms were located from difference Fourier maps. Anisotropic thermal parameters were assigned to all non-hydrogen atoms except the pyridinediimine carbon atoms, and the refinement on 468 least-squares parameters converged with R = 0.0536, wR = 0.0627, g = 0.00062 and a maximum least-squares shift/error of 0.05. The final difference map showed no features greater than ± 0.6eÅ^{-3} .

$[Mn_5(L1)_2(CH_3COO)_2(DMF)_2](ClO_4)_4.2DMF$

$C_{64}H_{90}Cl_4Mn_5N_{16}O_{28}$, well formed orange block, crystal dimensions 0.20 x 0.20 x 0.48 mm^3, triclinic, a = 10.750(5), b = 13.826(6), c = 15.953(17) Å, α = 86.52(7), β = 70.58(6), γ = 85.86(4)°, U = 2229(3) $Å^3$, space group $P\bar{1}$, Z = 1, F(000) = 1003. Using 3° ω-scans at a scan rate of 8.37° min^{-1}, and a background to scan ratio of 0.3, 5936 reflections were collected with 4 < 2θ < 45 °, index range: h 0/12, k -15/15, l -18/18, at 170K. Of these, 5804 were unique, and the 2668 having I >3 σ (I) were ultimately used in the structure refinement.

The structure was revealed by direct methods[109] and the remaining non-hydrogen atoms were located from difference Fourier maps. Two DMF molecules, O60 to C62 and O70 to C72, were half occupancy, and the temperature factor of N70 was fixed to be 0.02. Anisotropic thermal parameters were assigned to the two full occupancy manganese atoms (Mn1 and Mn2) and the two chlorine atoms of the perchlorate groups, and the refinement on 273 least-squares parameters converged with R = 0.1036, wR = 0.1308, g = 0.00340 and a maximum least-squares shift/error of 0.008. The final difference map showed no features greater than ± 1.9e$Å^{-3}$.

$[Mn(DAP)_2(H_2O)_2](ClO_4)_2$

$C_{18}H_{22}Cl_2Mn_1N_2O_{14}$, colourless block, crystal dimensions 0.47 x 0.78 x 0.88 mm^3, orthorhombic, a = 7.663(1), b = 9.221(1), c = 36.087(7) Å, U = 2549.9(7) $Å^3$, space group $P2_12_12_1$, Z = 4, F(000) = 1260. Using 1.6° ω-scans at a scan rate of 3.91° min^{-1}, and a background to scan ratio of 0.1, 2625 reflections were collected with 3 < 2θ < 50°, index range: h 0/10, k 0/11, l 0/43, at room temperature. Of these, 2599 were unique, and the 2000 having I >3 σ (I) were ultimately used in the structure refinement.

Direct methods[108] revealed the position of the manganese atom and the remaining non-hydrogen atoms were located from difference Fourier maps. Anisotropic thermal parameters were assigned to all non-hydrogen atoms, and the refinement on 334 least-squares parameters converged with R = 0.0691, wR = 0.1009, g = 0.00140 and a maximum least-squares shift/error of 0.3. The final difference map showed no features greater than ± 0.8e $Å^{-3}$.

$[Pb_2(H_2L5)(NCS)_3]NCS$

$C_{32}H_{38}N_{10}O_2Pb_2S_4$, irregular pale yellow block, crystal dimensions 0.16 x 0.18 x 0.20 mm^3, monoclinic, a = 11.947(3), b = 15.232(5), c = 21.392(5) Å, β = 96.14(2)°, U = 3870(2) $Å^3$, space group C2/c, Z = 4, F(000) = 2175. Using 1.6° ω-scans at a scan rate of 3.66° min^{-1}, and a background to scan ratio of 0.1, 2782 reflections were collected with 4 < 2θ < 45°, index range: h 0/13, k 0/17, l -24/24, at 170K. Of these, 2534 were unique, and the 1712 having I >3 σ (I) were ultimately used in the structure refinement.

A Patterson calculation[108] revealed the position of the lead atom and the remaining non-hydrogen atoms were located from difference Fourier maps. The fourth anion appeared to be very disordered and was not inserted, hence the final difference map shows some regions of substantial electron density. For further discussion of this point see Results and Discussion, Section 2.2. Anisotropic thermal parameters were assigned to the lead atom, terminally bound thiocyanate group (S31-C31-N31) and the macrocyclic nitrogen and oxygen atoms, and the refinement on 139 least-squares parameters converged with R = 0.0658, wR = 0.1063, g = 0.00407 and a maximum least-squares shift/error of 0.01. The final difference map showed no features greater than $\pm$ 8.2e $Å^{-3}$.

$[Mn^{II}Mn^{III}(L13)(O)(OH)(DMF)]_2(ClO_4)_4.2H_2O$

$C_{52}H_{78}Cl_4Mn_4N_{78}O_{14}$, brown block, crystal dimensions 0.18 x 0.22 x 0.41 mm^3, triclinic, *a* = 12.310(6), *b* = 13.266(9), *c* = 14.369(7) Å, α = 89.30(5), β = 74.02(4), γ = 70.26(4)°, U = 2115(2) $Å^3$, space group $P\bar{1}$, Z = 1, F(000) = 848. Using 2.1° ω-scans at a scan rate of 6° min^{-1} , and a background to scan ratio of 0.1, 3946 reflections were collected with 4 < 2θ < 40°, index range: h 0/12, k -13/13, l -14/14, at 140K. Of these, 3946 were unique, and the 1105 having I >3σ (I) were ultimately used in the structure refinement.

A Patterson calculation[108] revealed the position of the manganese atoms and the remaining non-hydrogen atoms were located from difference Fourier maps. The quality of this data collection did not warrant the insertion of hydrogen atoms; a recollection of the data on a better crystal is required. Anisotropic thermal parameters were assigned to the two manganese atoms and the two chlorine atoms of the perchlorate group, and the refinement on 221 least-squares parameters converged with R = 0.1468, wR = 0.1865, g = 0.0006 (not refined) and a maximum least-squares shift/error of 0.54. The final difference map showed no features greater than $\pm$ 1.5e $Å^{-3}$.

2.2 Results and Discussion

The ligands shown in Figure 37 have been investigated.

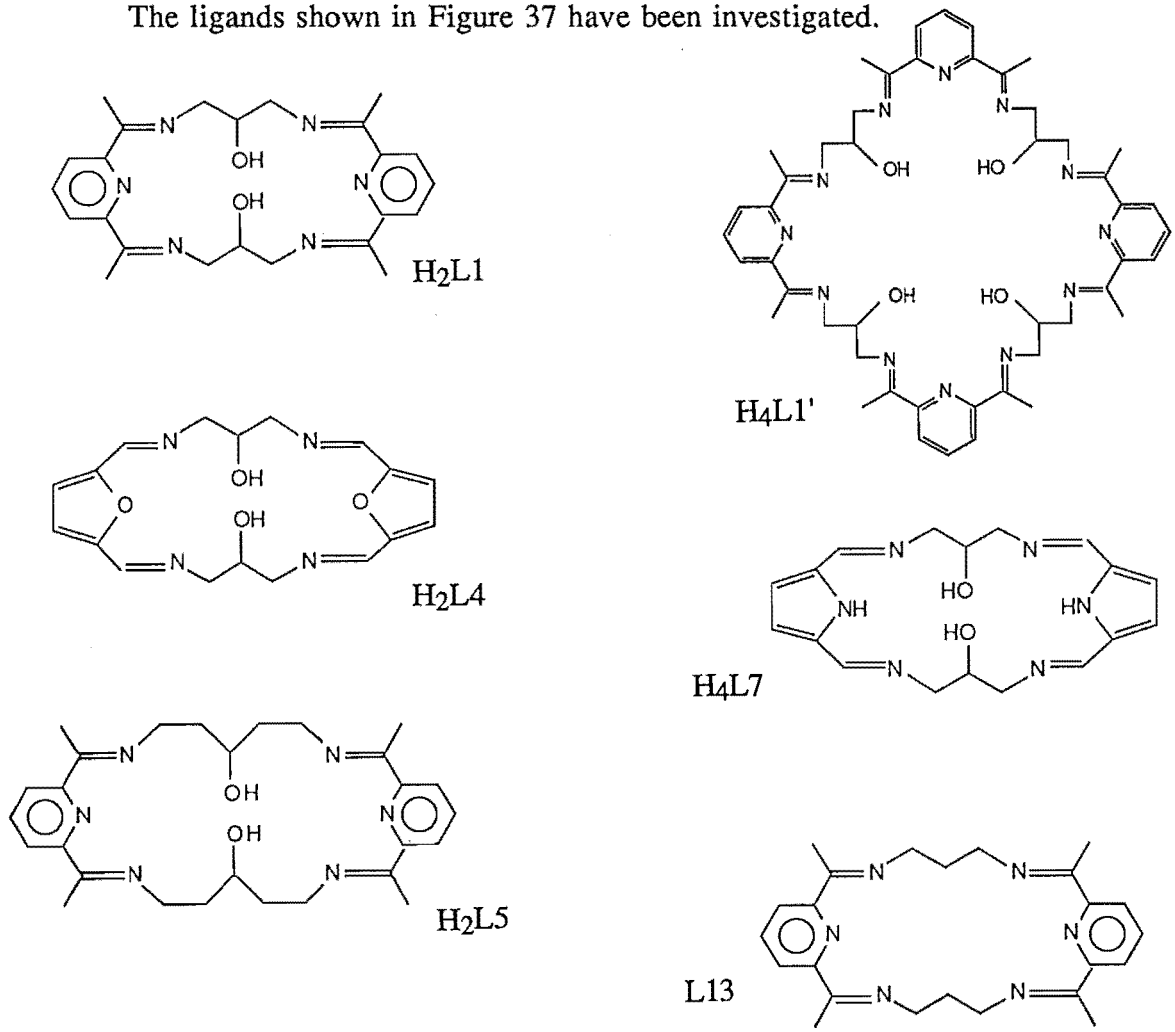

Figure 37: The ligands investigated in this work.

These ligands meet the OEC modelling requirements of nitrogen and/or oxygen donors. Variation in the nature of the nitrogen donor atoms is provided by the pyrrole-containing macrocycle H_4L7, and likewise a variation in the oxygen donor properties by the furan-containing macrocycle H_2L4. No oxygen donors are provided by macrocycle L13. The 20- and 24-membered macrocycles H_2L1, H_2L4, H_2L5, H_4 L7 and L13 are large enough to bind two transition metal atoms,[81,86,87,93,107,111] although H_2L7' (H_4L7 without the alcohol functions) has been found to bind only one copper(II) ion.[112] All of these ligands, except L13, provide alcohol oxygen atoms which can either twist away,[86,87] or bridge the bound metal ions as is proposed in many metalloproteins, including the OEC (Figures 9, 10).

These macrocycles have the ability to bind two or more transition metal ions and, except for L13, to provide bridges between them. This results in interactions between the metal ions which can be investigated by EPR and magnetic susceptibility studies. The Schiff-base macrocyclic chemistry involved in the ring expansion (2+2) to (4+4), that is H_2L1 to H_4L1', has also been investigated.

No transition metal complexes of H_2L4 or H_4L7 have been characterised to date. However, the barium complex of H_2L4 was prepared in good yield towards the end of this work, and attempts to characterise manganese complexes can now be undertaken. Difficulty was experienced with the pyrrole-containing macrocycle although the metal-free and template syntheses of this ligand had been reported previously by Fenton.[113] The product resulting from these syntheses was very insoluble and therefore hard to characterise or react further. Attempts to produce manganese complexes of H_4L7 were unsuccessful. The chemistry of these two macrocycles will not be discussed further here.

The rich chemistry of the manganese complexes of H_2L1, H_4L1' and L13; the structural characterisation of a manganese(II) complex of DAP; and a dilead complex of H_2L5 with unusual single-atom thiocyanate bridging *via* the nitrogen atom are presented and discussed in this Section.

X-Ray Structure Determinations

Structures of the Mn(II) Complexes of H_2L1 and H_4L1'

The structures of eight manganese(II) complexes of H_2L1 and one tetramanganese(II) complex of H_4L1' have been determined and are discussed next. These complexes will be referred to by the coordinated anion name rather than the long systematic name or an uninformative code number. For example, the $[Mn_2(HL1)(Cl)_2]_2(ClO_4)_2.2DMF.H_2O$ complex will be referred to as the chloride complex. The tetramanganese complexes are discussed first, followed by the pentamanganese acetate complexes of H_2L1.

In all of the tetramanganese complexes the manganese atoms are seven-coordinate with approximate pentagonal bipyramidal geometry. The donors in the pentagonal plane are the three nitrogen atoms of the macrocyclic pyridinediimine unit and two bridging alcohol oxygens, also from the macrocycle.

When chloride or azide is present a dimer of binucleating macrocycles is formed.[114] The structures of the cations are shown in Figures 38 and 39 respectively, and selected interatomic distances and angles are given in Tables 2 and 3. The chloride complex has a C_2 axis passing through Cl(2) and Cl(3), whereas the azide complex has no crystallographically imposed symmetry. Nonetheless, the structures are quite similar, dimeric with the two macrocyclic units linked by bridging chloro or azido groups. The macrocyles are maintained in an "eclipsed" arrangement by these bridges, allowing hydrogen bonding (dotted lines Figures 38 and 39) between alkoxide and alcohol groups on adjacent monodeprotonated macrocycles; for the chloride O(1) - O(2') = 2.48(1)Å while for the azide O(1)-O(3) = 2.43(1)Å and O(2)-O(4) = 2.44(1)Å.

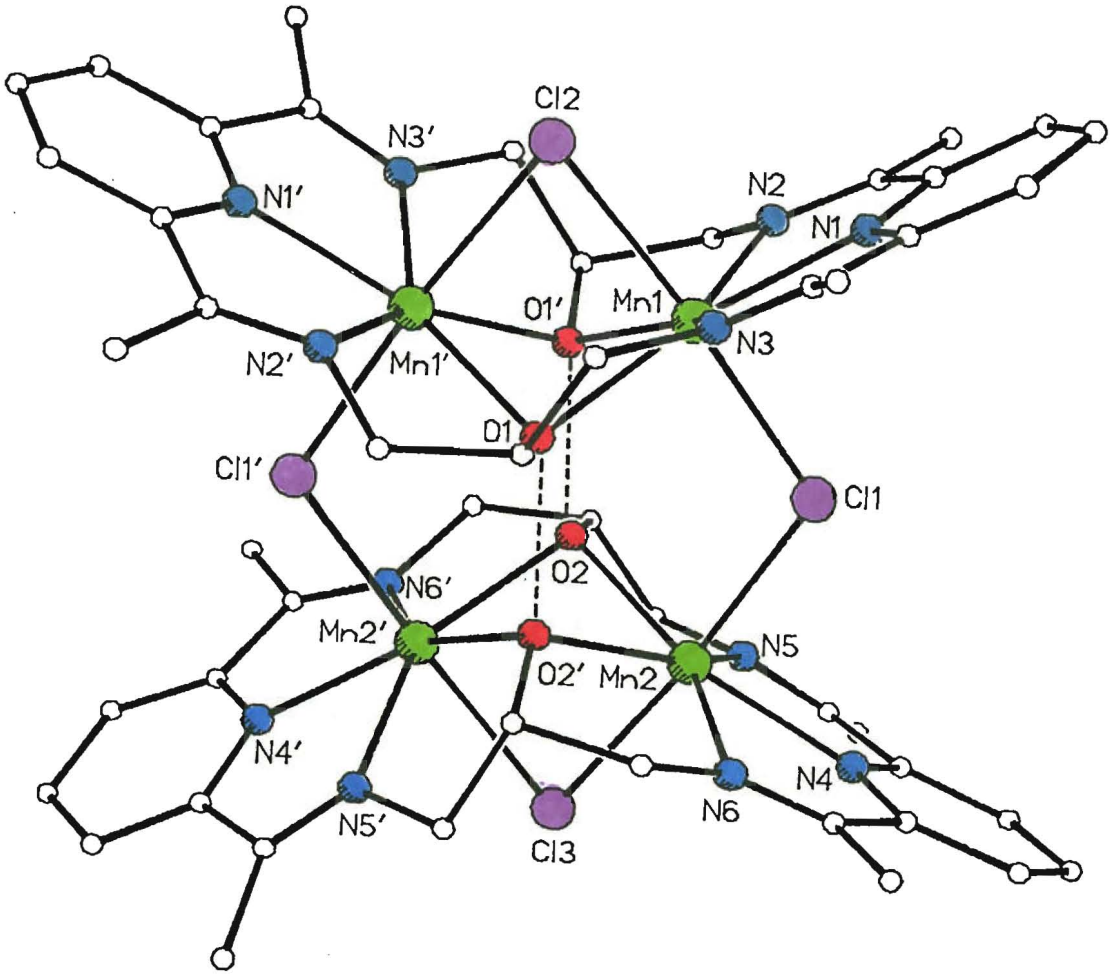

Figure 38: Perspective view of the cation $[Mn_2(HL1)(Cl)_2]_2^{2+}$, hydrogen bonds are shown as dotted lines.

Table 2: Selected interatomic distances and angles for $[Mn_2(HL1)(Cl)_2]_2(ClO_4)_2.2DMF.H_2O$

Interatomic Distances (Å)							
Mn1-N1	2.219(9)	Mn1-N2	2.279(9)	Mn1-O1	2.285(7)	Mn1-N3	2.248(8)
Mn1-Cl1	2.549(3)	Mn1-Cl2	2.611(4)	Mn1-O1'	2.269(7)	Mn2-N4	2.232(9)
Mn2-N5	2.279(9)	Mn2-O2	2.283(7)	Mn2-N6	2.298(8)	Mn2-Cl1	2.541(3)
Mn2-Cl3	2.599(4)	Mn2-O2'	2.270(7)	Mn1-Mn2	4.300(2)	Mn1-Mn1'	3.125(3)
Mn2-Mn2'	3.107(3)	O1-O2'	2.48(1)				

Bond Angles (°)					
N1-Mn1-N2	69.7(3)	N1-Mn1-O1	142.6(3)	N2-Mn1-O1	147.6(3)
N1-Mn1-N3	70.9(3)	N2-Mn1-N3	139.0(3)	O1-Mn1-N3	72.4(3)
N1-Mn1-Cl1	90.2(3)	N2-Mn1-Cl1	88.0(3)	O1-Mn1-Cl1	91.8(2)
N3-Mn1-Cl1	103.1(2)	N1-Mn1-Cl2	94.7(3)	N2-Mn1-Cl2	93.0(2)
O1-Mn1-Cl2	84.8(2)	N3-Mn1-Cl2	79.4(2)	Cl1-Mn1-Cl2	175.0(1)
N1-Mn1-O1'	143.0(3)	N2-Mn1-O1'	73.3(3)	O1-Mn1-O1'	74.3(3)
N3-Mn1-O1'	144.2(3)	Cl1-Mn1-O1'	90.4(2)	Cl2-Mn1-O1'	85.2(2)
Mn1-O1-C9	118.2(6)	Mn1-O1-Mn1'	86.7(2)	C9-O1-Mn1'	116.9(6)
N4-Mn2-N5	70.7(3)	N4-Mn2-O2	142.7(3)	N5-Mn2-O2	72.7(3)
N4-Mn2-N6	69.5(3)	N5-Mn2-N6	138.9(3)	O2-Mn2-N6	147.8(3)
N4-Mn2-Cl1	90.7(3)	N5-Mn2-Cl1	100.7(3)	O2-Mn2-Cl1	89.1(2)
N6-Mn2-Cl1	89.7(2)	N4-Mn2-Cl3	93.9(3)	N5-Mn2-Cl3	77.1(2)
O2-Mn2-Cl3	84.8(2)	N6-Mn2-Cl3	95.7(2)	Cl1-Mn2-Cl3	173.9(1)
N4-Mn2-O2'	141.9(3)	N5-Mn2-O2'	144.5(3)	O2-Mn2-O2'	75.3(3)
N6-Mn2-O2'	72.7(3)	Cl1-Mn2-O2'	93.8(2)	Cl3-Mn2-O2'	85.1(2)
Mn2-O2-C21	117.4(6)	Mn2-O2-Mn2'	86.2(2)	C21-O2-Mn2'	116.9(6)
Mn1-Cl1-Mn2	115.7(1)	Mn1-Cl2-Mn1'	73.6(1)	Mn2-Cl3-Mn2'	73.5(1)

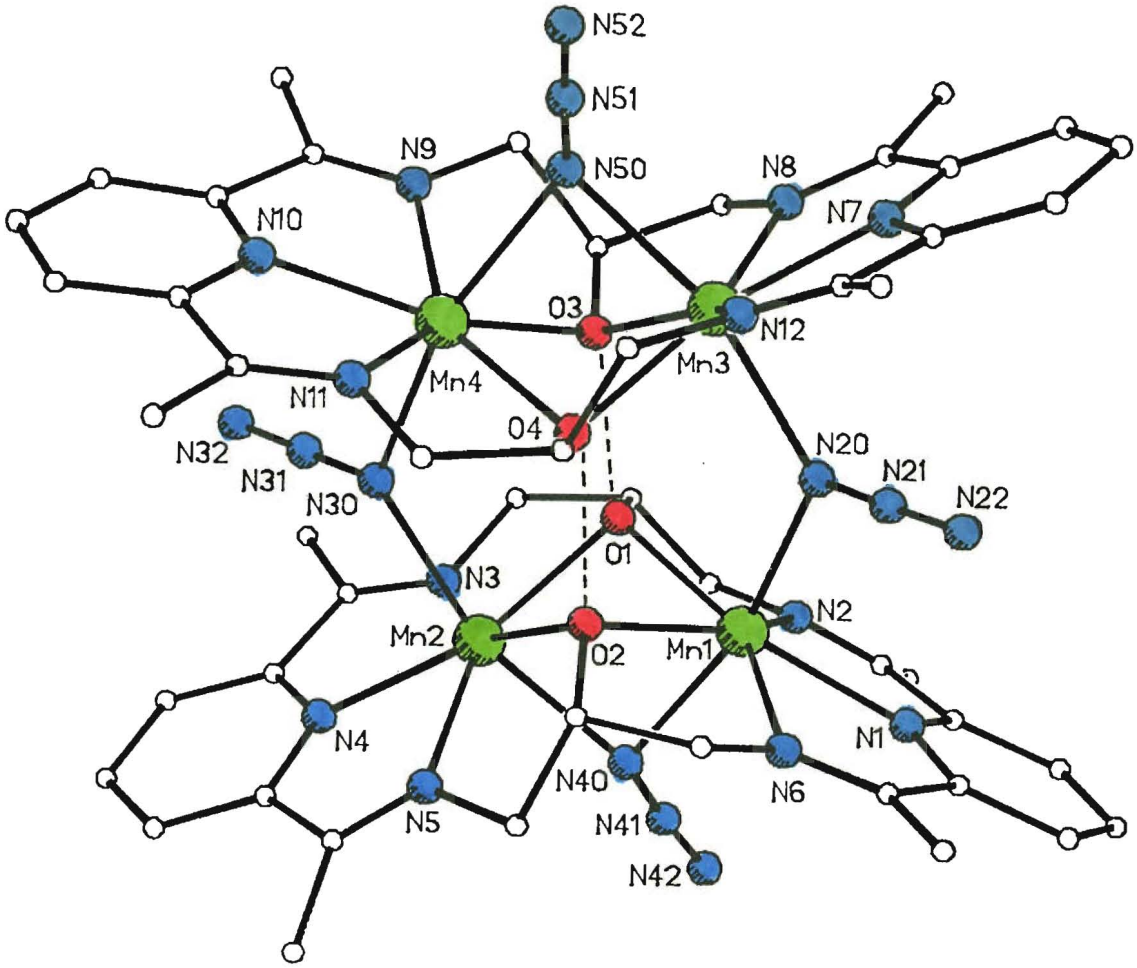

Figure 39: Perspective view of the cation $[Mn_2(HL1)(N_3)_2]_2^{2+}$, hydrogen bonds are shown as dotted lines.

In both cases the two manganese atoms within each macrocycle are also bridged by an anionic ligand and the intramolecular bridge angles are considerably smaller (chloride 73.5(1), 73.6(1)°; azide 84.7(2), 83.1(2)°) than the intermolecular equivalents (chloride 115.7(1)°; azide 126.3(2), 128.3(2)°). This is largely a consequence of the different Mn-Mn distances spanned by these bridges. Hence, all of the exogenous chloride or azide anions bridge manganese axial sites; Cl(1), N(20) and N(30) hold the dimeric structures together, while Cl(2), Cl(3), N(40) and N(50) bridge the two manganese atoms within each macrocycle. The angles made by the azide bridges are greater than the angles made by the chloride bridges because of the shorter Mn-N bond lengths which are due to the smaller radius of nitrogen *vs* chlorine. The macrocyclic rings have folded conformations. The angles between the manganese pentagonal planes within each macrocycle are 113.8° and 113.1° for the chloride and 116.1° and 122.0° for the azide. Two uncoordinated perchlorate anions are also present in each structure.

Table 3: Selected interatomic distances and angles for $[Mn_2(HL1)(N_3)_2]_2(ClO_4)_2.3MeCN$

Interatomic Distances (Å)							
Mn1-N1	2.242(6)	Mn1-N2	2.276(6)	Mn1-O1	2.246(5)	Mn1-O2	2.287(4)
Mn1-N6	2.302(6)	Mn1-N20	2.276(6)	Mn1-N40	2.301(6)	Mn2-O1	2.263(5)
Mn2-N3	2.256(6)	Mn2-N4	2.218(6)	Mn2-N5	2.261(6)	Mn2-O2	2.256(4)
Mn2-N30	2.357(6)	Mn2-N40	2.307(6)	Mn3-N50	2.332(6)	Mn3-N7	2.238(5)
Mn3-N8	2.290(6)	Mn3-O3	2.222(4)	Mn3-O4	2.282(5)	Mn3-N12	2.286(6)
Mn3-N20	2.326(6)	Mn4-N50	2.337(6)	Mn4-O3	2.276(4)	Mn4-N9	2.272(6)
Mn4-N10	2.222(5)	Mn4-N11	2.284(6)	Mn4-O4	2.201(4)	Mn4-N30	2.308(6)
Mn1-Mn2	3.103(1)	Mn1-Mn3	4.106(2)	Mn2-Mn4	4.199(2)	Mn3-Mn4	3.097(1)
Mn1-Mn4	5.172(1)	Mn2-Mn3	5.187(1)	O1-O3	2.43(1)	O2-O4	2.44(1)

Bond Angles (°)					
N1-Mn1-N2	69.9(2)	N1-Mn1-O1	142.6(2)	N2-Mn1-O1	72.8(2)
N1-Mn1-O2	140.9(2)	N2-Mn1-O2	144.5(2)	O1-Mn1-O2	75.6(2)
N1-Mn1-N6	69.6(2)	N2-Mn1-N6	137.4(2)	O1-Mn1-N6	147.3(2)
O2-Mn1-N6	71.7(2)	N1-Mn1-N20	98.1(2)	N2-Mn1-N20	109.1(2)
O1-Mn1-N20	90.4(2)	O2-Mn1-N20	86.8(2)	N6-Mn1-N20	89.3(2)
N1-Mn1-N40	96.3(2)	N2-Mn1-N40	79.8(2)	O1-Mn1-N40	80.7(2)
O2-Mn1-N40	79.5(2)	N6-Mn1-N40	91.8(2)	N20-Mn1-N40	165.1(2)
O1-Mn2-N3	72.7(2)	O1-Mn2-N4	143.5(2)	N3-Mn2-N4	70.9(2)
O1-Mn2-N5	145.7(2)	N3-Mn2-N5	139.0(2)	N4-Mn2-N5	70.2(2)
O1-Mn2-O2	75.9(2)	N3-Mn2-O2	148.2(2)	N4-Mn2-O2	139.8(2)
N5-Mn2-O2	72.6(2)	O1-Mn2-N30	85.5(2)	N3-Mn2-N30	87.1(2)
N4-Mn2-N30	89.7(2)	N5-Mn2-N30	105.2(2)	O2-Mn2-N30	85.8(2)
O1-Mn2-N40	80.2(2)	N3-Mn2-N40	99.1(2)	N4-Mn2-N40	108.4(2)
N5-Mn2-N40	81.4(2)	O2-Mn2-N40	80.0(2)	N30-Mn2-N40	161.9(2)
Mn1-O1-Mn2	87.0(2)	Mn1-O1-C9	119.3(4)	Mn2-O1-C9	115.8(4)
Mn1-O2-Mn2	86.1(1)	Mn1-O2-C21	116.0(4)	Mn2-O2-C21	118.0(4)
N7-Mn3-N8	70.2(2)	N7-Mn3-O3	142.9(2)	N8-Mn3-O3	72.7(2)
N7-Mn3-O4	140.3(2)	N8-Mn3-O4	149.4(2)	O3-Mn3-O4	76.7(2)
N7-Mn3-N12	69.6(2)	N8-Mn3-N12	137.5(2)	O3-Mn3-N12	146.1(2)
O4-Mn3-N12	72.1(2)	N7-Mn3-N20	90.0(2)	N8-Mn3-N20	94.6(2)
O3-Mn3-N20	92.1(2)	O4-Mn3-N20	86.0(2)	N12-Mn3-N20	98.7(2)
N7-Mn3-N50	104.6(2)	N8-Mn3-N50	95.7(2)	O3-Mn3-N50	79.8(2)
O4-Mn3-N50	79.2(2)	N12-Mn3-N50	81.5(2)	N20-Mn3-N50	164.4(2)
O3-Mn4-N9	72.6(2)	O3-Mn4-N10	139.5(2)	N9-Mn4-N10	69.6(2)
O3-Mn4-N11	149.6(2)	N9-Mn4-N11	137.5(2)	N10-Mn4-N11	70.3(2)
O3-Mn4-O4	77.3(2)	N9-Mn4-O4	147.3(2)	N10-Mn4-O4	142.5(2)
N11-Mn4-O4	72.4(2)	O3-Mn4-N30	84.1(2)	N9-Mn4-N30	98.1(2)
N10-Mn4-N30	87.6(2)	N11-Mn4-N30	93.5(2)	O4-Mn4-N30	91.1(2)
O3-Mn4-N50	78.6(2)	N9-Mn4-N50	81.1(2)	N10-Mn4-N50	108.5(2)
N11-Mn4-N50	99.1(2)	O4-Mn4-N50	80.7(2)	N30-Mn4-N50	162.1(2)
Mn3-O3-Mn4	87.0(2)	Mn3-O3-C33	117.6(4)	Mn4-O3-C33	117.2(4)
Mn3-O4-Mn4	87.4(2)	Mn3-O4-C45	118.1(4)	Mn4-O4-C45	118.8(4)
Mn1-N20-Mn3	126.3(2)	Mn2-N30-Mn4	128.3(2)	Mn1-N40-Mn2	84.7(2)
Mn3-N50-Mn4	83.1(2)				

The presence of thiocyanate ions also results in the formation of a dimer (Figure 40),[62(b)] the two halves of which are crystallographically independent. Selected interatomic distances and angles are given in Table 4. In this case the exogenous anion only forms intramolecular bridges, the dimer being held together by two intermolecular Mn-O bonds (Mn2-O4, Mn4-O2) and a hydrogen bond between O1 and O3 (dotted line in Figure 40). Each manganese atom has a nitrogen atom from thiocyanate as one axial donor; Mn1 and Mn2 are bridged by N80, while Mn3 and Mn4 are bridged by N50.

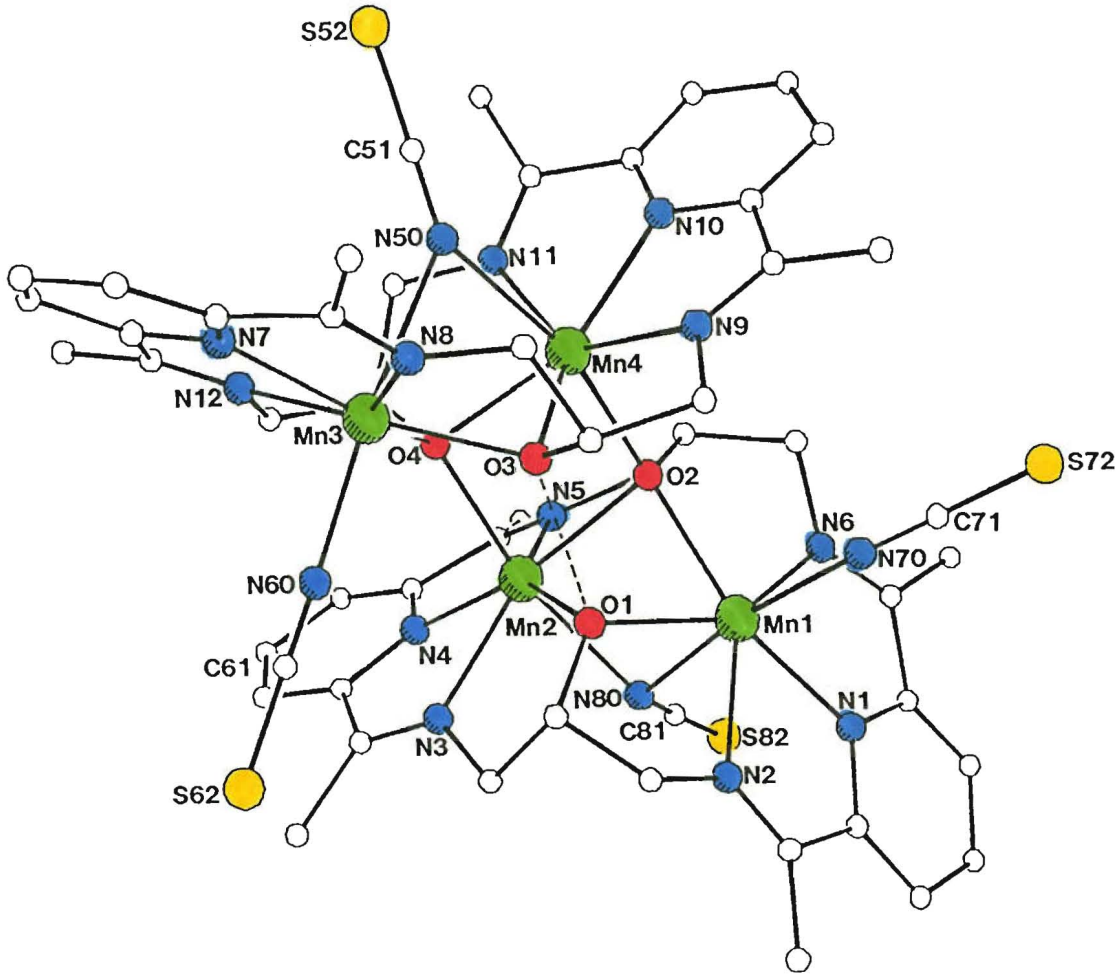

Figure 40: Perspective view of the cation $[Mn_4(HL1)(L1)(NCS)_4]^+$, the hydrogen bond is shown as a dotted line.

The axial coordination of Mn1 and Mn3 is completed by the nitrogen donor of terminally bound thiocyanate (N70 and N60 respectively). For Mn2 and Mn4 the seventh donor is an alkoxide oxygen from the adjacent macrocycle, O4 and O2 respectively. This leads to the macrocycles being in a "twisted" conformation (O4 over Mn2, Mn4 over O2, and O3 over O1) rather than the "eclipsed" conformation (Mn above Mn) adopted by the chloride and azide complexes. The alkoxide oxygen atoms O1 and O3 bridge two manganese atoms and are linked by a hydrogen bond; the hydrogen atom was located from difference Fourier maps. O2 and O4 are triply bridging, forming the corners of an incomplete Mn_4O_4 cubane. The axial sites on Mn1 and Mn3 are blocked by strongly coordinated N-terminal thiocyanate anions which prevent them from binding to O3 and O1 to complete the cubane. The macrocycles are folded such that the angle between the mean planes of Mn1, N1, N2, N6, O1, O2 and of Mn2, N3, N4, N5, O1, O2 is 104.6° and that between Mn3, N7, N8, N12, O3, O4 and of Mn4, N9, N10, N11, O3, O4 is 108.6°.

Table 4: Selected interatomic distances and angles for $[Mn_4(HL1)(L1)(NCS)_4]NCS$

Interatomic Distances (Å)							
Mn1-O1	2.244(11)	Mn1-O2	2.314(10)	Mn1-N1	2.241(12)	Mn1-N2	2.323(15)
Mn1-N6	2.264(14)	Mn1-N70	2.242(14)	Mn1-N80	2.461(12)	Mn2-O1	2.277(11)
Mn2-O2	2.247(10)	Mn2-O4	2.229(9)	Mn2-N3	2.304(14)	Mn2-N4	2.251(13)
Mn2-N5	2.288(13)	Mn2-N80	2.388(12)	Mn3-O3	2.242(10)	Mn3-O4	2.300(10)
Mn3-N7	2.277(13)	Mn3-N8	2.333(13)	Mn3-N12	2.289(13)	Mn3-N50	2.441(14)
Mn3-N60	2.163(15)	Mn4-O2	2.211(8)	Mn4-O3	2.238(11)	Mn4-O4	2.251(10)
Mn4-N9	2.304(13)	Mn4-N10	2.237(14)	Mn4-N11	2.322(14)	Mn4-N50	2.410(12)
Mn1-Mn2	3.134(5)	Mn1-Mn3	5.768(5)	Mn1-Mn4	4.077(5)	Mn2-Mn3	4.032(5)
Mn2-Mn4	3.315(5)	Mn3-Mn4	3.135(5)	O1-O3	2.42(1)		

Bond Angles (°)					
O1-Mn1-O2	73.0(4)	O1-Mn1-N1	138.3(4)	O2-Mn1-N1	140.6(4)
O1-Mn1-N2	71.3(4)	O2-Mn1-N2	143.6(4)	N1-Mn1-N2	70.0(5)
O1-Mn1-N6	146.0(4)	O2-Mn1-N6	73.9(4)	N1-Mn1-N6	69.7(5)
N2-Mn1-N6	139.6(4)	O1-Mn1-N70	110.1(4)	O2-Mn1-N70	104.0(4)
N1-Mn1-N70	87.7(5)	N2-Mn1-N70	94.5(5)	N6-Mn1-N70	85.3(5)
O1-Mn1-N80	80.8(4)	O2-Mn1-N80	81.7(4)	N1-Mn1-N80	81.9(4)
N2-Mn1-N80	86.0(4)	N6-Mn1-N80	87.0(4)	N70-Mn1-N80	168.7(4)
O1-Mn2-O2	73.7(4)	O1-Mn2-O4	94.1(3)	O2-Mn2-O4	82.9(3)
O1-Mn2-N3	72.8(4)	O2-Mn2-N3	146.0(4)	O4-Mn2-N3	104.5(4)
O1-Mn2-N4	141.3(5)	O2-Mn2-N4	144.3(5)	O4-Mn2-N4	97.7(4)
N3-Mn2-N4	68.6(5)	O1-Mn2-N5	145.0(4)	O2-Mn2-N5	75.0(4)
O4-Mn2-N5	97.2(4)	N3-Mn2-N5	134.8(4)	N4-Mn2-N5	69.5(5)
O1-Mn2-N80	81.8(4)	O2-Mn2-N80	84.8(4)	O4-Mn2-N80	167.6(4)
N3-Mn2-N80	85.5(4)	N4-Mn2-N80	92.7(4)	N5-Mn2-N80	80.2(4)
O3-Mn3-O4	74.7(4)	O3-Mn3-N7	141.0(4)	O4-Mn3-N7	141.7(4)
O3-Mn3-N8	72.2(4)	O4-Mn3-N8	142.4(4)	N7-Mn3-N8	68.8(5)
O3-Mn3-N12	148.3(4)	O4-Mn3-N12	73.6(4)	N7-Mn3-N12	69.5(5)
N8-Mn3-N12	136.8(4)	O3-Mn3-N50	79.0(4)	O4-Mn3-N50	81.6(4)
N7-Mn3-N50	91.4(4)	N8-Mn3-N50	75.2(5)	N12-Mn3-N50	94.9(5)
O3-Mn3-N60	94.1(5)	O4-Mn3-N60	102.4(4)	N7-Mn3-N60	90.3(5)
N8-Mn3-N60	97.2(5)	N12-Mn3-N60	94.0(5)	N50-Mn3-N60	170.9(5)
O2-Mn4-O3	94.1(3)	O2-Mn4-O4	83.2(3)	O3-Mn4-O4	75.7(4)
O2-Mn4-N9	94.8(4)	O3-Mn4-N9	71.5(4)	O4-Mn4-N9	146.9(5)
O2-Mn4-N10	100.5(4)	O3-Mn4-N10	139.0(4)	O4-Mn4-N10	143.7(5)
N9-Mn4-N10	69.3(5)	O2-Mn4-N11	102.5(4)	O3-Mn4-N11	142.6(4)
O4-Mn4-N11	73.3(4)	N9-Mn4-N11	138.5(5)	N10-Mn4-N11	70.6(5)
O2-Mn4-N50	166.2(4)	O3-Mn4-N50	79.8(4)	O4-Mn4-N50	83.3(4)
N9-Mn4-N50	94.9(4)	N10-Mn4-N50	92.1(4)	N11-Mn4-N50	76.3(4)
Mn1-O1-Mn2	87.8(4)	Mn3-O3-Mn4	88.8(4)	Mn1-O2-Mn4	128.6(4)
Mn2-O4-Mn4	95.4(4)	Mn1-O2-Mn2	86.8(3)	Mn2-O4-Mn3	125.8(5)
Mn2-O2-Mn4	96.1(4)	Mn3-O4-Mn4	87.1(3)		

An unusual feature of this complex is the presence of four distinctly different coordination geometries for the thiocyanate ions, in addition to the uncoordinated counter ion. One of the two terminal thiocyanate groups is bonded in approximately linear fashion [Mn3-N60-C61 173(1)°], whereas the other is distinctly bent (Mn1 - N70 - C71 = 128(1)°). A similar effect is observed for the two bridging thiocyanates; N80 - C81 - S82 is inclined at 33(1)° to the Mn1, Mn2, N80 plane but N50-C51-S52 makes an angle of only 7(1)° with the Mn3, Mn4, N50 plane. In addition, the Mn-N-C angles show wide variation; 139(1)° and 119(1)° for Mn1- and Mn2 - N80 - C81 respectively compared with 133(1)° and 145(1)° for Mn3- and

Mn4 - N50 - C51. There are no striking inter- or intramolecular interactions to account for these differences; the environments of the two terminal thiocyanates and of the two bridging groups, while not identical, show no major differences. The individual geometries can be ascribed to a number of weak interactions and to crystal packing effects. For example, S72 is *ca.* 3.8 Å from six macrocyclic ring atoms, three from the same asymmetric unit (N6, C23, C36) and three from an adjacent unit (C15, C16, and C46). Any straightening of the N70 - C71 - S72 angle is prevented by this network of interactions. There are eight other structurally characterised examples of N-bridging thiocyanate ligands.[53,111,115,116] In most cases the N-bridging thiocyanate is associated with an infrared band in the region below 2000cm^{-1} (see the Discussion of $[Pb_2(H_2L5)(NCS)_3]NCS$). The infrared spectrum (in nujol) of this complex shows four peaks due to the C-N stretch of the thiocyanates at *ca.* 2085, 2065, 2045 and 2025cm^{-1} and the band is broadened on the low energy side, but there is no distinct signal below 2000cm^{-1}. A systematic study of 1,1-NCS bridges by Nelson *et al* has shown that such blue shifts are commonly observed where μ-OR bridging is also present.[53]

Single crystal X-ray structural analysis of the formate and 4Mn acetate complexes revealed another type of dimer. These two cations are almost isostructural (Figures 41 and 42), as seen by least-squares fitting of the manganese coordination spheres. Selected interatomic distances and angles are given in Tables 5 and 6 respectively. Each half of the face-to-face dimer contains one binuclear macrocycle and an acetate (or formate) group bridging the two manganese(II) atoms. The dimer is held together by four manganese-alkoxide oxygen bonds, resulting in formation of an Mn_4O_4 cubane core similar to that observed with the (4+4) macrocycle (Figure 19A). The cation has crystallographically imposed symmetry; a C_2 axis passes through the centres of the cubane faces bounded by Mn(1), O(1), Mn(1') and O(1') and by Mn(2), O(2), Mn(2') and O(2'). Formation of the cubane requires that the two macrocycles be "staggered" with respect to each other, rather than "eclipsed" as in the chloride and azide complexes. In comparison the thiocyanate structure is twisted to an intermediate stage so that it resembles neither the chloride nor the acetate structures. Another difference between these acetate and formate structures and the previous ones is that the macrocyclic ligands are almost planar; the angle between the mean planes defined by Mn1, N1, N2, N6, O1, O2 and Mn2, N3, N4, N5, O1, O2 is 150.5° for the acetate and 148.4° for the formate. This demonstrates that the saturated section in this macrocycle is quite flexible and will adjust to suit the number and preferred geometry of coordinated metal ions. In the present case the controlling factor appears to be the axial ligation of the manganese atoms. In each case, one axial ligand is an alkoxide from the second macrocycle and the other is an oxygen atom from a bridging acetate (or formate) group. It is the former interaction which results in Mn_4O_4 cubane formation.

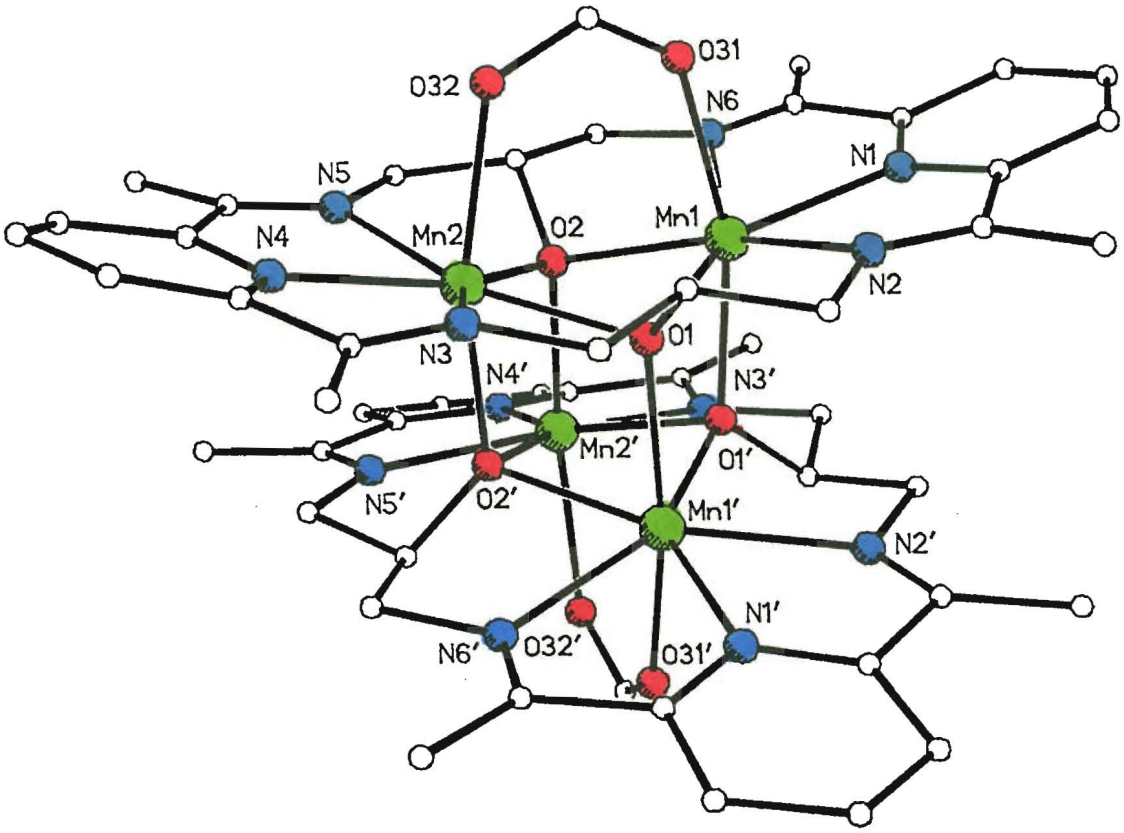

Figure 41: Perspective view of the cation $[Mn_2(L1)(HCOO)]_2^{2+}$

Table 5: Interatomic distances and angles for $[Mn_2(L1)(HCOO)]_2(ClO_4)_2.DMF.H_2O$

Interatomic Distances (Å)							
Mn1-N1	2.244(6)	Mn1-N2	2.346(7)	Mn1-O1	2.189(5)	Mn1-O2	2.196(5)
Mn1-N6	2.367(6)	Mn1-O31	2.251(6)	Mn1-O1'	2.213(5)	Mn2-O1	2.168(6)
Mn2-N3	2.351(6)	Mn2-N4	2.257(7)	Mn2-N5	2.366(7)	Mn2-O2	2.188(5)
Mn2-O32	2.254(6)	Mn2-O2'	2.231(6)	Mn1-Mn1'	3.459(2)	Mn1-Mn2	3.176(2)
Mn1-Mn2'	3.477(2)	Mn2-Mn2'	3.485(2)				

Bond Angles (°)					
N1-Mn1-N2	70.2(2)	N1-Mn1-O1	139.8(2)	N2-Mn1-O1	69.9(2)
N1-Mn1-O2	138.2(2)	N2-Mn1-O2	151.4(2)	O1-Mn1-O2	81.9(2)
N1-Mn1-N6	68.5(2)	N2-Mn1-N6	137.1(2)	O1-Mn1-N6	151.5(2)
O2-Mn1-N6	70.1(2)	N1-Mn1-O31	89.8(2)	N2-Mn1-O31	84.5(2)
O1-Mn1-O31	91.7(2)	O2-Mn1-O31	91.6(2)	N6-Mn1-O31	84.2(2)
N1-Mn1-O1'	107.1(2)	N2-Mn1-O1'	101.6(2)	O1-Mn1-O1'	76.0(2)
O2-Mn1-O1'	75.4(2)	N6-Mn1-O1'	101.0(2)	O31-Mn1-O1'	163.1(2)
O1-Mn2-N3	70.0(2)	O1-Mn2-N4	138.3(2)	N3-Mn2-N4	68.9(2)
O1-Mn2-N5	152.0(2)	N3-Mn2-N5	136.7(2)	N4-Mn2-N5	69.6(2)
O1-Mn2-O2	82.6(2)	N3-Mn2-O2	152.0(2)	N4-Mn2-O2	139.0(2)
N5-Mn2-O2	69.8(2)	O1-Mn2-O32	93.8(2)	N3-Mn2-O32	83.8(2)
N4-Mn2-O32	88.2(2)	N5-Mn2-O32	83.1(2)	O2-Mn2-O32	92.9(2)
O1-Mn2-O2'	75.6(2)	N3-Mn2-O2'	101.8(2)	N4-Mn2-O2'	106.6(2)
N5-Mn2-O2'	101.4(2)	O2-Mn2-O2'	75.7(2)	O32-Mn2-O2'	165.2(2)
Mn1-O1-Mn2	93.6(2)	Mn1-O1-C9	110.7(4)	Mn2-O1-C9	112.1(4)
Mn1-O1-Mn1'	103.6(2)	Mn2-O1-Mn1'	105.0(2)	C9-O1-Mn1'	126.7(4)
Mn1-O2-Mn2	92.8(2)	Mn1-O2-C21	111.3(4)	Mn2-O2-C21	111.6(5)
Mn1-O2-Mn2'	103.5(2)	Mn2-O2-Mn2'	104.1(2)	C21-O2-Mn2'	127.7(5)

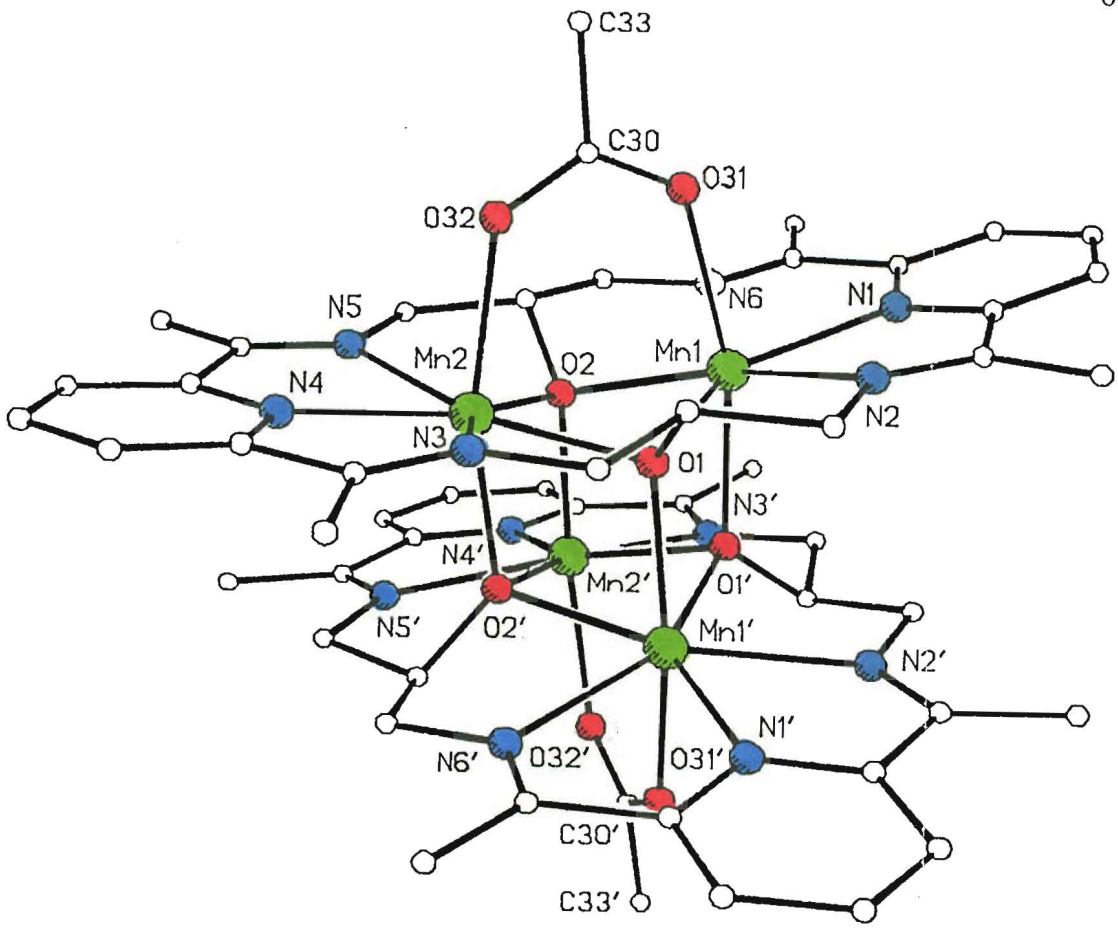

Figure 42: Perspective view of the cation $[Mn_2(L1)(CH_3COO)]_2^{2+}$

Table 6: Selected interatomic distances and angles for $[Mn_2(L1)(CH_3COO)]_2(ClO_4)_2.2DMF.5H_2O$

Bond Lengths (Å)							
Mn1-N1	2.248(5)	Mn1-N2	2.340(5)	Mn1-O1	2.180(4)	Mn1-O2	2.177(4)
Mn1-N6	2.369(5)	Mn1-O31	2.289(7)	Mn1-O1'	2.244(6)	Mn2-O1	2.165(4)
Mn2-N3	2.348(5)	Mn2-N4	2.251(5)	Mn2-N5	2.349(5)	Mn2-O2	2.188(4)
Mn2-O32	2.278(7)	Mn2-O2'	2.228(6)	Mn2-O1	2.165(4)	Mn1-Mn1'	3.491(1)
Mn1-Mn2	3.158(1)	Mn1-Mn2'	3.470(1)	Mn2-Mn2'	3.485(1)		

Bond Angles (°)					
N1-Mn1-N2	69.9(2)	N1-Mn1-O1	139.2(2)	N2-Mn1-O1	70.0(2)
N1-Mn1-O2	138.0(2)	N2-Mn1-O2	152.1(2)	O1-Mn1-O2	82.4(1)
N1-Mn1-N6	69.1(2)	N2-Mn1-N6	137.2(2)	O1-Mn1-N6	151.7(2)
O2-Mn1-N6	69.7(2)	N1-Mn1-O31	90.7(2)	N2-Mn1-O31	84.6(2)
O1-Mn1-O31	92.8(2)	O2-Mn1-O31	93.0(2)	N6-Mn1-O31	84.2(2)
N1-Mn1-O1'	104.7(2)	N2-Mn1-O1'	100.6(2)	O1-Mn1-O1'	75.6(2)
O2-Mn1-O1'	75.5(2)	N6-Mn1-O1'	101.1(2)	O31-Mn1-O1'	164.5(2)
O1-Mn2-N3	69.8(2)	O1-Mn2-N4	138.9(2)	N3-Mn2-N4	69.9(2)
O1-Mn2-N5	151.9(2)	N3-Mn2-N5	137.3(2)	N4-Mn2-N5	69.2(2)
O1-Mn2-O2	82.5(2)	N3-Mn2-O2	152.0(2)	N4-Mn2-O2	138.2(2)
N5-Mn2-O2	69.8(2)	O1-Mn2-O32	92.9(2)	N3-Mn2-O32	84.8(2)
N4-Mn2-O32	91.1(2)	N5-Mn2-O32	84.3(2)	O2-Mn2-O32	92.7(2)
O1-Mn2-O2'	76.1(2)	N3-Mn2-O2'	100.9(2)	N4-Mn2-O2'	104.2(2)
N5-Mn2-O2'	100.4(2)	O2-Mn2-O2'	75.6(2)	O32-Mn2-O2'	164.7(2)
Mn1-O1-Mn2	93.3(2)	Mn1-O1-C9	111.4(4)	Mn2-O1-C9	111.6(4)
Mn1-O1-Mn1'	104.2(2)	Mn2-O1-Mn1'	103.8(2)	C9-O1-Mn1'	127.1(4)
Mn1-O2-Mn2	92.7(2)	Mn1-O2-C21	110.6(4)	Mn2-O2-C21	111.0(4)
Mn1-O2-Mn2'	104.0(2)	Mn2-O2-Mn2'	104.2(2)	C21-O2-Mn2'	128.4(4)

The pentagonal planes of the two manganese atoms within each macrocycle must be approximately coplanar to allow formation of this core.

When $[Mn_4(L1')](ClO_4)_4.2H_2O$ (Figure 19A)[62(b)] was recrystallised from DMF a slightly different structure was formed and it is shown in Figure 43. Selected interatomic distances and angles are given in Table 7. The large (4+4) macrocycle is wrapped around a Mn_4O_4 core. The alcohol groups are deprotonated and each one bridges three manganese atoms. The macrocycle is able to wrap around this cluster by virtue of the flexible propane linkages which permit a 90° twist of the ligands between successive rigid pyridinediimine units. A crystallographic two-fold axis passes through the centres of the cubane faces defined by Mn1, O2, Mn1', O2' and Mn2, O1, Mn2', O1'.

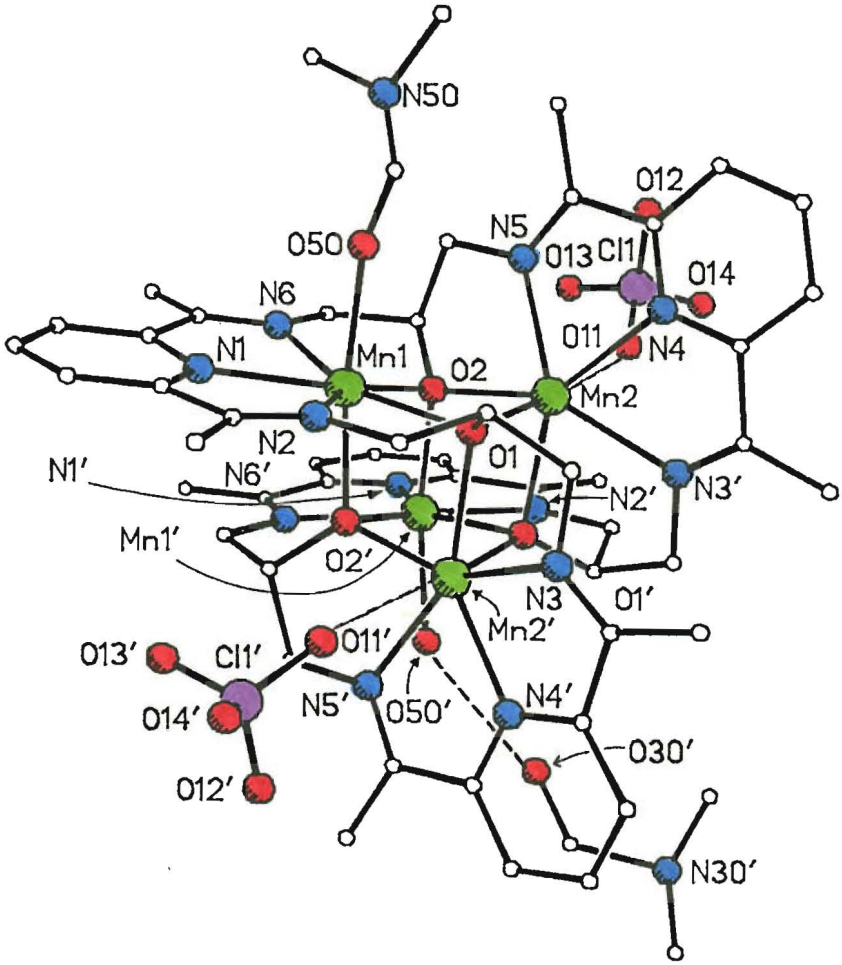

Figure 43: Perspective view of the cation $[Mn_4(L1')(H_2O)_{1.6}(DMF)_3(ClO_4)_2]^{2+}$, hydrogen bonds are shown as dotted lines.

The only significant difference between this structure and that of $[Mn_4(L1')](ClO_4)_4.2H_2O$ (Figure 19A) is that in this case two of the semi-coordinated perchlorate anions have been replaced by a 20% occupancy DMF bound *via* 050, coincident with an 80% occupancy water molecule (050) which is hydrogen

bonded to a 80% occupancy DMF molecule. The Mn1-O50 bond length of 2.312(9)Å implies this is coordinated whereas the Mn2-O11 separation of 2.897 Å indicates that the perchlorate is only semi-coordinated. In the structure shown in Figure 19A the two semi-coordinated perchlorate groups were at distances of 2.610(2) and 2.728(2)Å. It appears that in the present case the stronger coordination by O50 at two of the open axial coordination sites leads to weaker coordination by ClO_4^- at the other two axial sites, indicating some interaction between the manganese atoms through the cluster.

Table 7: Selected interatomic distances and angles for $[Mn_4(L1')(H_2O)_{1.6}(DMF)_3(ClO_4)_2](ClO_4)_2$

Interatomic Distances (Å)							
Mn1-N1	2.270(7)	Mn1-N2	2.314(7)	Mn1-O1	2.195(5)	Mn1-O2	2.307(5)
Mn1-N6	2.309(7)	Mn1-O50	2.312(9)	Mn1-O2'	2.193(7)	Mn2-O1	2.134(5)
Mn2-N4	2.284(8)	Mn2-N5	2.275(9)	Mn2-O2	2.145(5)	Mn2-O1'	2.289(7)
Mn2-N3'	2.326(7)	Mn2-O11	2.897(2)	Mn1-Mn2	3.279(2)	Mn1-Mn1'	3.515(2)
Mn1-Mn2'	3.362(2)	Mn2-Mn2'	3.445(2)	O50-O30	2.89(1)	O50-O40	2.79(1)

Bond Angles (°)					
N1-Mn1-N2	69.0(3)	N1-Mn1-O1	141.1(2)	N2-Mn1-O1	72.3(2)
N1-Mn1-O2	139.6(2)	N2-Mn1-O2	151.0(2)	O1-Mn1-O2	78.9(2)
N1-Mn1-N6	69.8(3)	N2-Mn1-N6	137.5(3)	O1-Mn1-N6	148.6(2)
O2-Mn1-N6	71.4(2)	N1-Mn1-O50	85.2(3)	N2-Mn1-O50	80.1(3)
O1-Mn1-O50	90.9(3)	O2-Mn1-O50	103.6(2)	N6-Mn1-O50	86.5(3)
N1-Mn1-O2'	100.4(3)	N2-Mn1-O2'	95.0(3)	O1-Mn1-O2'	80.2(2)
O2-Mn1-O2'	77.0(2)	N6-Mn1-O2'	102.2(3)	O50-Mn1-O2'	170.8(2)
O1-Mn2-N4	107.2(2)	O1-Mn2-N5	105.4(2)	N4-Mn2-N5	68.7(3)
O1-Mn2-O2	83.9(2)	N4-Mn2-O2	141.0(3)	N5-Mn2-O2	72.3(3)
O1-Mn2-O1'	77.6(2)	N4-Mn2-O1'	139.3(2)	N5-Mn2-O1'	150.6(2)
O2-Mn2-O1'	79.1(2)	O1-Mn2-N3'	102.9(2)	N4-Mn2-N3'	68.4(3)
N5-Mn2-N3'	133.8(3)	O2-Mn2-N3'	146.9(3)	O1'-Mn2-N3'	71.1(3)
Mn1-O1-Mn2	98.5(2)	Mn1-O1-C9	115.9(5)	Mn2-O1-C9	128.1(5)
Mn1-O1-Mn2'	97.1(2)	Mn2-O1-Mn2'	102.3(2)	C9-O1-Mn2'	110.0(5)
Mn1-O2-Mn2	94.8(2)	Mn1-O2-C21	111.0(5)	Mn2-O2-C21	119.2(5)
Mn1-O2-Mn1'	102.7(2)	Mn2-O2-Mn1'	101.6(2)	C21-O2-Mn1'	123.0(6)

In fact two general types of products were isolated from the acetate preparation; the first was the dimer $[Mn_2(L1)(CH_3COO)]_2(ClO_4)_2.H_2O.2DMF$ which is described above, and the second was a 5Mn structural type. There were three slight variations in the pentamanganese structures due to the binding of a series of different groups in the macrocycle fold; these are shown in Figures 44 and 45. Selected interatomic distances and angles are given in Tables 8, 9 and 10. In each case the $[Mn_5(L)_2(CH_3COO)_2(X)_2]^{y+}$ cation (X = ClO_4^- and y = 2; X = $(H_2O)_2(ClO_4^-)$ and y = 2; X = DMF, and y = 4) consists of two folded, binuclear macrocyclic units bridged by an octahedrally coordinated manganese atom (Mn3) and two acetate groups. The structures are centrosymmetric; Mn3 is located on a centre of symmetry, bonded to the two deprotonated alkoxide groups O1 and O2 from each macrocycle and to both acetate groups.

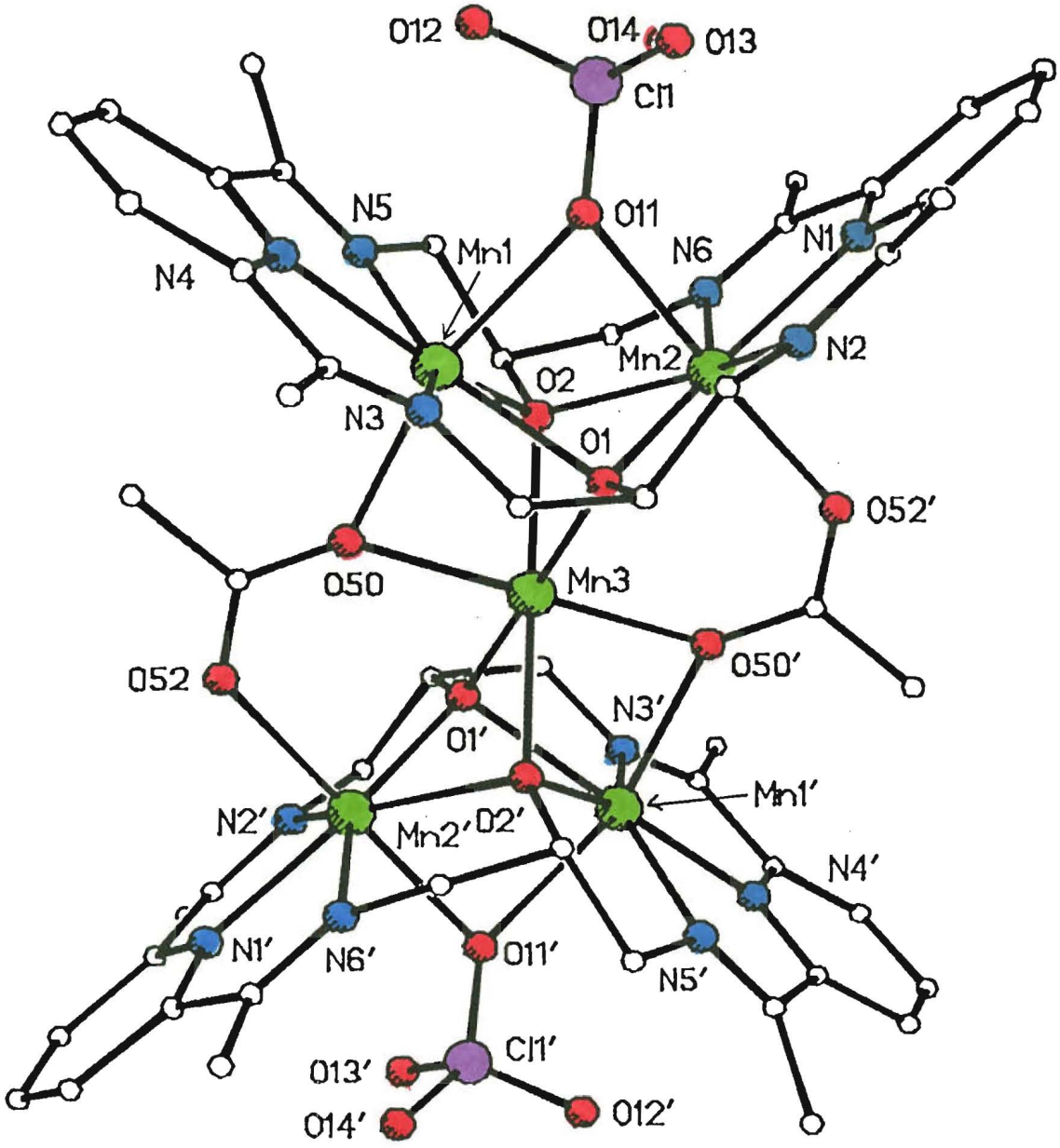

Figure 44: Perspective view of the cation $[Mn_5(L1)_2(CH_3COO)_2(ClO_4)_2]^{2+}$

The acetate ions each bridge three manganese atoms, one from each macrocycle plus Mn3 and exhibit both single- and three-atom bridging modes. Mn2 and Mn3 are linked by a three-atom acetate bridge but Mn1 and Mn3 are bridged by a single oxygen atom O50 of the acetate group. Mn1 and Mn2 are seven-coordinate and have approximate pentagonal bipyramidal geometry. The pentagonal plane contains the macrocyclic donor atoms (three nitrogen donors and two alkoxide groups), the axial ligands are acetate and an oxygen atom from the group bound in the macrocyclic cavity.

Table 8: Selected interatomic distances and angles for $[Mn_5(L1)_2(CH_3COO)_2(ClO_4)_2](ClO_4)_2.3MeCN$

Interatomic Distances (Å)							
Mn1-O1	2.222(7)	Mn1-N3	2.256(9)	Mn1-N4	2.200(9)	Mn1-N5	2.228(9)
Mn1-O2	2.229(7)	Mn1-O50	2.235(9)	Mn1-O11	2.298(9)	Mn2-N1	2.210(11)
Mn2-N2	2.261(11)	Mn2-O1	2.194(7)	Mn2-O2	2.193(8)	Mn2-N6	2.268(10)
Mn2-O11	2.428(9)	Mn2-O52'	2.157(9)	Mn3-O1	2.181(9)	Mn3-O2	2.182(8)
Mn3-O50	2.209(7)	Mn3-O1'	2.181(9)	Mn3-O2'	2.182(8)	Mn3-O50'	2.209(7)
Mn1-Mn2	3.112(2)	Mn1-Mn3	3.025(2)	Mn2-Mn3	3.243(2)		

Bond angles (°)					
O1-Mn1-N3	74.4(3)	O1-Mn1-N4	143.8(4)	N3-Mn1-N4	70.2(4)
O1-Mn1-N5	141.4(3)	N3-Mn1-N5	142.8(3)	N4-Mn1-N5	72.8(4)
O1-Mn1-O2	68.5(3)	N3-Mn1-O2	142.4(3)	N4-Mn1-O2	147.4(3)
N5-Mn1-O2	74.8(3)	O1-Mn1-O50	82.4(3)	N3-Mn1-O50	88.5(4)
N4-Mn1-O50	103.8(3)	N5-Mn1-O50	103.3(3)	O2-Mn1-O50	80.5(3)
O1-Mn1-O11	83.6(3)	N3-Mn1-O11	100.1(4)	N4-Mn1-O11	95.1(4)
N5-Mn1-O11	80.1(30)	O2-Mn1-O11	82.4(3)	O50-Mn1-O11	160.9(3)
N1-Mn2-N2	72.1(4)	N1-Mn2-O1	144.7(4)	N2-Mn2-O1	72.7(3)
N1-Mn2-O2	140.4(3)	N2-Mn2-O2	137.3(3)	O1-Mn2-O2	69.7(3)
N1-Mn2-N6	70.5(4)	N2-Mn2-N6	141.4(4)	O1-Mn2-N6	143.0(3)
O2-Mn2-N6	73.4(3)	N1-Mn2-O11	86.7(3)	N2-Mn2-O11	74.8(3)
O1-Mn2-O11	81.2(3)	O2-Mn2-O11	80.2(3)	N6-Mn2-O11	93.8(3)
N1-Mn2-O52'	91.8(4)	N2-Mn2-O52'	94.2(4)	O1-Mn2-O52'	93.8(3)
O2-Mn2-O52'	107.5(3)	N6-Mn2-O52'	96.1(4)	O11-Mn2-O52'	168.8(3)
O1-Mn3-O2	70.1(3)	O1-Mn3-O50	83.9(3)	O2-Mn3-O50	82.1(3)
O1-Mn3-O1'	180.0(1)	O2-Mn3-O1'	109.9(3)	O50-Mn3-O1'	96.1(3)
O2-Mn3-O2'	180.0(1)	O50-Mn3-O2'	97.9(3)	O50-Mn3-O50'	180.0(1)
Mn1-O1-Mn2	89.6(3)	Mn1-O1-Mn3	86.8(3)	Mn2-O1-Mn3	95.7(3)
Mn1-O1-C9	115.7(6)	Mn2-O1-C9	119.6(7)	Mn3-O1-C9	136.6(7)
Mn1-O2-Mn2	89.4(3)	Mn1-O2-Mn3	86.6(3)	Mn2-O2-Mn3	95.7(3)
Mn1-O2-C21	117.2(6)	Mn2-O2-C21	118.9(6)	Mn3-O2-C21	136.4(8)
Mn1O50-Mn3	85.8(3)	Mn1-O50-C51	138.3(8)	Mn3-O50-C51	131.6(9)
Mn1-O11-Mn2	82.3(3)	Mn1-O11-C11	142.6(5)	Mn2-O11-C11	132.8(5)

When X=ClO_4^-, the coordinated perchlorate ion occupies the cavity created by the folding of the macrocycle with O11 acting as a single atom bridge linking Mn1 and Mn2. The bond lengths are inequivalent (Mn1-O11 2.298(9), Mn2-O11 2.428(9)Å) but both are significantly shorter than the only other example of single atom bridging by perchlorate (2.56(3) and 2.60(3) Å in an aromatic sandwich complex, bis(*o*-xylene)silver(I) perchlorate[117]), probably because of the difference in the ionic radius of Mn(II) *vs* Ag(I). A water molecule can also be bound in the fold (Figure 45A, Mn1-O40 2.301(4), Mn2-O40 2.494(4)Å). In this case hydrogen bonding occurs between the bound water molecule, and both a second water molecule O60 (2.70(1)Å) and O11 of a perchlorate group (2.76(1)Å). When DMF is bound in the cavity the bonding is again inequivalent; Mn1-O40 2.287(16) and Mn2-O40 2.537(18)Å (Figure 45B).

In each case the macrocycles are folded to approximately the same extent, as indicated by the angles between the planes defined by Mn1, N3, N4, N5, O1, O2 *vs* Mn2, N1, N2, N6, O1, O2; 105.7° X = ClO_4^-, 106.3° X = $(H_2O)_2(ClO_4^-)$; 105.2° X = DMF.

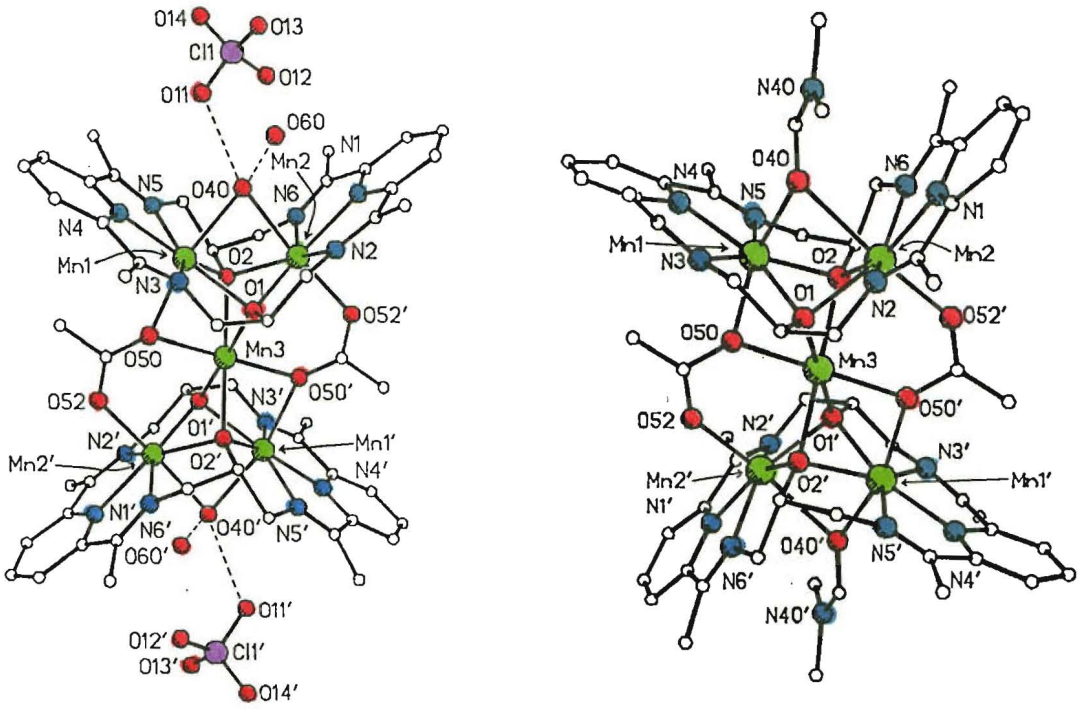

45A 45B

Figure 45: Perspective view of the cations $[Mn_5(L1)_2(CH_3COO)_2(H_2O)_4(ClO_4)_2]^{2+}$ (A) and $[Mn_5(L1)_2(CH_3COO)_2(DMF)_2]^{4+}$ (B), hydrogen bonds are shown as dotted lines.

Table 9: Selected interatomic distances and angles for $[Mn_5(L1)_2(CH_3COO)_2(H_2O)_4(ClO_4)_2](ClO_4)_2.6MeCN$

Interatomic Distances (Å)							
Mn1-O1	2.216(4)	Mn1-N3	2.260(7)	Mn1-N4	2.207(5)	Mn1-N5	2.241(7)
Mn1-O2	2.222(5)	Mn1-O40	2.301(4)	Mn1-O50	2.237(4)	Mn2-N1	2.229(5)
Mn2-N2	2.266(6)	Mn2-O1	2.210(5)	Mn2-O2	2.181(4)	Mn2-N6	2.277(7)
Mn2-O40	2.494(4)	Mn2-O52'	2.161(4)	Mn3-O1	2.194(4)	Mn3-O2	2.162(5)
Mn3-O50	2.207(4)	Mn3-O1'	2.194(4)	Mn3-O2'	2.162(5)	Mn3-O50'	2.207(4)
Mn1-Mn2	3.091(1)	Mn1-Mn3	3.023(1)	Mn1-Mn1'	6.046(1)	Mn1-Mn2'	5.454(1)
Mn2-Mn3	3.243(1)	Mn2-Mn2'	6.485(1)	O40-O60	2.70(1)	O40-O11	2.76(1)

Bond Angles (°)					
O1-Mn1-N3	74.1(2)	O1-Mn1-N4	145.3(2)	N3-Mn1-N4	71.5(2)
O1-Mn1-N5	142.3(2)	N3-Mn1-N5	142.8(2)	N4-Mn1-N5	71.4(2)
O1-Mn1-O2	68.8(2)	N3-Mn1-O2	142.5(2)	N4-Mn1-O2	145.8(2)
N5-Mn1-O2	74.7(2)	O1-Mn1-O40	85.2(2)	N3-Mn1-O40	98.0(2)
N4-Mn1-O40	94.4(2)	N5-Mn1-O40	82.0(2)	O2-Mn1-O40	85.0(2)
O1-Mn1-O50	82.1(2)	N3-Mn1-O50	88.9(2)	N4-Mn1-O50	102.2(2)
N5-Mn1-O50	101.6(2)	O2-Mn1-O50	80.4(2)	O40-Mn1-O50	163.3(2)
N1-Mn2-N2	70.8(2)	N1-Mn2-O1	144.1(2)	N2-Mn2-O1	73.7(2)
N1-Mn2-O2	140.7(2)	N2-Mn2-O2	139.7(2)	O1-Mn2-O2	69.7(2)
N1-Mn2-N6	70.9(2)	N2-Mn2-N6	141.2(2)	O1-Mn2-N6	142.9(2)
O2-Mn2-N6	73.3(2)	N1-Mn2-O40	85.8(2)	N2-Mn2-O40	76.9(2)
O1-Mn2-O40	80.9(2)	O2-Mn2-O40	81.3(1)	N6-Mn2-O40	94.1(2)
N1-Mn2-O52'	91.3(2)	N2-Mn2-O52'	94.8(2)	O1-Mn2-O52'	97.2(2)
O2-Mn2-O52'	105.7(2)	N6-Mn2-O52'	92.3(2)	O40-Mn2-O52'	171.7(2)
O1-Mn3-O2	70.3(2)	O1-Mn3-O50	83.3(1)	O2-Mn3-O50	82.4(2)

continued over...

Table 9: continued

Bond Angles (°)					
O2-Mn3-O1'	109.7(2)	O50-Mn3-O1'	96.7(1)	O50-Mn3-O2'	97.6(2)
O1'-Mn3-O2'	70.3(2)	O1-Mn3-O50'	96.7(1)	O1'-Mn3-O50'	83.3(1)
Mn1-O1-Mn2	88.6(2)	Mn1-O1-Mn3	86.5(2)	Mn2-O1-Mn3	94.8(2)
Mn1-O1-C9	116.7(3)	Mn2-O1-C9	120.9(4)	Mn3-O1-C9	136.0(4)
Mn1-O2-Mn2	89.2(2)	Mn1-O2-Mn3	87.2(2)	Mn2-O2-Mn3	96.6(2)
Mn1-O2-C21	118.2(3)	Mn2-O2-C21	119.5(4)	Mn3-O2-C21	134.1(3)
Mn1-O40-Mn2	80.2(1)	Mn1-O50-Mn3	85.7(1)	Mn1-O50-C51	139.8(4)
Mn3-O50-C51	133.6(4)				

Table 10: Selected interatomic distances and angles for $[Mn_5(L1)_2(CH_3COO)_2(DMF)_2](ClO_4)_4 2DMF$

Interatomic Distances (Å)							
Mn3-O1	2.114(13)	Mn3-O2	2.219(15)	Mn3-O50	2.198(16)	Mn1-O1	2.229(17)
Mn1-N3	2.264(16)	Mn1-N4	2.133(23)	Mn1-N5	2.288(20)	Mn1-O2	2.189(13)
Mn1-O50	2.222(16)	Mn1-O40	2.287(16)	Mn2-N1	2.234(18)	Mn2-N2	2.264(17)
Mn2-O1	2.179(15)	Mn2-O2	2.203(13)	Mn2-N6	2.259(19)	Mn2-O40	2.537(18)
Mn2-O52'	2.091(17)	Mn1-Mn2	3.083(5)	Mn1-Mn3	3.013(5)	Mn1-Mn1'	6.027(5)
Mn1-Mn2'	5.419(5)	Mn2-Mn3	3.218(4)	Mn2-Mn2'	6.436(5)		

Bond Angles (°)					
O1-Mn3-O2	70.6(5)	O1-Mn3-O50	82.2(5)	O2-Mn3-O50	82.8(6)
O2-Mn3-O1'	109.4(5)	O50-Mn3-O1'	97.8(5)	O1-Mn3-O2'	109.4(5)
O50-Mn3-O2'	97.2(6)	O1-Mn1-N3	74.1(6)	O1-Mn1-N4	146.5(6)
N3-Mn1-N4	72.5(7)	O1-Mn1-N5	143.3(6)	N3-Mn1-N5	142.5(8)
N4-Mn1-N5	70.1(7)	O1-Mn1-O2	69.0(5)	N3-Mn1-O2	142.0(7)
N4-Mn1-O2	144.2(7)	N5-Mn1-O2	75.1(6)	O1-Mn1-O50	79.2(6)
N3-Mn1-O50	99.3(6)	N4-Mn1-O50	104.4(7)	N5-Mn1-O50	89.0(6)
O2-Mn1-O50	82.9(5)	O1-Mn1-O40	83.6(6)	N3-Mn1-O40	78.2(6)
N4-Mn1-O40	91.5(7)	N5-Mn1-O40	103.5(7)	O2-Mn1-O40	88.6(5)
O50-Mn1-O40	162.6(7)	N1-Mn2-N2	69.6(7)	N2-Mn2-O1	73.5(6)
N2-Mn2-O2	143.2(6)	O1-Mn2-O2	69.7(5)	N1-Mn2-N6	71.3(6)
N2-Mn2-N6	139.1(7)	O1-Mn2-N6	137.7(7)	O2-Mn2-N6	74.0(6)
N1-Mn2-O40	86.9(6)	N2-Mn2-O40	91.4(6)	O1-Mn2-O40	78.9(6)
O2-Mn2-O40	82.2(5)	N6-Mn2-O40	75.2(6)	N1-Mn2-O52'	91.5(7)
N2-Mn2-O52'	94.2(7)	O1-Mn2-O52'	106.3(7)	O2-Mn2-O52'	95.5(6)
N6-Mn2-O52'	98.1(7)	O40-Mn2-O52'	173.3(6)	N1-Mn2-O1	140.0(5)
N1-Mn2-O2	145.3(6)	Mn3-O1-Mn1	87.8(5)	Mn3-O1-Mn2	97.1(5)
Mn1-O1-Mn2	88.7(6)	Mn3-O1-C9	134.0(15)	Mn1-O1-C9	118.5(14)
Mn2-O1-C9	118.8(13)	Mn3-O2-Mn1	86.3(5)	Mn3-O2-Mn2	93.4(6)
Mn1-O2-Mn2	89.1(4)	Mn3-O2-C21	139.4(12)	Mn1-O2-C21	116.4(13)
Mn2-O2-C21	118.6(11)	Mn3-O50-Mn1	85.9(5)	Mn3-O50-C51	134.0(18)
Mn1-O50-C51	137.1(16)	Mn1-O40-Mn2	79.2(5)	Mn1-O40-C40	131.1(17)
Mn2-O40-C40	134.3(15)				

Structure of $[Mn^{II}Mn^{III}(L13)(O)(OH)(DMF)]_2(ClO_4)_4.2H_2O$

The structure of the cation is shown in Figure 46 and selected interatomic distances and angles are given in Table 11. The two halves of this dimer are related by a centre of inversion. The brown colour of this complex indicated that some oxidation had occurred. From the stoicheiometry and the bond lengths shown in Figure 47, Mn1 and Mn1' are assigned the +III oxidation state and Mn2 and Mn2' are assigned the original oxidation state of +II.

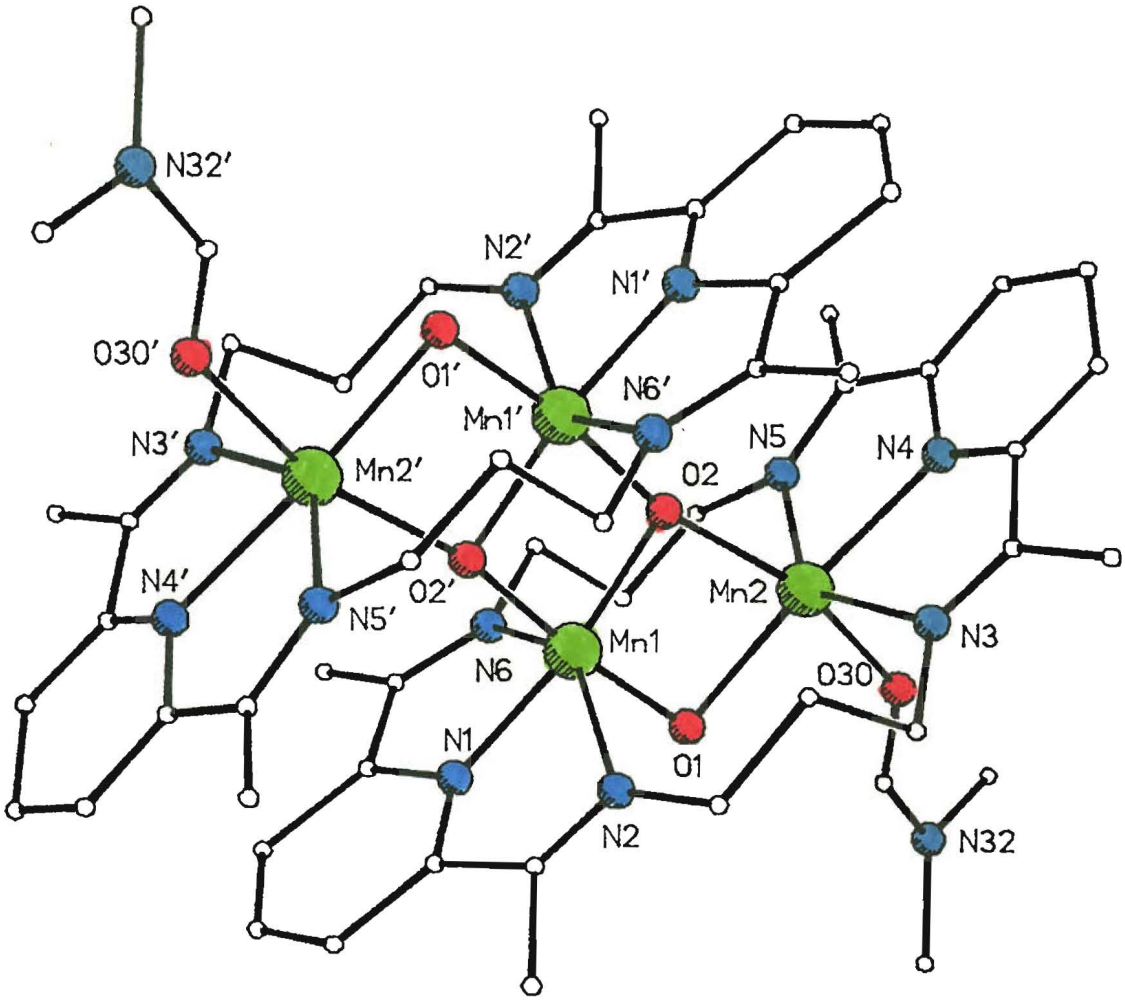

Figure 46: Perspective view of the cation $[Mn^{II}Mn^{III}(L13)(O)(OH)(DMF)]_2^{4+}$

Assignment of oxidation states from structural data is not a trivial exercise because often the bond lengths vary with donor atom type, coordination number and geometry. However, in the present case the situation is simplified as each manganese atom is six coordinate and has an approximately equivalent set of donor atoms. The bond distances to Mn2 and Mn2' are in the range normally observed for Mn(II) complexes (see complexes of H_2L1, Tables 2-10). The bond lengths to Mn1 and Mn1' are significantly shorter except those to N2 and N6 which are longer, perhaps due to a Jahn-Teller type distortion. Charge considerations require that two of the four oxygen donors must have a two minus charge and the other two a single minus charge. O2 and O2' each bind to three manganese atoms whereas O1 and O1' bind to only two. This, combined with the planar geometry about O2 and O2', suggests that these oxygen donors are the oxo ions, while O1 and O1' are hydroxo. DMF is bound, *via* the oxygen atom (O30 and O30'), as the sixth donor to Mn2 and Mn2'. The macrocycle is in a "step" conformation; the angle between the mean planes defined by Mn1, N1, N2, N6, O2 and Mn2, N3, N4, N5, O1 is only 7.5° but the planes are 1.8 $\pm$ 0.3Å apart.

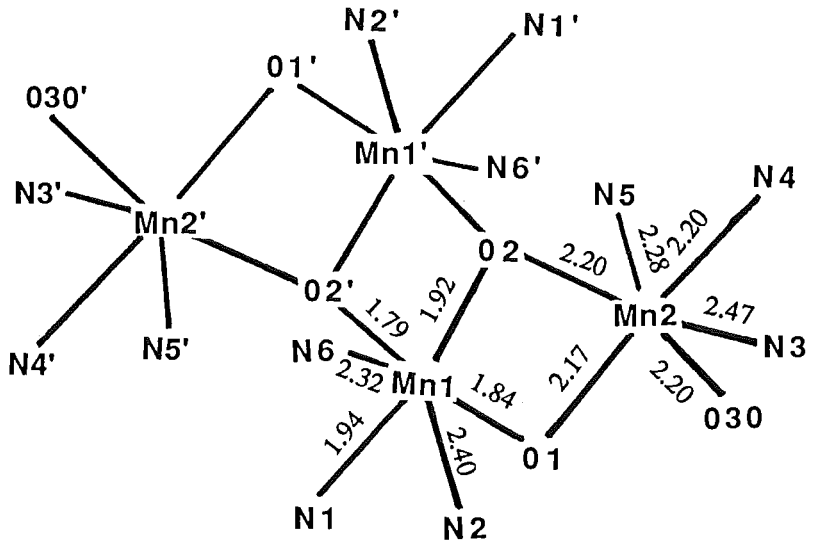

Figure 47

Table 11: Selected interatomic distances and angles for $[Mn^{II}Mn^{III}(L13)(O)(OH)(DMF)]_2(ClO_4)_4.2H_2O$

Bond Lengths (Å)							
Mn1-N1	1.936(52)	Mn1-N2	2.404(56)	Mn1-N6	2.315(56)	Mn1-O1	1.844(35)
Mn1-O2	1.916(36)	Mn1-O2'	1.787(37)	Mn2-N3	2.246(57)	Mn2-N4	2.198(53)
Mn2-N5	2.283(56)	Mn2-O1	2.165(34)	Mn2-O2	2.200(36)	Mn2-O30	2.205(46)
Mn1-Mn2	3.049(11)	Mn1-Mn1'	2.774(19)	Mn1-Mn2'	3.962(11)	Mn2-Mn2'	6.503(20)
O1-O2	2.670(40)	O2-O2'	2.460(40)				

Bond Angles (°)					
N1-Mn1-N2	73.7(22)	N1-Mn1-N6	77.0(22)	N2-Mn1-N6	148.1(17)
N1-Mn1-O1	95.1(19)	N2-Mn1-O1	86.5(16)	N6-Mn1-O1	83.9(17)
N1-Mn1-O2	169.7(21)	N2-Mn1-O2	115.4(19)	N6-Mn1-O2	95.1(18)
O1-Mn1-O2	90.5(15)	N1-Mn1-O2'	90.9(19)	N2-Mn1-O2'	98.7(18)
N6-Mn1-O2'	94.0(18)	O1-Mn1-O2'	173.0(16)	O2-Mn1-O2'	83.1(15)
N3-Mn2-N4	69.9(21)	N3-Mn2-N5	141.2(17)	N4-Mn2-N5	71.5(21)
N3-Mn2-O1	98.6(16)	N4-Mn2-O1	167.7(22)	N5-Mn2-O1	120.2(17)
N3-Mn2-O2	94.5(17)	N4-Mn2-O2	100.6(18)	N5-Mn2-O2	97.1(16)
O1-Mn2-O2	75.4(14)	N3-Mn2-O30	96.2(18)	N4-Mn2-O30	95.0(18)
N5-Mn2-O30	82.4(17)	O1-Mn2-O30	90.4(15)	O2-Mn2-O30	163.4(16)
Mn1-O1-Mn2	98.7(17)	Mn1-O2-Mn2	95.3(17)	Mn1-O2-Mn1'	96.9(15)
Mn2-O2-Mn1'	166.8(21)				

Structure of $[Mn(DAP)_2(H_2O)_2](ClO_4)_2$

The cation $[Mn(DAP)_2(H_2O)_2]^{2+}$ is shown in Figure 48 and selected bond lengths and angles are given in Table 12. The manganese atom is eight-coordinate. The two DAP groups are bound such that the angle between the planes they define is 85.2°. However, these six donor atoms do not define octahedral coordination about the Mn(II) because two water molecules are also bound. The DAP is bound unsymmetrically; in each case one of the two carbonyl oxygens is not bound as strongly as the other. The water molecules are bound on the opposite side of the manganese atom to the weak DAP carbonyl bonds to manganese.

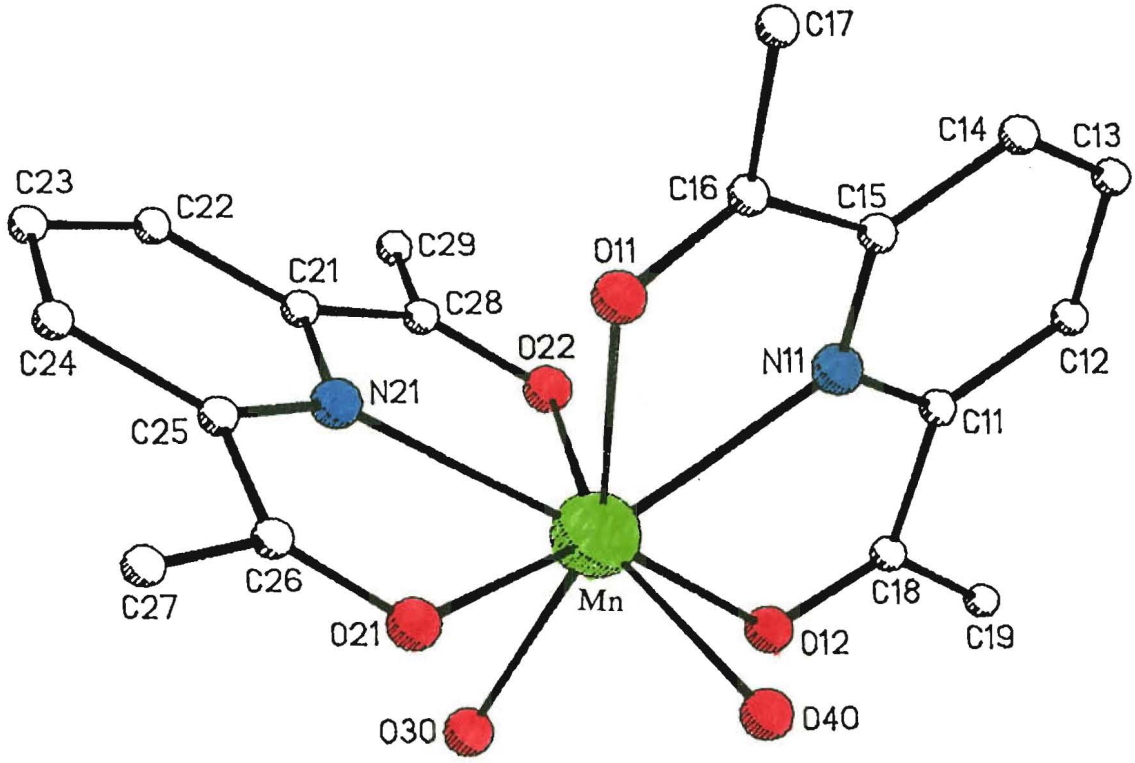

Figure 48: Perspective view of the cation $[Mn(DAP)_2(H_2O)_2]^{2+}$

Table 12: Selected bond lengths and angles for $[Mn(DAP)_2(H_2O)_2](ClO_4)_2$

Bond Lengths (Å)							
Mn-N11	2.310(6)	Mn-O11	2.493(8)	Mn-O12	2.331(7)	Mn-N21	2.299(7)
Mn-O21	2.369(8)	Mn-O22	2.438(7)	Mn-O30	2.208(7)	Mn-O40	2.213(8)

Bond Angles (°)					
N11-Mn-O11	65.8(2)	N11-Mn-O12	70.3(2)	O11-Mn-O12	135.6(3)
N11-Mn-N21	117.4(2)	O11-Mn-N21	74.5(3)	O12-Mn-N21	134.7(2)
N11-Mn-O21	132.4(3)	O11-Mn-O21	72.0(3)	O12-Mn-O21	142.0(2)
N21-Mn-O21	68.6(2)	N11-Mn-O22	77.9(2)	O11-Mn-O22	104.0(2)
O12-Mn-O22	72.1(2)	N21-Mn-O22	67.1(2)	O21-Mn-O22	134.7(2)
N11-Mn-O30	142.5(3)	O11-Mn-O30	151.7(3)	O12-Mn-O30	72.6(3)
N21-Mn-O30	85.6(2)	O21-Mn-O30	82.2(3)	O22-Mn-O30	85.9(3)
N11-Mn-O40	86.6(3)	O11-Mn-O40	92.2(3)	O12-Mn-O40	78.9(3)
N21-Mn-O40	142.3(3)	O21-Mn-O40	73.8(3)	O22-Mn-O40	150.3(3)
O30-Mn-O40	91.6(3)				

Structure of $[Pb_2(H_2L5)(NCS)_3]NCS$

This cation is shown in Figure 49 and selected bond lengths and angles are given in Table 13. The two halves of the H_2L5 macrocycle are related by a C_2 axis which passes through N31 perpendicular to the plane defined by the alkyl chains. The N31-C31-S31 thiocyanate is disordered between two sites around this axis as shown in Figure 49. The alkyl carbons C8, C9, C10, C11 and C12 lie approximately in a plane (maximum deviation 0.15 Å). The two pyridinediimine groups are folded out of this plane, defining two further planes which intersect at 50.1°. The pyridinediimine planes intersect the mean plane of the alkyl carbon atoms at angles

of 69.0 and 61.1°. The lead atoms have distorted geometry; the three nitrogen atoms of the pyridinediimine unit are donors in one plane, with approximate axial coordination from a terminal SCN^- (S21) and a bridging NCS^- (N31) group. The gap in the coordination sphere is probably occupied by the lone pair of the lead atom. The alcohol groups of H_2L5 are not coordinated, and are twisted out of the cavity.

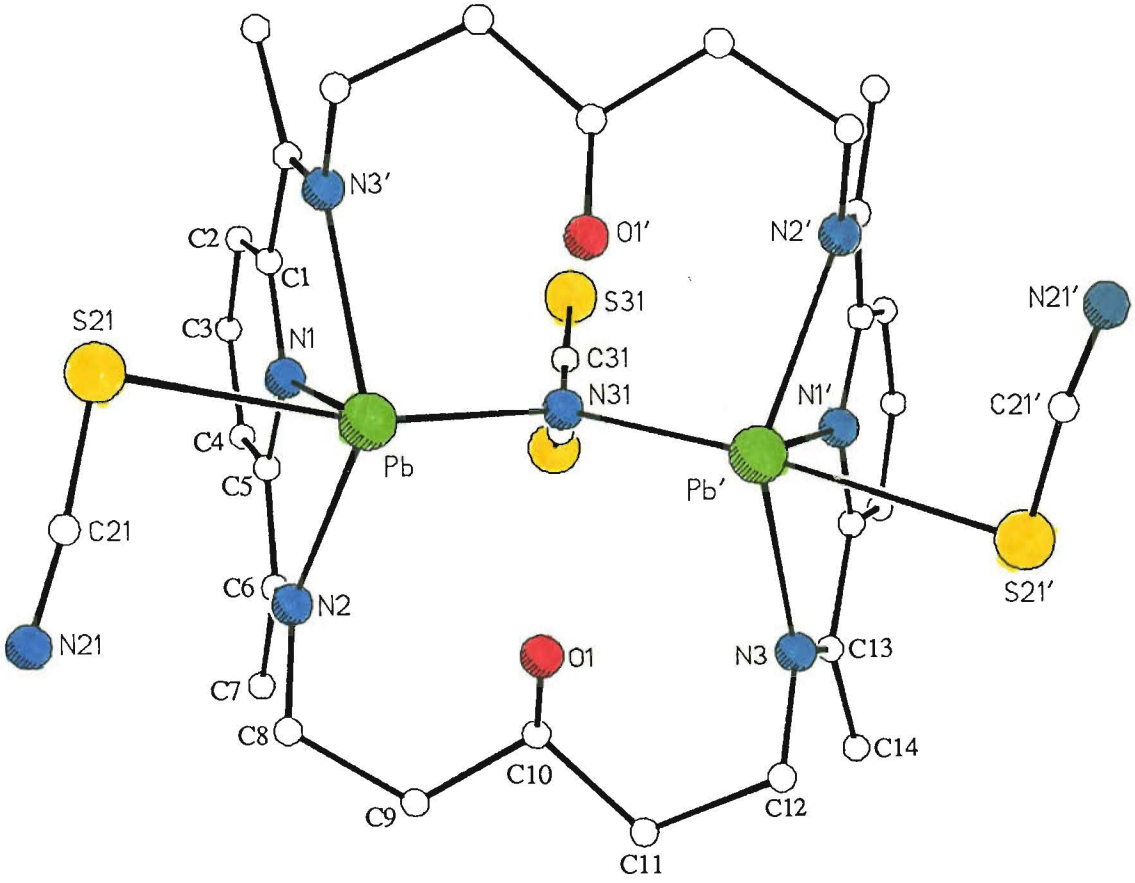

Figure 49: Perspective view of the cation $[Pb_2(H_2L5)(NCS)_3]^+$

Table 13: Selected interatomic distances and angles for $[Pb_2(H_2L5)(NCS)_3]NCS$

Interatomic Distances (Å)							
Pb-N1	2.466(20)	Pb-N2	2.566(22)	Pb-S21	2.901(8)	Pb-N31	2.705(22)
Pb-N3'	2.505(20)	Pb-Pb'	4.055(2)				

Bond Angles (°)					
N1-Pb-N2	62.2(7)	N1-Pb-S21	85.6(5)	N2-Pb-S21	90.8(5)
N1-Pb-N31	74.1(7)	N2-Pb-N31	87.3(6)	S21-Pb-N31	158.0(5)
N1-Pb-N3'	65.3(7)	N2-Pb-N3'	126.2(7)	S21-Pb-N3'	74.0(5)
N31-Pb-N3'	89.4(5)	Pb-N31-C31	126.4(34)	Pb-N31-C31'	127.5(37)
Pb-N31-Pb'	96.1(11)				

Results and Discussion of Complexes of H_2L1 and H_4L1'

Ring Expansion From a (2+2) to a (4+4) Macrocycle

The tetramanganese complexes of the (4+4) macrocycle H_4L1' (Figures 19A and 43) were formed by a transmetallation reaction of $[Ba(H_2L1)(H_2O)_2](ClO_4)_2$ with manganese(II) perchlorate. The ^{252}Cf PDMS data for the barium starting material (Figure 50) shows a peak at 671 a.m.u. which is assigned to $[Ba(H_2L1)(ClO_4)]^+$. There is no signal at twice the mass to indicate a BaH_4L1' species and the absence of an extensive fragmentation pattern indicates that it is unlikely that a BaH_4L1' species disintegrated in the instrument. Parent ions at 1401 a.m.u., $[Mn_4(L1')(ClO_4)_3(H_2O)]^+$, and 1259 a.m.u., $[Mn_4(L1)_2(NCS)_3]^+$ indicate that both of these manganese complexes remain intact in the instrument (Figure 50). This fact supports the conclusion that there was no significant amount of barium (4+4) species present in the barium macrocycle preparation. That is, certainly not enough barium (4+4) macrocycle complex to give an observed yield of the manganese (4+4) complex of 35%. This means that the ring expansion from (2+2) to (4+4) must have occurred during or after the transmetallation reaction.[62(b)]

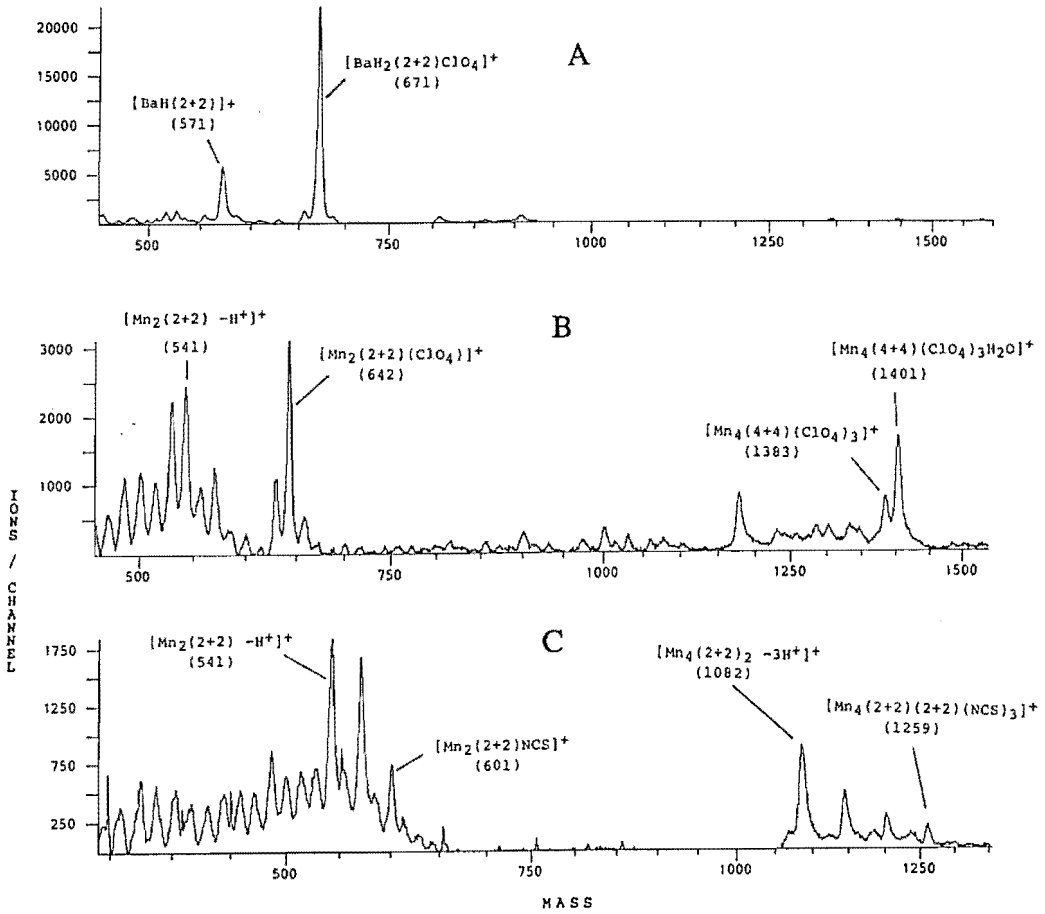

Figure 50: ^{252}Cf PDMS spectra of $[Ba(H_2L1)(H_2O)_2](ClO_4)_2$ (A), $[Mn(L1')(ClO_4)_4]$ (B) and $[Mn_4(HL1)(L1)(NCS)_4]NCS$ (C).

Before presenting a possible mechanism for this rearrangement the isomers and conformations which can be adopted by these macrocycles (H_2L1 and H_4L1') on

binding to a metal ion are discussed. When the alkoxide oxygen atoms bind to a metal ion the geometry at the attached alkyl carbon atoms C* are fixed as shown in Figure 51; either syn (both H* protons point in the same direction) or anti (pointing in opposite directions), with respect to the plane of the macrocycle.

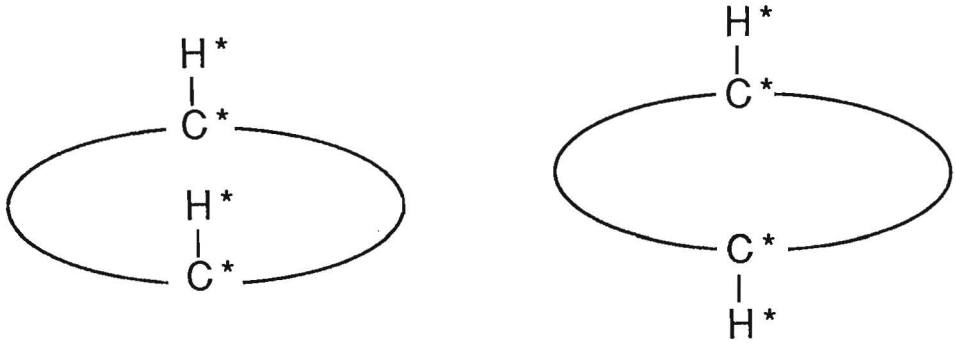

Figure 51

When barium(II) is employed as a template ion the resulting H_2L1 complex is the syn diastereoisomer as shown by the X-ray crystal structure determination by Bailey, Fenton and co-workers[80] (Figure 52). This configuration is required if the macrocycle is to fold around the single metal ion and bind through all of its donor atoms (including the alcohol oxygen atoms).

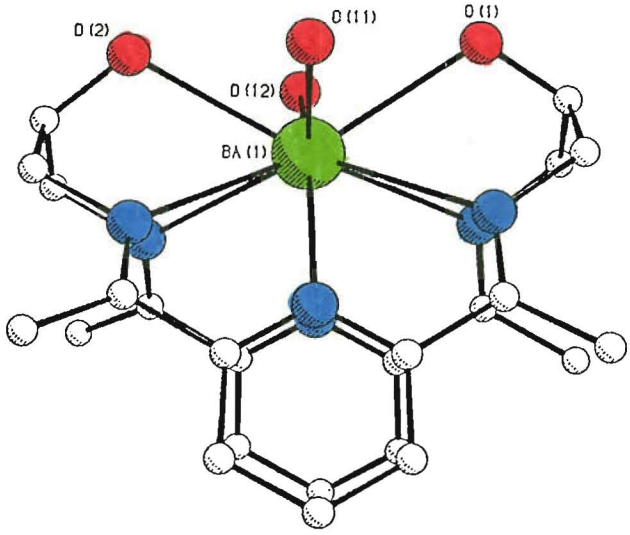

Figure 52: From reference 118.

Therefore transmetallation of the barium (2+2) complex with manganese(II) salts should, initially at least, form dimanganese (2+2) complexes which are also syn diastereoisomers. Imine linkages are readily hydrolysed so the diaminoalcohol group could be released by hydrolysis and replaced to yield the other (anti) diastereoisomer. A facile rearrangement of this type should result in isolation of the preferred diastereoisomer in the product.

The structure determinations of the chloride, azide, thiocyanate, formate, and both the 4Mn and 5Mn acetate complexes show that in each case the pairs of H* protons are syn with respect to their individual (2+2) macrocycles. However, the

two discrete (2+2) macrocycles can dimerise in one of the two ways outlined schematically in Figure 53.

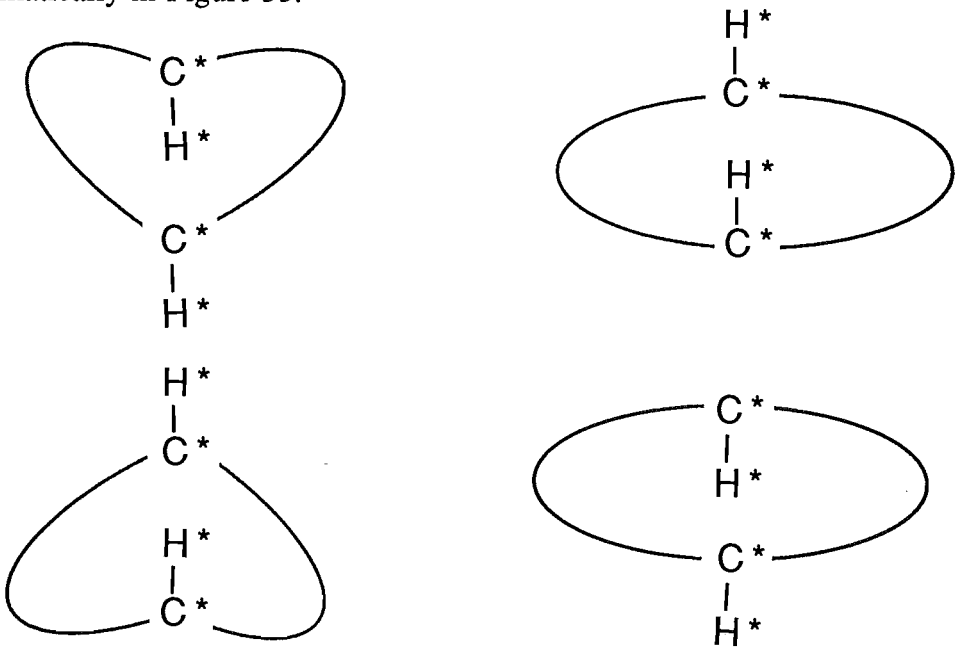

53A 53B

Figure 53

In the cases where the macrocycle is folded and accommodates a single atom bridge (i.e. the chloride, azide, thiocyanate and 5Mn acetate structures) the dimer produced is of the 53A type with all H* protons pointing to the centre of the cluster. Once the macrocycle is folded in this way it can only dimerise from the open side, i.e. with the protons in the 53A conformation. There are no single atom bridges in the formate and 4Mn acetate structures and in order to form the Mn_4O_4 cubane core (which requires the two manganese pentagonal planes within a (2+2) macrocycle to be approximately coplanar) the macrocycle must adopt a planar conformation. Dimerisation occurs from the less crowded side such that the alkoxy-C* bonds point away from the cubane core, and the H* protons are in the 53B conformation.

In contrast, the (4+4) macrocycle wraps around the Mn_4O_4 cubane core by a series of 90° twists between successive pyridinediimine units (and manganese pentagonal planes) which requires the geometry at C* to alternate (equivalent to the anti diastereoisomer for the (2+2) case). For the (4+4) to be formed from the barium (2+2) complex which is in the syn conformation implies that overall two inversions of configuration at C* centers must occur during the rearrangement. Inversion requires hydrolysis and replacement of the diaminoalcohol group to give the opposite configuration at C*. This inversion could possibly be achieved without the loss of the diaminoalcohol oxygen from the Mn_4O_4 core, by a rotation of the hydrolysed diamine about the oxygen-C* bond.

A possible route from the (2+2) to the ring expanded (4+4) macrocycle is outlined in Figure 54. This scheme indicates how the minimum requirements of two

inversions of configuration at the C* centre and rotation of two pentagonal planes through 90° could be satisfied.

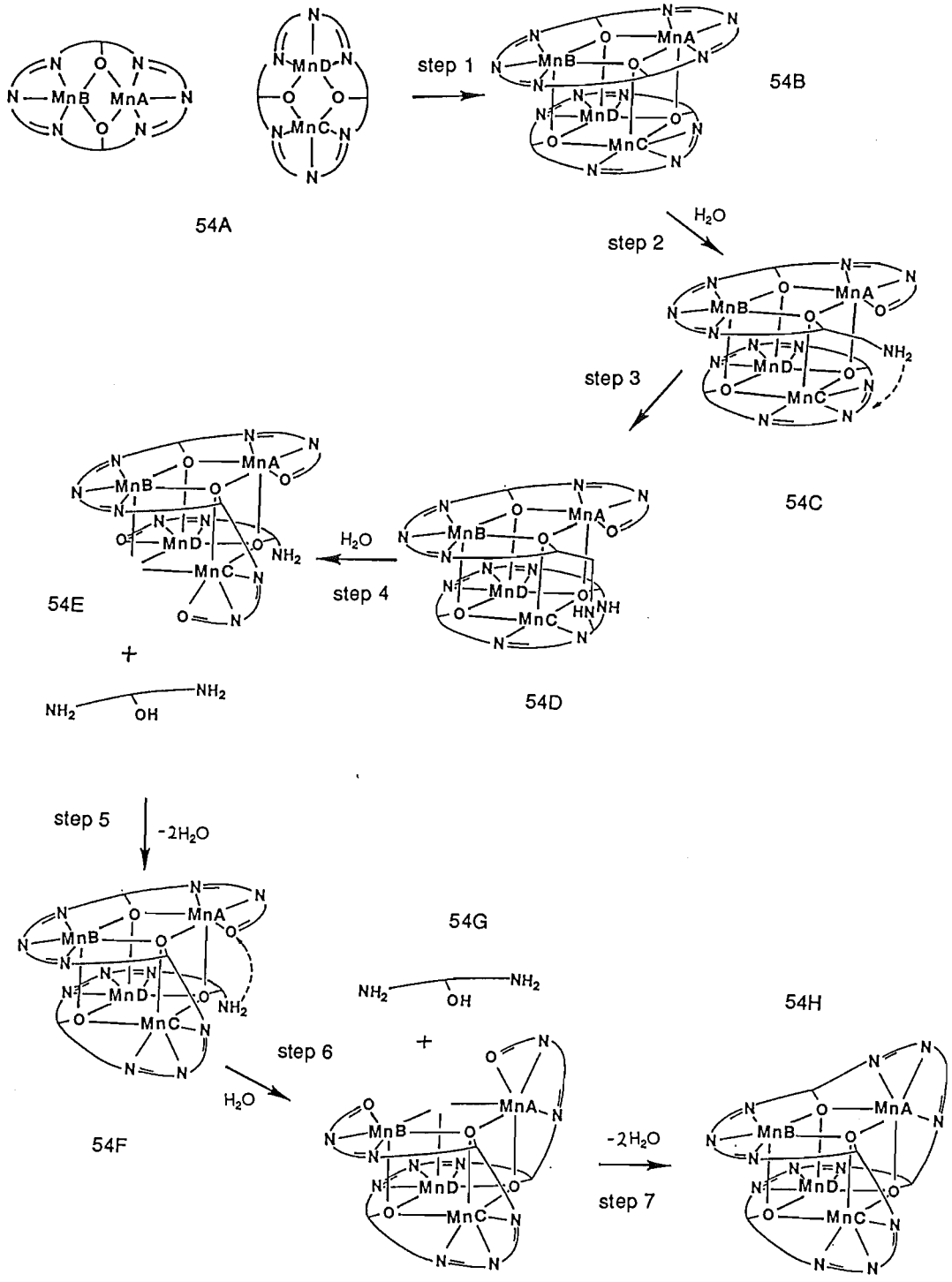

Figure 54

The first step is a face-to-face dimerisation where two dimanganese (2+2) macrocycles come together in a staggered conformation forming four intermolecular Mn-O bonds (54B). The formate and 4 Mn acetate structures model this intermediate which must have the 53B conformation as outlined earlier. The

resulting Mn_4O_4 cubane core then acts as a template for the ring expansion rearrangement. Hydrolysis of an imine bond (e.g. bound to MnA) in one macrocycle produces a free amine group (step 2) which can rotate down and attack an imine bond (bound to MnC) in the adjacent macrocycle (step 3). Similar nucleophilic attack by amine groups has been demonstrated by Nelson in transamination reactions of related complexes (Figure 29).[76] One of the resulting C-N single bonds (54D) then breaks either reforming 54C, or leaving a new intermolecular imine link and releasing another free amine (54E). The new intermolecular imine link requires the pyridinediimine unit, and hence the pentagonal plane of MnC, to twist 90° from its original orientation. For this to occur the diaminoalcohol group on the other side of this pyridinediimine group from the new imine link must hydrolyse (step 4). The resulting gap in the cubane core is then filled by binding a diaminoalcohol group to give the opposite configuration, which can condense with the two free carbonyl groups of MnC and MnD to link up one side of the new macrocycle (step 5). Step 6 involves a second intermolecular attack by the remaining free amine on the free carbonyl group (of MnA). Again formation of the new intermolecular imine link causes the pyridinediimine unit to twist through 90°, and a diaminoalcohol group to hydrolyse (step 6) and recondense in the opposite configuration (step 7). This results in the (4+4) macrocycle (54H) with the conformation at C* alternating as observed in the (4+4) structure determinations (Figures 19A and 43).

When chloride or azide ions are present no ring expansion occurs. These anions bridge the manganese atoms in adjacent macrocycles forcing them into an eclipsed formation preventing Mn_4O_4 cubane formation. In the thiocyanate structure two intermolecular Mn-O bonds form the beginning of an Mn_4O_4 cube but it is not completed because two terminally bound thiocyanate groups block the other two manganese axial sites. No rearrangement is observed. The formate and 4Mn acetate structures represent intermediate 54B (Figure 54) in the rearrangement scheme. An Mn_4O_4 cubane forms as the two dimanganese macrocycles dimerise in a staggered face-to-face orientation because the formate/acetate anions do not compete with the alkoxide oxygens for the axial coordination sites on the manganese. However, the rearrangement does not proceed any further because the 1,3-bridging formate/acetate anions prevent the 90° twist (of one manganese pentagonal plane relative to the second in the same macrocycle) required to complete the formation of the new intermolecular imine links (i.e. Figure 54, steps 4 and 6). Hydrolysis of imine bonds (e.g. Figure 54, step 2) may occur but the bridging anions ensure the same bonds reform.

Nothing is isolated from solution if the transmetallation of the barium (2+2) compound with manganese perchlorate is carried out in anhydrous conditions which supports the conclusion that hydrolysis is an important feature of this rearrangement reaction. The $[Mn_4(L1')](ClO_4)_4$ complex can also be prepared directly using

Mn(II) as the template ion instead of transmetallating the $[Ba(H_2L1)(H_2O)_2](ClO_4)_2$ complex. This implies that the H_4L1' tetramanganese complex is the thermodynamically stable product and should form in solution in the absence of strongly coordinating anions. Hence, it would be expected that there would not be any significant anion dissociation in the chloride, azide, thiocyanate, formate, 4Mn or 5Mn acetate complexes in solution. If the anions did dissociate in solution then, from the proposed scheme (Figure 54), H_4L1' ought to be formed.

Results of conductivity studies of these complexes in MeCN and DMF (recrystallisation solvents) are shown in Table 14 along with the literature ranges.[119]

Table 14: Conductivity measurements, Λ_m ohm^{-1} cm^2 mol^{-1}, ? indicates extrapolation.

EXPERIMENTAL RESULTS

Complex	Λ_m (DMF)	Λ_m (MeCN)	slope(MeCN)
$[Mn_2(HL1)(Cl)_2]_2(ClO_4)_2$	125	270	620
$[Mn_2(HL1)(N_3)_2]_2(ClO_4)_2$	121	239	670
$[Mn_4(HL1)(L1)(NCS)_4]NCS$	110	135	
$[Mn_2(L1')](ClO_4)_4$	245	460	930

LITERATURE RANGES

Complex	Λ_m(DMF)	Λ_m (MeCN)	slope (MeCN)
1:1	65-90	120-160	~ 350
1:2	130-170	220-300	~ 750
1:3	200-240	340-420	~ 1050?
1:4	~ 300?	~ 500?	~ 1400?

The values obtained indicate that the anions do not dissociate significantly. For example, possible fragments of the chloride complex, $[Mn_2(HL1)(Cl)]_2(ClO_4)_2(Cl)_2$ 1:4 electrolyte and $[Mn_2(HL1)(Cl)_{1.5}]_2(ClO_4)_2Cl$ 1:3 electrolyte are discounted by the 1:2 value obtained. The values for the H_4L1' complex are lower than those expected for a 1:4 electrolyte which may indicate some association of the perchlorate anions as observed in the crystal structure (Figure 19A). The value obtained for the thiocyanate complex in DMF is quite high for a 1:1 electrolyte and may indicate some anion dissociation, however, this complex was always recrystallised from MeCN. Other than the thiocyanate complex in DMF the Λ_m values fall at the lower end of the expected (literature) ranges. This is probably due to the low ionic mobilities of

these bulky cations compared to the smaller ions of simple salts which have greater ionic mobilities and hence larger Λ_m values.

Unfortunately, conductivity measurements at a single concentration do not unambiguously determine the molecular complexity v in complexes $[MnL_n]_vX_{yv}$ (e.g. v=2 $[Mn_2(HL1)X_2]_2Y_2$, 1:2 *vs* two v=1 $[Mn_2(HL1)X_2]Y$ 1:1) in solution because an assumed molecular weight is used to calculate Λ_m (their equivalent weights are the same).[119,120] To resolve this problem a series of Λ measurements at low concentrations are obtained, and a plot of Λ_e vs $\sqrt{c_e}$ constructed, because the Onsager equation (higher terms omitted[121]) shows that this should give a straight line with a slope of $(\alpha\Lambda_o + \beta)$:

$$\Lambda_e = \Lambda_o - (\alpha\Lambda_o + \beta)\sqrt{c_e} \qquad (4)$$

where Λ_e = equivalent conductivity $= \frac{\kappa}{c_e}$

κ = specific conductivity $= \frac{\text{cell constant}}{\text{measured resistance}}$

c_e = equivalent concentration; for MX_n $c_e = nc_m$

c_m = molar concentration

Λ_o = equivalent conductance at infinite dilution

$$\alpha = \frac{0.986 \times 10^6\, \omega\sqrt{z_1 + z_2}}{(DT)^{3/2}}$$

$$\beta = \frac{29.0\,(z_1 + z_2)^{3/2}}{(DT)^{1/2}\eta}$$ for derivation of α and β see reference 122

$$\omega = \frac{2q}{1 + \sqrt{q}}\, z_1 z_2$$

$$q = \frac{z_1 z_2 \Lambda_o}{(z_1 + z_2)(z_2 l_1 + z_1 l_2)}$$

z_i = charge on type i ion

l_i = equivalent ionic conductance of ion i at infinite dilution; $\Lambda_o = \Sigma l_i$

D = dielectric constant

T = temperature (K)

η = viscosity (Poise)

As the slope of the line depends on z_i it can be used to distinguish $[Mn_2(HL1)X_2]_2Y_2$ from $[Mn_2(HL1)X_2]Y$. If the l_i values for the ions involved are known, then the slope can be calculated.[123,124] Experimental and calculated values vary[125] but in MeCN the values indicated in Table 14 for 1:1 and 1:2 electrolytes are good estimates for simple electrolytes.

To test the available acetonitrile and resistance meter a Λ_e vs $\sqrt{c_e}$ graph was plotted for $(C_2H_5)_4NBr$ (Figure 55). Measurement of large resistances, > 5 k Ω, exposed the solution to unacceptably large voltages (± 6.5 V); which caused the reading of resistance to drop visibly during measurement giving rise to the sudden upwards curve at lower concentrations in Figure 55.

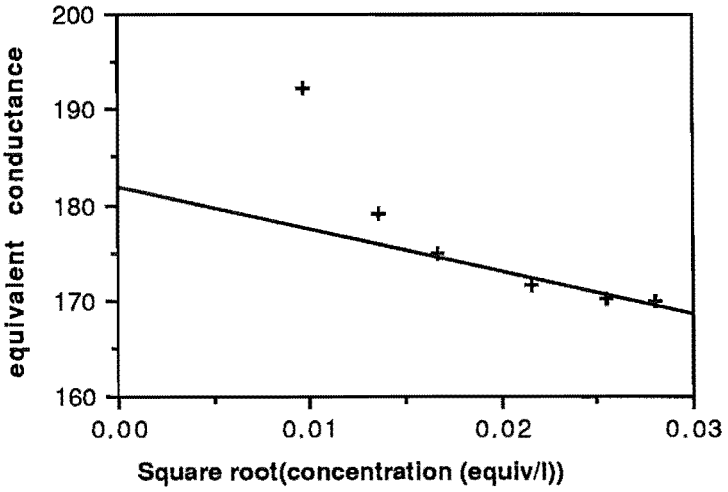

Figure 55

Hence it was decided to neglect any points in this area. This is not ideal as it limits the concentration range which can be studied; the maximum concentration is limited to *ca.* 1 mmol l^{-1} due to the limited solubility of these complexes and because of the problems of ion association at higher concentrations.The four remaining points in Figure 55 give a line of slope 443 and intercept 182 which agree quite well with the literature values of 426 and 185.5 respectively.[124]

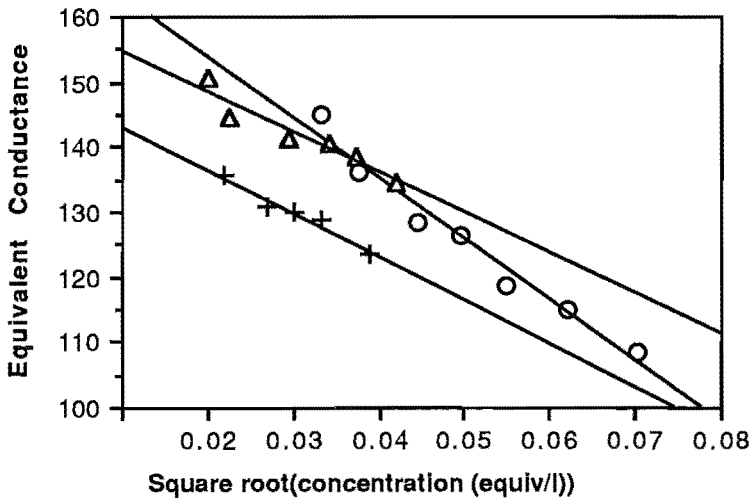

Figure 56: Concentration dependence of the equivalent conductance for the chloride (Δ), azide (+) and $[Mn_4(L1')](ClO_4)_4$ (O) complexes.

Figure 56 shows the results for the chloride, azide and $[Mn_4(L1')](ClO_4)_4$ complexes in MeCN. The slopes of the chloride and azide lines are lower than the average value for a 1:2 electrolyte but are closer to 1:2 than 1:1 slopes. The H_4L1' complex also gives a low slope, matching 1:3 not 1:4. As the "one off" measurement was also close to a 1:3 value it seems likely that the complex in solution is a $[Mn_4L1'(ClO_4)](ClO_4)_3$ species.

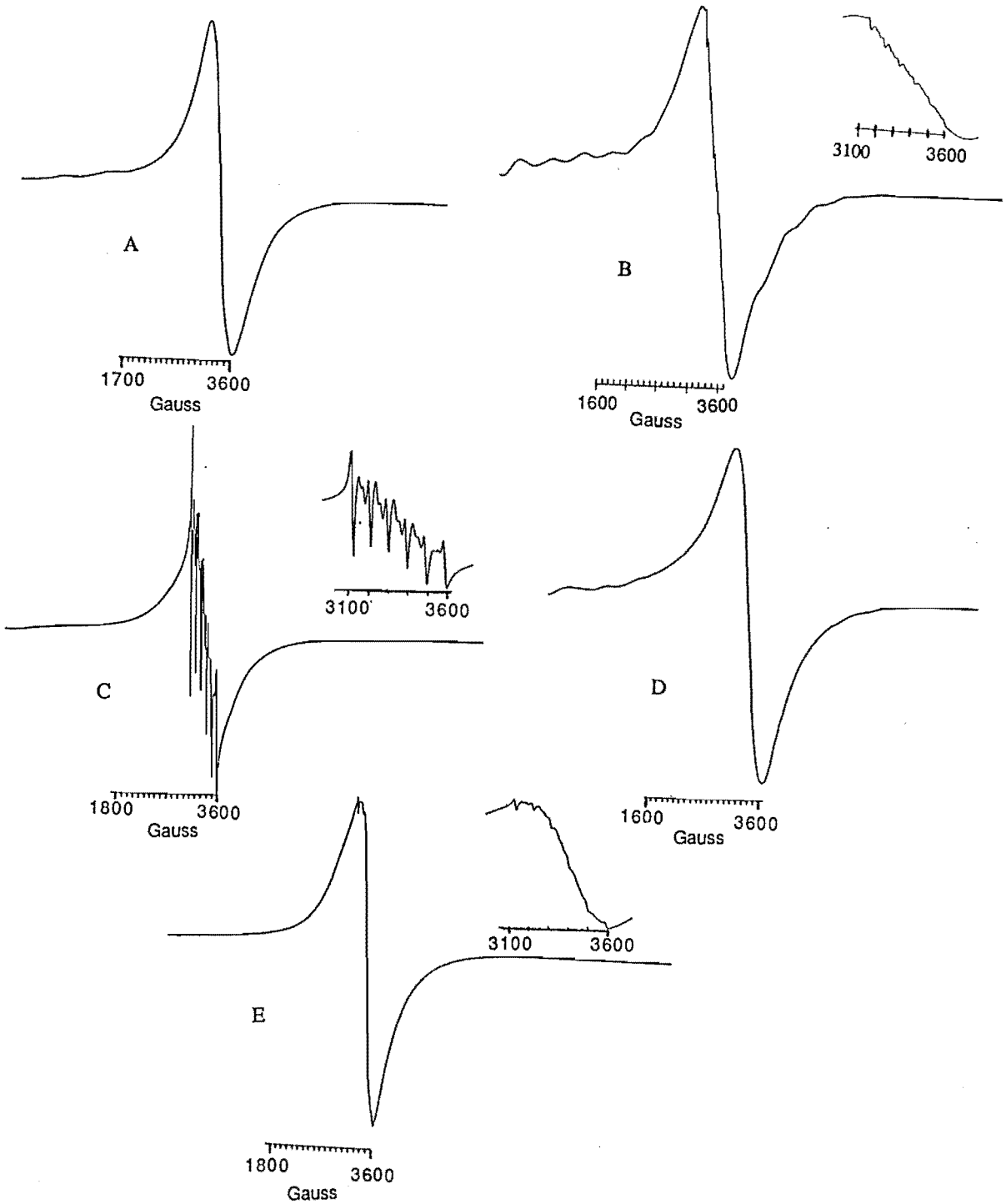

Figure 57: EPR spectra of the chloride (A), azide (B), thiocyanate (C), 4Mn acetate (D) and $[Mn_4(L1')](ClO_4)_4$ (E) complexes.

EPR spectra of these complexes, in DMF/toluene glasses (Figure 57), indicate that they are polynuclear because the six line spectrum characteristic of

uncoupled or mononuclear Mn(II) is not observed.[126] However, mononuclear impurity is evident in the EPR spectra of the azide and $[Mn_4(L1')](ClO_4)_4$ complexes, and the thiocyanate complex shows only an uncoupled signal. Taken with the DMF conductivity result this may suggest that there is some decomposition of the thiocyanate complex in DMF solutions; although the EPR signal could arise from a loss of magnetic coupling rather than complete dissociation. To check out these possibilities the thiocyanate complex should be recrystallised from DMF several times and then a single crystal X-ray unit cell determination (and if necessary a structure determination) carried out to see whether or not rearrangement to a (4+4) structure has occurred. It is possible that the DMF will not be wet enough to facilitate the hydrolysis reactions required during the ring expansion.

Formation of Penta- and Tetramanganese Acetate Complexes of H_2L1

Attempts were made to determine what factors control the formation of the 4Mn acetate structure (Figure 42) in some cases and the 5Mn acetate structure (Figures 44 and 45) in others. A major problem in this exercise was the difficulty in identifying which product(s) were present in a given sample. Unfortunately, the analytical figures are very similar, and consequently slight differences in solvent content can cause relatively large variations. Slight differences in the positioning and intensity of the imine and pyridine absorptions at *ca.* 1650 and 1570 cm^{-1} in the infrared spectrum were observed but these did not correlate very well with the identified products (identification by a single crystal X-ray unit cell determination) and may be ascribed to the presence of differing amounts of solvent (H_2O, DMF). Mass spectrometry was tried but even using the "gentle" ^{252}Cf PDMS technique no parent ions were observed.[127] As the fragments are the same in both cases no information was gained from these studies. Single crystal X-ray unit cell determinations can distinguish unambiguously between the various products; however, this gives rise to two further problems. Firstly, the bulk sample may not necessarily be the same as the single crystal analysed although in no case were different crystal morphologies observed in a single sample. Secondly, the recrystallisation step may result in a changed product. X-ray powder diffraction seems the obvious method to be used on any bulk sample as it can be matched against a predicted powder pattern derived from the single crystal X-ray data for the 4Mn or 5Mn structures. However, none of the experimentally determined patterns matched the predicted ones, possibly due to solvent loss, so the only conclusions which could be drawn were from comparisons of the experimentally determined spectra. One interesting observation was that the crystals initially obtained from the 5Mn reaction solution (Experimental Section) gave no powder diffraction pattern, possibly because the crystal lattice collapsed when the solvent molecules were lost.

The powder isolated from the 4Mn preparation (Experimental Section) gave the powder pattern shown in Figure 58. This pattern was also observed for other samples which had been shown to contain some 4Mn complex by single crystal X-ray unit cell determinations.

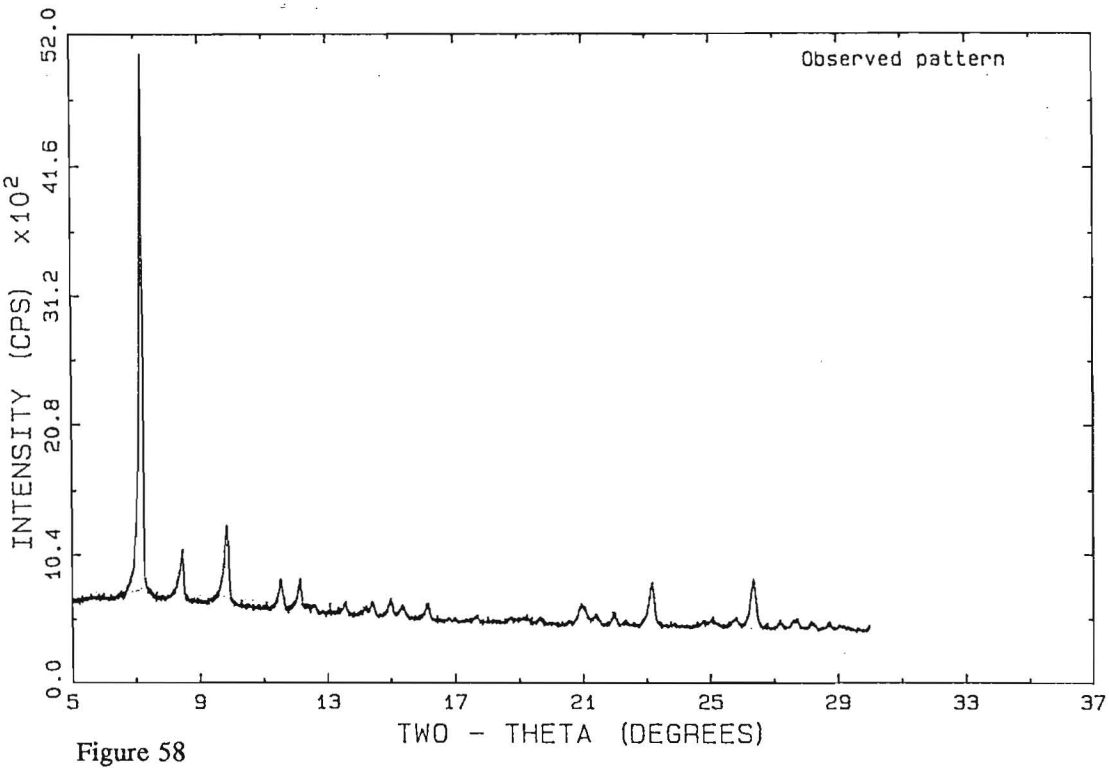

Figure 58

It seems likely that the polymeric structure of $Mn(CH_3COO)_2.4H_2O$ (Figure 59) is an important factor in determining which structure is isolated.[128] There are marked similarities between the manganese acetate structure and the central core of the 5Mn complex (Figures 44 and 45).

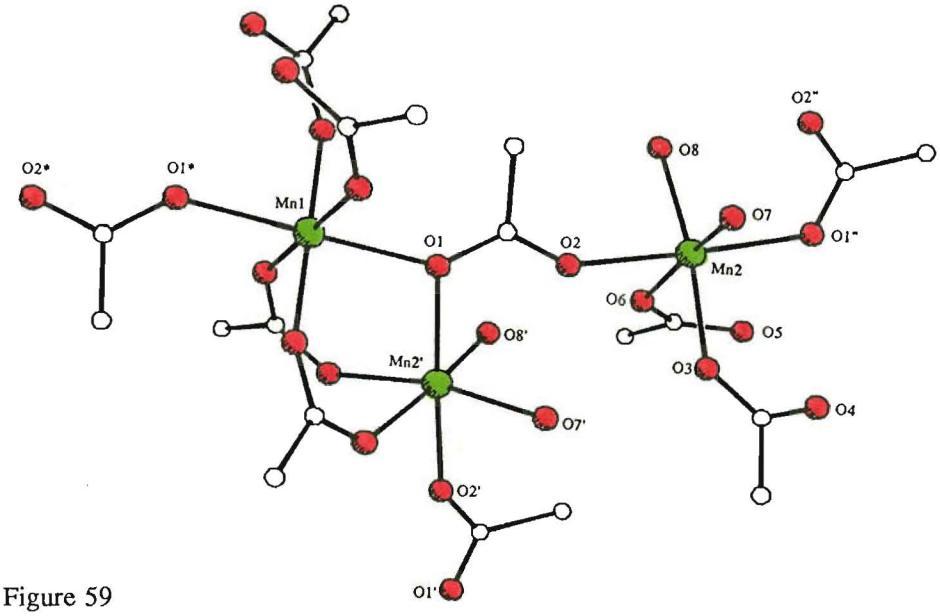

Figure 59

The two types of bridging acetate observed in the 5Mn complex are present; three atom bridges between two manganese atoms and acetate bridges over three

manganese atoms. It seems possible that when fragments of this manganese acetate structure persist in solution the 5Mn acetate structure is formed. The 4Mn complex may then result from either the 5Mn structure breaking down in a strongly coordinating solvent (e.g. DMF) or from smaller manganese acetate fragments being present during the transmetallation reaction. It is therefore quite possible that the products isolated initially are generally mixtures of both of these complexes. Recrystallisation of such mixtures will tend to give one complex, that is, fractional crystallisation will probably occur. To test the proposal that the degree of disintegration of the $Mn(CH_3COO)_2.4H_2O$ structure is important a series of reactions were carried out. The results are summarised in Table 15.

Table 15: Results of the variations in reaction conditions for the preparation of the manganese acetate complexes of H_2L1.

Mn:L1 Ratio	Pretreatment of Manganese Acetate	Reaction Volume/Time	Observations Identification	Product
5:2	Freshly dissolved 20 ml methanol	70 ml/1 hr	Crystals on cooling	% Mn 16.9†. Recryst. from $MeCN/Et_2O \rightarrow$ Figure 44 5Mn structure‡
5:2	Dissolved in 20 ml methanol 10 min prior to addition	70 ml/1 hr	Crystals on cooling	% Mn 16.4†. Recryst. from $MeCn/Et_2O \rightarrow$ Figure 44 5Mn structure‡
5:2	Dissolved in 20 ml methanol 5 days prior to addition	70 ml/1 hr	Crystals on cooling	% Mn 16.3†. Recryst. from $DMF/Et_2O \rightarrow$ Figure 45B 5Mn structure‡
2:1	Refluxed in 60 ml methanol for 105 min prior to addition	60 ml/3.5 hr	Thick ppt after after 30 min	Recryst. from $DMF/Et_2O \rightarrow$ Figure 43 4Mn structure‡

† Details of the manganese analysis procedure are given in A.I. Vogel, "A Textbook of Quantitative Inorganic Analysis" 3rd ed., Longman, London, 1972, 434. The unsolvated 5Mn structure should contain 16.6% Mn whereas the unsolvated 4Mn structure should contain 15.7% Mn.

‡ From a single crystal X-ray unit cell determination.

Dissolving the manganese acetate in methanol for up to 5.5 days before carrying out the reaction did not prevent 5Mn formation. However, when the solution was refluxed for 105 min first, only the 4Mn complex was identified. The Mn:L1 ratio was also different in this experiment, however, previous experiments with this ratio had yielded a 5Mn product. These observations are consistent with the above proposal. They also show that one recrystallisation from DMF/Et_2O yields the 5Mn complex with bound DMF. Several recrystallisations from a coordinating solvent like DMF may result in the 5Mn structure breaking down to the 4Mn structure, or perhaps down to a $[Mn_4(L1')(H_2O)_{1.6}(DMF)_3]^{4+}$ complex, as if the acetate anions dissociate to allow cubane formation they may also allow ring expansion to occur if left long enough in such solvents. Ring expansion seems unlikely as the 4Mn acetate complex gives an EPR signal which implies the presence of only polynuclear

species in DMF/toluene solutions (Figure 57D). These possibilities have not yet been tested.

EXAFS, XANES, Cyclic Voltammetry and Magnetic Susceptibility Studies

This series of complexes fulfils the OEC requirements of four manganese ions bridged by oxygen atoms and coordinated by oxygen and/or nitrogen donors. Variations in the number and type of the bridging groups has produced a valuable series of structural types.

The $[Mn_4(L1')](ClO_4)_4$ complex (Figure 19A) contains a fairly symmetrical Mn_4O_4 cubane core, with all of the Mn-Mn distances being very similar (Mn1-Mn2 3.330, Mn1-Mn1' 3.442, Mn1-Mn2' 3.334, Mn2-Mn2' 3.451 Å). This core is more symmetrical than that which occurs in the OEC (Section 1.2) however, the first two shells of scattering atoms (Figure 60)[129] do occur at approximately the same distance (after offsetting all distances by an arbitrary constant) as in the $\theta=15°$ oriented samples (Figure 5).

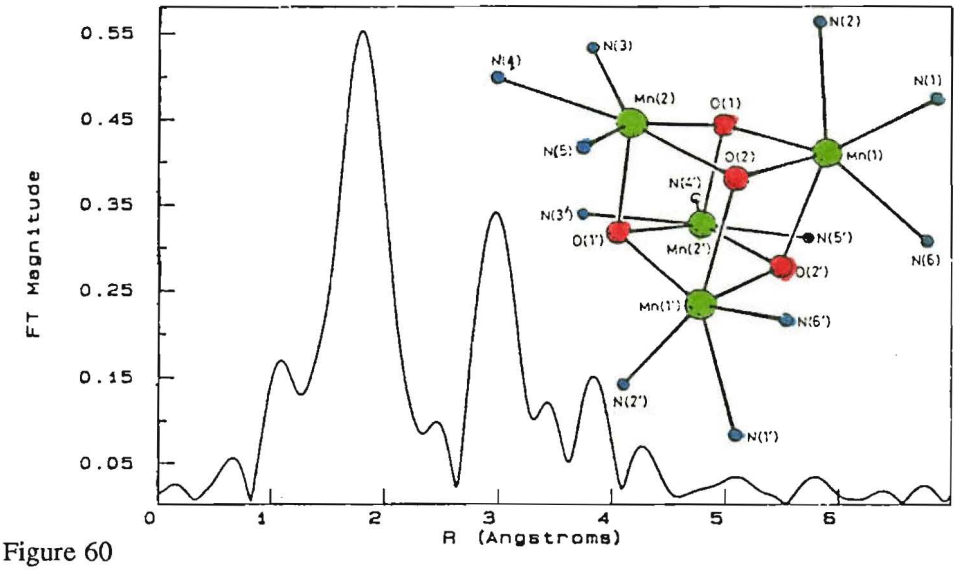

Figure 60

Likewise the acetate dimer (Figure 42) contains a slightly less symmetrical Mn_4O_4 core (Mn1-Mn2 3.158, Mn1-Mn1' 3.491, Mn1-Mn2' 3.470, Mn2-Mn2' 3.485 Å). A bigger variation in the Mn-Mn separations is observed in the chloride and azide complexes; for the chloride (Figure 38, Table 2) the values are 3.111, 3.127, 4.308 and 5.318 Å, while for the azide (Figure 39, Table 3) the values are 3.097, 3.103, 4.106, 4.199, 5.172 and 5.187 Å. The preliminary EXAFS results for the chloride complex are shown in Figure 61. The Mn-O/N, Mn-Cl, "short" Mn-Mn (3.1 Å) and "long" 4.3 Å Mn-Mn interactions all show up fairly clearly. This complex is of particular interest as an OEC model because of the presence of chloride ions. In this case the Mn-Cl interaction can be seen quite distinctly but if the Mn-Cl bonds were a little longer it could be difficult to distinguish this peak from the "short" Mn-Mn

peak. As this complex is much less symmetrical than the (Mn_4 O_4) cubanes it is of interest to examine oriented crystals. Suitable single crystals have been supplied to Cramer for study. The thiocyanate dimer has the least symmetrical arrangement of manganese atoms with the Mn-Mn separation varying from 3.134 to 5.768 Å. A sample of this complex will also be characterised by EXAFS.

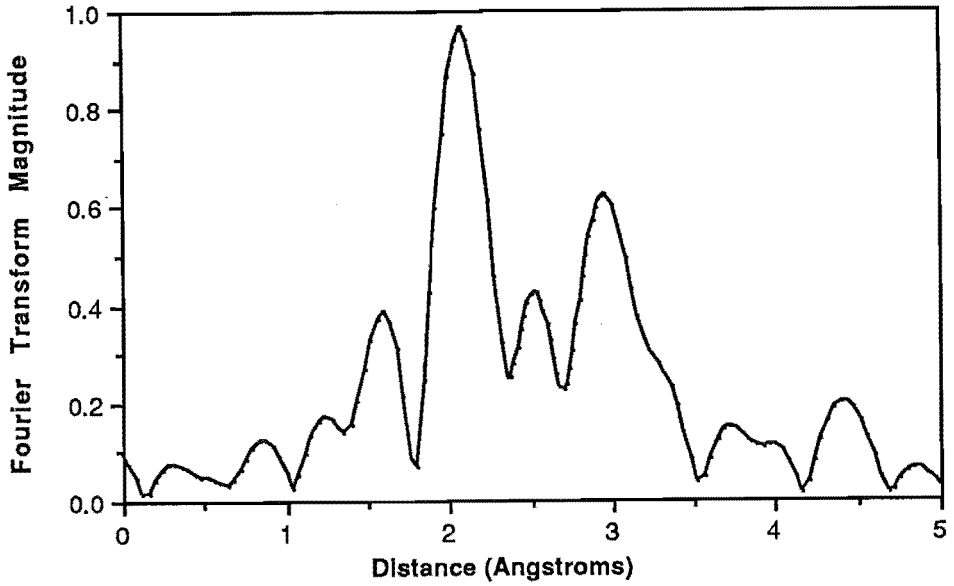

Figure 61

L-edge XANES spectra for the chloride and thiocyanate complexes are shown in Figure 62[129] along with two mixed-valence Mn(II)Mn(III) complexes.

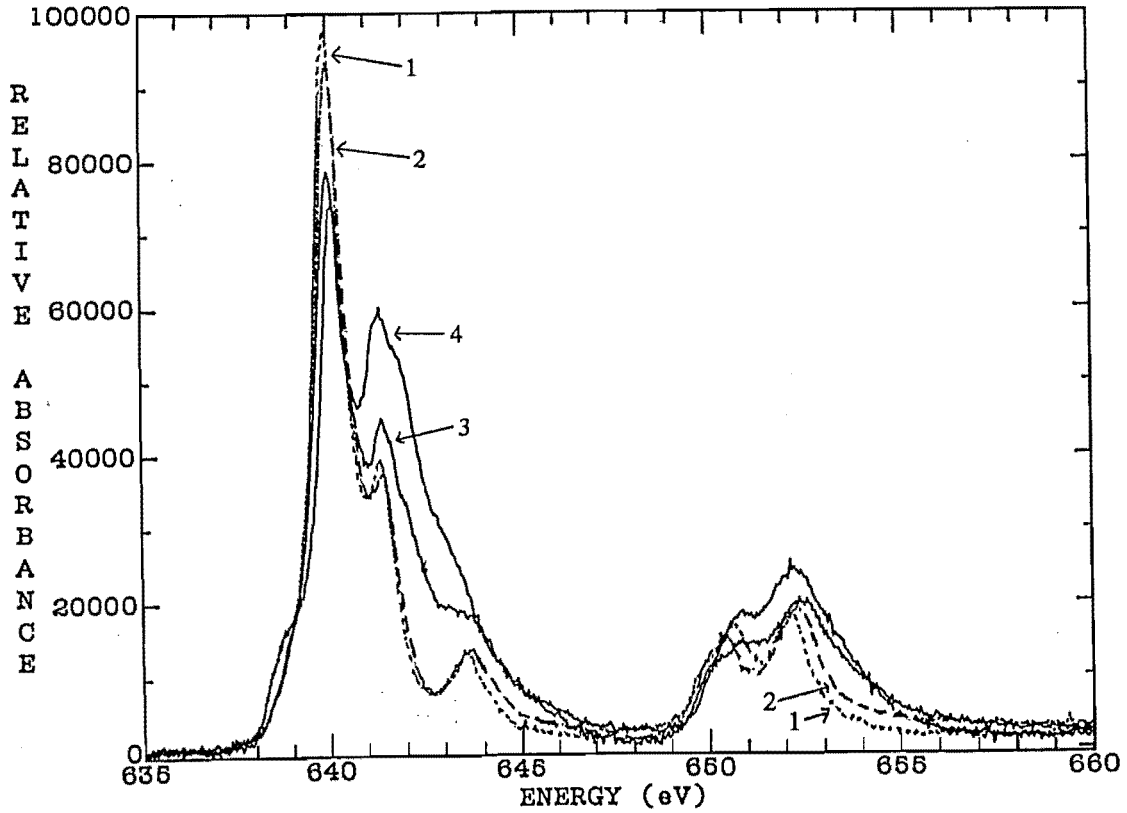

Figure 62: L-edge XANES for the chloride (1), thiocyanate (2) and two Mn(II)Mn(III) (3 and 4) complexes.

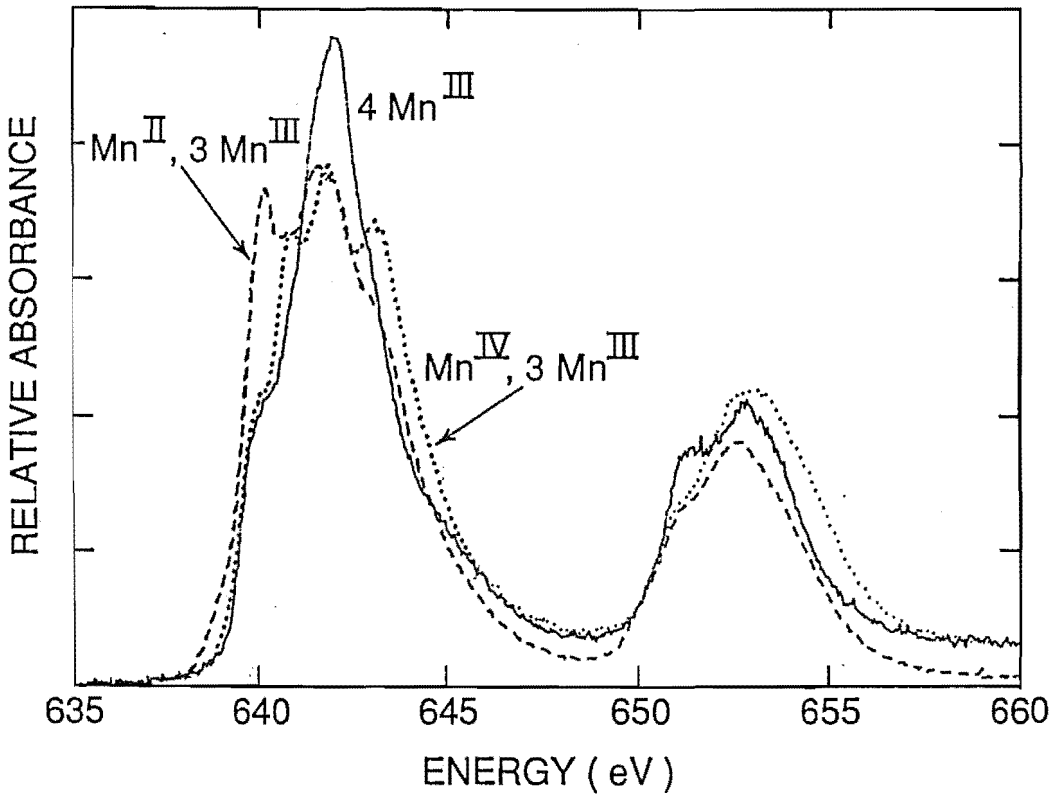

Figure 63

These results along with those for Christou's tetranuclear complexes (Figure 63)[32] show that L-edge spectra give well defined peaks which give a good indication of the oxidation states present.

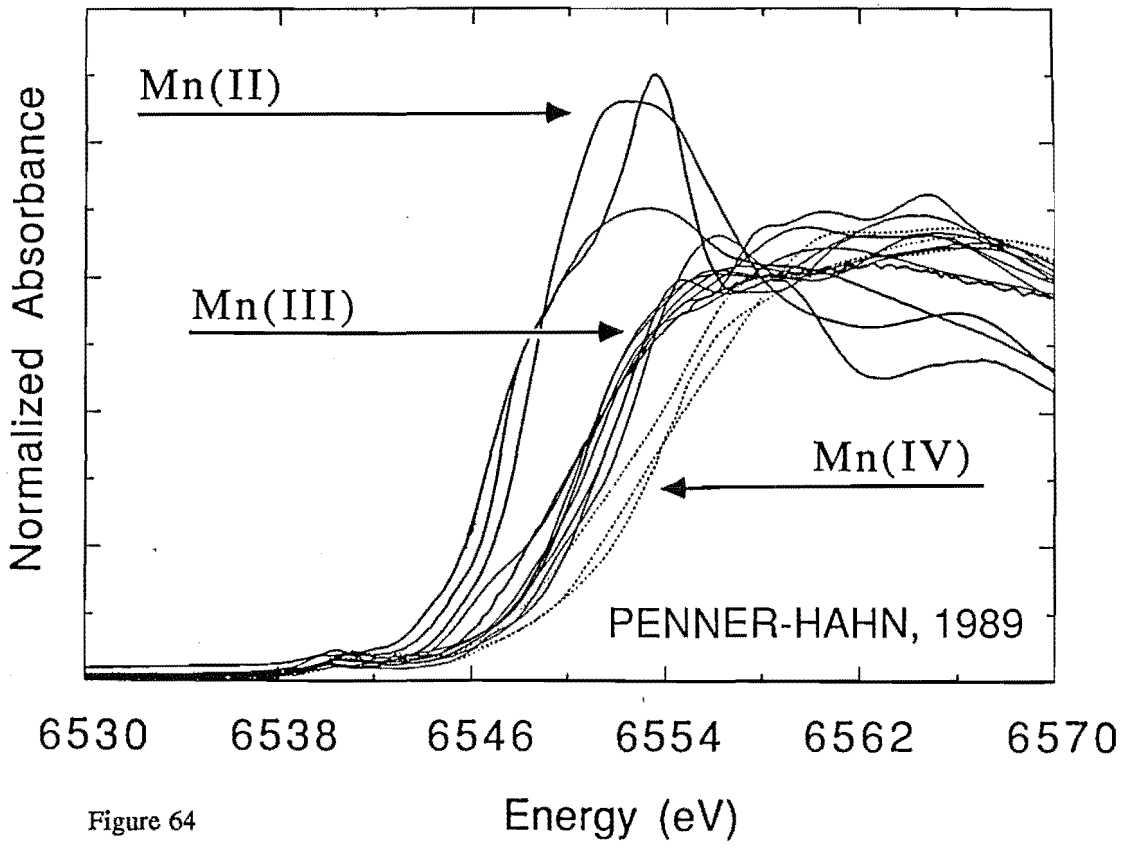

Figure 64

These results contrast with the broad features obtained from K-edge spectra (Figure 64).[32] The database Cramer is generating will be very useful when interpreting L-edge spectra of the OEC itself.

These tetramanganese complexes are good structural models for the OEC but they are all in the +II oxidation level which is too low to match the expected oxidation levels of the OEC (Table 1). These are, therefore, poor models for the spectroscopic properties of the photosynthetic system. Unfortunately, none of these complexes have been successfully oxidised. Cyclic voltammetric studies indicate that oxidation of the manganese ions occurs irreversibly. Attempts to oxidise these complexes chemically, using Ce(IV) or Br_2, have been equally unsuccessful to date, resulting only in tacky brown precipitates. The factor most likely to affect the oxidation process is the expected preference of Mn(III), d^4, for octahedral geometries rather than the existing pentagonal bipyramidal arrangement. This may lead to the imine links of the macrocycle being hydrolysed to allow such a change in geometry to occur. The isolation of the Mn(II)Mn(III) complex of L13 (in which there is no seven-coordination) supports the conclusion that the geometry is important (see the discussion of the mixed-valence tetramanganese complex of L13).

Latour and Tuchagues[126] have measured accurate magnetic susceptibility data as a function of temperature (300 to 5 K) for the chloride, azide, thiocyanate and perchlorate complexes. Tuchagues has partially analysed these results but the theoretical calculations are complex and require large amounts of computer time. Therefore, for all but the fairly symmetrical perchlorate [Mn_4O_4] cubane complex (Figure 19A)[62(b)] the rigorous calculations await the arrival of a new computer. Tuchagues repeated the published preparation of the perchlorate complex independently and published the results of the theoretical calculations and observed magnetic susceptibility as a function of temperature.[64] Because this complex is fairly symmetrical the calculations are a little simpler than for the other less symmetrical complexes which are under study. The reason that these theoretical calculations are so complex is that each manganese(II) ion has a large number of unpaired electrons (5) and there are four of them interacting with each other. Additionally, for four interacting manganese ions six J values can be defined. As an example these are shown on the perchlorate cubane in Figure 65. In this case the Mn-Mn distances fall in two groups which simplifies the problem somewhat because $J_1 \approx J_3 \approx J_5 \approx J_6 \neq J_2 \approx J_4$. Calculations with two J values were compared with (the further simplified) calculations using a single J value, and it was found that, in this instance, a single J value of -0.51 cm^{-1} modelled the data well. This represents a small antiferomagnetic interaction, however, the strongest reported antiferromagnetic coupling between two manganese(II) ions is only J = -4.5 cm^{-1}.[46(d),64]

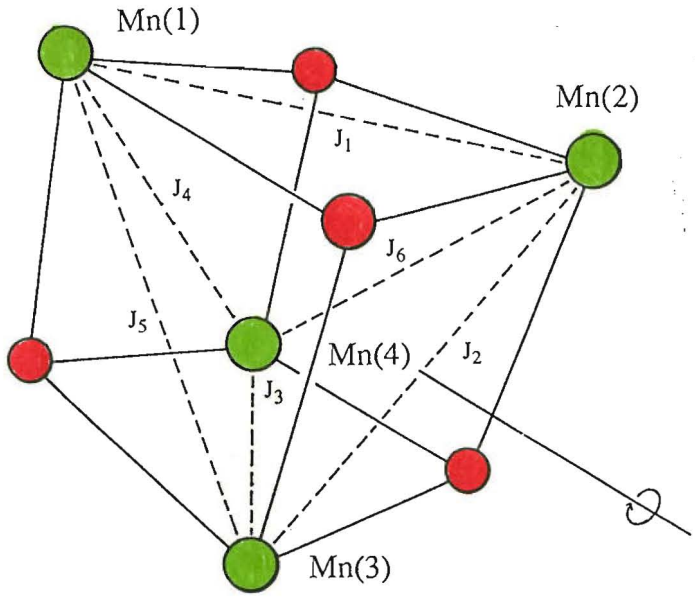

Figure 65

The variation in magnetic moment (per manganese) *vs* temperature for the chloride, azide, thiocyanate and $[Mn_4(L1')](ClO_4)_4$ complexes is shown in Figure 66. The detailed analysis of the less symmetrical chloride, azide and thiocyanate complexes has not been carried out yet, however, initial results indicate the presence of similar or slightly greater antiferromagnetic coupling than was found in the perchlorate complex.

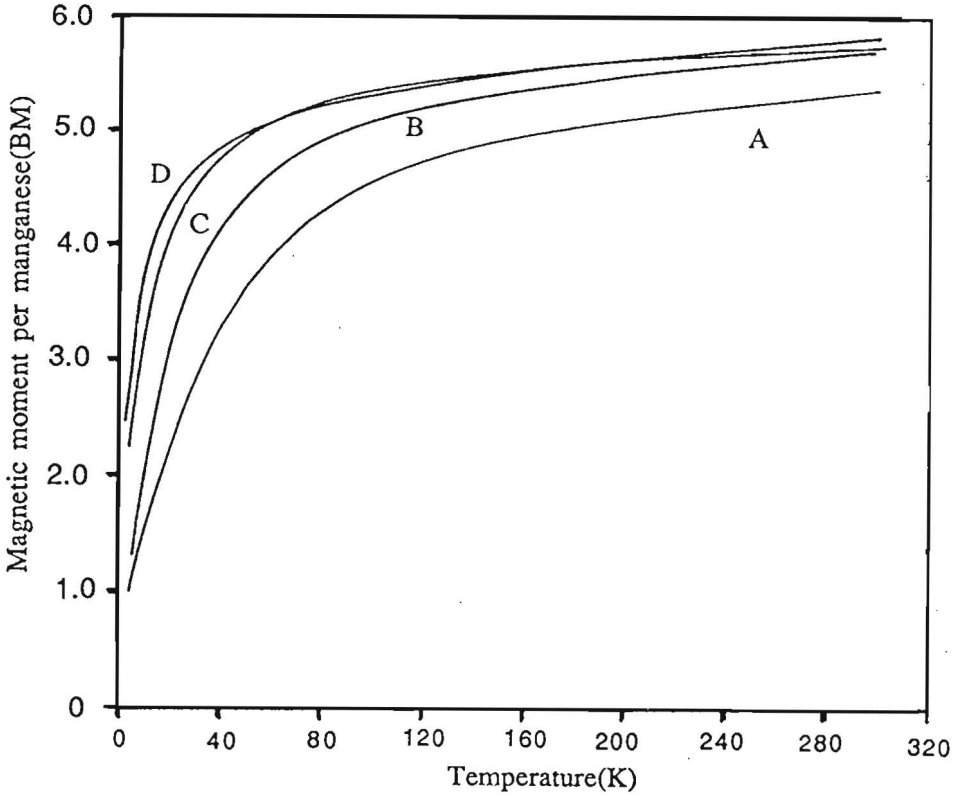

Figure 66: Magnetic susceptibility vs temperature for the chloride (A), azide (B), thiocyanate (C) and $[Mn_4(L1')](ClO_4)_4$ (D) complexes.

Concluding Comments

The manganese(II) chemistry of H_2L1 and H_4L1' described in this Chapter has been totally different to that observed for copper(II),[86,87] iron(II) and iron(III).[81] No other transition metal ions have been seen to promote the formation of dimeric H_2L1 complexes, or to allow the ring expansion to H_4L1 to occur. All of the copper(II) and iron(III) complexes of H_2L1 are dinuclear and monomeric. Iron(II) is an effective template for H_2L1 formation but iron(III) is not. Therefore it seems likely that iron(II) can accept the N_3O_2 pentagonal plane of donors provided by the H_2L1 or H_4L1' macrocycle. If this is so then combined with the similar ionic radii of manganese(II) and iron(II), 0.82 and 0.78 Å respectively,[76(a)] and the identical charge on the metal ions there seems to be no reason why very similar chemistry should not be observed. No iron(II) complexes have been characterised yet but the iron(III) compounds formed by air oxidation are binuclear and monomeric. It is possible that the unidentified iron(II) precursor is an $[Fe_4O_4]$ dimer-type of cluster which breaks in half upon oxidation to iron(III). The only obvious reasons for the d^5 iron(III) not paralleling the d^5 manganese(II) chemistry are the higher charge on the resulting clusters, and the smaller ion size of iron(III) 0.65Å compared to Mn(II) 0.82Å.[76(a)]

Pentagonal bipyramidal geometry is observed for all of the manganese(II) ions in complexes of H_2L1 and H_4L1' (except the 5Mn acetate structures which have a central octahedral manganese(II) ion). This geometry is not very common. Most other structurally characterised examples are complexes of more constrained ligands; either conjugated noncyclic ligands with five donor atoms in a planar geometry,[130,131,132,133] or smaller, more rigid macrocycles.[134,135,136,137] These are discussed further in Section 3.2. In this case the H_2L1 macrocycle is quite flexible; for example the Cu(II) complex has tetragonal geometry.[86,87] Therefore pentagonal bipyramidal geometry is not enforced by the H_2L1 ligand.

All of the manganese(II) complexes were orange in colour. The electronic spectra reveal ligand transitions (assigned by comparison with the barium(II) complex of H_2L1) at *ca.* 240 nm (*ca.* ε = 16,000) and 290 nm (*ca.* ε = 62,000). No bands could be unambiguously assigned to charge transfer transitions, although the absorption at 290 nm tails into the visible, possibly due to an underlying charge transfer transition. This tail gives rise to the observed orange colouration and is absent in the white barium complex.

Discussion of the Mixed-Valence Tetramanganese Complex of L13

It is interesting to compare the preparation of this mixed-valence tetramanganese complex with those of the complexes of H_2L1. While attempts to oxidise the tetramanganese complexes of H_2L1 were unsuccessful, removing the two alcohol functions from the alkyl chains to form the L13 macrocycle allows facile air oxidation of two Mn(II) centres to Mn(III). In all the tetramanganese(II) complexes of H_2L1 the two oxygen donors complete the pentagonal plane of coordination of the Mn(II) ions. As Mn(III) prefers octahedral geometries, the absence of these donors in the L13 macrocycle means that oxidation of Mn(II) is no longer disfavoured for geometrical reasons.

The central oxo ions are held quite close to each other (2.46 Å) and therefore this tetranuclear cluster can be thought of as model for an intermediate stage of the OEC water oxidation process; two water molecules have been bound to the cluster and deprotonated, but as yet no O-O bond has been formed. The hexairon(III) complexes characterised by Lippard (Figure 67) represent the water oxidation intermediates on either side of this manganese complex.[138]

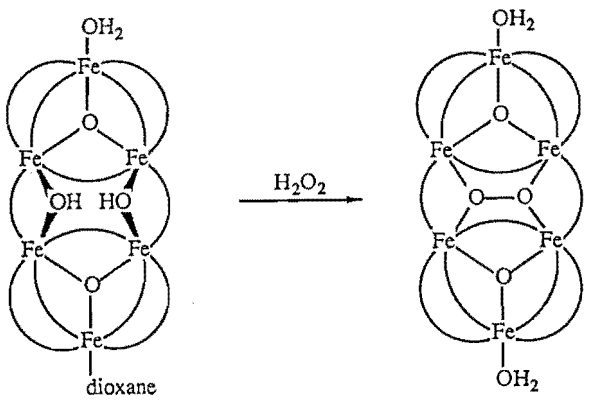

67A 67B

Figure 67

Complex 67A has the water bound and singly deprotonated. The O3-O4 separation of 2.46(1) Å is the same as is observed for the manganese complex. In the OEC cycle further deprotonation (bound oxo ions) would be followed by O-O bond formation giving bound peroxide as shown in 67B (Figure 67). 67B is generated in the laboratory from 67A by a simple ligand substitution reaction (one peroxide for two hydroxides). Consideration of these complexes prompted the proposal of the new OEC cycle shown in Figure 68.

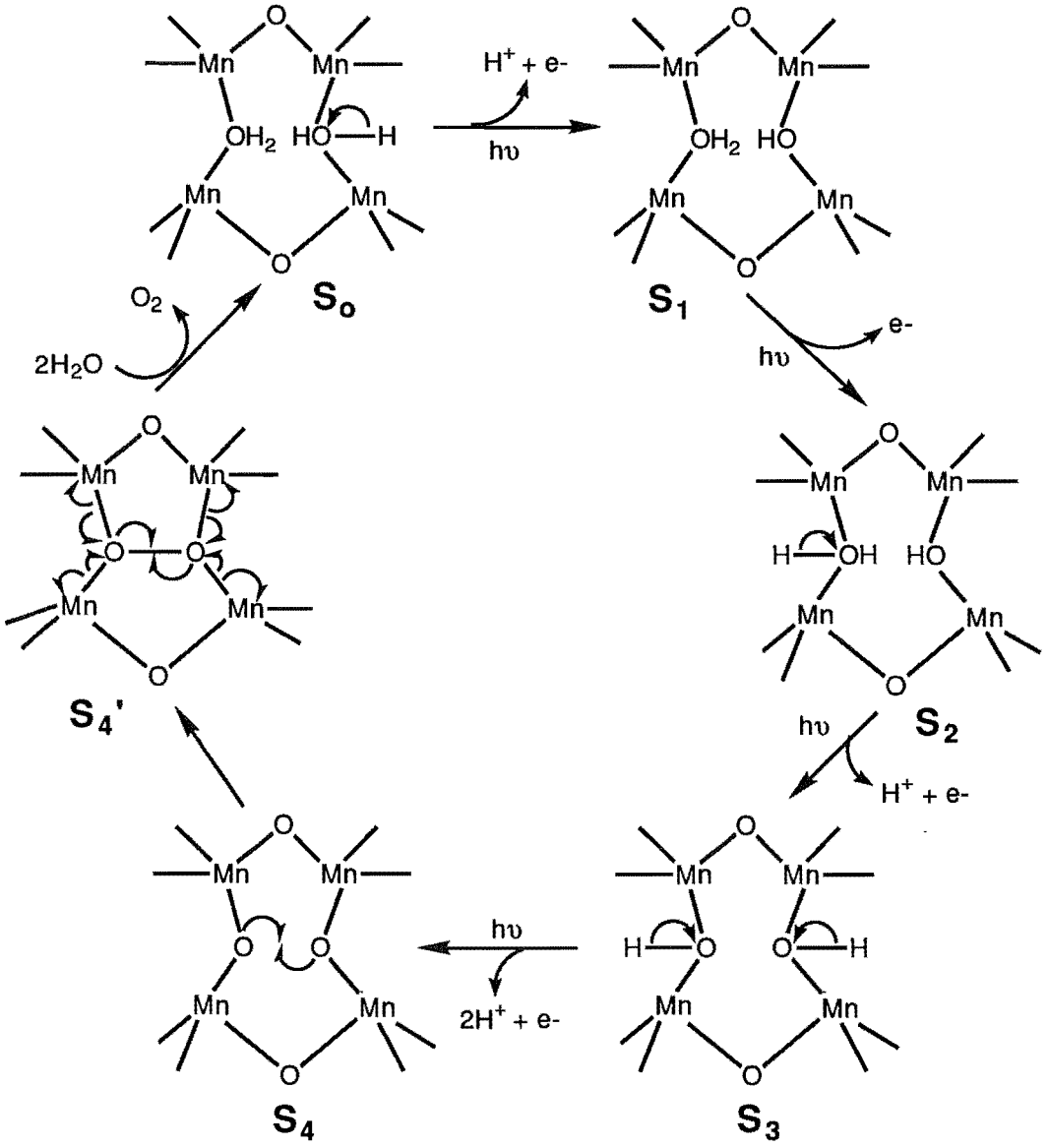

Figure 68

Four manganese ions are held in a tetranuclear cluster with oxygen bridging. The bound water (S_0) is deprotonated in several steps giving rise to the 1, 0, 1, 2 pattern of proton release observed for the OEC as $S_0 \rightarrow S_1$, $S_1 \rightarrow S_2$, $S_2 \rightarrow S_3$, $S_3 \rightarrow S_0$ (Section 1.2).No oxidation of the bound water molecules occurs until S_4; rather the oxidising equivalents are stored up in the form of more highly oxidised manganese centres (Table 1, set B). S_2 and S_3 have a positive surplus of charge relative to S_0 which may be balanced by coordination of chloride ions. These features are consistent with current data on the OEC (Section 1.2). 67A with the two bridging hydroxide ions represents the S_3 state, and 67B the S_4' state with bound peroxide. The manganese complex of L13 is a structural model for the proposed S_4 state, containing two bridging oxo ions. Very little movement is required during the oxidation of water by this proposed scheme.

More work is needed on this complex; the preparation needs to be refined, a bulk sample crystallised and further characterised by EXAFS, XANES, EPR, cyclic

voltammetry, magnetic susceptiblity, chemical reactivity and so on. This complex has the potential to produce many more exciting results.

Results and Discussion of Complexes of DAP and H_2L5

$[Mn(DAP)_2(H_2O)_2](ClO_4)_2$

Rather unusual eight-coordinate manganese(II) is a feature of this complex. In most structurally characterised examples eight-coordinate manganese(II) is observed when bi- or multidentate ligands[139] (e.g. bidentate nitrate[140] or acetate (Figure 22A)[69]) are bound. DAP acts as a tridentate ligand with a restricted bite angle which effectively compresses the coordination by these three donors thus allowing the larger coordination number. As manganese(II) is a d^5 ion there are no geometrical preferences to overcome.

$[Pb_2(H_2L5)(NCS)_3]NCS$

A very similar dilead complex of the related macrocycle L5' has been structurally characterised by Nelson, Drew and co-workers (Figure 69A).[116]

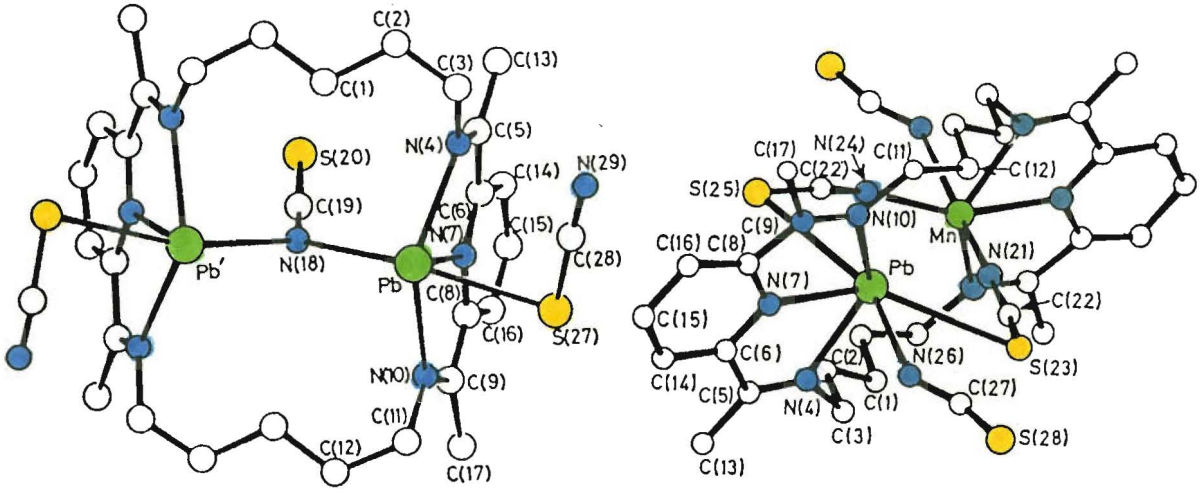

69A 69B

Figure 69

The L5' macrocycle differs from H_2L5 only in that it contains no pendant alcohol groups. As the alcohol groups of H_2L5 do not bind to the lead atom this has little effect on the overall structure. In both cases the N-bridging thiocyanate group is disordered about the C_2 axis. Such single atom N- only thiocyanate bridging is rare;[53,62(b),111,115,116] the L5' structure was the first involving lead. A more common mode of NCS^- bridging is the 1,3-bridging observed in the heterobinuclear $PbMn(L5')(NCS)_4$ structure (Figure 69B).[141] In this case the L5' macrocycle has a different conformation, allowing the metal-metal separation to increase to 4.857(2)Å.

There are slight geometrical differences between the two dilead structures of H_2L5 and L5', which are summarised in Figure 70.

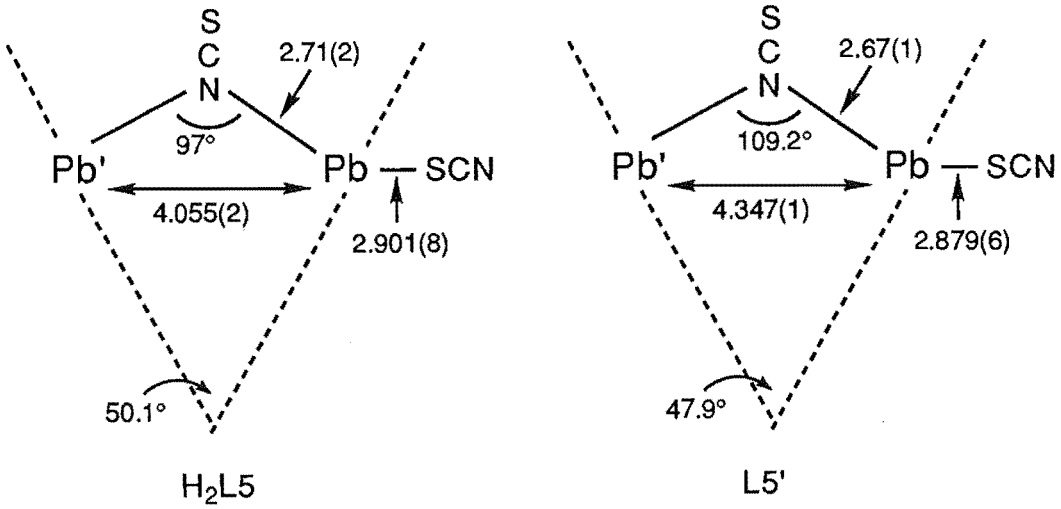

Figure 70

The L5' macrocycle is slightly more folded which allows greater separation of the lead atoms. In the L5' structure the N-bridging thiocyanate and terminally S-bonded thiocyanate are both more tightly bound than in the H_2L5 case. These differences in bonding are reflected in the infrared spectra of these two complexes. As expected more tightly bound thiocyanate groups of the L5' complex give rise to absorptions at lower energy; N-bridging NCS H_2L5 1983 cm^{-1} → L5' 1970 cm^{-1} and S-terminal NCS H_2L5 2060 cm^{-1} → L5' 2019, 2041 cm^{-1}. The remaining absorption in this region is assigned to the uncoordinated (fourth) thiocyanate ion; H_2L5 2083 cm^{-1} and L5' 2084 cm^{-1}. The unusually low energy thiocyanate absorption at $\leq$ 2000 cm^{-1} is thought to be a characteristic of single atom N-bridging thiocyanate.[53,111,115] The infrared data on $[Pb_2(H_2L5)(NCS)_3]NCS$, though in agreement with that of Nelson, do not match the values (2000, 2025 and 2070 cm^{-1}) reported by Fenton, Drew and co-workers for a dilead complex of the same macrocycle with the same anions and stoicheiometry.[80] It is difficult to see why there would be any difference in the thiocyanate geometries and hence the reason for the substantial discrepancy is not clear. As stated in the Experimental Section the fourth anion was not located in the structural analysis of $[Pb_2(H_2L5)(NCS)_3]^+$ as it appeared to be severely disordered. It is interesting to note that similar difficulties were experienced in the structure determination of the L5' complex by Nelson, Drew and co-workers, who comment that the fourth thiocyanate anion was "not located with any certainty". A cylinder of electron density was observed *ca.* 3.5Å from the lead atom and two tightly constrained, quarter occupancy NCS^- groups were fitted inside it. This, and the symmetry related cylinder, accounted for the final NCS^- anion. In the H_2L5 structure a region of remaining electron density was located in a position similar to the L5' case, relative to the macrocycle. No significant electron density was found within 3.1Å of the lead atom. It was not considered worthwhile to try to force a

constrained, disordered NCS^- group to this remaining electron density. From the infrared absorption at 2083 cm^{-1} and comparisons with the data on L5' it appears that there must be a free thiocyanate ion in the structure (rather than a perchlorate ion due to the method of preparation).

Chapter 3

COMPLEXES OF THE ARM LIGANDS

3.1 Experimental

Preparation of Free Ligands

HL3

Initially this was prepared by the method of Johnson *et al.*[142] 2-Pyridinecarbaldehyde (0.68 g, 0.0064 mol) dissolved in benzene (20 ml) was added to a mixture of ethanolamine (0.40 g, 0.0065 mol) and benzene (60 ml). The resultant mixture was brought to reflux and the azeotrope removed until no further water was produced. Evaporation of the remaining benzene under reduced pressure left a yellow oil which was pumped *in vacuo* overnight. Occasionally the oil solidified overnight to give white crystals. The oil was used promptly without further purification. Yield 0.95 g, 6.3 mmol, 99%

HL3 can also be obtained by simply adding equimolar amounts of 2-pyridinecarbaldehyde and ethanolamine together in a small volume of methanol. Evaporation of the solvent overnight followed by pumping *in vacuo* yielded the same yellow oil. The addition of one drop of 70% $HClO_4$ to this reaction had no effect on the reaction.

Infrared spectrum *inter alia* 3280(m,b), 2880(m,b), 1650(m), 1590(m) cm^{-1}

Electronic spectrum (CH_3OH) λ_{max} = 273 nm, ε = 5,600; λ_{max} = 234 nm, ε = 10,000; λ_{max} = 197 nm, ε = 17,500

NMR spectra ($CDCl_3$):

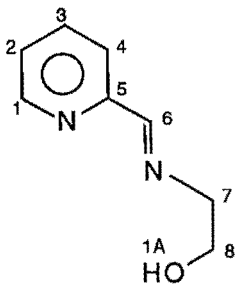

^{1}H H1 8.61(dd); H2 7.30(m); H3 7.71(m); H4 7.90(dd); H6 8.40(s); H7 3.95(m); H8 3.83(m) ppm.
These were assigned using homonuclear decoupling experiments and ^{1}H-^{1}H homonuclear two-dimensional correlation spectroscopy.

^{13}C C1 149.27; C2 124.75; C3 136.50; C4 121.39; C5 153.88; C6 163.42; C7 63.26; C8 61.95 ppm.
These assignments were confirmed using ^{1}H-^{13}C heteronuclear two-dimensional correlation spectroscopy.

(L3')ClO_4 or (L3')(p-$CH_3C_6H_4SO_3$)

Several methods of obtaining $(L3')^+$, that is the 2-(2-hydroxyethyl)-3-(2-pyridyl)-imidazo[1,5-a]-pyridinium cation, as either a perchlorate or p-toluenesulphonate salt, follow:

Method 1: Ethanolamine (0.29 g, 4.8 mmol) was brought to reflux in 15 ml of ethanol. Pyridinecarbaldehyde (0.5 g, 4.7 mmol) in 10 ml of ethanol was added dropwise followed by $HClO_4$ (0.67 g 70% $HClO_4$, 4.7 mmol) in ethanol (10 ml). The resulting yellow solution deepened to a gold colour as it was refluxed for 2.5 hr. After cooling and evaporation of solvent (over a period of hours) discoloured yellow-brown crystals were filtered from the green-yellow solution. Further crops were obtained after more evaporation of solvent. Yield 0.32 g, 0.9 mmol, 40%.

Method 2: p-Toluenesulphonic acid (0.9 g, 4.7 mmol) in 10 ml ethanol was added to the pyridinecarbaldehyde (0.5 g, 4.7 mmol, in 10 ml of ethanol) solution, and the combination dripped into a refluxing ethanol (15 ml) solution of ethanolamine (0.29 g, 4.8 mmol). The red-gold solution was refluxed for 2.5 hr after which it was yellow-brown in colour. This solution slowly evaporated down to an oil which was pumped *in vacuo*. Addition of MeCN allowed some of the amine p-toluenesulphonate salt byproduct to be filtered off. Evaporation and pumping *in vacuo* left (L3')(p-toluenesulphonate) as a gold oil contaminated with some amine salt. Approximate yield (subtracting the amine salt from NMR ratio) 0.34 g, 0.8 mmol, 34%.

Method 3: 2-Pyridinecarboxaldehyde (1g, 9.3 mmol) dissolved in ethanol (20ml) was slowly added to a refluxing ethanol solution of ethanolamine (0.58g, 9.5 mmol in 30ml), $Mn(ClO_4)_2$ .6HO (3.41g, 9.4 mmol) in ethanol (20 ml) was added and refluxing continued for 2.5 hr. On cooling and evaporation of solvent (over several weeks) a crystalline product was obtained. Yield 0.6 g, 1.8 mmol, 38%. Recrystallisation from methanol by diethylether diffusion yielded colourless crystals of X-ray quality.[143]

Infrared spectrum *inter alia* 3540(m), 1660(w), 1590(m), 1560(m), 1100(s,b)
Electronic spectrum (CH_3CH_2OH) λ_{max} = 315 nm, ε = 11,300; λ_{max} = 204, ε = 36,000

Density (by flotation in $CHCl_3/CCl_4$) 1.52 g cm^{-3}

NMR spectra ($CDCl_3$):

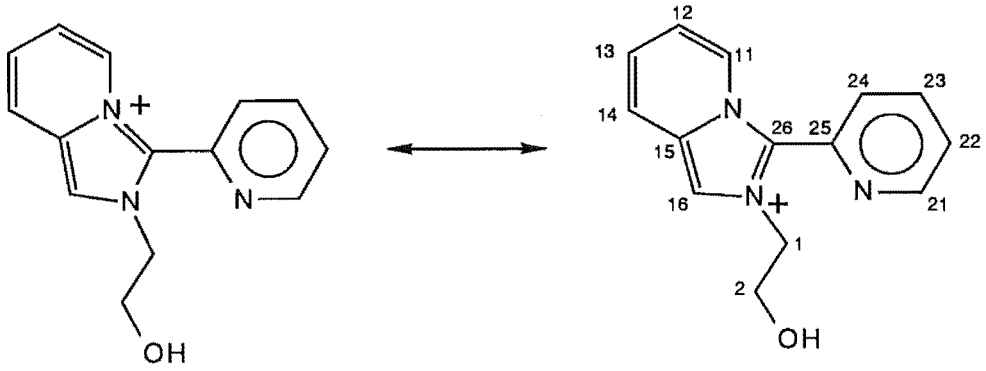

^1H H1 3.97(t); H2 4.68(t); H11 8.53(bd), J=7.5; H12 7.20(bt), J=7.0; H13 7.38(bdd), J=9.3, 6.6; H14 7.91(bd), J=9.3; H16 8.35(s); H21 8.95(bd),J=5.0; H22 7.75(ddd)J=7.7, 4.9, 1.3; H23 8.20(td), J=7.7, 1.7; H24 8.12(bd) ppm, J=7.7, 1.7 Hz

These were assigned using homonuclear decoupling experiments.

^{13}C C1 53.93; C2 61.79; C11 124.14; C12 119.97; C13 126.88; C14 119.84; C16 116.46; C21 152.70; C22 128.04; C23 139.87; C24 128.68 ppm

The assignments of these complex spectra were confirmed using ^1H-^{13}C heteronuclear two-dimensional correlation spectroscopy:

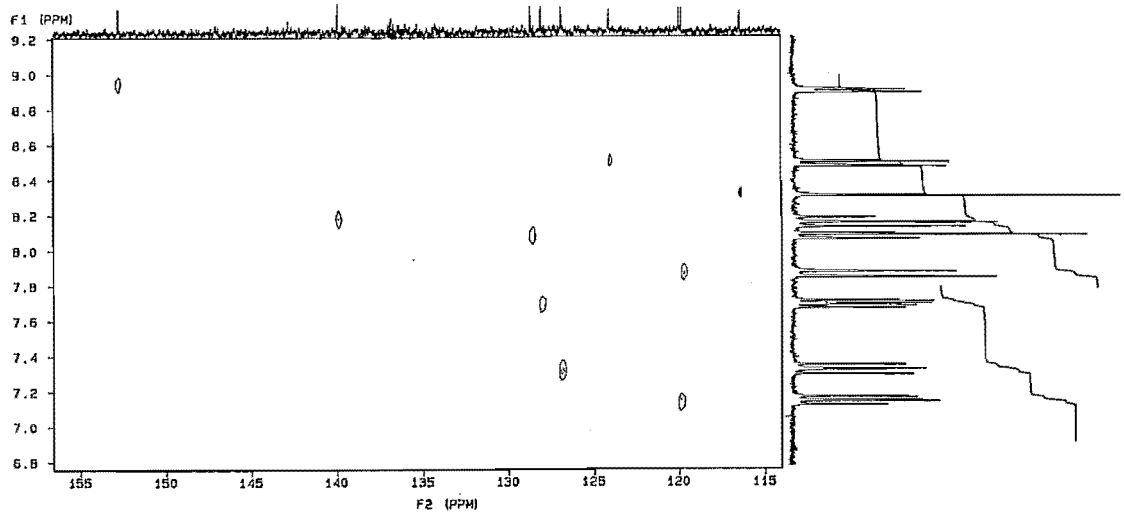

$[H_4L12]_2(ClO_4)_2Cl_2$

2,6-Pyridinedicarboxylic acid chloride (0.49 g, 2.4 mmol) was dissolved in 50 ml of benzene and ethanolamine (0.57 g, 9.3 mmol) was added, followed by a further 200 ml of benzene. This mixture was refluxed for 20 min (removing the benzene/water azeotrope) by which time the reaction volume had been reduced to 50 ml. The benzene solution was decanted off the undissolved brownish oil. The oil was washed with benzene and then dried by evaporation under reduced pressure. After standing for five days the oil solidified. This off-white solid was dissolved in

20 ml of warm methanol and $NaClO_4.H_2O$ (0.84 g, 6.0 mmol, 25% excess) added, followed by three drops of 70% $HClO_4$. Overnight colourless crystals formed. Yield 0.32 g, 0.8 mmol, 34%.

Infrared spectrum *inter alia* 3490(s,b), 3350(s,b), 1655(s,b), 1100(s,b) cm^{-1}.

Analysis Calculated: C 33.9; H 4.4; N 10.8%

Found: C 33.9; H 4.3; N 10.9%

NMR spectra (D_2O) :

H_2L12 is

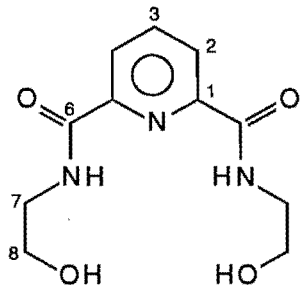

^1H H2, H3 8.08(m); H7 3.51(t); H8 3.72(t) ppm

^{13}C C1 148.82; C2 125.77; C3 140.66; C7 42.43; C8 60.91 ppm

These assignments were confirmed using ^1H-^{13}C heteronuclear two-dimensional correlation spectroscopy.

Preparation of Complexes of H_2L2

$[Mn(H_2L2)(H_2O)_2](ClO_4)_2$

DAP (1 g, 6.1 mmol) and $Mn(ClO_4)_2.6H_2O$ (2.22 g, 6.1 mmol) in 50 ml of ethanol were brought to reflux. Ethanolamine (0.75 g, 12.2 mmol) in ethanol (10 ml) was added and refluxing continued for 10 hr. A yellow powder formed after some solvent had evaporated and was collected by filtration. Further solvent evaporation led to the formation of yellow crystals suitable for a single crystal X-ray structure determination. Yield 1.9 g, 3.53 mmol, 60%.

Infrared spectrum *inter alia* 3310(s,b), 1650(m), 1610(m), 1590(m), 1100(s,b) cm^{-1}

Analysis Calculated: C 29.0; H 4.3; N 7.8 %

Found: C 29.2; H 4.4; N 7.9 %

$Mn(H_2L2)(NCS)_2$

This complex was made as for $Mn(H_2L2)(H_2O)_2](ClO_4)_2$ but in methanol (30 + 10 ml) rather than ethanol. After refluxing overnight, NaNCS (1.0 g, 12 mmol) was added to the gold coloured solution. After a further 15 min reflux the solution was allowed to cool and the resulting yellow precipitate was collected by filtration. Further crops including yellow crystals suitable for single crystal X-ray structural analysis were obtained after solvent evaporation. Yield 1.65 g, 3.93 mmol, 65%.

Infrared spectrum *inter alia* 3350(s,b), 2080(m), 2015(s), 1650(m), 1590(m) cm^{-1}

Magnetic moment (293K) = 5.99 BM

Analysis Calculated: C 42.9; H 4.5; N 16.7%

Found: C 42.7; H 4.5; N 16.8%

$Mn(H_2L2)(N_3)_2$

DAP (0.5 g, 3.1 mmol) and $Mn(ClO_4)_2.6H_2O$ (1.11 g, 3.1 mmol) were brought to reflux in 55 ml of methanol. Ethanolamine (0.38 g, 6.2 mmol) in methanol (5 ml) was added and the orange solution refluxed for 30 min before addition of a suspension of sodium azide (0.39 g, 6.2 mmol) in methanol (20 ml). The clear orange-brown solution was refluxed a further hour after which time the solution was again orange. Orange needles crystallised as the solution cooled slowly, but they proved to be twinned. A good single crystal for X-ray structural analysis was obtained after slow evaporation of the solvent. Yield 0.64 g, 1.65 mmol, 55%.

Infrared spectrum *inter alia* 3190(s,b), 2045(s), 1655(m), 1595(m) cm^{-1}

Analysis Calculated: C 40.2%; H 4.9%; N 32.5%

Found: C 40.0%; H 4.9%; N 32.2%

$[Co(H_2L2)_2](ClO_4)_3$

DAP (1 g, 6.1 mmol) and $Co(ClO_4)_2.6H_2O$ (2.24 g, 6.1 mmol) dissolved in methanol (40 ml) were brought to reflux. Ethanolamine (0.75 g, 12.2 mmol) in methanol (20 ml) was added causing the pink solution to turn dark brown. The solution was refluxed for 6 hr, cooled, and the dark brown product collected by filtration the following day. Further crops were obtained after solvent evaporation. Recrystallisation by vapour diffusion of diethylether into MeCN solutions gave brown crystalline material, yield *ca.* 0.5 g, 0.6 mmol, 20%.

Infrared spectrum *inter alia* 3350(m,b), 1590(m), 1085(s,b) cm^{-1}

Magnetic moment (293K) = 0.84 BM

Electronic spectrum (DMF) λ_{max} = 424 nm, ε = 3,300; plus further bands in the u.v.

Analysis Calculated for $[Co(H_2L2)_2](ClO_4)_3.0.5$ MeCN:

C 37.0; H 4.5; N 10.4%

Found: C 37.2; H 4.5; N 10.1%

FAB ms $[Co(H_2L2)(HL2)(ClO_4)]^+$ m/e = 656 a.m.u.

$[Ni(H_2L2)_2](ClO_4)_2.H_2O$

DAP (1 g, 6.1 mmol) and excess ethanolamine (1.75 g, 28.7 mmol) were refluxed in a benzene/dry methanol mixture, removing the azeotrope, for many hours. Most of the excess ethanolamine separated from the final benzene (only) solution allowing it to be removed. This preparation of H_2L2 (infrared spectrum showed only a small $\upsilon_{C=O}$) was used immediately in the following reaction.†

$Ni(ClO_4)_2.6H_2O$ (0.75 g, 2.1 mmol) in 15 ml dry methanol was added to free H_2L2 (2.1 mmol) in 15 ml benzene. The resulting clear yellow brown solution was stoppered and allowed to stand for two days. After evaporating the solution down to 10 ml under reduced pressure isopropanol was added until the solution became cloudy. Then benzene and methanol were added until the solution cleared again. Slow evaporation over two months yielded red-brown crystals suitable for a single crystal X-ray structural determination, in a brown oil.

Infrared spectrum *inter alia* 3370(s,b), 1635(w), 1585(m), 1100(s,b) cm^{-1}

Electronic spectrum (CH_3OH) λ_{max} = 804 nm, ε = 40; λ_{max} = 242 nm, ε = 3,000; λ_{max} = 204 nm, ε = 3,800

FAB ms $[Ni(H_2L2)_2]ClO_4^+$ m/e = 655 a.m.u.

†Many attempts to obtain a reproducible preparation of this free ligand failed. Two reasons for this difficulty are: firstly the imine bonds formed are not stable and readily hydrolyse to give back the starting materials, and secondly the ketone carbonyl is not as reactive as (for example) the aldehyde which readily formed HL3.

$[Ni(H_2L2)(NCS)_2]_2$

$Ni(ClO_4)_2.6H_2O$ (2.46 g, 6.7 mmol) in methanol (10 ml) was added to a refluxing methanolic solution (50 ml) of DAP (1 g, 6.1 mmol). This was followed by the dropwise addition of ethanolamine (0.75 g, 6.1 mmol) in methanol (5 ml), and finally the addition of NaNCS (1.10 g, 13.6 mmol) in methanol (15 ml). The resulting mid-green solution was refluxed for 3 hr over which time the solution became darker green. The solution was allowed to cool slowly and the green crystalline solid which precipitated was collected by filtration. Further crops were obtained after slow evaporation of the solvent. Yield 0.76 g, 1.8 mmol, 30%. Recrystallisation from DMF containing excess NaNCS in ethanol, by vapour diffusion of diethylether, produced green plates suitable for a single crystal X-ray structure determination.

Infrared spectrum *inter alia* 3300(m,b), 2090(s), 1640(m), 1595(m) cm^{-1}

Electronic spectrum (DMF) $\lambda_{max} \approx$ 885 nm, ε = 70; λ_{max} = 585 nm, ε = 40; plus further bands in the u.v.

Analysis Calculated: C 42.5; H 4.5; N 16.5%

Found: C 42.6; H 4.6; N 16.2%

Preparation of Complexes of HL3

$(L3')ClO_4$ and $Mn(HL3)(NCS)_2$ and $[Mn(HL3)(NCS)_2]_x$

HL3 (0.5 g, 3.3 mmol) in ethanol (5 ml) was added dropwise to an ethanolic solution (5 ml) of manganese(II) perchlorate (1.21 g, 3.3 mmol). A solution of sodium thiocyanate (0.54 g, 6.7 mmol) in 8 ml ethanol was added, followed by 5 ml of

isopropanol. A mixture of products was obtained on rapid evaporation (by maintaining an air flow over the solution) of the solvents. The yellow-brown solid formed was physically separated from some green oil. Crystals of (L3')ClO_4 (1%) were obtained by vapour diffusion of diethylether into a methanol solution of the green oil. The acetonitrile-soluble portion of the yellow-brown solid yielded poor quality crystals by vapour diffusion of diethylether into the acetonitrile solution. A recrystallisation by the same method using methanol/diethylether gave yellow crystals (1%) identified as $Mn(HL3)_2(NCS)_2$ by a single crystal X-ray structure determination. The golden crystalline material left undissolved by acetonitrile was readily soluble in methanol and was recrystallised by vapour diffusion of diethylether to give clusters of yellow crystals of the polymer $[Mn(HL3)(NCS)_2]_x$. Elemental analysis (results below) indicated the purity of this yellow crystalline polymer (*ca.* 20% yield calculated on $[Mn(HL3)(NCS)_2]_x$).

Infrared spectra for:

$Mn(HL3)_2(NCS)_2$ *inter alia* 3440(m,b), 2070(s,b), 1645(w), 1590(m) cm^{-1}

$[Mn(HL3)(NCS)_2]_x$ *inter alia* 3360(m,b), 2080(s,b), 1650(w), 1595(m) cm^{-1}

$[Mn(HL3)(NCS)_2]_x$	Analysis	Calculated:	C 37.4; H 3.1; N 17.4%
		Found:	C 37.8; H 3.2; N 17.4%

$[Ni(HL3)_2](ClO_4)_2$

HL3 (0.5 g, 3.3 mmol) in methanol (10 ml) was added dropwise to a green methanolic solution (10 ml) of $Ni(ClO_4)_2.6H_2O$ (1.22 g, 3.3 mmol). Isopropanol (6 ml) was added to the resulting dark yellow-brown solution and it was put aside to allow slow evaporation of the solvents. When almost all the solvent had evaporated a yellow-brown crystalline precipitate was isolated and washed with isopropanol (10 ml). Yield 0.36 g, 0.65 mmol, 40%. Recrystallisation by vapour diffusion of diethylether into a methanol solution of this complex yielded clusters of yellow-brown needles of poor quality; however a single crystal X-ray structure determination was carried out.

Infrared spectrum *inter alia* 3350(s,b), 1660(m), 1605(m), 1085(s,b) cm^{-1}

FAB ms $[Ni(HL3)_2(ClO_4)]^+$ m/e = 457 a.m.u

$[Cu(HL3)(H_2O)_2(ClO_4)]_2(ClO_4)_2$

A methanol solution (5 ml) of HL3 (1 g, 6.7 mmol) was added dropwise to a light blue solution of $Cu(ClO_4)_2.6H_2O$ (2.48 g, 6.7 mmol in 5 ml of methanol), causing a green colour to develop. A small amount of isopropanol was added and the solution evaporated quickly at room temperature in a fumehood. The resulting green solid was collected and washed with 20 ml of isopropanol, leaving an aqua blue crystalline compound which was dried *in vacuo*. Yield 0.99 g, 1.1 mmol, 33%.

A crystal suitable for X-ray structural analysis was obtained from a similar preparation (70% scale) using 25 ml of a 1:1 mixture of dichloromethane:methanol as the reaction solvent. After most of the solvent had evaporated nothing had precipitated so a little toluene was added and further evaporation allowed. The resulting clusters of aqua blue crystals were filtered off and washed with methanol.
Infrared spectrum *inter alia* 3310(m,b), 1650(w), 1605(m), 1100(s,b) cm^{-1}
Magnetic moment (293 K) = 1.88 BM
Analysis calculated for $[Cu(HL3)(H_2O)_2]_2(ClO_4)_4.2H_2O$:

C 20.6; H 3.4; N 6.0%

Found: C 20.2; H 3.1; N 5.8%

$[Zn(HL3)(H_2O)_2(ClO_4)]_2(ClO_4)_2$

This complex was prepared in the same way as $(L3')ClO_4$ except that the scale was halved and $Zn(ClO_4)_2.6H_2O$ (1.75 g, 4.7 mmol) was substituted for $Mn(ClO_4)_2..6H_2O$. On cooling and evaporation of the solvent over several weeks a pinkish-white crystalline solid was obtained. This was collected by filtration and washed with a very small amount of methanol followed by chloroform. Further solvent evaporation from the filtrate resulted in a golden oil which, on pumping *in vacuo*, produced crystals of $[Zn(HL3)]_2(ClO_4)_4$ as colourless blocks which were suitable for single crystal X-ray structural analysis. These crystals were hygroscopic and redissolved if left exposed to the atmosphere overnight. Overall yield 0.78 g, 0.9 mmol, 38%.
Infrared spectrum *inter alia* 3400(m,b), 1650(w), 1590(m), 1100(s,b) cm^{-1}
Analysis Calculated: C 21.3; H 3.1; N 6.2%

Found: C 21.1; H 3.0; N 6.0%

FAB ms $[Zn_2HL3)_2(H_2O)_2(ClO_4)_4H]^+$ m/e = 861 a.m.u.
NMR spectra (CD_3CN):

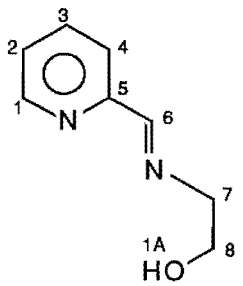

^1H H1 8.45(d); H2 7.82(m); H3 8.33(m); H4 8.12(d); H6 8.93(s); H7 4.09(m); H8 3.90(m); H1A 4.621(t) ppm

^{13}C C1 150.27; C2 130.61; C3 143.17; C4 129.52; C5 147.25; C6 164.77; C7 55.93; C8 59.94 ppm

Preparation of Complexes of HL6 and L6'

$[Mn(HL6)(L6')]_2(ClO_4)_4.2solvent$

2-Acetylpyridine (2 g, 16.5 mmol) in 5 ml of ethanol was added dropwise to a refluxing ethanol solution (60 ml) of ethanolamine (1.02 g, 16.7 mmol), followed by $Mn(ClO_4)_2.6H_2O$ (5.98 g, 16.5 mmol) in 10 ml of ethanol. The resulting gold solution was refluxed 3 hr, allowed to cool, then some was solvent removed under reduced pressure. On standing, a shiny brown microcrystalline powder precipitated in the stoppered flask. Further evaporation under reduced pressure, followed by standing allowed brown crystals of $[Mn(HL6)(L6')]_2(ClO_4)_4.2EtOH$ suitable for an X-ray structure determination to grow. A further crop of yellow-brown powder was obtained. Yield 0.73 g, 0.5 mmol, 20%. Vapour diffusion of diethylether into an acetonitrile solution of the brown powder yielded crystals of $[Mn(HL6)(L6')]_2(ClO_4)_4.2MeCN$ which were also characterised by a single crystal X-ray structure determination, as they had a completely different unit cell and crystal system to those crystals obtained from the reaction solution.
Infrared spectrum *inter alia* 3440(m,b), 1645(m), 1620(m), 1600(m), 1100(s,b) cm^{-1}

Preparation of Complexes of H_2L9

$[Mn(H_2L9)(NCS)_2]_x$

A methanol solution (50 ml) of DAP (1 g, 6.1 mmol) and Mn $(ClO_4)_2.6H_2O$ (1.56 g, 4.3 mmol) was refluxed for 5 min then propanolamine (0.92 g, 12.3 mmol) was added. After an hour NaSCN (0.99 g, 12.3 mmol) was added to the orange solution and refluxing continued for 30 min. The initial yellow precipitate (the infrared spectrum showed that this contained no NCS^-) was removed by filtration. Clusters of gold crystals suitable for X-ray analysis grew in the filtrate overnight. These were collected and washed with ethanol. Yield 0.75 g, 1.7 mmol (calculated on monomer molecular weight), 39%.
Infrared spectrum *inter alia* 3480(m,b), 3290(m,b), 2080(s), 1640(w), 1620(w), 1590(m) cm^{-1}.

$[Ni(H_2L9)_2](ClO_4)_2$

Propanolamine (0.34 g, 4.8 mmol) in 10ml of methanol was added to a refluxing methanol (40ml) solution of DAP (0.40 g, 2.5 mmol) and $Ni(ClO_4)_2.6H_2O$ (0.88 g, 2.4 mmol) causing the colour to change from green to dark red-brown. Slow evaporation of the solvent allowed the formation of crystals suitable for single crystal analysis.

Infrared spectrum *inter alia* 3330(s,b), 1625(m), 1590(m), 1100(s,b) cm^{-1}

$[Ni(H_2L9)(NCS)_2]_x$

$Ni(ClO_4)_2.6H_2O$ (2.24g, 6.1mmol) in methanol (10ml) was added to a refluxing methanol (50ml) solution of DAP (1g, 6.1mmol). The dropwise addition of propanolamine (0.92g, 12.2mmol) in methanol (5ml) caused the yellow-green solution to turn dark brown. NaNCS (1.00g, 12.2mmol) in 15ml methanol was quickly added and the dark brown solution refluxed a further 40min. Four days later green crystals suitable for X-ray analysis were filtered from the brown solution. A dichroic brown/green crystal was shown to be the same compound by an X-ray unit cell determination. After slow evaporation of solvent further crops of green crystalline product were obtained. Yield 1.83 g, 4.1 mmol, 66% calculated on monomer molecular weight.

Infrared spectrum *inter alia* 3400(m,b), 3310(m), 2120(s), 2100(s), 1635(w), 1595(m) cm^{-1}

Analysis Calculated: C 45.1; H 5.1; N 15.5%

Found: C 45.1; H 5.1; N 15.1%

Electronic spectra (solid) λ_{max} = 920 nm, λ_{max} = 580 nm

(DMF) $\lambda_{max} \approx$ 892 nm, ε = 30; λ_{max} = 586 nm, ε = 15; plus further bands in the u.v.

Crystallography

General Data

Crystals suitable for single crystal X-ray structural analysis were obtained as described in the Experimental Section. X-ray crystallographic data were collected on a Nicolet R3m four-circle diffractometer using graphite-monochromated Mo-K_α radiation (λ=0.71069). The cell parameters were determined by least-squares refinement of 14 to 22 accurately centered reflections in the range $5 < 2\theta < 35^o$. Crystals suitable for X-ray crystallography were usually coated with a hydrocarbon oil and transferred into the low temperature gas stream of the diffractometer. The crystal stability was monitored by recording three check reflections every 97 reflections and no significant variations were observed for any data sets. The data sets were corrected for Lorentz and polarisation effects, and unless otherwise stated, an empirical absorption correction was applied, based on ψ-scan data. Hydrogen atoms were inserted at calculated positions using a riding model with thermal parameters equal to 1.2U of their carrier atoms. The function minimised in the refinement was $\Sigma w(|F_o| - |F_c|)^2$ where $w = [\sigma^2 (F_o) + gF_o^2]^{-1}$. Final atom coordinates and numbering schemes are given in Appendix A, and tables of selected interatomic distances and angles are given in Section 3.2. All programs used in data

reduction and final refinement were contained in the SHELXTL (version 4.0) package.[108] SHELXTL or SHELXS[109] programs were employed to solve the structures, and in some cases the intermediate refinement was performed using SHELX76.[110]

(L3')ClO_4

$C_{14}H_{14}ClN_3O_5$, colourless triangular prism, crystal dimensions 0.45 x 0.45 x 0.60 x 0.20 mm^3, monoclinic, a = 10.781(3), b = 17.519(6), c = 8.155(3) Å, β = 105.01(3)°, U = 1487.1(9) $Å^3$, space group $P2_1/n$, Z = 4, F(000) = 704. Using 1.6° ω-scans at a scan rate of 3.90° min^{-1} , and a background to scan ratio of 0.1, 2859 reflections were collected with $4 < 2\theta < 50°$, index range: h 0/13, k 0/21, l -10/10, at room temperature. Of these, 2611 were unique, and the 1804 having $I > 3\sigma(I)$ were ultimately used in the structure refinement.

A Patterson calculation[108] revealed the position of the chlorine atom and the remaining non-hydrogen atoms were located from difference Fourier maps. Anisotropic thermal parameters were assigned to all non-hydrogen atoms and the refinement on 208 parameters converged with R = 0.053 , wR = 0.067, g = 0.0004 and a maximum least-squares shift/error of 0.012 . The final difference map showed no features greater than ± 0.38e $Å^{-3}$.

[Mn(H_2L2)(H_2O)$_2$](ClO_4)$_2$

$C_{13}H_{23}Cl_2MnN_3O_{12}$, irregular yellow block, crystal dimensions 0.16 x 0.41 x 0.53 mm^3, monoclinic, a = 16.142(3), b = 12.222(3), c = 11.047(3) Å, β = 94.41(2)°, U = 2173.1(9) $Å^3$, space group C2/c, Z = 4, F(000) = 1108. Using 1.6° ω-scans at a scan rate of 3.91° min^{-1} , and a background to scan ratio of 0.1, 2157 reflections were collected with $4 < 2\theta < 50°$, index range: h 0/20, k 0/15, l -14/14, at 298 K. Of these, 2088 were unique, and the 1683 having $I > 3\sigma(I)$ were ultimately used in the structure refinement.

A Patterson calculation[108] revealed the position of the manganese and chlorine atoms and the remaining non-hydrogen atoms were located from difference Fourier maps. Two-fold rotational disorder about Cl-O14, of the 0.7 occupancy perchlorate oxygen atoms O11, O12 and O13, was modelled by the insertion of the 0.3 occupancy atoms O15, O16 and O17. Anisotropic thermal parameters were assigned to all non-hydrogen atoms, except O15, O16 and O17, and the refinement on 154 parameters converged with R = 0.0638 , wR = 0.0990, g = 0.001365 and a maximum least-squares shift/error of 0.009 . The final difference map showed no features greater than ± 0.6 e $Å^{-3}$.

$Mn(H_2L2)(NCS)_2$

$C_{15}H_{19}MnN_5O_2S_2$, yellow block, crystal dimensions 0.31x 0.41 x 0.62 mm^3, monoclinic, a = 9.902(2), b = 12.581(2), c = 15.203(3) Å, β = 101.46(2)°, U = 1856.1(6) $Å^3$, space group I2/a , Z = 4, F(000) = 868. Using 1.6° ω-scans at a scan rate of 2.93° min^{-1} , and a background to scan ratio of 0.1, 2503 reflections were collected with 4 < 2θ < 50°, index range: h 0/12, k 0/15, l -19/19, at 298 K. Of these, 1638 were unique, and the 1503 having I >3 σ (I) were ultimately used in the structure refinement.

A Patterson calculation[108] revealed the position of the manganese atom and the remaining non-hydrogen atoms were located from difference Fourier maps. Anisotropic thermal parameters were assigned to all non-hydrogen atoms and the refinement on 115 parameters converged with R = 0.0416 , wR = 0.0714, g = 0.0033 and a maximum least-squares shift/error of 0.094 . The final difference map showed no features greater than ± 0.6 e $Å^{-3}$.

$Mn(H_2L2)(N_3)_2$

$C_{13}H_{19}MnN_9O_2$, irregular orange block, crystal dimensions 0.24x 0.27 x 0.40 mm^3, orthorhombic, a = 18.643(7), b = 12.616(3), c = 7.127(3) Å, U = 1676(1)$Å^3$, space group Pbcn , Z = 4, F(000) = 804. Using 1.4° ω-scans at a scan rate of 4.88° min^{-1} , and a background to scan ratio of 0.25, 1736 reflections were collected with 4 < 2θ < 50°, index range: h 0/23, k 0/16, l 0/9, at 173 K. Of these, 1479 were unique, and the 815 having I >3 σ (I) were ultimately used in the structure refinement.

Direct methods[109] revealed the structure and the remaining non-hydrogen atoms were located from difference Fourier maps. Anisotropic thermal parameters were assigned to all non-hydrogen atoms and the refinement on 115 parameters converged with R = 0.0407 , wR = 0.0525, g = 0.00146 and a maximum least-squares shift/error of 0.002 . The final difference map showed no features greater than ± 0.36 e $Å^{-3}$.

$[Ni(H_2L2)_2](ClO_4)_2.H_2O$

$C_{26}H_{40}Cl_2NiN_6O_{13}$, irregular brown block, crystal dimensions 0.25 x 0.47 x 0.47 mm^3, tetragonal, a = 10.109(1), c = 16.540(2) Å, U = 1690.2(5) $Å^3$, space group $P\bar{4}2_1c$, Z = 2, F(000) = 808 Using 1.4° ω -scans at a scan rate of 3.91° min^{-1} , and a background to scan ratio of 0.5, 1723 reflections were collected with 4 < 2θ < 50°, index range: h 0/13, k 0/13 , l -0/20, at room temperature. Of these, 857 were unique, and the 554 having I >3 σ (I) were ultimately used in the structure refinement.

A Patterson calculation[108] revealed the position of the nickel atom and the remaining non-hydrogen atoms were located from difference Fourier maps.

Hydrogen atoms were inserted on all but the quarter occupancy water molecule O20. Anisotropic thermal parameters were assigned to all non-hydrogen atoms and the refinement on 110 parameters converged with R = 0.0896, wR = 0.1238, g = 0.00633 and a maximum least-squares shift/error of 0.024 . The final difference map showed no features greater than $\pm$ 0.87 e Å^{-3} .

[Ni(H_2L2)(NCS)$_2$]$_2$

$C_{30}H_{38}N_{10}Ni_2O_4S_4$, green plate, crystal dimensions 0.06 x 0.30 x 0.46 mm^3, monoclinic, *a* = 12.623(4), *b* =10.799(3), *c* = 14.174(5) Å, β = 106.61 (3)°, U = 1851(1) Å^3, space group $P2_1/n$, Z = 2, F(000) = 880. Using 1.6° ω-scans at a scan rate of 4.88° min^{-1} , and a background to scan ratio of 0.1, 3588 reflections were collected with 4 < 2θ < 50°, index range: h 0/16, k 0/13 , l -17/17, at 173 K. Of these, 3248 were unique, and the 2414 having I >3 σ (I) were ultimately used in the structure refinement.

A Patterson calculation[108] revealed the position of the nickel atom and the remaining non-hydrogen atoms were located from difference Fourier maps. Anisotropic thermal parameters were assigned to all non-hydrogen atoms and the refinement on 226 parameters converged with R = 0.0343 , wR = 0.0445, g = 0.00067 and a maximum least-squares shift/error of 0.011 . The final difference map showed no features greater than $\pm$ 0.6 e Å^{-3} .

Mn(HL3)$_2$(NCS)$_2$

$C_{18}H_{20}MnN_6O_2S_2$, irregular yellow block, crystal dimensions 0.22 x 0.66 x 0.75 mm^3, orthorhombic, *a* = 9.786(4), *b* = 12.748(4), *c* = 17.615(6) Å, U = 2197(1)Å^3, space group $Pna2_1$, Z = 4, F(000) = 972. Using 1.7° ω-scans at a scan rate of 5.86° min^{-1} , and a background to scan ratio of 0.3, 1669 reflections were collected with 4 < 2θ < 45°, index range: h 0/11, k 0/14, l 0/19, at 150 K. Of these, 1526 were unique, and the 1356 having I >3 σ (I) were ultimately used in the structure refinement.

A Patterson calculation[108] revealed the position of the manganese atom and the remaining non-hydrogen atoms were located from difference Fourier maps. Hydrogen atoms were inserted on all atoms except the alkoxy oxygens O1 and O10. Anisotropic thermal parameters were assigned to all non-hydrogen atoms, except the carbon atoms of the pyridine rings, and the refinement on 213 parameters converged with R = 0.0306 , wR = 0.0395, g = 0.00050 and a maximum least-squares shift/error of 0.015 . The final difference map showed no features greater than $\pm$ 0.38e Å^{-3} .

$[Mn(HL3)(NCS)_2]_x$

$[C_{10}H_{10}MnN_4O_1S_2]_x$, irregular yellow plate, crystal dimensions 0.16 x 0.35 x 0.5 mm^3, monoclinic, a = 16.718(8), b = 5.788(2), c = 28.135(11) Å, β = 91.61(3)°, U = 2721(2) $Å^3$, space group I2/a , Z = 8, F(000) = 1304. Wycoff-scans (ie. peak top ω-scans) using a 0.5° scan width and 0.9° steps at a scan rate of 4.88° min^{-1} , and a background to scan ratio of 0.3, 4232 reflections were collected with $4 < 2\theta < 45°$, index range: h 0/19, k 0/7, l -31/31, at 150 K. Of these, 1769 were unique, and the 1476 having I >3 σ (I) were ultimately used in the structure refinement.

A Patterson calculation[109] revealed the structure and the remaining non-hydrogen atoms were located from difference Fourier maps. Anisotropic thermal parameters were assigned to all non-hydrogen atoms and the refinement on 164 parameters converged with R = 0.0273 , wR = 0.0394, g = 0.0006 (not refined) and a maximum least-squares shift/error of 0.018 . The final difference map showed no features greater than ± 0.46e $Å^{-3}$.

$[Ni(HL3)_2](ClO_4)_2$

$C_{16}H_{20}Cl_2N_4NiO_{10}$, small yellow-brown needle, crystal dimensions, orthorhombic, a = 18.190(13), b =7.539(6), c = 15.931(6) Å, U = 2185(2) $Å^3$, space group $Pna2_1$, Z = 4, F(000) = 1144. Using 2.4° ω-scans at a scan rate of 3.91° min^{-1} , and a background to scan ratio of 0.3, 1675 reflections were collected with $4 < 2\theta < 45°$, index range: h 0/9, k 0/18 , l 0/20, at 140 K. Of these, 1481 were unique, and the 517 having I >2 σ (I) were ultimately used in the structure refinement. No absorption correction was applied. The data were of low intensity due to poor crystal quality.

A Patterson calculation[109] revealed the structure and the remaining non-hydrogen atoms were located from difference Fourier maps. The pyridine rings were fixed to be hexagonal. No hydrogen atoms were inserted. Anisotropic thermal parameters were assigned only to the nickel atom and the refinement on 93 parameters converged with R = 0.1274 , wR = 0.1200, g = 0.0006 (not refined) and a maximum least-squares shift/error of 0.75. The final difference map showed no features greater than ± 1.24 e $Å^{-3}$.

$[Cu(HL3)(H_2O)_2(ClO_4)]_2(ClO_4)_2$

$C_{16}H_{28}Cl_4Cu_2N_4O_{22}$, blue block, crystal dimensions 0.16 x 0.38 x 0.63 mm^3, monoclinic, a = 15.132(11), b = 9.235(8)), c = 23.030(17) Å, β = 102.32(5)°, U = 3144(4) $Å^3$, space group C2/c , Z = 4, F(000) = 1816. Using 2.2° ω-scans at a scan rate of 4.88° min^{-1} , and a background to scan ratio of 0.3, 2278 reflections were collected with $4 < 2\theta < 45°$, index range: h 0/17, k 0/10, l -25/25, at 150 K. Of

these, 2049 were unique, and the 938 having I >3 σ (I) were ultimately used in the structure refinement.

Direct methods[108] revealed the structure and the remaining non-hydrogen atoms were located from difference Fourier maps. Anisotropic thermal parameters were assigned to the copper atom, and to all oxygen atoms except O23 and O24, and the refinement on 157 parameters converged with R = 0.0793 , wR = 0.1018, g = 0.00213 and a maximum least-squares shift/error of 0.011 . The final difference map showed no features greater than ± 1.06e Å^{-3} .

$[Zn(HL3)(H_2O)_2(ClO_4)]_2(ClO_4)_2$

$C_{16}H_{28}Cl_4N_4O_{22}Zn_2$, colourless block, crystal dimensions 0.40 x 0.56 x 0.68 mm^3, monoclinic, *a* = 15.114(7), *b* = 9.428(3), *c* = 22.649(9) Å, β = 100.86(3)°, U = 3170(2) Å^3, space group C2/c , Z = 4, F(000) = 1826. Using 1.7° ω-scans at a scan rate of 4.19° min^{-1} , and a background to scan ratio of 0.4, 3066 reflections were collected with 4 < 2θ < 50°, index range: h 0/18, k 0/12, l -27/27, at 150 K. Of these, 2785 were unique, and the 2260 having I >3 σ (I) were ultimately used in the structure refinement.

Direct methods[109] revealed the structure and the remaining non-hydrogen atoms were located from difference Fourier maps. Anisotropic thermal parameters were assigned to all non-hydrogen atoms and the refinement on 217 parameters converged with R = 0.0391 , wR = 0.0500, g = 0.00027 and a maximum least-squares shift/error of 0.015 . The final difference map showed no features greater than ± 0.82e Å^{-3} .

$[Mn(HL6)(L6')]_2(ClO_4)_4.2EtOH$

$C_{50}H_{60}Cl_4Mn_2N_8O_{22}$, irregular brown block, crystal dimensions 0.18 x 0.19 x 0.25 mm^3, orthorhombic, *a* = 23.987(7), *b* = 12.697(3), *c* = 19.355(5) Å, U = 5895(3)Å^3, space group $Pca2_1$, Z = 4, F(000) = 2840. Using 1.4° ω-scans at a scan rate of 2.93° min^{-1} , and a background to scan ratio of 0.1, 4308 reflections were collected with 4 < 2θ < 45°, index range: h 0/26, k 0/14, l 0/21, at 170 K. Of these, 2447 were unique, and the 2260 having I >3 σ (I) were ultimately used in the structure refinement.

Direct methods[109] revealed the structure and the remaining non-hydrogen atoms were located from difference Fourier maps. Anisotropic thermal parameters were assigned to all manganese, chlorine, oxygen and nitrogen atoms as well as to the carbon atoms of the ethanol molecules (C60, C61, C70, C71) and the refinement on 544 parameters converged with R = 0.0876 , wR = 0.1146, g = 0.00423 and a maximum least-squares shift/error of 0.081 . The final difference map showed no features greater than ± 1.99e Å^{-3} .

$[Mn(HL6)(L6')]_2(ClO_4)_4.2MeCN$

$C_{50}H_{56}Cl_4Mn_2N_{10}O_{20}$, irregular brown block, crystal dimensions 0.30 x 0.30 x 0.40 mm^3, monoclinic, a = 10.391(7), b = 24.451(23), c = 11.558(6) Å, β = 92.31(5)° U = 2934(4) $Å^3$, space group $P2_1/n$, Z = 2, F(000) = 1408. Using 2.8° ω-scans at a scan rate of 7.32° min^{-1} , and a background to scan ratio of 0.3, 4172 reflections were collected with $4 < 2\theta < 45°$, index range: h 0/12, k 0/27, l -13/13, at 180 K. Of these, 3815 were unique, and the 1325 having I >3 σ (I) were ultimately used in the structure refinement.

A Patterson calculation[108] revealed the position of the manganese atom and the remaining non-hydrogen atoms were located from difference Fourier maps. Anisotropic thermal parameters were assigned to the manganese atom and the two perchlorate groups and the refinement on 228 parameters converged with R = 0.1181, wR = 0.1460, g = 0.00220 and a maximum least-squares shift/error of 0.008 . The final difference map showed no features greater than $\pm$ 1.92e $Å^{-3}$.

$[Mn(H_2L9)(NCS)_2]_x$

$[C_{17}H_{23}MnN_5O_2S_2]_x$, irregular yellow block, crystal dimensions 0.38 x 0.38 x 0.48 mm^3, monoclinic, a = 14.387(3), b = 10.045(2), c = 15.528(4) Å, β = 115.10(2)°, U = 2032.1(9) $Å^3$, space group $P2_1/n$, Z = 4, F(000) = 932. Using 1.2° ω-scans at a scan rate of 5.33° min^{-1} , and a background to scan ratio of 0.5, 4877 reflections were collected with $4 < 2\theta < 54°$, index range: h 0/16, k 0/11, l -17/17, at 173 K. Of these, 4447 were unique, and the 3478 having I >3 σ (I) were ultimately used in the structure refinement. The data were corrected for extinction effects.

A Patterson calculation revealed the position of the manganese atom and the remaining non-hydrogen atoms were located from difference Fourier maps. Anisotropic thermal parameters were assigned to all non-hydrogen atoms and the refinement on 245 parameters converged with R = 0.0308 , wR = 0.0393, g = 0.000346 and a maximum least-squares shift/error of 0.02 . The final difference map showed no features greater than $\pm$ 0.3e $Å^{-3}$.

$[Ni(H_2L9)_2](ClO_4)_2$

$C_{30}H_{46}Cl_2N_6NiO_{12}$, irregular red-brown block, crystal dimensions 0.20 x 0.30 x0.49 mm^3, monoclinic, a = 19.482(4), b = 10.438(2), c = 21.324(5) Å, β = 123.48(2)°, U = 3616(2) $Å^3$, space group C2/c, Z =4 , F(000) = 1704 . Using 1.4° ω-scans at a scan rate of 4.88° min^{-1} , and a background to scan ratio of 0.5 ,3469 reflections were collected with $4 < 2\theta < 50°$, index range: h 0/24, k 0/13, l -26/26, at 153K. Of these, 3186 were unique, and the 2572 having I >3 σ (I) were ultimately used in the structure refinement.

A Patterson calculation[108] revealed the position of the nickel atom and the remaining non-hydrogen atoms were located from difference Fourier maps. Anisotropic thermal parameters were assigned to all non-hydrogen atoms and the refinement on 231 least-squares parameters converged with R = 0.0409 , wR = 0.0555, g = 0.00067 and a maximum least-squares shift/error of 0.02 . The final difference map showed no features greater than $\pm$ 0.6e Å^{-3} .

$[Ni(H_2L9)(NCS)_2]_x$

$[C_{17}H_{23}N_5NiO_2S_2]_x$, green plate, crystal dimensions 0.13 x 0.22 x0.59 mm^3, monoclinic, a = 14.922(7), b = 9.305(4), c = 16.140(7) Å, β = 114.50(3)°, U = 2039(1) Å^3, space group $P2_1/c$, Z =4 , F(000) = 944 . Using 1.9° ω-scans at a scan rate of 4.19° min^{-1} , and a background to scan ratio of 0.5 , 4338 reflections were collected with 4 < 2θ < 50°, index range: h 0/19, k 0/12, l -20/20, at 140K. Of these, 3792 were unique, and the 2049 having I >3 σ (I) were ultimately used in the structure refinement.

Direct methods[109] revealed the structure and the remaining non-hydrogen atoms were located from difference Fourier maps. Anisotropic thermal parameters were assigned to all non-hydrogen atoms and the refinement on 245 least-squares parameters converged with R = 0.0490 , wR = 0.0456, g = 0.00018 and a maximum least-squares shift/error of 0.03 . The final difference map showed no features greater than $\pm$ 0.56e Å^{-3} .

3.2 Results and Discussion

The noncyclic ligands employed in this work are shown in Figure 71. They all contain one or two flexible alkyl chains which terminate in an alcohol group. These compounds will be referred to as "one arm" or "two arm" ligands throughout this Chapter.

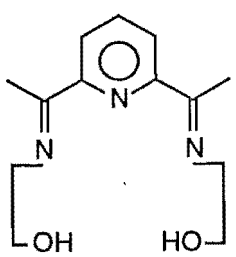

H_2L 2

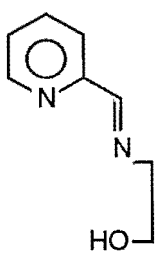

HL3

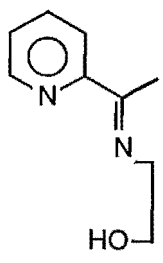

HL6

Figure 71

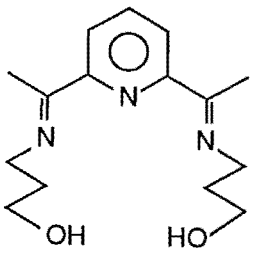

H_2L9

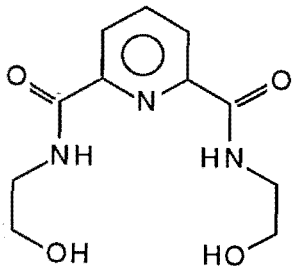

H_2L12

Figure 71 continued

X-ray Structure Determinations

A brief discussion of the restrictions that the coordination of pyridinediimine or pyridineimine units can place on metal ions is presented before the structures are described.

The two planar units are shown in Figure 72. Generally they restrict $\theta_{1,2}$ (N1-M-N2) and $\theta_{1,3}$ (N1-M-N3) to a value between 68° and 78°.

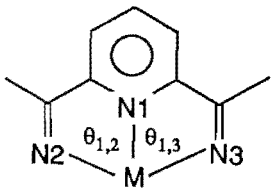

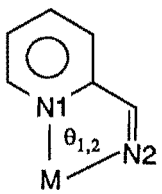

Figure 72

Thus a metal ion of appropriate radius, without a strong stereochemical preference, can take up angles close to those (θ = 72°) required for a regular pentagonal geometry in this plane. However, if the metal ion prefers a tetragonal type geometry in this plane (e.g. octahedral) then some distortion will be observed as θ can not increase to 90°. The effective ionic radius of 6-coordinate Ni^{2+} is 83 pm whereas that of 6-coordinate Mn^{2+} is 97 pm;[144] thus bonds to nickel can be shorter, allowing the angle θ to increase. This is what is observed in the following structures; typically Ni-N1 bonds are 0.12Å shorter than the Mn-N1 bonds, and θ is correspondingly larger at *ca.* 78° for Ni(II) complexes compared to 68° for Mn(II) complexes.

Structure of $(L3')ClO_4$

Figure 73 shows the cation, including the atom labelling scheme, and selected bond lengths and angles are shown in Table 16.[143] Schematic diagrams of the cation in its two resonance forms A and B are shown in Figure 74; 74A includes selected bond lengths (Å), and 74B shows selected ^3J coupling constants (Hz). The

structure consists of a positively charged imidazo[1,5-*a*]pyridinium ring with pyridine and hydroxyethyl substituents on the (five membered) imidazo ring. Formation of an ionic compound is likely to be due to the poor leaving ability of the hydroxyethyl substituent.

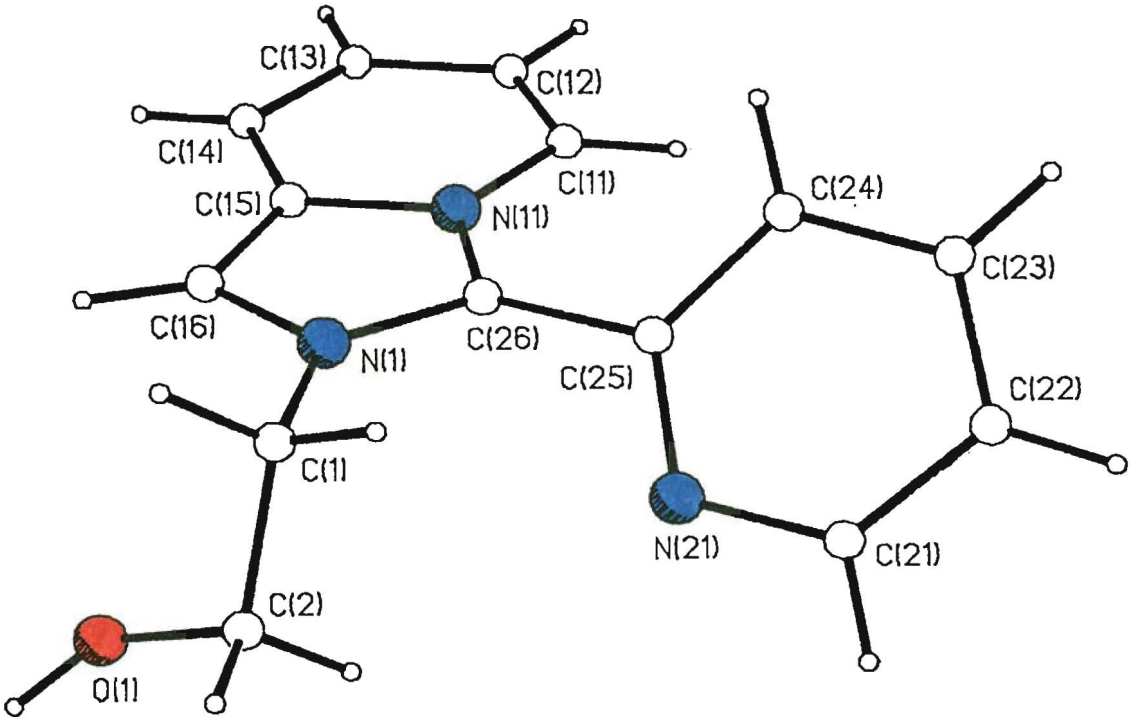

Figure 73: Perspective view of the cation $(L3')^+$

Table 16: Selected bond lengths (Å) and angles for $(L3')ClO_4$

Bond Lengths (Å)							
N11-C11	1.396(4)	N11-C15	1.407(5)	N11-C26	1.352(5)	C11-C12	1.326(6)
C12-C13	1.424(6)	C13-C14	1.330(6)	C14-C15	1.428(6)	C15-C16	1.368(5)
C16-N1	1.349(5)	N21-C21	1.332(6)	N21-C25	1.339(5)	C21-C22	1.379(7)
C22-C23	1.361(6)	C23-C24	1.370(6)	C24-C25	1.385(5)	C25-C26	1.473(5)
C26-N1	1.342(4)	N1-C1	1.484(5)	C1-C2	1.496(6)	C2-O1	1.399(6)

Bond Angles (°)					
C11-N11-C15	120.9(3)	C1-N11-C26	129.8(3)	C15-N11-C26	109.3(3)
N11-C11-C12	119.1(3)	C11-C12-C13	121.4(4)	C12-C13-C14	121.0(4)
C13-C14-C15	119.4(4)	N11-C15-C14	118.2(3)	N11-C15-C16	105.6(3)
C14-C15-C16	136.1(4)	C15-C16-N1	107.5(3)	C21-N21-C25	115.5(4)
N21-C21-C22	124.9(4)	C21-C22-C23	118.1(4)	C22-C23-C24	119.2(4)
C23-C24-C25	118.7(4)	N21-C25-C24	123.6(4)	N21-C25-C26	115.5(3)
C24-C25-C26	120.9(3)	N11-C26-C25	126.1(3)	N11-C26-N1	106.2(3)
C25-C26-N1	127.6(3)	C16-N1-C26	111.4(3)	C16-N1-C1	122.4(3)
C26-N1-C1	126.0(3)	N1-C1-C2	112.2(3)	C1-C2-O1	109.4(4)

The angle between the mean planes of the imidazo[1,5-*a*]pyridinium ring and the pyridine ring is 43.2°. This large twist prevents the steric strain which a coplanar arrangement (with the hydrogen atoms very close to each other) would produce. The bond lengths show that the imidazo[1,5-*a*]pyridinium ring is not aromatic; double

bonds are localised at C11-C12 and C13-C14 (Figure 74A). This is also evident from the ^3J coupling constants shown in Figure 74B.

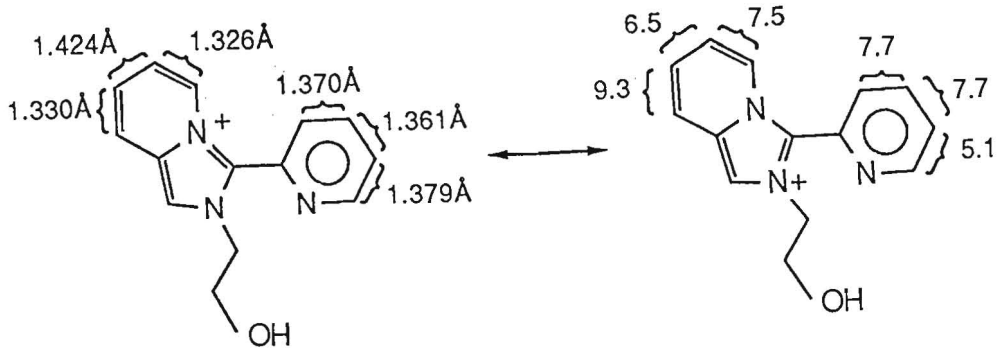

74A 74B

Figure 74

Structures of the Complexes of H_2L2

The structures of the monomeric complexes $[Mn(H_2L2)(H_2O)_2](ClO_4)_2$, $Mn(H_2L2)(NCS)_2$ and $Mn(H_2L2)(N_3)_2$ are shown in Figures 75, 76 and 77 (cation only for the perchlorate compound). Selected bond lengths and angles are given in Tables 17, 18 and 19 respectively.

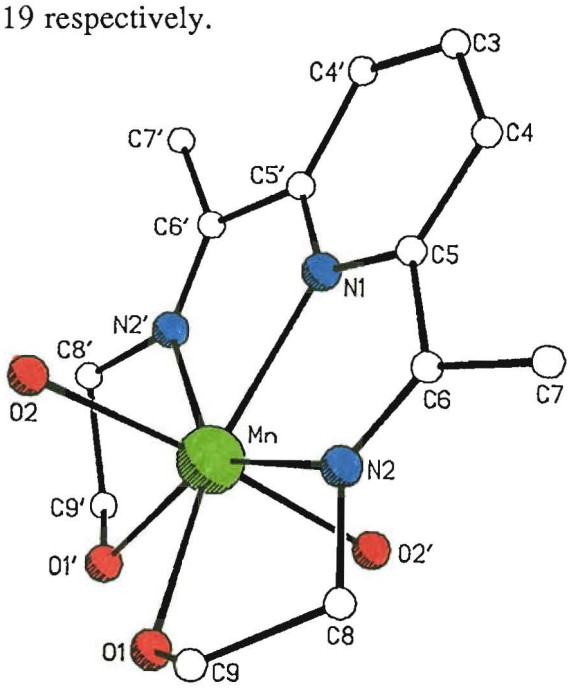

Figure 75: Perspective view of the cation $[Mn(H_2L2)(H_2O)_2]^{2+}$

In each of these structures the manganese(II) atom has approximate pentagonal bipyramidal geometry. The donors in the pentagonal plane are the three nitrogen atoms and two oxygen atoms of H_2L2 and a two fold rotation axis passes through Mn, N1 and C3. In these examples the pyridinediimine unit provides an average angle at the manganese(II) atom of $\theta_{1,2} = 68.7 \pm 0.7°$ which results in a small distortion from regular pentagonal geometry (72°). The axial donors are the anions

in the thiocyanate and azide complexes, whereas water is bound in preference to perchlorate in the perchlorate compound.

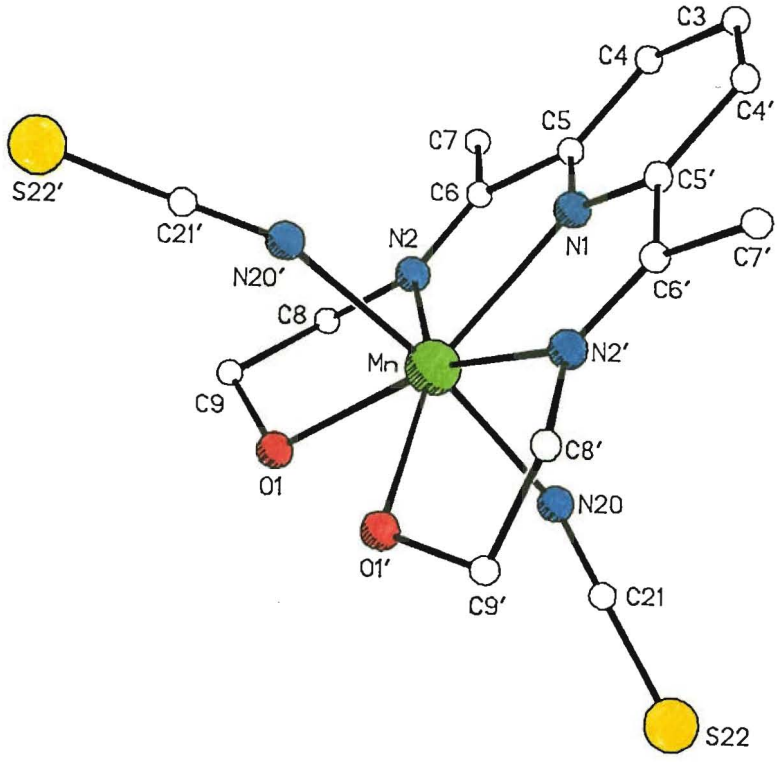

Figure 76: Perspective view of $Mn(H_2L2)(NCS)_2$

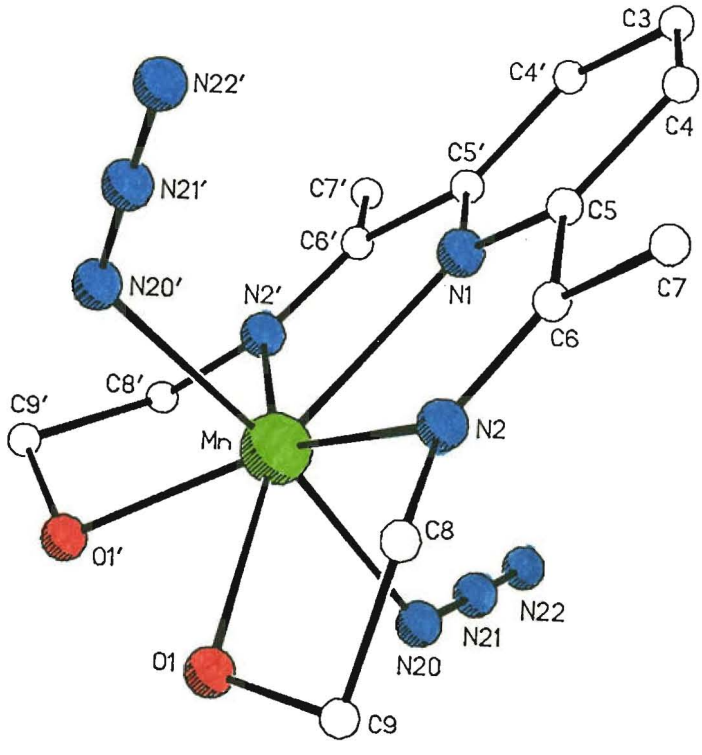

Figure 77: Perspective view of $Mn(H_2L2)(N_3)_2$

Table 17: Selected bond lengths and angles for $[Mn(H_2L2)(H_2O)_2](ClO_4)_2$

Bond Lengths (Å)							
Mn-N1	2.266(5)	Mn-O2	2.223(4)	Mn-O1	2.261(3)	Mn-N2	2.286(4)

Bond Angles (°)					
N1-Mn-N2	69.4(1)	N1-Mn-O1	140.7(1)	N2-Mn-O1	72.3(1)
N1-Mn-O2	92.0(1)	N2-Mn-O2	95.3(1)	O1-Mn-O2	83.0(1)
N2-Mn-N2'	138.8(2)	O1-Mn-N2'	148.1(1)	O2-Mn-N2'	86.1(1)
O1-Mn-O1'	78.6(2)	O2-Mn-O1'	93.9(1)	O2-Mn-O2'	176.0(2)

Table 18: Selected bond lengths and angles for $Mn(H_2L2)(NCS)_2$

Bond Lengths (Å)							
Mn-N1	2.296(2)	Mn-N2	2.326(2)	Mn-O1	2.316(3)	Mn-N20	2.212(2)

Bond Angles (°)					
N1-Mn-N2	68.6(1)	N1-Mn-O1	139.3(1)	N2-Mn-O1	70.8(1)
N1-Mn-N20	93.5(1)	N2-Mn-N20	92.2(1)	O1-Mn-N20	90.4(1)
N2-Mn-N2'	137.2(1)	O1-Mn-N2'	152.0(1)	N20-Mn-N2'	90.4(1)
O1-Mn-O1'	81.4(1)	N20-Mn-O1'	84.3(1)	N20-Mn-N20'	173.0(1)

Table 19: Selected bond lengths and angles for $Mn(H_2L2)(N_3)_2$

Bond Lengths (Å)							
Mn-N1	2.303(5)	Mn-N2	2.312(4)	Mn-O1	2.303(3)	Mn-N20	2.222(4)

Bond Angles (°)					
N1-Mn-N2	68.2(1)	N1-Mn-O1	138.7(1)	N2-Mn-O1	71.1(1)
N1-Mn-N20	93.5(1)	N2-Mn-N20	97.0(2)	O1-Mn-N20	84.3(1)
N2-Mn-N2'	136.4(2)	O1-Mn-N2'	151.8(1)	N20-Mn-N2'	85.6(2)
O1-Mn-O1'	82.7(2)	N20-Mn-O1'	90.5(1)	N20-Mn-N20'	173.1(2)

The structure of the nickel(II) complex obtained when perchlorate is the anion is another monomer (cation Figure 78, Table 20), but it is different to the manganese complexes described above because the metal ion is bound to two H_2L2 ligands (*via* the nitrogen atoms only). The nickel atom is on a $\bar{4}$ special position and the asymmetric unit contains only half of one H_2L2 ligand. The two H_2L2 ligands are bound such that the angle between the mean planes of the two sets of three nitrogen donors is 90°. Angles at the nickel(II) atom due to the pyridinediimine unit are only $\theta_{1,2}$ = 77.0(3)°, although this is larger than the θ = 68.7° found for the previous Mn(II) complexes. As expected, this corresponds to a smaller Ni-N1 bond length, 1.981(13)Å, as compared with the average Mn-N1 bond length of 2.288Å. The overall geometry of the nickel atom approaches octahedral.

Table 20: Selected bond lengths and angles for $Ni(H_2L2)_2](ClO_4)_2.H_2O$

Bond Lengths (Å)			
Ni-N1	1.98(1)	Ni-N2	2.12(1)

continued ...

Table 20 continued

Bond Angles (°)					
N1-Ni-N2	77.0(3)	N1-Ni-N1'	180.0(1)	N1-Ni-N2'	103.0(3)
N2-Ni-N2*	153.9(6)	N2-Ni-N2'	92.9(1)	N2-Ni-N2"	92.9(1)

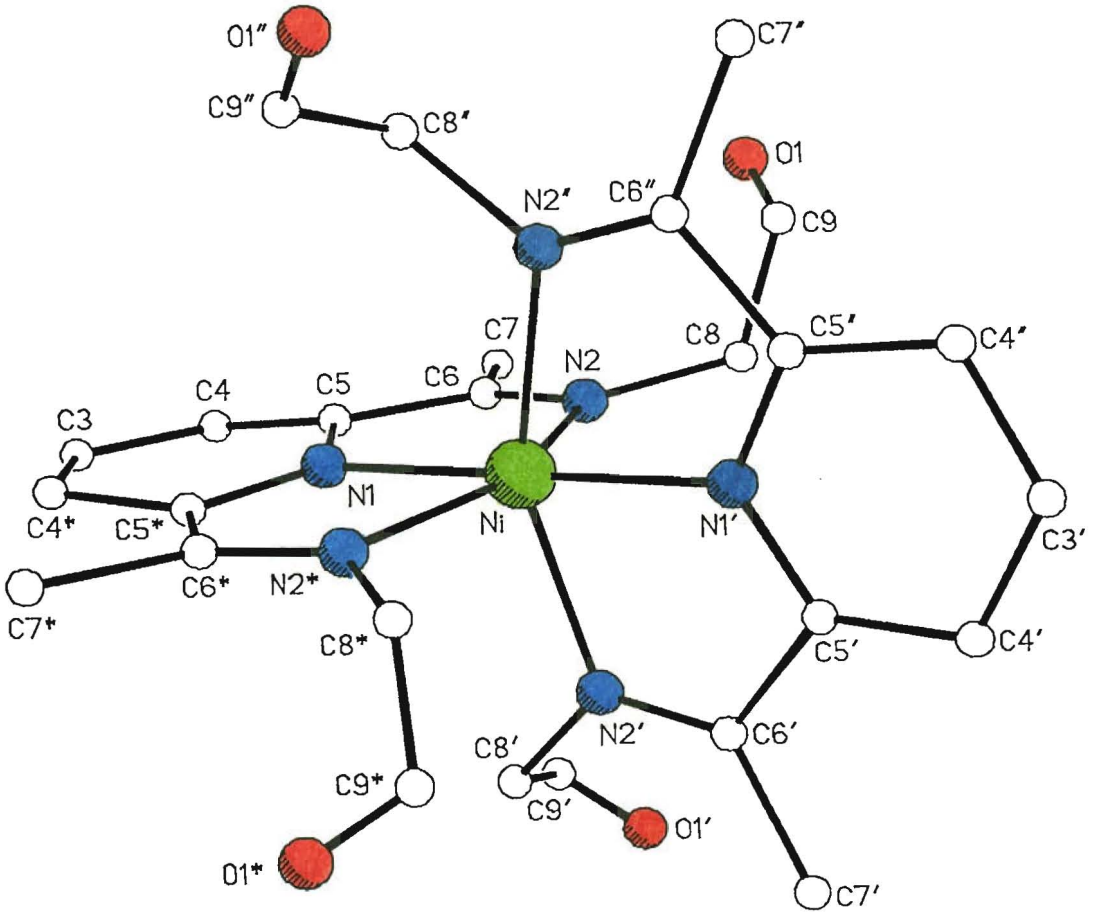

Figure 78: Perspective view of the cation $[Ni(H_2L2)_2]^{2+}$

A nickel(II) dimer is formed when strongly coordinating thiocyanate ions are present (Figure 79, Table 21). The geometry about the nickel atom is closer to octahedral than in the previous nickel complex because only one pyridinediimine is bound per nickel atom ($\theta_{1,2}$ = 76.6(1)°, $\theta_{1,3}$ = 77.0(1)°). The other coordination sites are filled by two nitrogen atoms of terminal thiocyanate groups and by one alcohol (O2', O2) group (of the H_2L2 ligand bound to the other nickel atom of the dimer). Thus the dimer is held together by the intermolecular coordination of two arms. The two thiocyanate groups and the alcohol oxygen donors are less geometrically constrained ligands than the pyridinediimine unit and make angles which approach 90° between each other, about the nickel atom (Table 21).

Table 21: Selected bond lengths and angles for $[Ni(H_2L2)(NCS)_2]_2$

Bond Lengths (Å)							
Ni-N1	1.992(3)	Ni-N2	2.199(3)	Ni-N3	2.128(3)	Ni-N70	2.022(3)
Ni-N60	2.033(3)	Ni-O2'	2.140(2)				

continued ...

Table 21 continued

Bond Angles (°)					
N1-Ni-N2	76.6(1)	N1-Ni-N3	77.0(1)	N2-Ni-N3	153.5(1)
N1-Ni-N70	171.7(1)	N2-Ni-N70	109.1(1)	N3-Ni-N70	96.8(1)
N1-Ni-N60	94.4(1)	N2-Ni-N60	90.0(1)	N3-Ni-N60	94.4(1)
N70-Ni-N60	91.6(1)	N1-Ni-O2'	91.0(1)	N2-Ni-O2'	85.2(1)
N3-Ni-O2'	92.9(1)	N70-Ni-O2'	83.7(1)	N60-Ni-O2'	171.7(1)

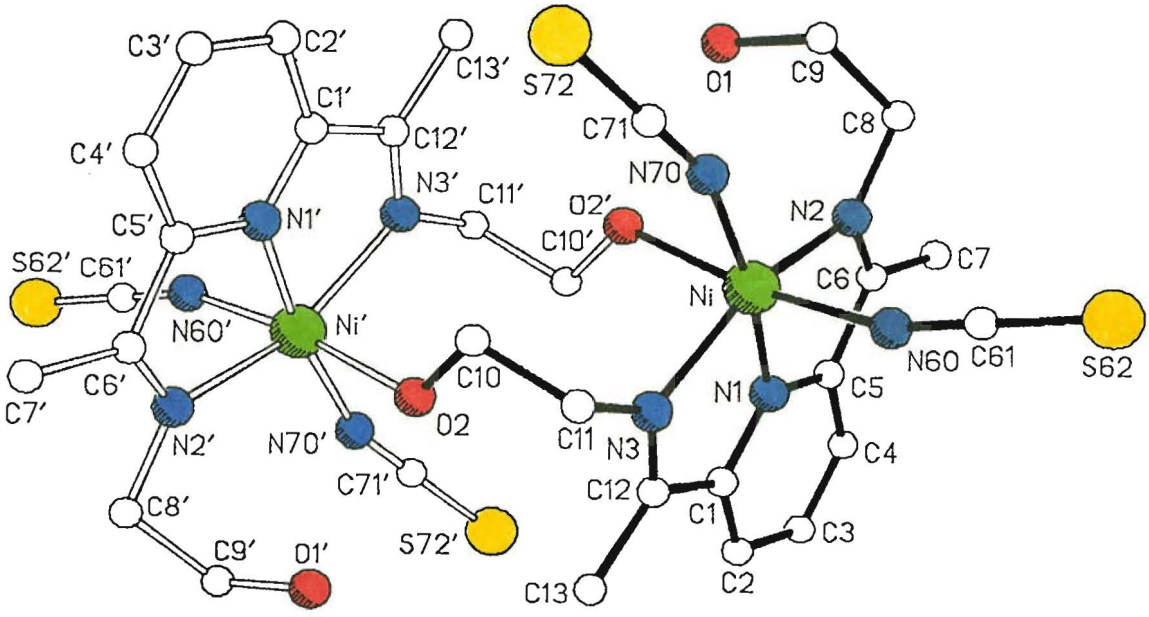

Figure 79: Perspective view of $[Ni(H_2L2)(NCS)_2]_2$

Structures of the Complexes of HL3

Two complexes of HL3 with Mn(II) and NCS^- have been structurally characterised. The first is a monomer (Figure 80, Table 22).

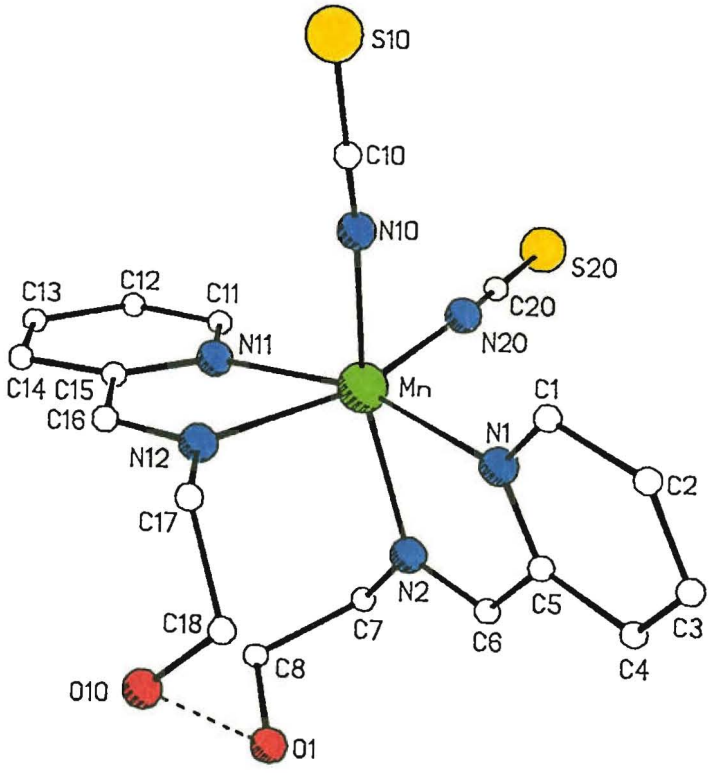

Figure 80: Perspective view of $Mn(HL3)_2(NCS)_2$

Two HL3 ligands and two thiocyanate groups are bound to a manganese(II) atom in a geometry approaching octahedral. The distortion is again due to the restricted angle that the pyridineimine unit contributes ($\theta_{1,2}$ 72.7(1)°, $\theta_{11,12}$ 72.6(1)°). The mean planes of the two pyridine rings are at 75.2° to each other. The two alcohol arms of the HL3 ligands twist away from the central manganese atom; a disordered hydrogen bond links them (O1-O10 2.819Å).

Table 22: Selected interatomic distances and angles for $Mn(HL3)_2(NCS)_2$

Bond Lengths (Å)							
Mn-N1	2.296(3)	Mn-N2	2.277(4)	Mn-N11	2.300(3)	Mn-N12	2.292(3)
Mn-N10	2.174(4)	Mn-N20	2.136(4)	O1-O10	2.819(7)		

Bond Angles (°)					
N1-Mn-N2	72.7(1)	N1-Mn-N11	164.8(1)	N2-Mn-N11	97.9(1)
N1-Mn-N12	96.4(1)	N2-Mn-N12	97.3(1)	N11-Mn-N12	72.6(1)
N1-Mn-N10	88.8(1)	N2-Mn-N10	161.5(1)	N11-Mn-N10	100.3(1)
N12-Mn-N10	85.0(1)	N1-Mn-N20	102.4(1)	N2-Mn-N20	89.9(1)
N11-Mn-N20	89.2(1)	N12-Mn-N20	161.1(1)	N10-Mn-N20	93.8(2)

The second complex is a polymer (Figure 81, Table 23). Again the six-coordinate manganese atom has distorted geometry due to the bound pyridineimine group ($\theta_{1,2}$ 72.1(1)°) but only one HL3 ligand is bound.

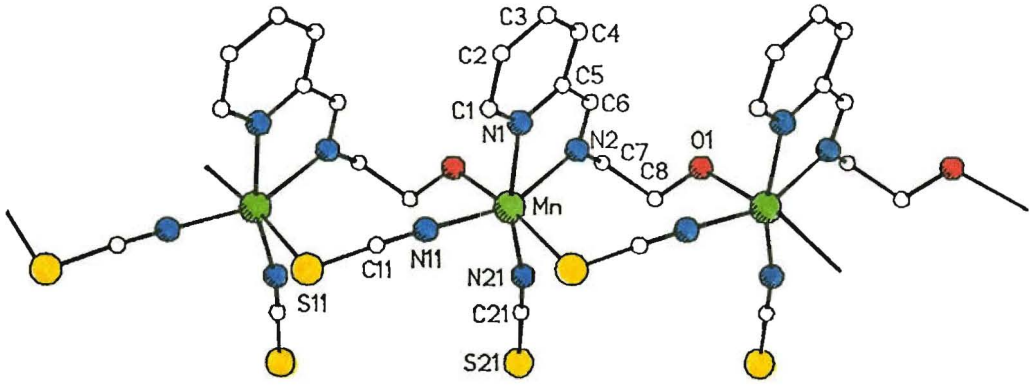

Figure 81: Perspective view of $[Mn(HL3)(NCS)_2]_x$

Table 23: Selected bond lengths and angles for $[Mn(HL3)(NCS)_2]_x$

Bond Lengths (Å)							
Mn-N1	2.286(3)	Mn-N2	2.268(2)	Mn-N11	2.145(3)	Mn-N21	2.154(3)
Mn-O1'	2.269(2)	Mn-S11'	2.685(1)				

Bond Angles (°)					
N1-Mn-N2	72.1(1)	N1-Mn-N11	91.4(1)	N2-Mn-N11	157.1(1)
N1-Mn-N21	164.7(1)	N2-Mn-N21	93.4(1)	N11-Mn-N21	103.9(1)
N1-Mn-O1'	97.1(1)	N2-Mn-O1'	82.1(1)	N11-Mn-O1'	84.3(1)
N21-Mn-O1'	85.5(1)	N1-Mn-S11'	88.0(1)	N2-Mn-S11'	104.3(1)
N11-Mn-S11'	90.5(1)	N21-Mn-S11'	90.9(1)	O1'-Mn-S11'	172.8(1)

The other angles are slightly closer to 90° (Table 23) as the donors are not so constrained. These donors are the nitrogen atom of a terminally bound NCS^-, one

nitrogen atom and one sulphur atom from each 1,3-bridging NCS^-, and finally the alcohol oxygen of an HL3 arm from another unit. The 1,3-bridging NCS^- and the alcohol oxygen atom intermolecular bridge hold the linear polymeric chain together. The pyridine rings are lined up parallel to each other at a separation of 3.97(1)Å.

The monomeric cation of the poorly refined structure of $[Ni(HL3)_2](ClO_4)_2$ is shown in Figure 82. Two HL3 ligands provide all of the donor atoms, giving the central nickel(II) atom approximate octahedral geometry. No further analysis of this structure is warranted because the errors in all of the structural parameters are large due to the lack of good data, resulting from poor crystal quality.

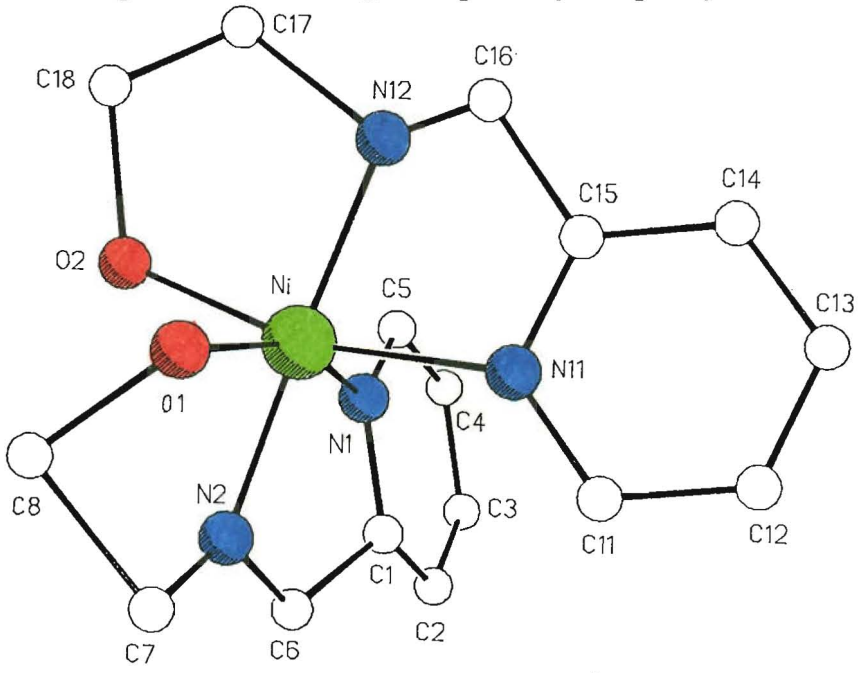

Figure 82: Perspective view of the cation $[Ni(HL3)_2]^{2+}$

The copper(II) and zinc(II) complexes of HL3 are almost isomorphous. Hence, only the cation of the zinc complex is shown (Figure 83); the numbering scheme is the same for the copper complex. Selected bond lengths and angles are shown in Tables 24 and 25 for the zinc and copper complexes respectively.

Table 24: Selected bond lengths and angles for $[Zn(HL3)(H_2O)_2(ClO_4)]_2(ClO_4)_2$

Bond Lengths (Å)							
Zn-N1	2.122(3)	Zn-N2	2.107(3)	Zn-O2	2.031(3)	Zn-O3	2.051(3)
Zn-O11	2.342(3)	Zn-O1'	2.105(3)				

Bond Angles (°)					
N1-Zn-N2	78.8(1)	N1-Zn-O2	94.2(1)	N2-Zn-O2	165.1(1)
N1-Zn-O3	169.5(1)	N2-Zn-O3	91.8(1)	O2-Zn-O3	93.8(1)
N1-Zn-O11	88.1(1)	N2-Zn-O11	87.2(1)	O2-Zn-O11	79.3(1)
O3-Zn-O11	86.6(1)	N1-Zn-O1'	98.6(1)	N2-Zn-O1'	102.6(1)
O2-Zn-O1'	91.4(1)	O3-Zn-O1'	88.1(1)	O11-Zn-O1'	168.9(1)

These complexes are dimeric with the monomer units linked by the alcohol arms (O1, O1'). In both cases the metal ion has a geometry which approximates to octahedral;

the donor atoms in the HL3 plane are the two nitrogen atoms of HL3 and two water molecules. Axial coordination by O11 of the perchlorate group is weak in both complexes (Zn-O11 2.342; Cu-O11 2.526Å), however in the copper complex this is accentuated by a Jahn-Teller distortion. This distortion is also evident in the axial Cu-O1' distance of 2.282Å which is 0.3Å longer than the average Cu-(in the plane donor) bond lengths. In comparision the Zn-O1' distance of 2.105Å is within the range of values 2.031-2.122Å found for the Zn-(in the plane donors). There are numerous hydrogen-bonding interactions between the bound water molecules and the perchlorate groups. No attempt was made to place the hydrogen atoms of the water molecules (O2 and O3) appropriately as there were so many interactions.

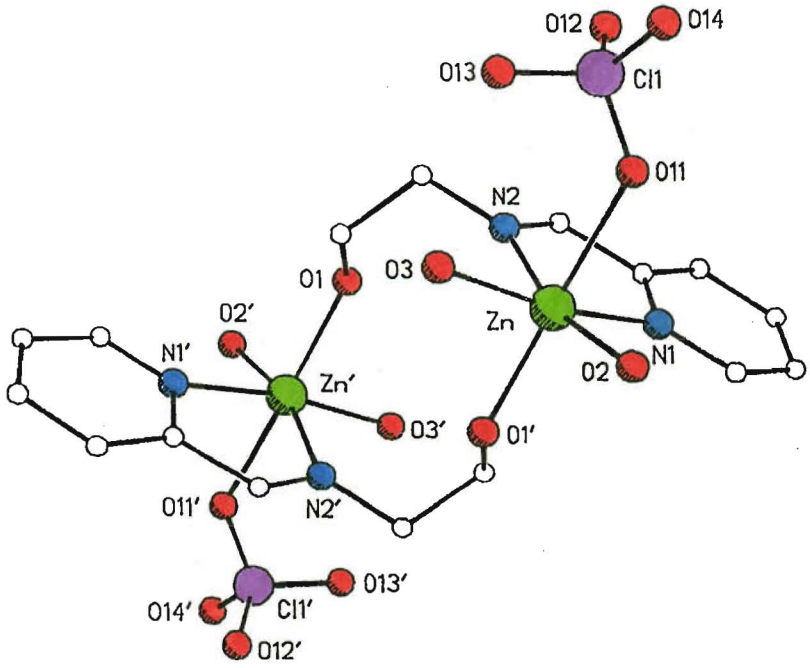

Figure 83: Perspective view of the cation $[Zn(HL3)(H_2O)_2(ClO_4)]_2^{2+}$

Table 25: Selected bond lengths and angles for $[Cu(HL3)(H_2O)_2(ClO_4)]_2(ClO_4)_2$

Bond Lengths (Å)							
Cu-N1	1.975(17)	Cu-N2	1.952(18)	Cu-O2	2.004(16)	Cu-O3	1.973(14)
Cu-O11	2.526(16)	Cu-O1'	2.282(14)				

Bond Angles (°)					
N1-Cu-N2	82.2(7)	N1-Cu-O2	93.6(6)	N2-Cu-O2	169.0(6)
N1-Cu-O3	174.2(7)	N2-Cu-O3	94.0(6)	O2-Cu-O3	89.3(6)
N1-Cu-O11	88.8(6)	N2-Cu-O11	87.6(7)	O2-Cu-O11	82.2(6)
O3-Cu-O11	86.7(6)	N1-Cu-O1'	98.8(6)	N2-Cu-O1'	100.3(6)
O2-Cu-O1'	90.3(6)	O3-Cu-O1'	86.1(6)	O11-Cu-O1'	169.7(6)

Structure of the Manganese(II) Complex of HL6 and L6'

Two $[Mn(HL6)(L6')]_2(ClO_4.2$solvent complexes were structurally characterised because they had completely different unit cells. When the solvent was ethanol the complex had no imposed symmetry and crystallised in the orthorhombic crystal system whereas when the solvent was acetonitrile the asymmetric unit contained only half of the complex (the other half was generated by a centre of inversion) and the crystal system was monoclinic. These two complexes are almost isostructural. The only difference appears to be a change in the conformation of the alkyl arms of HL6. Hence, only the former complex will be described. The dimeric complex consists of two six-coordinate manganese(II) ions each with a geometry approaching octahedral (Figure 84, Table 26).

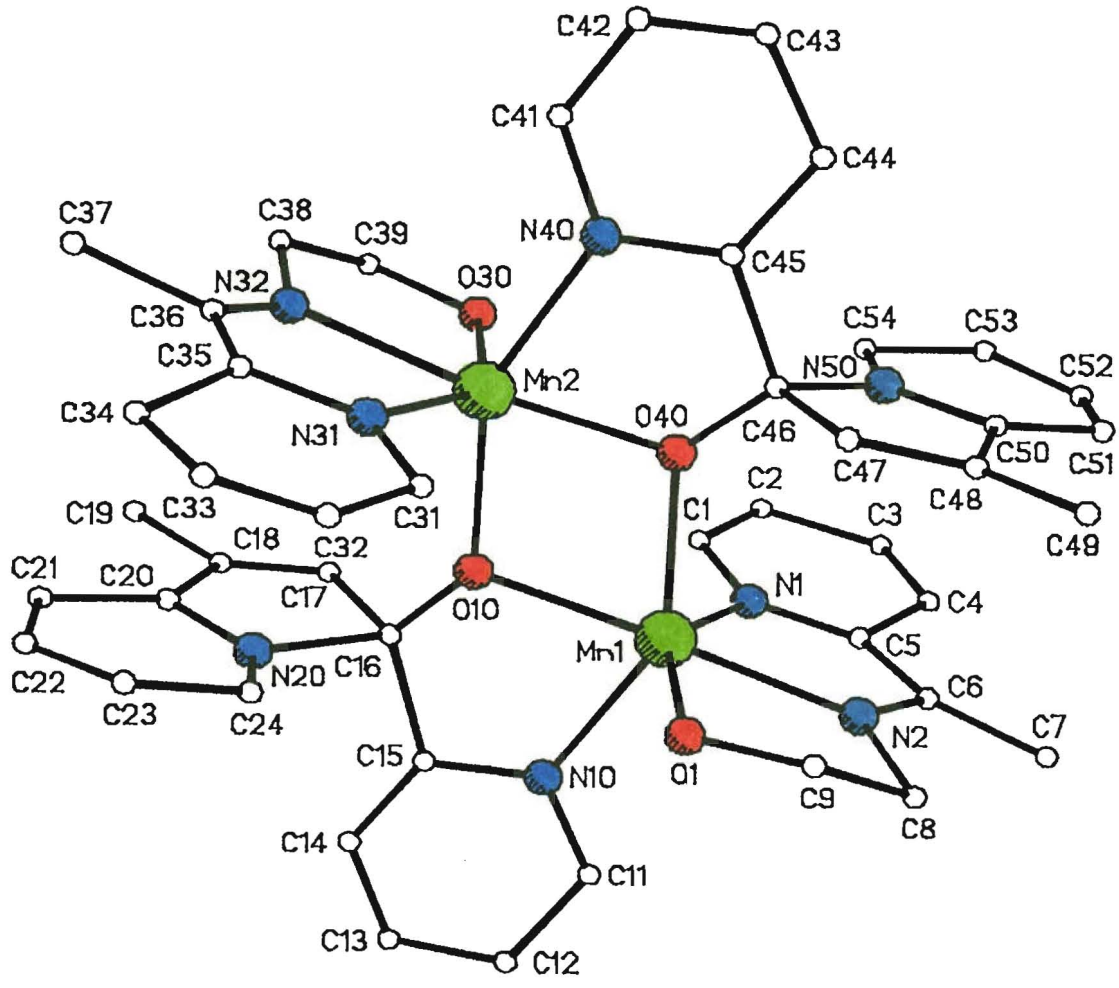

Figure 84: Perspective view of the cation $[Mn(HL6)(L6')]_2^{4+}$

The HL6 ligand binds to the manganese atom *via* two nitrogen atoms and an alcohol group. The average angle at manganese due to HL6 binding is 72 ± 3°. The other donors, a pyridine nitrogen and two bridging oxygen atoms, are from L6'. The Mn_2O_2 core is a rhombus; the internal angles at manganese are acute (76.5(4)° and 73.8(4)°) whereas the internal angles at oxygen are obtuse (104.9(4)° and 104.8(4)°). This matches the preference of oxygen for tetrahedral angles (109.5°)

and shows the irregular nature of the six-coordinate manganese(II) environment. The HL6 pyridine rings (N1 → C5 and N31 → C35) and the L6' pyridine rings which share two atoms with the five membered ring (N50 → C54 and N20 → C24 respectively) lie above one another (*ca.* 10° from parallel) at an average distance of 3.5 ± 0.2 Å, which indicates some π-π interaction. The L6' ligand is twisted at the saturated carbon of the five membered ring C16 (or C46), such that the mean planes of the respective pyridine rings lie at an angle of 89.9° (or 88.0°). C16 and C46 are distorted tetrahedra; C16 is more distorted than C46, suggesting that the C16-O10 bond still maintains some double bond character (C16-O10 1.295(24)Å, O10-C16-C15 117.1(17)°, O10-C16-C17 113.4(17)°, O10-C16-N20 113.7(18)°) at the expense of bonds to C17 and N20 (C16 - C17 1.676(29), C16 - N20 1.636(31)Å).

Table 26: Selected interatomic distances and angles for $[Mn(HL6)(L6')]_2(ClO_4)_4.2EtOH$

Interatomic Distances (Å)							
Mn1-N1	2.203(14)	Mn1-N2	2.211(15)	Mn1-O1	2.213(12)	Mn1-N10	2.230(13)
Mn1-O10	2.182(11)	Mn1-O40	2.185(11)	C15-C16	1.518(29)	C16-C17	1.676(29)
C16-N20	1.636(31)	C16-O10	1.295(24)	O10-Mn2	2.117(11)	Mn2-N31	2.287(16)
Mn2-N32	2.281(18)	Mn2-O30	2.230(14)	Mn2-N40	2.225(14)	Mn2-O40	2.119(11)
C45-C46	1.529(25)	C46-C47	1.506(23)	C46-N50	1.502(23)	C46-O40	1.368(20)
Mn1-Mn2	3.409(10)	O10-O40	2.622(25)				

Bond Angles (°)					
N1-Mn1-N2	73.3(5)	N1-Mn1-O1	146.8(5)	N2-Mn1-O1	73.5(5)
N1-Mn1-N10	93.8(5)	N2-Mn1-N10	106.9(5)	O1-Mn1-N10	94.1(5)
N1-Mn1-O10	108.2(5)	N2-Mn1-O10	177.7(5)	O1-Mn1-O10	104.9(4)
N10-Mn1-O10	71.4(5)	N1-Mn1-O40	92.0(5)	N2-Mn1-O40	108.0(5)
O1-Mn1-O40	99.8(4)	N10-Mn1-O40	144.8(5)	O10-Mn1-O40	73.8(4)
C15-C16-C17	112.4(17)	C15-C16-N20	102.7(16)	C17-C16-N20	94.9(14)
C15-C16-O10	117.1(17)	C17-C16-O10	113.4(17)	N20-C16-O10	113.7(18)
Mn1-O10-C16	118.6(12)	Mn1-O10-Mn2	104.9(4)	C16-O10-Mn2	135.3(12)
O10-Mn2-N31	93.3(5)	O10-Mn2-N32	110.4(6)	N31-Mn2-N32	69.7(6)
O10-Mn2-O30	100.1(5)	N31-Mn2-O30	142.9(6)	N32-Mn2-O30	73.2(6)
O10-Mn2-N40	148.7(5)	N31-Mn2-N40	92.1(5)	N32-Mn2-N40	100.4(6)
O30-Mn2-N40	93.9(5)	O10-Mn2-O40	76.5(4)	N31-Mn2-O40	111.8(5)
N32-Mn2-O40	173.1(5)	O30-Mn2-O40	104.9(5)	N40-Mn2-O40	72.9(5)
C45-C46-C47	113.0(15)	C45-C46-N50	107.4(13	C47-C46-N50	100.7(13)
C45-C46-O40	108.6(13)	C47-C46-O40	116.5(14)	N50-C46-O40	110.0(14)
Mn1-O40-Mn2	104.8(4)	Mn1-O40-C46	130.0(10)	Mn2-O40-C46	124.0(10)

Structures of the Complexes of H_2L9

The structure of the manganese(II) complex of H_2L9 with thiocyanate present is a polymer (Figure 85, Table 27). The manganese(II) ion has a geometry approximating to octahedral. The three nitrogen atoms of the pyridinediimine unit are held at θ angles of 71.0(1) and 71.2(1)°. Two thiocyanate groups are bound N-terminally to the manganese atom. The final site is occupied by the alcohol oxygen (O1') of one arm from another unit; it is this twisted intermolecular link which holds the polymer together. There is a sharp twist in this arm leading to the mean planes of successive pyridine rings making angles of 76° with each other.

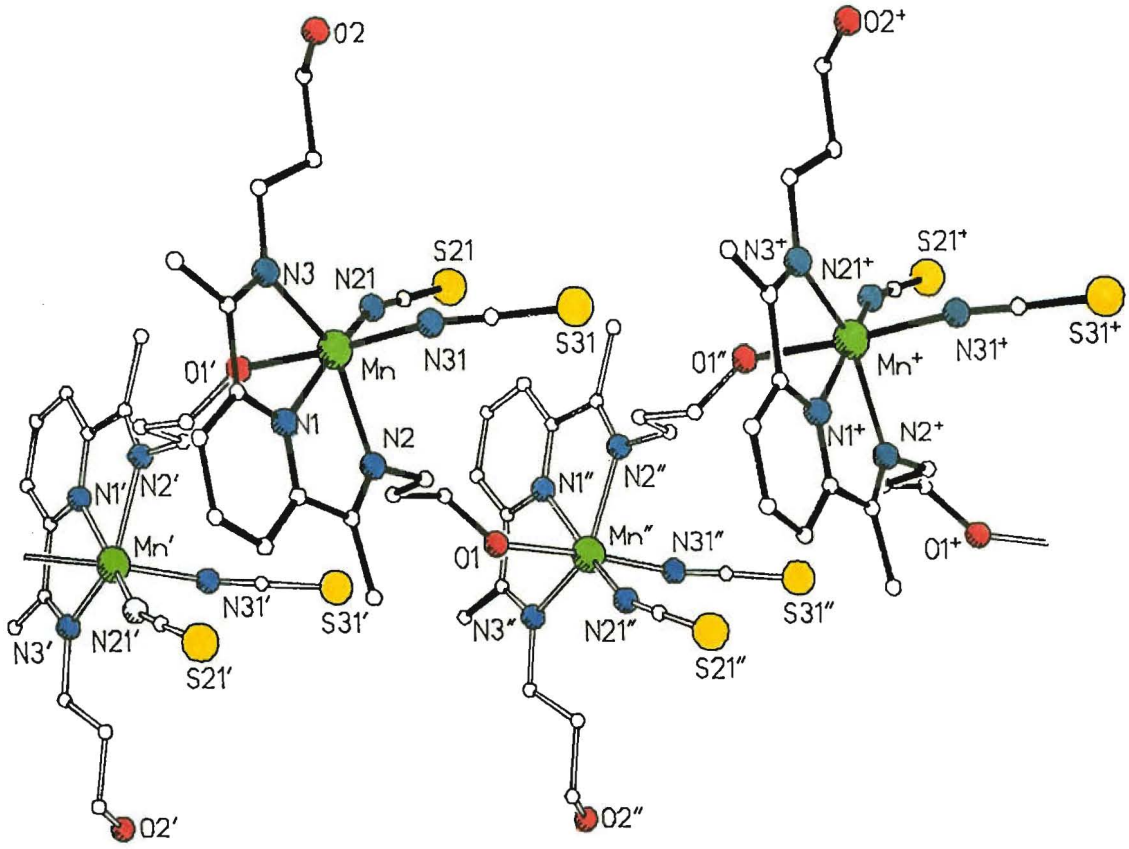

Figure 85: Perspective view of $[Mn(H_2L9)(NCS)_2]_x$

Table 27: Selected bond lengths and angles for $[Mn(H_2L9)(NCS)_2]_x$

Bond Lengths (Å)							
Mn-N1	2.219(2)	Mn-N2	2.280(1)	Mn-N3	2.304(2)	Mn-N21	2.130(2)
Mn-N31	2.167(2)	Mn-O1'	2.282(2)				

Bond Angles (°)					
N1-Mn-N2	71.0(1)	N1-Mn-N3	71.2(1)	N2-Mn-N3	142.0(1)
N1-Mn-N21	163.9(1)	N2-Mn-N21	97.7(1)	N3-Mn-N21	120.0(1)
N1-Mn-N31	98.3(1)	N2-Mn-N31	89.5(1)	N3-Mn-N31	92.8(1)
N21-Mn-N31	92.8(1)	N1-Mn-O1'	85.4(1)	N2-Mn-O1'	93.6(1)
N3-Mn-O1'	86.4(1)	N21-Mn-O1'	84.0(1)	N31-Mn-O1'	175.7(1)

The nickel(II) complex of H_2L9 with ClO_4^- as counter ion is a monomer (cation Figure 86, Table 28) as seen in the $[Ni(H_2L2)_2](ClO_4)_2$ complex (Figure 78). Two H_2L9 ligands are bound by the nitrogen donors only giving a geometry approaching octahedral. This makes angles about the nickel atom due to the pyridinediimine unit of $\theta_{1,2} = 78.1(1)°$ and $\theta_{1,3} = 77.1(1)°$. These angles are closer to 90° than in the $[Mn(H_2L9)(NCS)_2]_x$ structure (71.1° average) because the nickel atom is significantly closer to N1 (Ni-N1 1.973(3)Å) than was the case for

the manganese atom (Mn-N1 2.219(2)Å). The angle between the two pyridine rings is 95.6°.

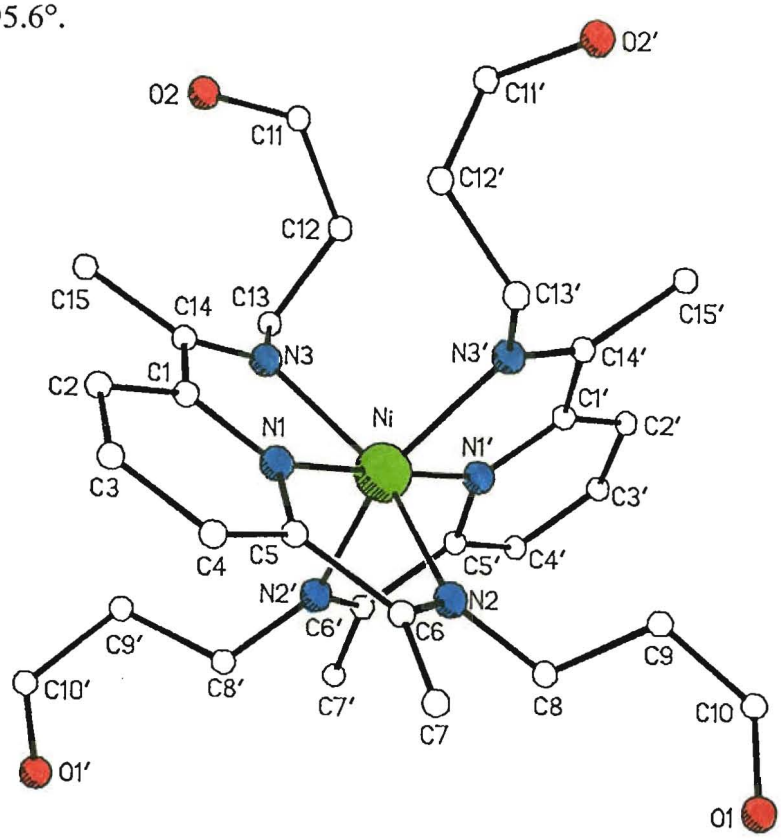

Figure 86: Perspective view of the cation $[Ni(H_2L9)_2]^{2+}$

Table 28: Bond lengths and angles for $[Ni(H_2L9)_2](ClO_4)_2$

Bond Lengths (Å)					
Ni-N1	1.973(3)	Ni-N2	2.106(2)	Ni-N3	2.125(2)

Bond Angles (°)					
N1-Ni-N2	78.1(1)	N1-Ni-N3	77.1(1)	N2-Ni-N3	154.7(1)
N1-Ni-N1'	178.9(1)	N2-Ni-N1'	102.7(1)	N3-Ni-N1'	102.2(1)
N2-Ni-N2'	90.7(1)	N3-Ni-N2'	90.1(1)	N3-Ni-N3'	99.8(1)

When thiocyanate is present a polymeric nickel(II) complex of H_2L9 is isolated (Figure 87). Each nickel atom is again six-coordinate with approximate octahedral coordination. The three nitrogen donors of the pyridinediimine unit again make angles of *ca.* 77° at the nickel centre due to the nickel atom moving in towards N1 (Ni-N1 1.993(4)Å). Two nitrogen atoms of terminally bound thiocyanate groups and the alcohol oxygen of an alkoxy arm from a different unit complete the coordination sphere. The mean planes of successive pyridine rings make angles of 63.7° with each other.

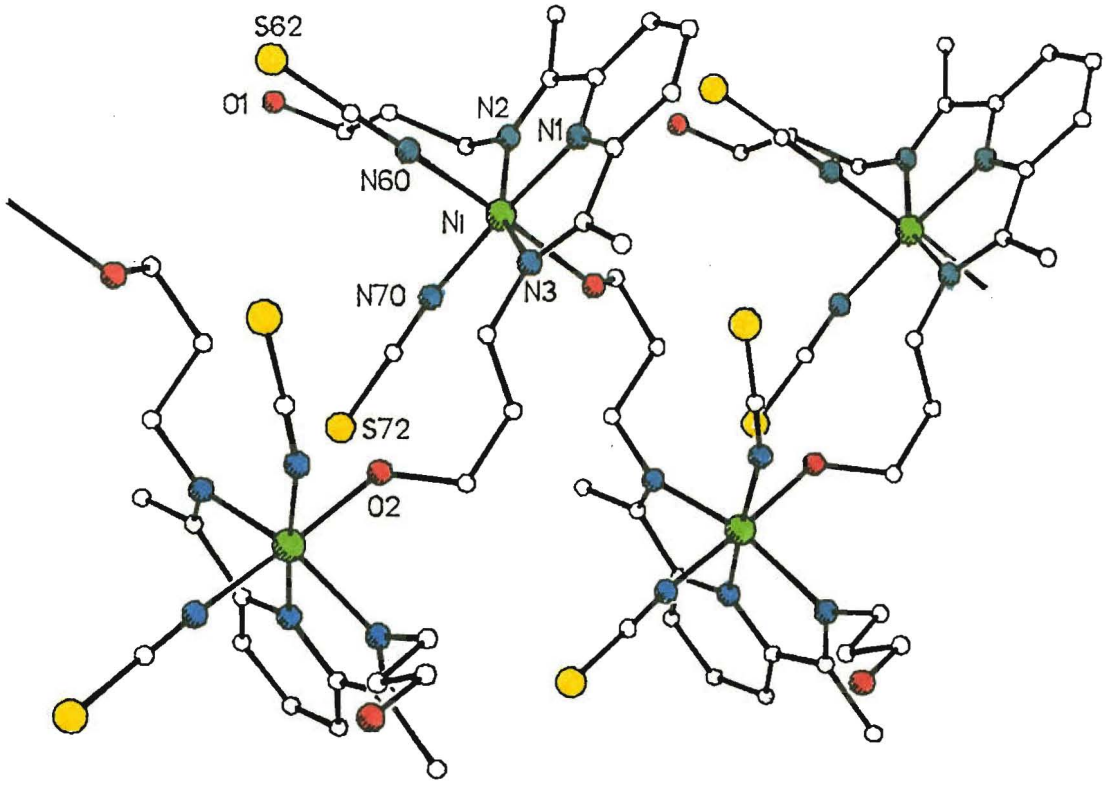

Figure 87: Perspective view of $[Ni(H_2L9)(NCS)_2]_x$

Table 29: Selected bond lengths and angles for $[Ni(H_2L9)(NCS)_2]_x$

Bond Lengths (°)							
Ni-N1	1.993(4)	Ni-N2	2.109(6)	Ni-N3	2.123(6)	Ni-N60	2.066(5)
Ni-N70	2.016(4)	Ni-O2'	2.177(4)				

Bond Angles (°)					
N1-Ni-N2	77.3(2)	N1-Ni-N3	77.6(2)	N2-Ni-N3	154.9(2)
N1-Ni-N60	93.1(2)	N2-Ni-N60	91.2(2)	N3-Ni-N60	90.6(2)
N1-Ni-N70	175.4(2)	N2-Ni-N70	102.1(2)	N3-Ni-N70	102.9(2)
N60-Ni-N70	91.5(2)	N1-Ni-O2'	88.1(2)	N2-Ni-O2'	91.0(2)
N3-Ni-O2'	87.7(2)	N60-Ni-O2'	177.7(2)	N70-Ni-O2'	87.3(2)

Results and Discussion of the H_2L2 Complexes

The two arm ligand H_2L2 was designed to be equivalent to half of the H_2L1 macrocycle (Figure 88). Removing the constraint due to the macrocyclic ring leaves the alcohol arms free to twist into appropriate conformations to bridge mononuclear complexes. Thus it was thought possible that clusters of transition metal ions would be held together by alcohol arm bridges as observed in related complexes (see discussion of HL3).

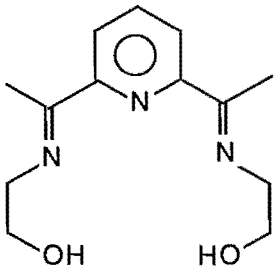

H_2L2

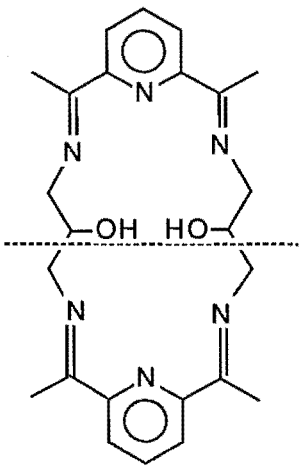

H_2L1

Figure 88

Free H_2L2 is difficult to synthesise as DAP is an unreactive aromatic ketone (i.e. less reactive than an aliphatic ketone which is in turn less reactive than an aldehyde)[145] and free H_2L2 itself is susceptible to hydrolysis. Therefore, other than the $[Ni(H_2L2)_2](ClO_4)_2$ complex, all of the complexes characterised were synthesised directly from DAP, ethanolamine and the transition metal salt. Successful formation of H_2L2 complexes was initially established from the replacement of the DAP carbonyl stretch at 1700 cm^{-1} with an imine absorption at *ca.* 1650 cm^{-1} in the infrared spectrum. The one exception was $[Co(H_2L2)_2](ClO_4)_3$ which showed no imine absorption (see later). The $[Mn(H_2L2)(H_2O)_2](ClO_4)_2$ complex has an extra absorption at 1610 cm^{-1} which is possibly due to the coordinated water.

The proposed stoicheiometries are in all cases supported by C, H and N elemental analyses and/or observation of the parent ion by mass spectrometry (Experimental Section). Single crystal X-ray structure determinations have been carried out for all but the $[Co(H_2L2)_2](ClO_4)_3$ complex.

All three structurally characterised manganese(II) complexes (Figures 75 to 77) are monomeric. It appears that the H_2L2 ligand provides its five donors in a pentagonal array which is acceptable to manganese(II). This leaves only the axial sites free for a bridging interaction by an anion. In the cases of the perchlorate, thiocyanate and azide complexes no bridging occurs. This is reflected in the normal uncoupled d^5 (5.8 - 6.0 BM expected[146]) room temperature magnetic moment of 5.99 BM found for the thiocyanate monomer. Conductivity measurements (Table 30) show that the thiocyanate and azide complexes are 1:1 electrolytes in DMF and methanol respectively, so there is some anion dissociation from the axial sites in solution. The perchlorate compound is a 1:2 electrolyte as is expected. As was observed for the macrocyclic complexes of manganese(II) described in the previous chapter, these monomers are yellow or orange in colour. The colour again arises from an absorption at *ca.* λ_{max} = 300 nm ($\varepsilon \approx 6{,}000$) which tails off into the visible.

Further intense ligand transitions or charge transfer absorption bands occur at higher energy.

Table 30: Conductivity measurements at *ca.* 1 mmol l^{-1}, Λ_m $ohm^{-1}cm^2$ mol^{-1}. Literature ranges are tabulated in Table 14.

Complex	Solvent	Λ_m
$[Mn(H_2L2)(H_2O)_2](ClO_4)_2$	MeOH	188
$Mn(H_2L2)(NCS)_2$	DMF	97
$Mn(H_2L2)(N_3)_2$	MeOH	105
$[Co(H_2L2)_2](ClO_4)_3$	MeCN	372
$[Ni(H_2L2)_2](ClO_4)_2$†	MeOH	178
$[Ni(H_2L2)(NCS)_2]_2$	DMF	108

† This complex was studied at a concentration of only 0.1 mmol l^{-1}

These manganese complexes have very similar properties to the pentagonal bipyramidal manganese(II) complexes of the (1+1) macrocycle 89A characterised by Nelson *et al* (89B: μ_{eff} (293 K) = 5.91 BM, Λ_m (MeCN) = 77, orange).[136]

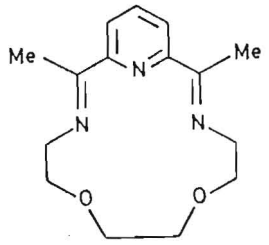

89A

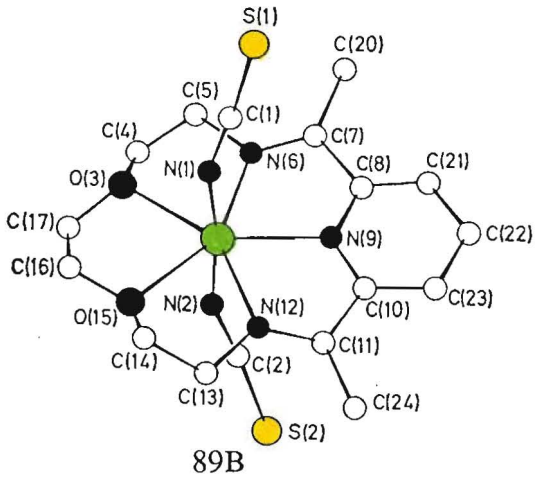

89B

Figure 89

The H_2L2 ligand, with it's flexible arms, acts as a planar N_3O_2 donor set as does the ring-constrained macrocycle 89A. This is an interesting feature of H_2L2 as it was thought that a ligand constrained to be planar was necessary to enforce pentagonal geometry at a metal ion. This requirement is met by either a fairly rigid macrocycle (e.g. above example), or a conjugated noncyclic ligand. This latter case is illustrated by the resonance-stabilised planar ligand 90A which gives the pentagonal bipyramidal manganese(II) complex shown in Figure 90B.[133]

These monomeric complexes are not very useful models for the OEC, although interest has been expressed by Cramer in the synthesis of an analogous chloride-containing complex. Based on the results to date this complex is expected to have two chloride ions bound to the axial sites, producing another manganese(II) monomer. The EXAFS and XANES spectra will be useful additions to the database

Cramer is generating; especially if these units stack so that the Mn-Cl vectors are aligned allowing oriented studies of the crystals.

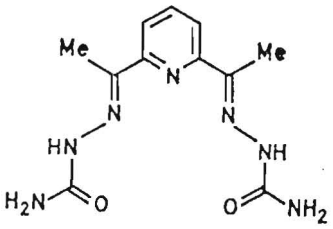

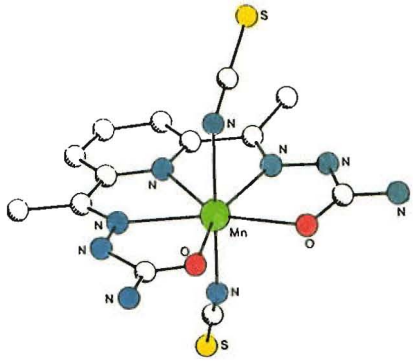

90A 90B

Figure 90

The structure of the cobalt complex was not verified by an X-ray structure determination because all of the crystals obtained were hopelessly twinned. However, the combination of results from other techniques, summarised below, indicates that this complex is $[Co^{III}(H_2L2)_2](ClO_4)_3$. Mass spectrometry indicated a parent ion at 656 a.m.u. which corresponds to $[Co(H_2L2)(HL2)(ClO_4)]^+$, and the complex acts as a 1:3 electrolyte in MeCN (Table 30). The oxidation state +III was assigned due to the room temperature magnetic moment of 0.84 BM which indicates a low spin d^6 configuration. The coordination of six imine-type nitrogen donors is consistent with a fairly large LFSE and the corresponding low spin configuration. The lack of an imine absorption in the infrared spectrum also correlates with the d^6 low spin system. This is a common characteristic of low spin Fe(II) (d^6) α-diimine complexes and is due to an increase in the metal-imine nitrogen bond strength because of extensive delocalisation (backbonding) of t_2-electrons from the metal into vacant π* orbitals of the α-diimine.[147] Finally, the C, H and N elemental analysis was also consistent with the formulation $[Co^{III}(H_2L2)_2](ClO_4)_3$.

The $[Ni(H_2L2)_2](ClO_4)_2$ complex is another structurally characterised monomer (Figure 78) with the expected 1:2 electrolyte behaviour in methanol; it was not characterised further. It is interesting to compare this structure with the ring-opened octahedral Ni(II) complex (91B) which resulted when Nelson attempted to complex the (1+1) macrocycle 91A (Figure 91).[148]

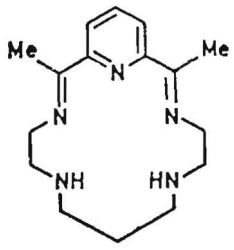

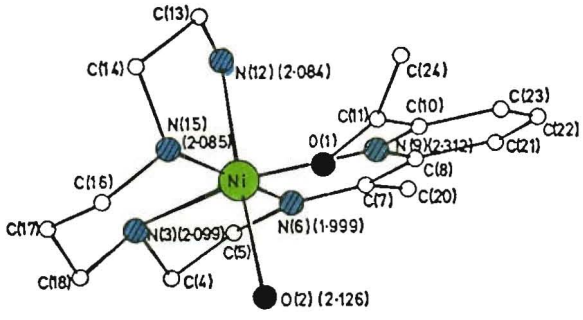

91A 91B

Figure 91

The strong stereochemical preference of the d^8 ion for tetragonal geometries is imposed on the ligand by promoting hydrolysis to release strain. In comparison, the planar (resonance stabilised) two arm ligand 90A led to a pentagonal bipyramidal nickel(II) complex (Figure 92).[130,131] In this case the multidentate ligand has a preferred planar conformation and this conformation is imposed on the d^8 metal ion producing the unusual geometry. H_2L2 can provide the same arrangement of donor atoms but because the arms are flexible they can (and do) twist out of the way so that the nickel atom can bind six nitrogen donors in a geometry approaching the preferred octahedral arrangement.

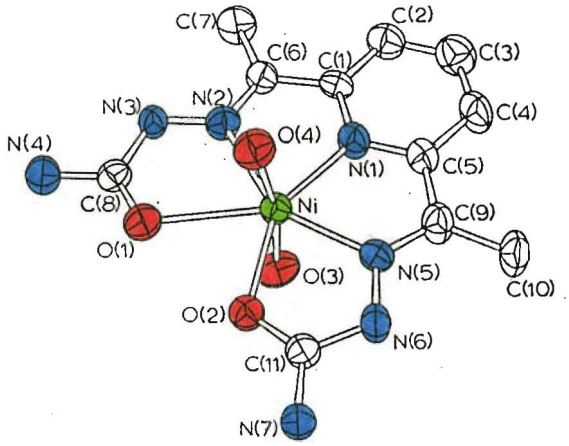

Figure 92

A dimer is formed by Ni(II) when NCS^- is present (Figure 79). The change in structure from the perchlorate complex due to the loss of one set of three imine-type nitrogen donors (from H_2L2), is compensated by two nitrogen donors (from NCS^-) and loss of some of the strain imposed by tbe coordination of two rigid pyridinediimine units. The sixth coordination site is occupied by the intermolecular alcohol bridge. This complex is not very soluble but on warming in DMF a solution of 1 mmol l^{-1} concentration was shown to have 1:1 electrolyte behaviour (Table 30). It is concluded that some dissociation accompanies dissolution. The electronic spectrum is very similar to that observed for a related pseudo-octahedral nickel(II) complex $[Ni(93)(NCS)](ClO_4)$ (Figure 93).[148]

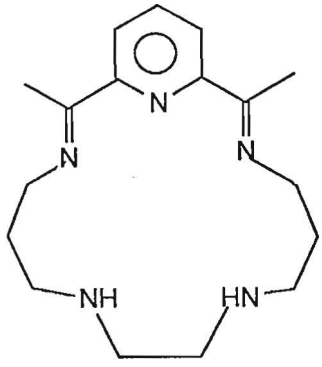

Figure 93

These absorptions are readily assigned for pseudo-octahedral nickel(II). The two lower energy bands $\lambda_{max} \approx 900$ nm, $\varepsilon \approx 70$; and $\lambda_{max} \approx 585$ nm, $\varepsilon \approx 40$ are d-d transitions, specifically the $^3A_{2g} \rightarrow {}^3T_{2g}$ and $^3A_{2g} \rightarrow {}^3T_{1g}$ (F) transitions. The third allowed transition, $^3A_{2g} \rightarrow {}^3T_{1g}$ (P) is at higher energy and is therefore hidden by the intense charge transfer/ligand transition absorptions.

Results and Discussion of the HL3 Complexes and Formation of (L3')ClO4

This arm ligand was chosen because it was thought that it might be compact enough, and flexible enough, to build clusters of bridged transition metal ions. The flexible arm could potentially provide bridges *via* the terminal alcohol group. An advantage of HL3 over H_2L1 and H_2L2 is that it provides a maximum of three donors so the metal ion will have vacant coordination sites which could be occupied by bridging groups.

Many related tridentate one-armed Schiff-base ligands have been successfully employed to build clusters of copper(II) ions bridged by oxygen atoms. Representative examples are shown in Figure 94.

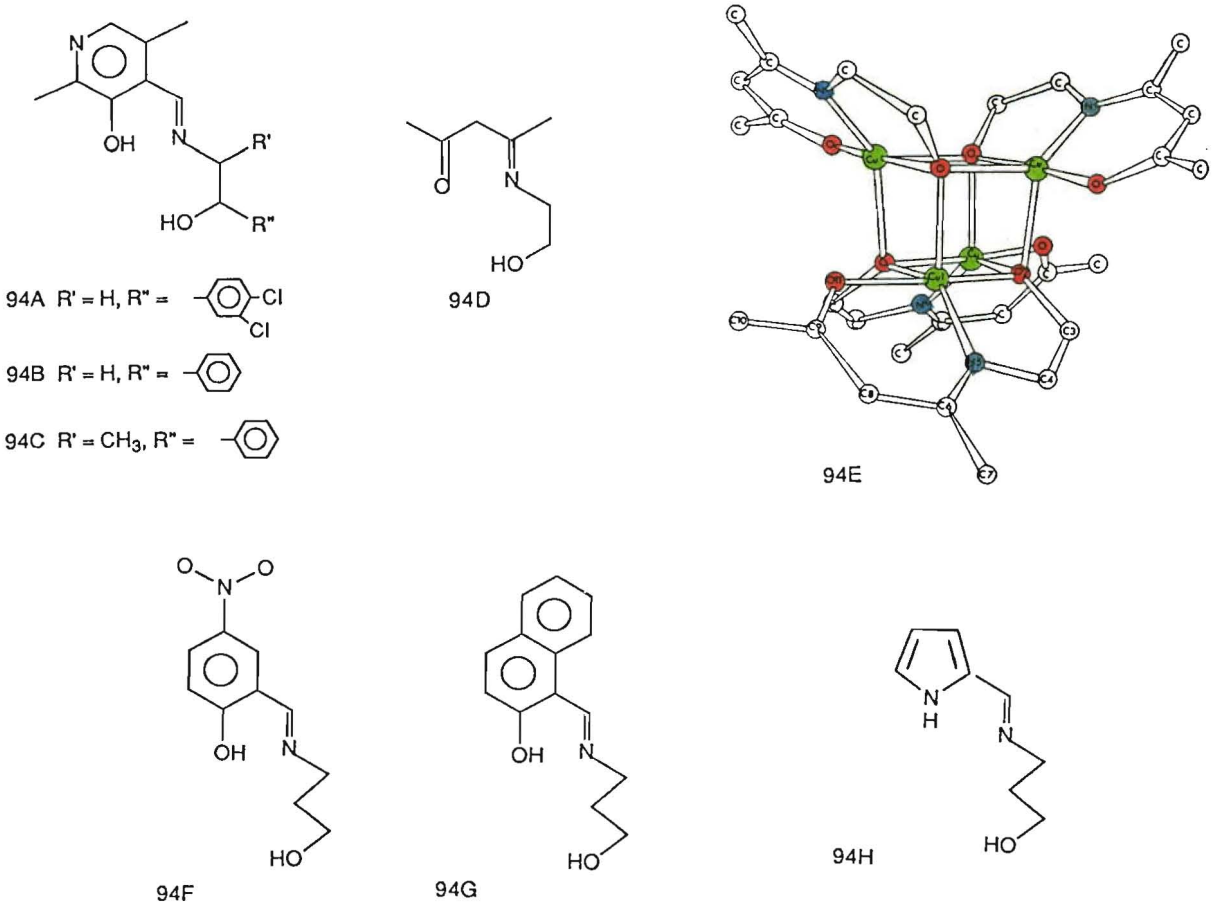

Figure 94

Figure 94 continued

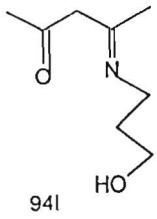

94I

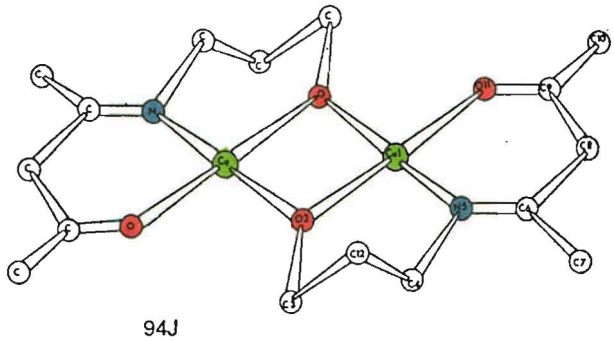

94J

The incorporation of an ethanolamine fragment (e.g. 94A[149], 94B[150], 94C[150], 94D[151]) generally leads to the formation of Cu_4O_4 cubane-type clusters of the general structural type shown in 94E.[151] However, a recent paper by Cros and Laurent[152] proposed a binuclear structure (94J) for the copper(II) complex of the one arm Schiff-base derived from 2'-aminoacetophenone and ethanolamine, on the basis of the mass spectrum and the temperature dependence of the magnetic moment. In comparison, when propanolamine is incorporated (e.g. 94F[153], 94G[154], 94H[155], 94I[151]) binuclear copper(II) complexes of the type shown in 94J[151] are formed. In all of these examples the arm alcohol group bridges two copper(II) ions. Therefore, it seemed that employing HL3 might well lead to the formation of clusters of transition metal ions.

Free HL3 is readily prepared as it is formed from a reactive aromatic aldehyde, however during the course of this work it was found that the chemistry of HL3 is complicated by a rearrangement reaction to form $(L3')^+$ (Figure 73). The transition metal complexes of HL3 which were characterised are discussed next, and finally a possible scheme for the rearrangement to $(L3')^+$ is proposed.

Discussion of the HL3 Complexes

The two manganese(II) complexes of HL3 and NCS^- which were structurally characterised were neither dimeric nor tetrameric. The first is monomeric with the alcohol arms uncoordinated (Figure 80) and the second is polymeric *via* 1,3-NCS^- bridging and intermolecular alcohol arm bridging (Figure 81). The latter complex is also significantly different to those shown in Figure 94 because the alcohol group does not bridge two manganese ions, it binds only to the manganese atom of the next unit in the polymer. The observation that the two products could be separated and recrystallised cleanly from the same reaction suggests that there is apparently little interconversion between the two structural types during recrystallisation. The mole ratio of one HL3:one manganese(II) employed in the synthesis is probably the

reason that the polymeric 1:1 complex predominates over the 1:2 monomeric complex.

The nickel(II) complex is a monomer (Figure 82) with two tridentate HL3 ligands, and two uncoordinated ClO_4^- anions. This structure is similar to that isolated when nickel(II) is complexed by a one arm thiol ligand (Figure 95).[156]

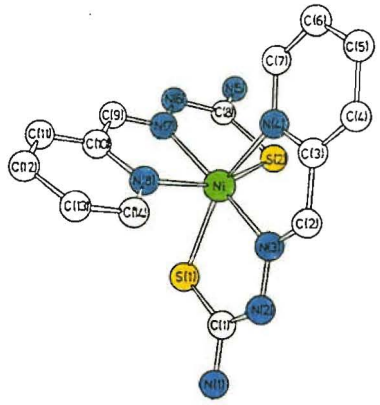

Figure 95

Dimers were obtained when copper(II) or zinc(II) complexed HL3 in the presence of ClO_4^- counter ions (Figure 83). Again these are different to the complexes shown in Figure 94 because the oxygen arms bind only to the copper (or zinc) atom of the second part of the dimer. That is, they do hold the dimer together but they do not bridge two metal ions. Because there are no one atom bridges and the intermolecular alcohol arms twist down to bind axially to the copper atom, the Cu-Cu separation is large (5.6 Å). This leads to a room temperature magnetic moment of 1.88 BM for this copper(II) complex, which is in the range expected for uncoupled octahedral d^9 ions (1.7 - 2.2 BM).[146] The visible spectrum (MeOH) shows only one broad d-d transition at 722 nm, $\varepsilon = 40$, which can be assigned to $^2Eg \rightarrow {}^2T_2$. Intense charge transfer or ligand transitions occurred in the ultraviolet.

In conclusion, no oxygen-bridged transition metal clusters were isolated using HL3, but several other structural types have been identified. A different synthetic approach may, however, lead to the formation of 94E and/or 94J structural types. For example, the copper and manganese complexes could be prepared under anhydrous conditions using only ClO_4^- counter ions. In both cases the absence of H_2O or NCS^- ligands to complete the coordination sphere might promote the formation of 94E or 94J type clusters.

Formation of L3 and (L3')$^+$

Schiff-bases such as HL3 are formed *via* a series of equilibria and the precise mechanism is pH dependent.[145] There is an optimum pH for the maximum rate of formation of a particular imine. This is because of a switch of the slowest (and therefore rate determining) step from acid-catalysed dehydration (Step 5) on the

high pH side, to attack of the amine on the carbonyl group (Step 1) on the low pH side of the optimum pH (see Figure 97).

HL3 can be formed quantitatively by several routes:

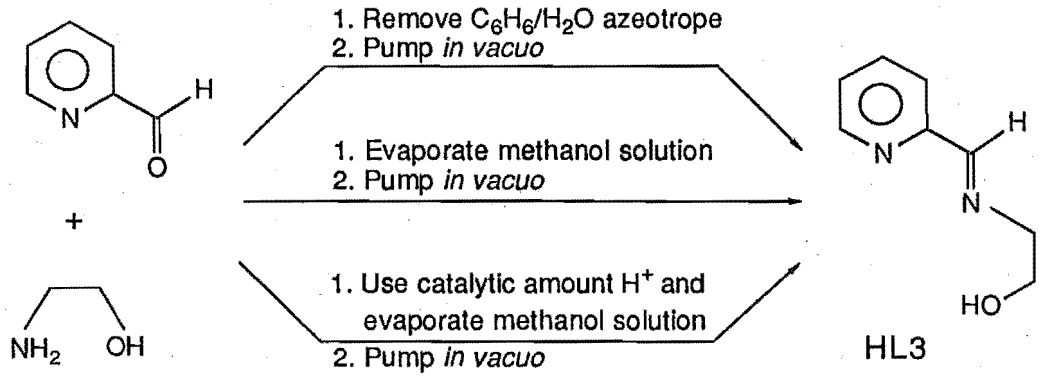

Figure 96

It therefore appears that the optimum pH for HL3 formation lies in the neutral or mildly acidic pH range. Schiff-bases like HL3 are known to be unstable with respect to hydrolysis. The rate of hydrolysis increases with acidity, allowing $(L3')^+$ formation to occur.

Figure 97 outlines a possible mechanism for formation of HL3 and $(L3')^+$ from 2-pyridinecarbaldehyde and ethanolamine based on those proposed for similar compounds.[157] $(L3')^+$ is formed when 2-pyridinecarbaldehyde and ethanolamine are reacted under acidic conditions (1:1 $HClO_4$ or p-toluenesulphonic acid:aldehyde) and, to some extent, in the presence of metal ions. The role of acid is probably to destabilise HL3 (i.e. enhanced hydrolysis), promoting $(L3')^+$ formation instead. $(L3')ClO_4$ has quite low solubility and crystallises out of ethanolic reaction solutions which contain mainly HL3 and 2-pyridinecarbaldehyde rather than $(L3')^+$ (5:1) *via* the equilibria shown in Figure 97. This conclusion was based on electronic spectra of ethanolic solutions; $(L3')^+$ has a characteristic absorption at 315 nm, $\varepsilon = 11{,}300$ which was readily compared with HL3 ($\lambda_{max} = 273$ nm, $\varepsilon = 5{,}600$; $\lambda_{max} = 234$ nm, $\varepsilon = 10{,}000$), although 2-pyridinecarbaldehyde has absorptions at similar wavelengths to HL3. On the other hand, $(L3')(p\text{-}CH_3C_6H_4SO_3)$ is quite soluble and therefore a shift of the equilibrium due to precipitation is not applicable. After solvent removal it remains as an oil, while some of the excess protonated amine precipitates as the p-toluenesulfonate salt. NMR of this oil shows the presence of the amine salt and $(L3')(p\text{-}CH_3C_6H_4SO_3)$ but no significant amounts of HL3.

To explain these observations it was necessary to determine whether or not $(L3')^+$ formation is reversible under these conditions. The electronic spectrum of $(L3')ClO_4$ in EtOH did not change over two months. Acidification to pH ≈ 1 did not change the absorption at 315 nm, although more acid did appear to cause aldehyde to be reformed (based on the electronic spectrum). Addition of base to pH ≈ 14 caused a white precipitate, but other than concentration effects, the electronic spectrum of

the solution was unchanged. Therefore within the reaction conditions employed $(L3')^+$ formation appears to be irreversible.

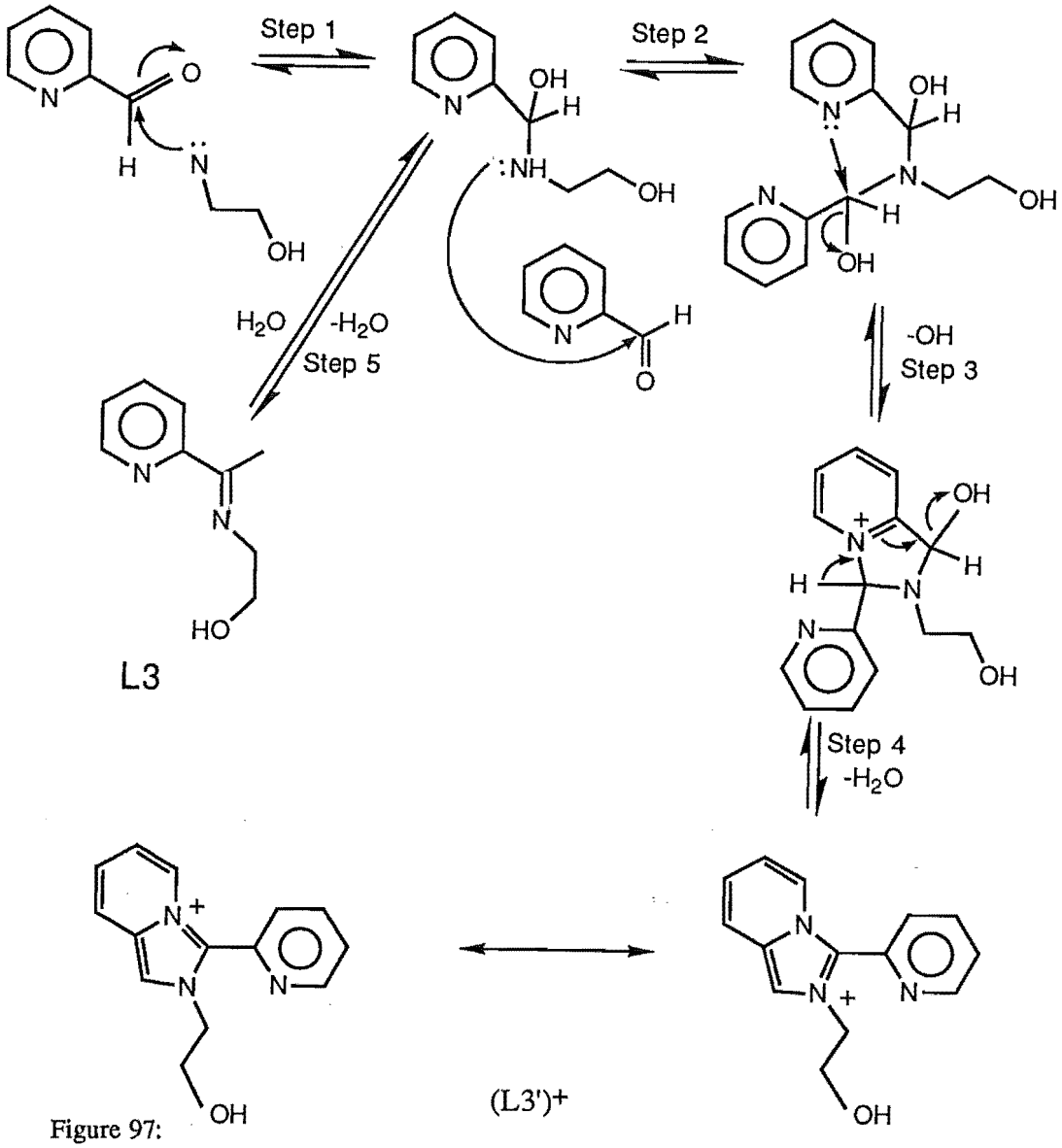

Figure 97:

This implies that in the HL3 forming reactions any $(L3')^+$ produced should be detected in the products. No $(L3')^+$ is detected, possibly because the pH is close to the optimum for fast reaction to produce HL3, and on the time scale employed (weeks not months) $(L3')^+$ did not have time to form in significant quantity.

Transition metal ions (e.g. Mn(II), Fe(III)) will provide slightly acidic pH conditions favouring fast, reversible formation of HL3. Because HL3 and the transition metal complexes of HL3 are very soluble the equilibrium allows slow, irreversible $(L3')ClO_4$ formation over a period of months. When Zn(II) was present $[Zn(HL3)(H_2O)_2]_2(ClO_4)_4$ was formed although small amounts of $(L3')^+$ were detected in the remaining oil. The manganese complexes $[Mn(HL3)_2(NCS)_2]$ and $[Mn(HL3)(NCS)_2]_x$ have been isolated quickly (days) from reactions of Mn(II) and HL3, with small amounts of $(L3')ClO_4$ also observed. Therefore, in conclusion, it

appears that in the presence of transition metal ions HL3 chemistry will be complicated by the formation of $(L3')^+$ to some extent.

Discussion of HL6 and the Rearrangement Product L6'

Initially interest in the one-armed ligands focused on making complexes of HL3 (Figure 71). However, as discussed above, this system was complicated by the formation of $(L3')^+$ (Figure 97). In order to prevent this rearrangement, which proceeds *via* loss of the aldehyde proton (Step 4, Figure 97), the aldehyde was replaced by the ketone 2-acetylpyridine. This prevented the previous rearrangement but, in addition to forming the desired Schiff-base HL6 (Figure 71), L6' (Figure 98) formed *via* an aldol condensation. Figure 98 shows a scheme by which L6' formation may occur.

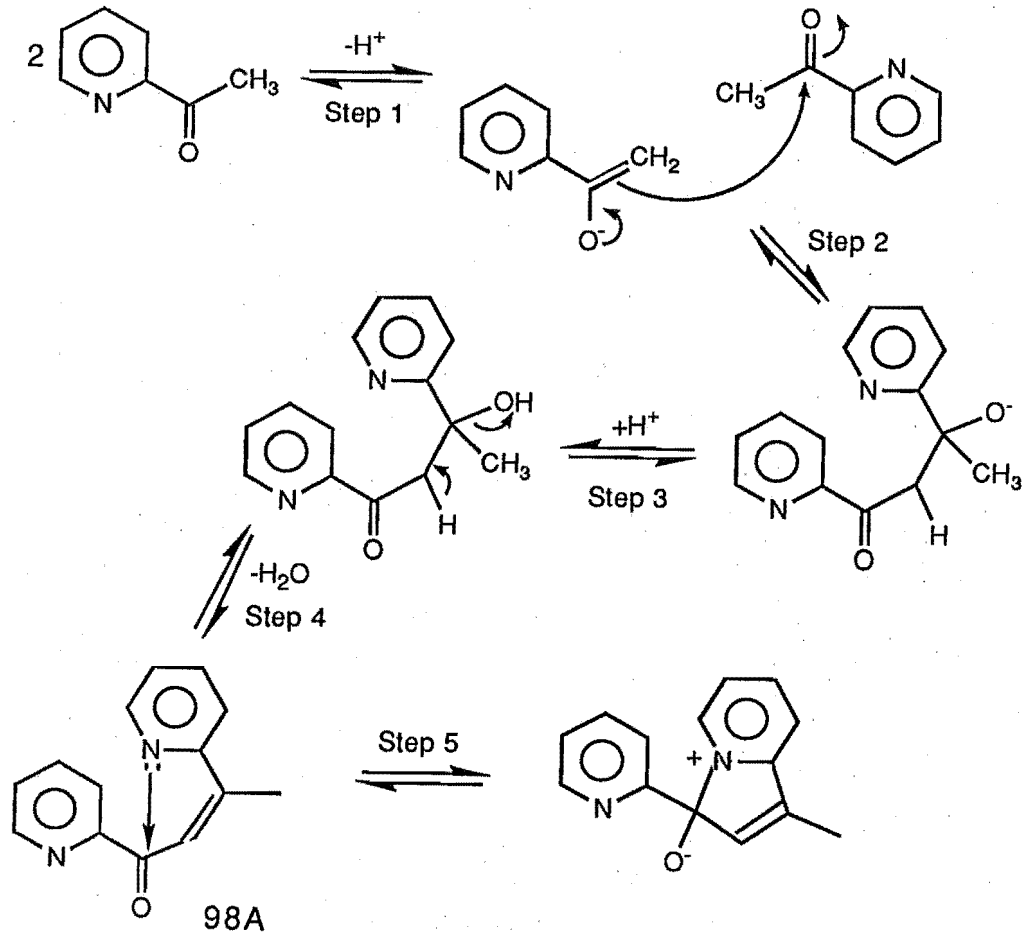

Figure 98

The first three steps are base-catalysed aldol-type reactions followed by a dehydration step, resulting in the αβ-unsaturated ketone (Figure 98A). Attack by the pyridine lone pair on the electron-deficient carbon of the carbonyl group (Step 5) results in L6'. In the preparation described in the Experimental Section the ketone was added to the solution of the amine. Possibly reversing the order of addition of these components (so the solution is less basic) could prevent L6' formation.

Results and Discussion of the H_2L9 Complexes

As the alcohol arms of the H_2L2 ligand only coordinate to a single manganese(II) ion no dimerisation or cluster formation occurred. The lengthening of each arm by one carbon to form H_2L9 was an attempt to disfavour planar pentagonal N_3O_2 coordination of manganese(II) by the H_2L9 ligand. Previous work with complexes of the macrocycle shown in Figure 93 found that the ligand was significantly folded such that the pyridine nitrogen (N9) lies 0.92 Å out of the mean plane of Mn, N6, N12, N16 and N19 (maximum deviation 0.04 Å) (Figure 99).[135]

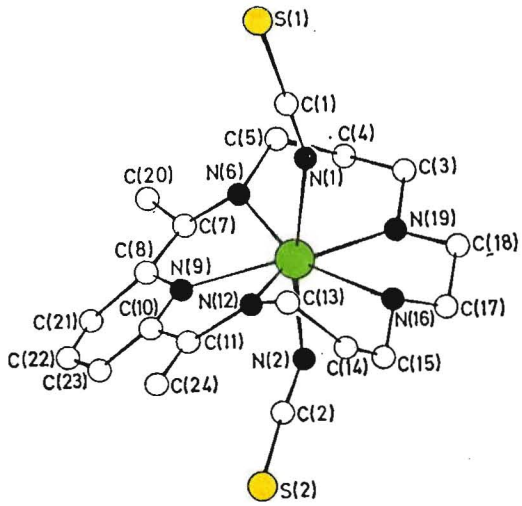

Figure 99

Therefore, as H_2L9 is noncyclic, it was expected that one or both of the alcohol arms would not bind to the manganese atom coordinated to the pyridinediimine unit of the same ligand. In this case the alcohol groups may bridge to another manganese complex, as seen in the nickel(II) complex of H_2L2 with NCS^-, (Figure 79) or they may not bind at all. As shown by the crystal structure of $[Mn(H_2L9)(NCS)_2]_x$ (Figure 85) this approach did prevent the formation of manganese(II) monomers but unfortunately led to polymeric species rather than finite clusters.

When only weakly coordinating ClO_4^- anions were available nickel(II) bound two pyridinediimine units preferentially (Figure 86), as seen before in the analagous H_2L2 complex (Figure 78). However, when NCS^- was present the nickel(II) coordinated two N-terminal NCS^- groups and an intermolecular bridging alcohol group instead of the second rigid pyridinediimine unit (Figure 87). In contrast to $[Ni(H_2L2)(NCS)_2]$ (Figure 79) this results in a polymeric structure, due to the extra length and flexibility of the three carbon arm. This polymer has electrolytic behaviour between that of a non-electrolyte and a 1:1 electrolyte which indicates some dissociation (Λ_m (calculated per monomer) = 45 in MeCN; 1:1 literature range 120 - 160) in solution. The solid state and DMF solution electronic spectra of this

polymer are very similar, indicating that the complex is largely intact in solution. The available solution electronic spectrometer was limited to a maximum wavelength of 900 nm, and an absorbance maximum was reached at around this value ($\varepsilon = 30$). The solid state electronic spectrum indicated that the maximum occurs at 920 nm ($^3A_{2g} \rightarrow {}^3T_{2g}$). A shoulder on this band occurred at 790 nm ($\varepsilon = 15$) and another absorbance ($^3A_{2g} \rightarrow {}^3T_{1g}$ (F) was identified at *ca.* 585 nm ($\varepsilon = 15$). An intense charge transfer band/ligand transition occurred in the u.v. region (*ca.* 280 nm) obscuring the final spin allowed d-d transition ($^3A_{2g} \rightarrow {}^3T_{1g}$ (P)). These results are very similar to those obtained for the $[Ni(H_2L2)(NCS)_2]_2$ complex.

Discussion of H_2L12

One possible reason for the difficulties experienced in trying to obtain complexes of manganese in higher oxidation states is the choice of Schiff-bases as ligands. The Schiff-base ligands used in this work are electron-rich, and most of them are unstable with respect to hydrolysis. Therefore synthesis of amide equivalents was attempted as these are known to stabilise high oxidation states by coordination of the deprotonated nitrogen atom.[158] For example 100A promotes the formation of a green manganese(IV) complex (Figure 100).[158]

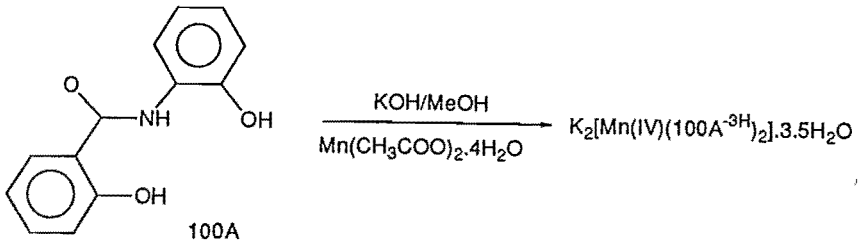

100A

Figure 100

Initially H_2L12 was synthesised rather than a macrocyclic amide because it avoided the added problems of polymer formation. The synthesis was straightforward and clean crystals were obtained. Subsequent work has indicated that simply mixing the two reactants and allowing them to stand for a week followed by the alcohol/ClO_4^- recrystallisation step may also be effective. The product was characterised by infrared spectroscopy, ^1H NMR, ^{13}C NMR and C, H and N elemental analysis. The carbonyl stretch appears at quite low energy, 1655 cm^{-1}, but this is usual for such amides (e.g. 100A 1620 cm^{-1}; 101A 1660 cm^{-1}; 101B 1676 cm^{-1}).[158,159,160]

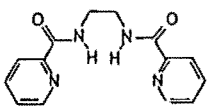

101A

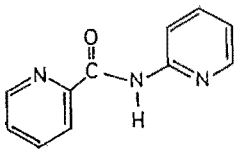

101B

Figure 101

The ^{1}H NMR spectrum is interesting because the two pyridyl protons appear as one broad signal at 8.08 ppm (360 MHz). This was confirmed by the relative integral of this signal and the alkyl proton signals, and by ^{1}H-^{13}C heteronuclear two-dimensional correlational spectroscopy which showed two carbon atoms to be coupled to this signal. Now that these characteristics have been established the synthesis of the related macrocyclic ligand H_6L14 (Figure 102) can be attempted with more confidence. Complexes of both H_2L12 and H_6L14 amide ligands with manganese could then be prepared and characterised.

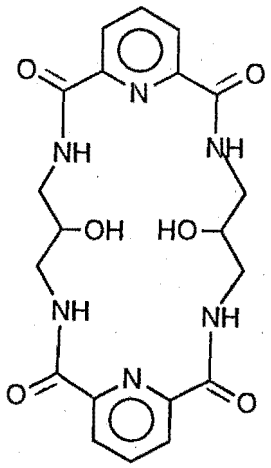

H_6L14

Figure 102

Appendix A

ATOMIC COORDINATES AND LABELLING SCHEMES

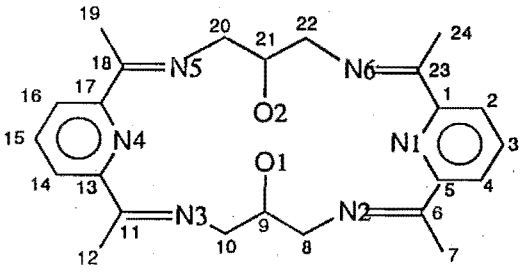

Figure 103: H_2L1 numbering scheme.

Table 31: Atomic coordinates ($x10^4$) for $[Mn_2(HL1)(Cl)_2]_2(ClO_4)_2.2DMF.H_2O$

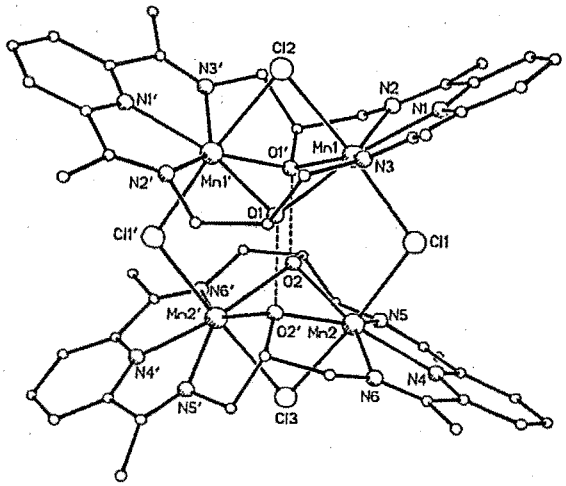

atom	x	y	z	atom	x	y	z
Mn1	8974(1)	4452(1)	2679(1)	C19	7306(10)	7445(6)	1370(6)
N1	7742(6)	3934(4)	2900(4)	N5	8366(6)	6732(4)	1830(4)
C1	7614(7)	3726(5)	3489(5)	C20	8926(8)	6714(4)	1297(4)
C2	6836(8)	3440(5)	3652(6)	C21	9469(7)	6138(5)	1265(5)
C3	6185(9)	3361(6)	3183(6)	O2	9731(4)	5943(3)	1876(3)
C4	6339(9)	3544(5)	2603(6)	C22	9678(7)	6198(5)	4145(4)
C5	7123(7)	3832(5)	2459(5)	N6	8924(6)	6468(4)	3779(4)
C6	7370(7)	4078(5)	1831(5)	C23	8210(7)	6657(5)	4012(5)
N2	8156(6)	4284(4)	1792(4)	C24	7965(8)	6651(6)	4702(5)
C7	6682(8)	4054(6)	1326(6)	Cl1	8084(2)	5402(1)	2816(1)
C8	8492(7)	4578(5)	1228(5)	Cl2	10000	3534(2)	2500
O1	10235(5)	4856(3)	3123(3)	Cl3	10000	7257(2)	2500
C9	10478(7)	4677(5)	3744(5)	Cl4	10190(3)	2033(2)	4960(2)
C10	9974(8)	4117(5)	3939(5)	O41	10110(10)	2526(6)	4558(7)

continued...

continued...

N3	9080(6)	4106(4)	3662(4)	O42	10297(18)	2282(12)	5544(13)
C11	8422(8)	3809(5)	3907(5)	O43	11149(12)	1868(9)	4899(7)
C12	8405(9)	3542(6)	4544(6)	O44	9585(18)	1670(13)	4892(14)
Mn2	8993(1)	6343(1)	2712(1)	O51	13346(10)	-23(6)	138(5)
N4	7781(6)	6874(4)	2974(4)	C52	12778(13)	81(7)	501(8)
C13	7532(8)	6901(5)	3579(5)	N53	11944(13)	-65(9)	433(8)
C14	6731(8)	7138(6)	3758(6)	C54	11557(21)	-352(11)	-89(10)
C15	6195(9)	7402(6)	3294(6)	C55	11316(17)	85(11)	856(13)
C16	6465(9)	7386(6)	2687(7)	O80	0	327(16)	7500
C17	7283(8)	7109(5)	2520(6)	O90	0	523(25)	2500
C18	7675(8)	7066(5)	1879(5)				

Table 32: Atomic coordinates (x10⁴) for $[Mn_2(HL1)(N_3)_2]_2(ClO_4)_2.3MeCN$

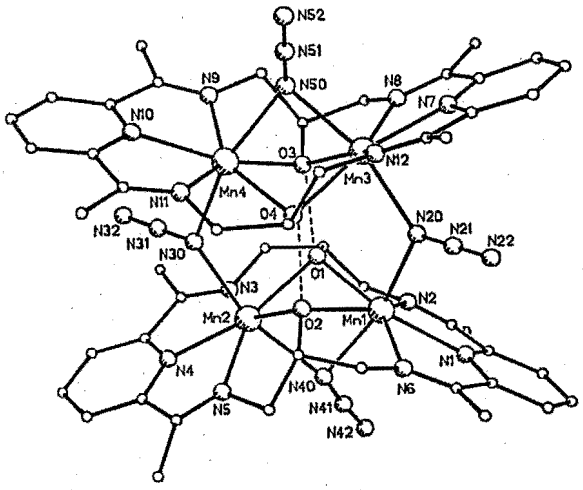

atom	x	y	z	atom	x	y	z
Mn1	3129(1)	6267(1)	3210(1)	C36	-1188(5)	8976(5)	522(5)
Mn2	1437(1)	7610(1)	3874(1)	C37	-199(5)	9976(4)	1263(4)
N1	4074(4)	5095(4)	3566(4)	C38	-931(5)	10637(5)	1378(5)
C1	4986(5)	5186(5)	3725(5)	C39	-753(6)	11405(5)	1709(5)
C2	5615(6)	4473(5)	3882(5)	C40	190(5)	11516(5)	1903(5)
C3	5287(6)	3656(5)	3878(6)	C41	903(5)	10824(4)	1765(4)
C4	4340(7)	3558(5)	3743(5)	N10	709(4)	10082(4)	1449(4)
C5	3733(5)	4299(5)	3595(5)	C42	1927(5)	10835(4)	1974(4)
C6	2681(6)	4321(4)	3499(5)	C43	2228(6)	11658(4)	2293(5)
C7	2147(6)	3512(5)	3735(6)	N11	2443(4)	10115(3)	1868(4)
N2	2286(4)	5052(3)	3289(4)	C44	3417(5)	9996(4)	2122(5)
C8	1236(5)	5219(4)	3348(5)	C45	3900(5)	9078(4)	1859(5)
C9	953(5)	6033(4)	2835(5)	O4	3177(3)	8467(3)	1901(3)
O1	1666(3)	6673(3)	2811(3)	C46	4513(5)	9130(4)	1008(5)
C10	-69(5)	6455(5)	3166(5)	N12	4656(4)	8262(4)	652(4)
N3	-2(4)	7052(4)	3813(4)	C47	5438(5)	7960(4)	214(4)
C11	-770(5)	7469(4)	4161(5)	C48	6381(5)	8378(5)	11(5)
C12	-1801(5)	7315(5)	4017(6)	N20	3859(4)	6466(4)	1876(4)
C13	-629(5)	8132(4)	4783(5)	N21	4728(5)	6394(4)	1814(4)
C14	-1368(6)	8629(5)	5256(5)	N22	5582(5)	6321(5)	1743(5)

continued...

continued...

C15	-1097(6)	9219(5)	5788(5)	N30	990(4)	8670(4)	2871(4)
C16	-128(6)	9299(5)	5859(5)	N31	124(4)	8833(4)	2914(4)
C17	591(5)	8777(4)	5362(5)	N32	-724(5)	8987(4)	2960(4)
N4	316(4)	8234(4)	4822(4)	N40	2222(4)	6431(4)	4501(4)
C18	1658(5)	8763(4)	5356(5)	N41	2100(4)	5788(4)	4943(4)
C19	2061(7)	9175(6)	6053(6)	N42	2013(6)	5152(5)	5340(5)
N5	2164(4)	8341(4)	4770(4)	N50	2624(4)	8678(4)	210(4)
C20	3201(5)	8140(5)	4700(5)	N51	3016(4)	9115(4)	-323(4)
C21	3637(5)	8126(4)	3778(4)	N52	3403(5)	9549(4)	-869(5)
O2	2985(3)	7756(3)	3285(3)	C11	4187(1)	1029(1)	4309(1)
C22	4635(5)	7639(4)	3657(5)	O11	3623(4)	1497(4)	3727(4)
N6	4499(4)	6693(4)	3687(4)	O12	5167(4)	1214(5)	4120(5)
C23	5223(5)	6129(5)	3747(5)	O13	4063(7)	141(4)	4276(6)
C24	6238(6)	6333(5)	3835(7)	O14	3856(5)	1329(5)	5119(4)
Mn3	3325(1)	7463(1)	884(1)	C12	995(2)	3701(2)	978(2)
Mn4	1745(1)	8908(1)	1530(1)	O21	1478(5)	2895(4)	661(5)
N7	4443(4)	6853(4)	-94(4)	O22	128(11)	3539(6)	1413(15)
C25	5350(5)	7110(4)	-196(5)	O23	1583(9)	4138(7)	1387(7)
C26	6110(6)	6630(5)	-650(5)	O24	732(12)	4245(7)	354(14)
C27	5898(6)	5892(5)	-1055(5)	N60	6821(11)	8193(8)	2112(7)
C28	4949(6)	5663(5)	-973(5)	C61	6655(7)	8827(7)	2465(6)
C29	4230(6)	6152(4)	-484(5)	C62	6538(12)	9569(8)	2892(7)
C30	3183(5)	5965(4)	-335(5)	N70	7014(9)	2653(9)	2094(11)
C31	2855(6)	5235(5)	-768(6)	C71	6283(8)	2300(7)	2101(8)
N8	2641(4)	6449(4)	197(4)	C72	5343(8)	1992(7)	2103(8)
C32	1626(5)	6308(4)	453(5)	N80	9609(14)	3088(11)	3475(12)
C33	1109(5)	7086(4)	968(5)	C81	9004(17)	3403(15)	3267(15)
O3	1781(3)	7429(3)	1457(3)	C82	8527(16)	4103(13)	2741(14)
C34	676(5)	7792(4)	406(5)	N90	8355(14)	6645(12)	1384(12)
N9	500(4)	8608(3)	838(4)	C91	8177(19)	6204(17)	1852(17)
C35	-255(5)	9121(4)	862(4)	C92	8066(21)	5569(18)	2412(18)

Table 33: Atomic coordinates ($x10^4$) for $[Mn_4(HL1)(L1)(NCS)_4]NCS.2H_2O$

atom	x	y	z	atom	x	y	z
Mn1	1605(1)	259(2)	1295(1)	C27	618(5)	5289(17)	-2428(10)
Mn2	1545(1)	2628(2)	1184(1)	C28	619(4)	4250(16)	-2457(10)
Mn3	1011(1)	3219(2)	-518(1)	C29	704(4)	3680(13)	-1922(8)
Mn4	825(1)	1894(2)	476(1)	C30	680(4)	2534(14)	-1889(8)
O1	1600(2)	1361(8)	539(4)	N8	799(3)	2165(10)	-1351(6)
O2	1206(2)	1405(8)	1268(4)	C31	513(4)	1959(16)	-2440(9)
O3	1100(2)	1606(7)	-202(4)	C32	753(4)	1124(11)	-1201(7)
O4	1124(2)	3289(8)	530(4)	C33	1013(4)	765(11)	-631(7)
N1	1952(3)	-714(10)	1956(6)	N9	712(3)	280(10)	87(6)
C1	1900(4)	-1023(12)	2491(7)	C34	898(4)	-138(12)	-308(7)
C2	2122(4)	-1586(13)	2919(8)	C35	529(4)	-296(12)	297(7)
C3	2399(4)	-1796(14)	2813(8)	C36	473(4)	-1423(13)	212(8)
C4	2466(4)	-1505(13)	2274(7)	C37	359(4)	252(13)	700(7)
C5	2232(4)	-961(12)	1838(7)	C38	157(4)	-239(14)	998(7)
C6	2254(4)	-620(12)	1232(7)	C39	6(4)	402(14)	1330(8)

continued...

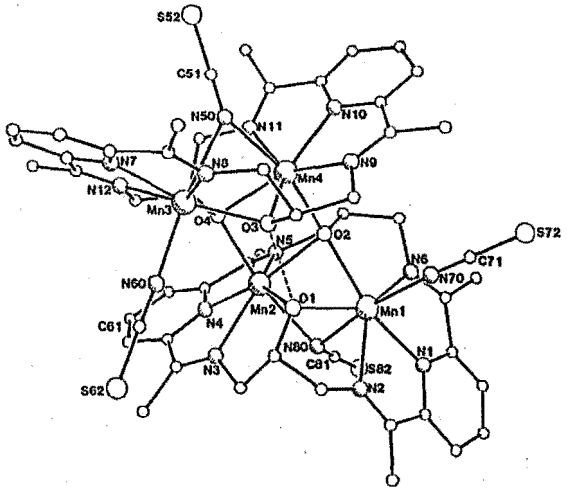

continued...

C7	2532(4)	-941(15)	1031(9)	C40	47(4)	1465(14)	1355(8)
N2	2036(3)	-58(10)	925(6)	N10	410(3)	1258(10)	732(6)
C8	2005(4)	367(13)	312(7)	C41	255(3)	1863(12)	1056(7)
C9	1852(3)	1395(12)	256(7)	C42	323(4)	2969(12)	1012(7)
C10	2091(4)	2207(12)	534(8)	N11	585(3)	3175(10)	888(5)
N3	1955(3)	3069(10)	791(5)	C43	85(4)	3725(15)	1086(9)
C11	2060(4)	3970(13)	862(7)	C44	674(3)	4169(12)	738(7)
C12	2330(4)	4348(14)	620(8)	C45	1028(4)	4200(12)	748(7)
C13	1946(4)	4629(13)	1282(7)	N12	969(3)	4890(10)	-272(5)
C14	2014(4)	5656(15)	1417(8)	C46	1086(4)	5102(12)	389(6)
C15	1917(4)	6114(15)	1882(8)	C47	889(4)	5558(13)	-674(8)
C16	1748(4)	5559(13)	2211(8)	C48	891(5)	6672(15)	-589(9)
C17	1681(4)	4556(12)	2038(7)	N50	498(3)	2738(10)	-408(6)
N4	1768(3)	4097(10)	1587(6)	C51	246(4)	2988(13)	-657(7)
C18	1513(3)	3815(11)	2361(7)	S52	-102(1)	3326(5)	-999(4)
C19	1498(4)	4058(15)	3006(8)	N60	1467(3)	3409(11)	-676(6)
N5	1409(3)	3005(9)	2062(5)	C61	1692(3)	3477(12)	-822(7)
C20	1271(4)	2161(12)	2316(7)	S62	2018(1)	3538(4)	-1043(2)
C21	1104(4)	1404(12)	1810(7)	N70	1354(3)	-1172(11)	911(6)
C22	1113(4)	298(12)	2079(7)	C71	1247(4)	-1800(15)	1170(8)
N6	1434(3)	-76(10)	2128(5)	S72	1091(1)	-2682(4)	1514(3)
C23	1592(3)	-677(11)	2556(7)	N90	1110(4)	-1388(14)	-1389(7)
C24	1490(4)	-1052(13)	3076(7)	C91	868(4)	-1386(15)	-1721(8)
N7	790(3)	4143(10)	-1372(6)	S92	524(1)	-1441(4)	-2200(3)
C25	789(4)	5157(13)	-1328(7)	N80	1922(3)	1627(10)	1898(5)
C26	694(4)	5796(15)	-1855(8)	C81	2019(3)	1532(12)	2425(7)
H1	1391	1495	186	S82	2146(1)	1385(4)	3175(2)

Table 34: Atomic coordinates (x10^4) for $[Mn_2(L1)(HCOO)]_2(ClO_4)_2.2DMF.H_2O$

atom	x	y	z	atom	x	y	z
Mn1	-222(1)	2100(1)	1444(1)	C18	542(3)	5732(6)	1702(5)
Mn2	564(1)	3621(1)	2089(1)	C19	382(4)	6690(6)	1561(6)
N1	-703(2)	1063(4)	712(4)	N5	264(3)	5037(4)	1560(4)
C1	-1127(3)	1292(5)	251(5)	C20	-267(3)	5046(6)	1171(5)
C2	-1432(3)	654(5)	-212(5)	C21	-385(3)	4052(5)	978(5)
C3	-1274(3)	-232(6)	-163(5)	O2	-242(2)	3556(3)	1708(3)
C4	-826(3)	-472(6)	274(5)	C22	-916(3)	3780(5)	634(5)
C5	-548(3)	193(5)	708(5)	N6	-903(2)	2779(4)	598(4)
C6	-47(3)	-4(5)	1214(5)	C23	-1251(3)	2294(6)	226(5)
C7	126(3)	-963(5)	1313(6)	C24	-1743(3)	2599(6)	-187(6)
N2	188(2)	700(4)	1524(4)	O31	183(2)	2337(4)	331(3)
C8	688(3)	679(5)	1993(5)	O32	736(2)	3421(4)	771(4)
C9	848(3)	1671(5)	2012(5)	C30	540(3)	2854(6)	254(6)
O1	472(2)	2188(4)	2306(3)	Cl	1503(1)	8604(2)	2906(2)
C10	1346(3)	1927(5)	2527(5)	O11	1885(3)	8039(6)	3319(5)
N3	1347(2)	2937(5)	2458(4)	O12	1492(3)	8489(5)	2023(4)
C11	1730(3)	3422(5)	2704(5)	O13	1027(3)	8332(6)	3119(5)
C12	2223(3)	3123(7)	3105(6)	O14	1609(3)	9515(5)	3128(5)
C13	1646(3)	4406(6)	2494(5)	O40	2285(3)	5253(7)	-229(6)
C14	2048(4)	5021(6)	2529(6)	C40	2312(5)	4503(11)	166(8)
C15	1926(4)	5902(7)	2306(6)	N40	1968(3)	3896(8)	1(5)
C16	1441(4)	6178(7)	2064(6)	C41	1553(4)	4016(9)	-615(8)
C17	1064(3)	5522(6)	2035(5)	C42	1989(5)	3027(10)	473(8)
N4	1178(3)	4664(4)	2265(4)	O50	2207(5)	985(10)	3894(9)

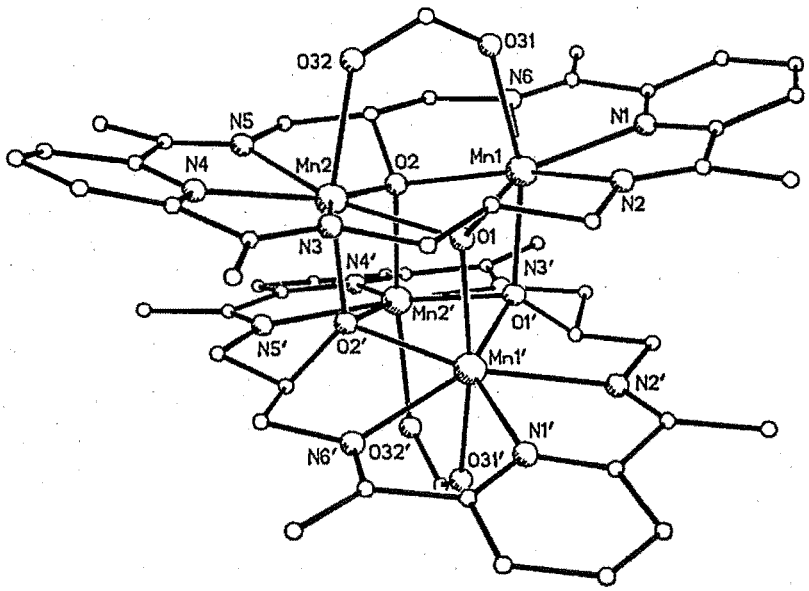

Table 35: Atomic coordinates (x104) for $[Mn_2(L1)(CH_3COO)]_2(ClO_4)_2.2DMF.5H_2O$

atom	x	y	z	atom	x	y	z
Mn1	-137(1)	2236(1)	1338(1)	N5	318(2)	5190(4)	1897(4)
Mn2	570(1)	3757(1)	2615(1)	C20	-150(2)	5209(4)	1068(4)
N1	-566(2)	1179(4)	275(4)	C21	-258(2)	4202(4)	781(4)
C1	-952(3)	1429(4)	-512(4)	O2	-177(2)	3694(3)	1572(3)
C2	-1231(3)	775(5)	-1162(5)	C22	-737(2)	3940(4)	5(4)
C3	-1089(3)	-128(5)	-994(5)	N6	-735(2)	2940(4)	-8(4)
C4	-690(3)	-379(5)	-223(5)	C23	-1045(3)	2436(5)	-628(4)
C5	-428(3)	292(4)	425(5)	C24	-1478(3)	2760(5)	-1449(5)
C6	21(3)	101(4)	1285(5)	O31	329(2)	2461(3)	643(3)
C7	167(3)	-869(4)	1526(5)	O32	826(2)	3540(3)	1548(3)
N2	238(2)	808(4)	1750(4)	C30	675(3)	2992(4)	874(5)
C8	696(2)	779(4)	2621(4)	C33	948(3)	2956(5)	337(5)
C9	851(2)	1787(4)	2782(5)	Cl	1633(1)	997(2)	9016(2)
O1	465(2)	2305(3)	2719(3)	O11	1308(5)	1336(5)	8240(7)
C10	1286(2)	2055(4)	3681(4)	O12	2009(3)	1598(6)	9458(7)
N3	1290(2)	3061(4)	3643(4)	O13	1465(7)	645(16)	9429(10)
C11	1626(3)	3576(4)	4219(4)	O14	1797(6)	206(7)	8796(15)
C12	2067(3)	3264(5)	5052(5)	O40	2413(6)	4038(10)	2218(10)
C13	1550(3)	4590(5)	4025(4)	C40	2390(6)	3112(12)	1856(12)
C14	1900(3)	5221(5)	4517(5)	N40	2275(5)	2350(9)	2047(9)
C15	1801(3)	6140(5)	4275(5)	C41	2030(5)	2445(9)	2645(9)
C16	1368(3)	6384(5)	3558(5)	C42	2375(8)	1354(14)	1854(15)
C17	1040(3)	5721(4)	3101(5)	O50	1531(3)	4896(5)	1832(5)
N4	1130(2)	4831(4)	3339(4)	O60	2815(4)	4023(6)	4181(7)
C18	572(2)	5894(4)	2271(4)	O70	2094(9)	-441(18)	8102(17)
C19	427(3)	6860(4)	1954(5)				

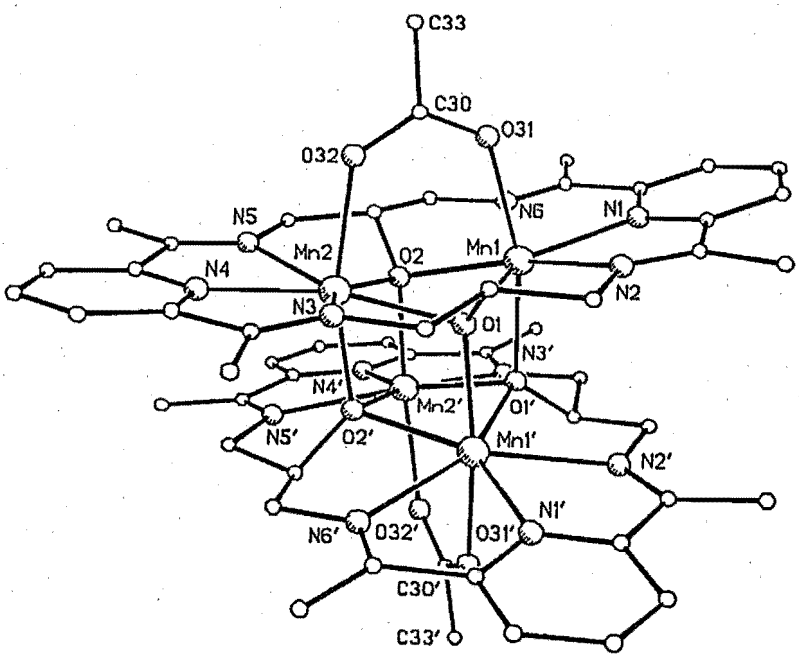

Table 36: Atomic coordinates (x10⁴) for $[Mn_4(L1')(H_2O)_{1.6}(DMF)_3(ClO_4)_2](ClO_4)_2$

atom	x	y	z	atom	x	y	z
Mn1	653(1)	8878(1)	2730(1)	C22	140(4)	10413(6)	1559(5)
Mn2	11(1)	7299(1)	1663(1)	N6	527(3)	10343(5)	2210(4)
N1	1143(3)	9979(5)	3409(4)	C23	746(4)	11069(6)	2544(5)
C1	1103(4)	10894(6)	3212(5)	C24	639(5)	12061(6)	2312(6)
C2	1388(4)	11594(7)	3630(5)	O50	1306(3)	8702(5)	2258(4)
C3	1719(4)	11321(8)	4220(6)	N50	1851(16)	8683(28)	1630(21)
C4	1772(4)	10368(8)	4398(6)	C50	1613	8394	1959
C5	1477(3)	9715(7)	3978(5)	C51	1878	9764	1446
C6	1506(4)	8655(7)	4092(5)	C52	2182(24)	8061(45)	1321(31)
C7	1881(4)	8288(8)	4725(6)	Cl1	-725(1)	7864(2)	-374(2)
N2	1233(3)	8170(5)	3632(4)	O11	-647(4)	7484(7)	294(4)
C8	1222(4)	7132(6)	3648(5)	O12	-278(3)	7723(5)	-574(4)
C9	937(3)	6758(5)	2945(5)	O13	-825(4)	8840(5)	-354(6)
O1	515(2)	7347(4)	2663(3)	O14	-1129(4)	7386(7)	-836(5)
C10	762(4)	5755(6)	3033(5)	Cl2	1911(1)	4199(3)	4206(2)
N3	363(3)	5825(5)	3363(4)	O21	1615(4)	3910(6)	3556(6)
C11	195(3)	5103(6)	3572(4)	O22	1950(7)	3627(9)	4735(7)
C12	340(4)	4095(6)	3510(6)	O23	1998(7)	5067(8)	4313(8)
C13	199(4)	5300(6)	1073(4)	O24	2351(8)	3882(25)	4093(14)
C14	421(4)	4616(7)	761(5)	C31	1655(9)	4861(14)	2089(11)
C15	734(4)	4903(7)	411(5)	C32	2108(9)	4782(16)	1168(12)
C16	844(4)	5863(7)	372(5)	N30	2003	5215	1679
C17	616(4)	6506(7)	690(5)	C30	1902(12)	6356(23)	1526(16)
N4	319(3)	6227(5)	1052(4)	O30	1696(5)	6983(10)	1836(7)
C18	663(4)	7541(7)	655(5)	N40	2211(7)	11672(14)	1983(9)
C19	955(5)	7952(8)	217(7)	C41	2029(9)	12248(15)	2409(12)
N5	413(3)	8033(5)	983(4)	C42	2471(8)	12027(14)	1579(10)
C20	403(4)	9066(6)	960(5)	C40	2048(8)	10793(16)	1851(11)
C21	2(4)	9424(7)	1274(5)	O40	1781(7)	10447(13)	2293(9)
O2	-42(2)	8797(4)	1802(3)				

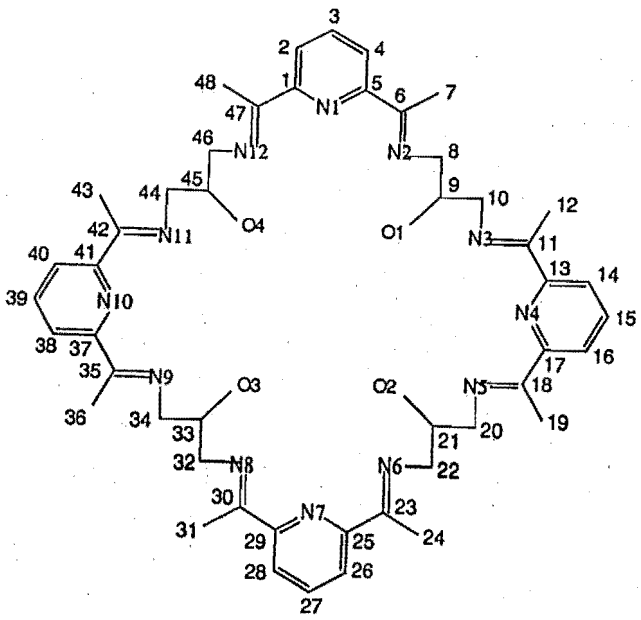

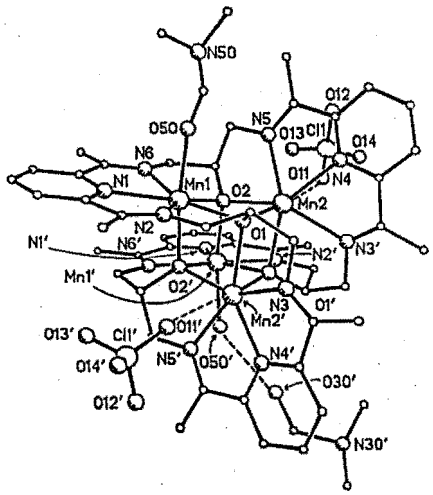

Figure 104: H_4L1' numbering scheme.

Table 37: Atomic coordinates (x10^4) for $[Mn_5(L1)_2(CH_3COO)_2(ClO_4)_2](ClO_4)_2.2H_2O$

atom	x	y	z	atom	x	y	z
Mn1	10074(1)	4507(1)	2038(1)	C19	11018(13)	2586(6)	3474(11)
Mn2	7876(1)	4364(1)	358(2)	N5	10558(7)	3471(4)	2248(7)
Mn3	10000	5000	0	C20	10031(10)	3062(5)	1439(9)
N1	6306(8)	3930(5)	293(8)	C21	9773(9)	3428(5)	424(10)
C1	6062(10)	3341(6)	-99(10)	O2	9542(6)	4081(4)	512(5)
C2	5027(11)	3067(7)	-215(10)	C22	8807(9)	3101(6)	-358(10)
C3	4325(11)	3409(7)	154(11)	N6	7808(8)	3329(5)	-189(8)
C4	4601(10)	3982(8)	596(10)	C23	6928(11)	3001(7)	-368(10)
C5	5635(9)	4256(7)	668(10)	C24	6744(11)	2346(7)	-840(13)
C6	6099(10)	4868(6)	1197(9)	O50	11312(6)	4942(4)	1434(6)
C7	5553(11)	5210(8)	1858(11)	C51	12340(10)	4947(6)	1639(10)
N2	7029(8)	5052(5)	1114(8)	O52	12795(7)	5203(4)	1094(7)
C8	7668(10)	5541(6)	1708(9)	C53	12967(11)	4623(8)	2572(11)
C9	8609(10)	5725(5)	1358(10)	Cl1	8050(5)	3642(3)	2687(5)
O1	8982(6)	5172(4)	943(6)	O11	8485(6)	4059(4)	2106(6)
C10	9534(10)	5982(5)	2250(9)	O12	8886(8)	3399(6)	3526(9)
N3	10073(8)	5438(4)	2874(7)	O13	7278(14)	4004(8)	3041(12)
C11	10629(11)	5487(6)	3765(10)	O14	7440(18)	3096(9)	2052(14)
C12	10805(15)	6085(7)	4430(12)	Cl2	3209(4)	2517(2)	2116(3)
C13	11124(10)	4873(6)	4257(9)	O21	2572(9)	2852(6)	1263(8)
C14	11752(13)	4783(8)	5228(11)	O22	3363(12)	2911(6)	2971(10)
C15	12188(15)	4192(7)	5543(12)	O23	2634(19)	1972(6)	2230(11)
C16	11979(12)	3672(7)	4908(11)	O24	4200(14)	2403(13)	1993(14)
C17	11331(9)	3774(6)	3931(10)	O60	3844(36)	6454(21)	3196(32)
N4	10944(8)	4368(5)	3632(7)	O70	2724(36)	6635(20)	3042(32)
C18	10963(11)	3256(6)	3114(11)				

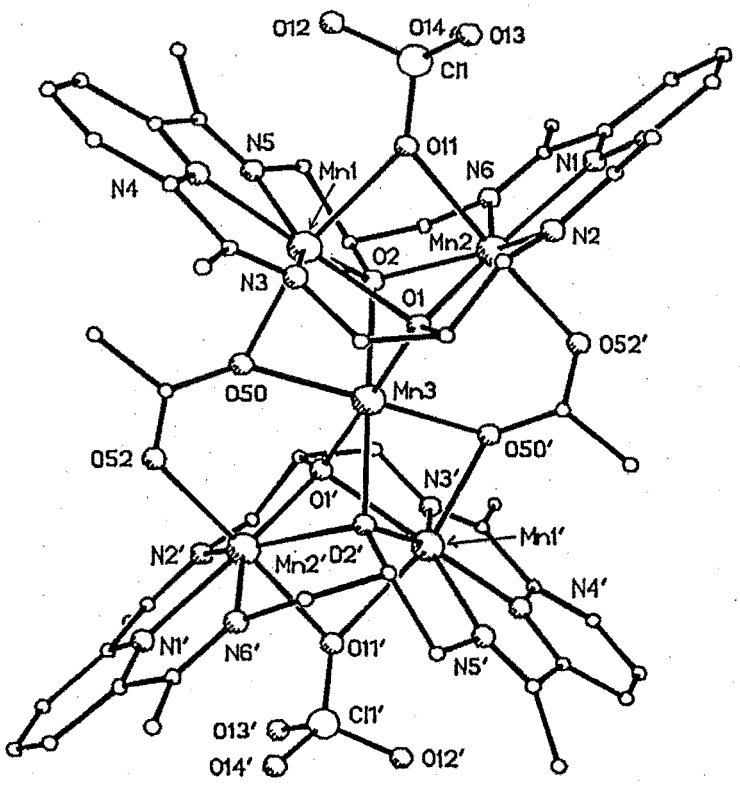

Table 38: Atomic coordinates (x10^4) for $[Mn_5(L1)_2(CH_3COO)_2(H_2O)_4(ClO_4)_2](ClO_4)_2.6MeCN$

atom	x	y	z	atom	x	y	z
Mn1	-2002(1)	1969(1)	-289(1)	O2	-1542(4)	438(3)	-825(3)
Mn2	-587(1)	982(1)	-2177(1)	C22	-2277(7)	-508(5)	-1830(5)
Mn3	0	0	0	N6	-1804(5)	135(4)	-2620(4)
N1	-783(5)	1393(4)	-3759(4)	C23	-2021(6)	228(5)	-3512(5)
C1	-1368(7)	900(5)	-4193(5)	C24	-2830(7)	-233(6)	-3917(5)
C2	-1321(7)	1004(5)	-5210(5)	O40	-2308(4)	2560(4)	-1879(3)
C3	-645(7)	1606(6)	-5749(6)	O50	-1320(4)	1012(3)	1040(3)
C4	-61(7)	2117(6)	-5283(5)	C51	-1618(7)	933(5)	1959(5)
C5	-142(6)	1997(5)	-4275(5)	O52	-1063(4)	239(4)	2528(3)
C6	375(7)	2536(5)	-3659(5)	C53	-2690(9)	1762(7)	2387(6)
C7	889(8)	3372(6)	-4125(5)	Cl1	-5162(2)	3116(2)	-3084(2)
N2	302(5)	2235(4)	-2745(4)	O11	-4748(6)	3102(5)	-2161(4)
C8	567(7)	2778(5)	-2004(5)	O12	-4516(9)	2173(7)	-3481(7)
C9	645(6)	2144(5)	-1005(5)	O13	-4874(10)	3952(8)	-3697(7)
O1	-30(4)	1431(3)	-892(3)	O14	-6437(7)	3288(7)	-2947(7)
C10	210(6)	2848(5)	-168(5)	Cl2	-1076(2)	-3511(2)	-2389(1)
N3	-1140(5)	3139(4)	28(4)	O21	-184(5)	-3014(4)	-2265(4)
C11	-1814(6)	3915(5)	468(5)	O22	-1412(5)	-4057(5)	-1502(4)
C12	-1402(7)	4736(5)	783(5)	O23	-2129(7)	-2775(5)	-2694(6)
N4	-3473(5)	3238(4)	358(4)	O24	-561(8)	-4196(5)	-3118(5)
C13	-3172(6)	3988(5)	677(5)	N70	3494(8)	791(7)	6628(6)
C14	-4041(7)	4727(6)	1201(5)	C70	3861(9)	358(8)	7602(7)
C15	-5239(7)	4667(6)	1390(5)	C71	4088(10)	50(8)	8325(7)
C16	-5550(7)	3896(5)	1043(5)	N80	4967(11)	1463(9)	4345(8)
C17	-4633(6)	3177(5)	525(5)	C80	4586(12)	2343(10)	4184(9)
C18	-4816(7)	2307(5)	80(5)	C81	4079(12)	3384(8)	4067(8)
C19	-6079(7)	2269(6)	40(6)	N90	2133(15)	5534(10)	4737(9)
N5	-3816(5)	1669(4)	-260(4)	C90	2379(12)	5694(10)	5437(10)
C20	-3764(6)	838(5)	-833(5)	C91	2691(12)	5916(10)	6284(9)
C21	-2519(6)	30(5)	-870(5)	O60	-2080(5)	4359(4)	-2768(5)

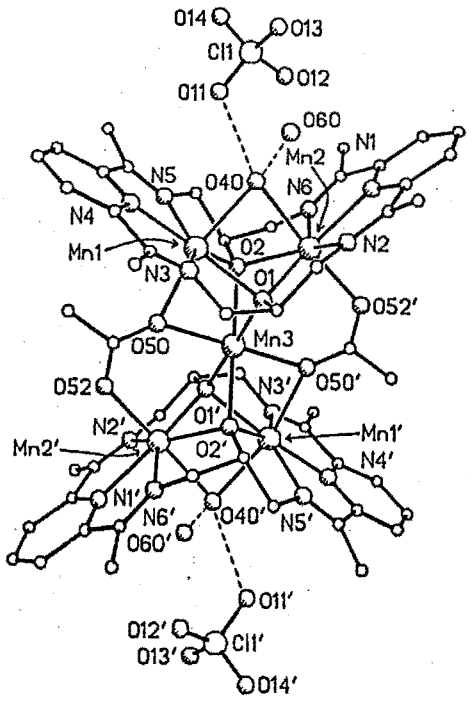

Table 39: Atomic coordinates (x10^4) for $[Mn_5(L1)_2(CH_3COO)_2(DMF)_2](ClO_4)_4.2DMF$

atom	x	y	z	atom	x	y	z
Mn1	-75(3)	4624(3)	3177(3)	N6	-1392(16)	2142(13)	4266(12)
Mn2	439(3)	2832(3)	4287(3)	C23	-1361(21)	1252(17)	4084(16)
Mn3	0	5000	5000	C24	-2427(21)	733(17)	3938(16)
N1	939(16)	1262(13)	4004(12)	Cl1	3450(7)	7162(6)	-1518(5)
C1	-43(21)	701(16)	3984(16)	O11	4626(22)	7732(17)	-1655(15)
C2	215(21)	-315(16)	3918(15)	O12	3716(19)	6215(16)	-1190(14)
C3	1446(21)	-690(18)	3842(15)	O13	2337(21)	7660(16)	-893(15)
C4	2422(22)	-96(17)	3858(15)	O14	3231(19)	7081(15)	-2355(14)
C5	2170(22)	903(18)	3876(16)	Cl2	3964(8)	2100(6)	6214(6)
C6	3119(22)	1642(17)	3844(16)	O21	4196(20)	2917(17)	5686(15)
N2	2655(17)	2522(14)	3831(12)	O22	3390(18)	2272(15)	7139(14)
C7	4471(23)	1337(20)	3828(18)	O23	2904(28)	1654(22)	5908(20)
C8	3385(21)	3393(16)	3782(16)	O24	4810(29)	1356(23)	6084(21)
C9	2688(21)	4253(17)	3464(15)	O50	-252(14)	5967(11)	3915(10)
O1	1322(13)	4232(11)	3925(10)	C51	-139(25)	6941(20)	3717(19)
C10	2992(21)	4237(17)	2456(15)	O52	-201(14)	7439(11)	4366(11)

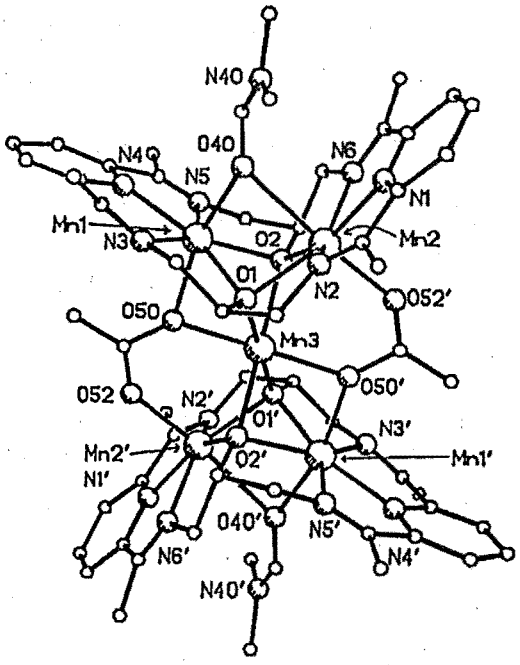

N3	1975(17)	4776(13)	2181(12)	C53	-79(27)	7265(21)	2862(18)
C11	2023(21)	4908(17)	1412(16)	O40	466(14)	3078(11)	2692(11)
C12	3193(27)	4604(22)	616(20)	C40	71(27)	2613(20)	2198(18)
N4	-294(19)	5126(15)	1940(14)	N40	781(22)	1848(17)	1853(16)
C13	789(21)	5332(17)	1230(15)	C41	2146(28)	1609(24)	1817(21)
C14	740(24)	5865(17)	517(17)	C42	176(29)	1186(23)	1372(21)
C15	-495(23)	6260(19)	466(18)	O60	2853(26)	2118(21)	9634(19)
C16	-1597(23)	5997(17)	1146(16)	C60	2734(57)	1578(45)	9091(42)
C17	-1471(20)	5465(15)	1865(15)	N60	3136(33)	712(26)	8852(24)
C18	-2592(23)	5215(18)	2719(17)	C61	4109(67)	388(53)	9200(49)
C19	-3975(21)	5448(18)	2723(17)	C62	2935(57)	165(43)	8241(39)
N5	-2268(18)	4842(14)	3330(13)	O70	2182(35)	9109(28)	1543(25)
C20	-3096(22)	4596(17)	4207(15)	C70	2808(46)	8330(37)	1228(35)
C21	-2435(19)	3768(15)	4667(15)	N70	3604(34)	7705(27)	1403(25)
O2	-1113(12)	4011(10)	4504(9)	C71	3763(45)	7763(35)	2171(31)
C22	-2498(20)	2813(15)	4257(15)	C72	4255(41)	6894(32)	872(30)

Table 40: Atomic coordinates for (x10^4) for $[Mn(DAP)_2(H_2O)_2](ClO_4)_2$

atom	x	y	z	atom	x	y	z
Mn	7611(2)	8351(1)	1103(1)	C26	10498(13)	6799(10)	1569(3)
N11	7499(10)	10663(7)	858(2)	O21	9967(10)	6792(8)	1251(2)
C11	6082(12)	11030(9)	646(2)	C27	12175(13)	6080(11)	1670(4)
C12	5897(14)	12382(10)	503(3)	C28	5285(12)	9421(9)	1803(2)
C13	7156(13)	13402(11)	576(3)	O22	5234(9)	9446(8)	1455(2)
C14	8551(13)	13013(10)	773(3)	C29	3845(14)	10004(11)	2020(3)
C15	8695(12)	11650(11)	914(2)	Cl1	7067(3)	3455(3)	1864(1)
C16	10221(12)	11120(10)	1144(2)	O1	6890(26)	2623(21)	2152(8)
O11	10189(10)	9888(8)	1256(2)	O2	5984(23)	3185(19)	1568(3)
C17	11713(14)	12126(13)	1229(3)	O3	6364(30)	4748(14)	2031(5)
C18	4863(13)	9789(10)	579(2)	O4	8572(20)	4031(19)	1763(5)
O12	5207(9)	8557(7)	711(2)	Cl2	2724(3)	5267(2)	315(1)
C19	3264(15)	10015(12)	340(4)	O5	3182(16)	5451(12)	692(2)
N21	7975(9)	8144(7)	1734(2)	O6	1903(13)	3888(9)	274(2)
C21	6851(13)	8776(9)	1975(2)	O7	1588(15)	6334(10)	190(3)
C22	7161(13)	8692(11)	2347(3)	O8	4203(12)	5317(13)	95(3)
C23	8619(16)	8033(15)	2486(3)	O30	6113(11)	6313(7)	1146(2)
C24	9774(15)	7405(12)	2244(3)	O40	8761(13)	7673(10)	568(2)
C25	9399(11)	7468(9)	1860(3)				

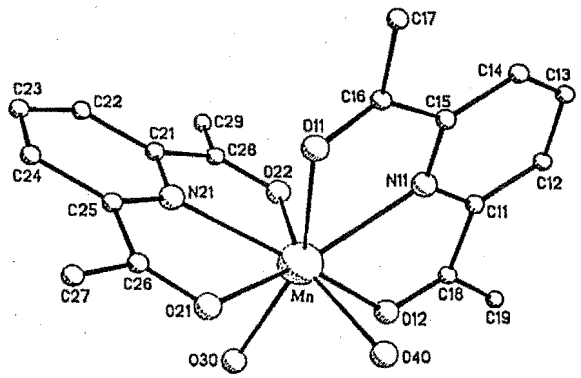

Table 41: Atomic coordinates (x10^4) for $[Pb_2(H_2L5)(NCS)_3](NCS)$

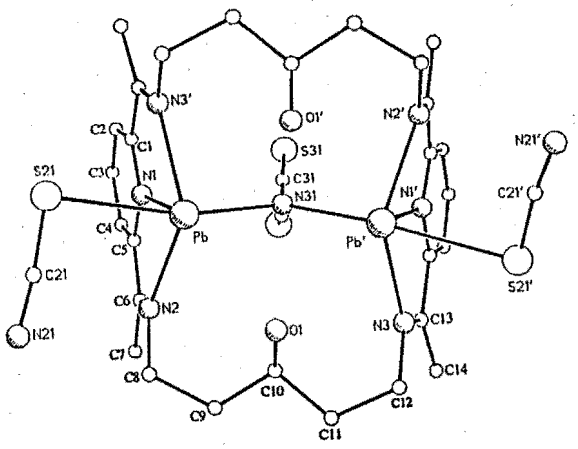

atom	x	y	z	atom	x	y	z
Pb	4665(1)	2984(1)	6551(1)	O1	6785(19)	2556(15)	7389(10)
N1	4477(18)	4444(13)	6053(9)	C11	8636(24)	2968(19)	7894(12)
C1	3438(21)	4834(17)	5952(11)	C12	8214(27)	2837(20)	8571(14)
C2	3316(25)	5731(18)	5727(13)	N3	7319(17)	3519(15)	8675(10)
C3	4254(25)	6168(23)	5624(13)	C13	7570(22)	4259(17)	8901(12)
C4	5280(23)	5786(17)	5715(12)	C14	8709(23)	4618(18)	9072(13)

continued...

continued...

C5	5419(23)	4885(17)	5914(12)	S21	3857(7)	2303(5)	5318(4)
C6	6456(21)	4419(17)	5977(12)	C21	5057(24)	1891(17)	5202(14)
C7	7526(25)	4821(20)	5862(14)	N21	5925(24)	1577(19)	5060(14)
N2	6404(18)	3638(15)	6117(10)	S31	4248(32)	5811(26)	7548(19)
C8	7378(24)	3034(18)	6125(13)	C31	4657(40)	4751(34)	7513(29)
C9	8212(24)	3156(18)	6746(12)	N31	5000	4159(22)	7500
C10	7694(24)	3146(18)	7360(12)				

Table 42: Atomic coordinates (x10^4) for $[Mn^{II}Mn^{III}(L13)(O)(OH)(DMF)]_2(ClO_4)_4.2H_2O$

atom	x	y	z	atom	x	y	z
Mn1	4835(8)	4139(7)	503(6)	N5	5847(42)	2916(36)	-2601(33)
Mn2	6623(10)	2736(8)	-1311(7)	C20	4529(55)	2746(49)	-2397(44)
N1	3644(48)	4016(42)	1659(38)	C21	3877(47)	2862(41)	-1407(36)
C1	2347(64)	4263(56)	1676(51)	C22	3449(44)	3980(38)	-1056(35)
C2	1192(71)	4320(61)	2576(56)	N6	3310(39)	4031(34)	-95(31)
C3	1744(65)	4261(53)	3392(49)	C23	2354(49)	4186(41)	615(38)
C4	2814(58)	4046(50)	3500(45)	C24	1088(54)	4301(45)	503(41)
C5	3791(55)	4019(46)	2613(42)	O1	5511(31)	2683(28)	134(24)
C6	5094(63)	3831(51)	2516(50)	O2	5770(34)	4427(30)	-707(25)
C7	5345(58)	3518(49)	3535(46)	O30	6980(38)	1018(33)	-1652(29)
N2	5817(44)	3764(34)	1766(33)	C31	6796(60)	502(54)	-1076(50)
C8	7027(61)	3470(52)	1756(45)	N32	6793(45)	-614(41)	-1312(38)
C9	7766(55)	3429(47)	678(43)	C33	7082(70)	-880(62)	-2381(58)
C10	8412(49)	2256(43)	123(37)	C34	6697(65)	-1327(57)	-461(51)
N3	8353(42)	2505(37)	-956(33)	Cl1	-1984(15)	5297(16)	3674(12)
C11	9379(62)	2667(53)	-1617(47)	O11	-1610(40)	5470(36)	2678(32)
C12	10510(56)	2520(49)	-1424(44)	O12	-1137(48)	5075(42)	4160(37)
C13	8937(58)	2847(47)	-2473(44)	O13	-3114(55)	5171(49)	4007(44)
C14	9855(66)	2868(57)	-3268(53)	O14	-2641(86)	6392(76)	4221(67)
C15	9557(61)	3188(53)	-4261(47)	Cl2	6423(23)	414(19)	2021(20)
C16	8427(56)	3220(50)	-4257(43)	O21	5793(87)	1345(76)	1676(68)
C17	7649(60)	3126(50)	-3411(46)	O22	6119(77)	-568(71)	2037(60)
N4	7996(51)	2868(42)	-2611(37)	O23	7508(86)	64(76)	1162(74)
C18	6486(64)	3158(53)	-3424(50)	O24	7005(126)	429(113)	2800(103)
C19	5990(61)	3289(52)	-4270(49)	O50	344(50)	2068(45)	1421(41)

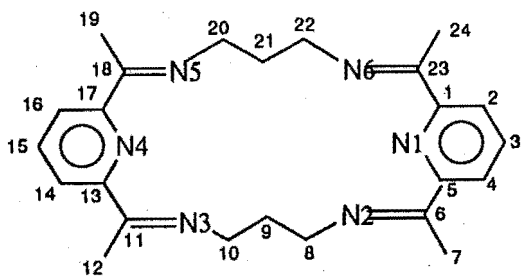

Figure 104: L13 numbering scheme.

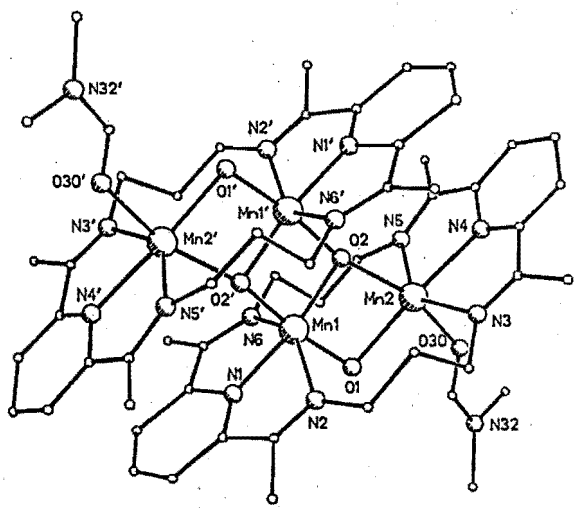

Table 43: Atomic coordinates (x10⁴) for (L3')ClO_4

atom	x	y	z	atom	x	y	z
N11	2689(2)	4165(2)	457(4)	C25	3790(3)	4106(2)	-1912(4)
C11	3039(3)	3466(2)	1265(4)	C26	3000(3)	4470(2)	-907(4)
C12	2606(4)	3285(2)	2595(5)	N1	2427(3)	5155(2)	-1162(4)
C13	1817(4)	3795(2)	3236(5)	C1	2394(4)	5676(2)	-2610(5)
C14	1478(3)	4469(2)	2507(5)	C2	3363(4)	6303(2)	-2141(6)
C15	1911(3)	4683(2)	1059(4)	O1	3070(3)	6760(2)	-884(4)
C16	1771(3)	5302(2)	4(4)	Cl	213(1)	6557(1)	3198(1)
N21	4655(3)	4560(2)	-2341(4)	O11	1525(3)	6419(2)	3395(4)
C21	5392(4)	4225(3)	-3213(5)	O12	89(3)	7087(2)	4487(4)
C22	5332(4)	3465(3)	-3660(5)	O13	-429(3)	5870(2)	3415(4)
C23	4429(4)	3022(3)	-3227(5)	O14	-339(4)	6877(3)	1599(4)
C24	3630(3)	3343(2)	-2358(4)				

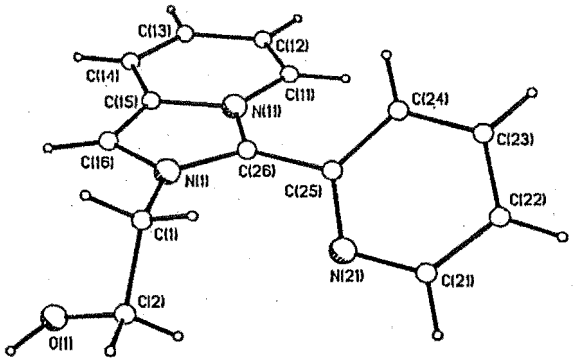

Table 44: Atomic coordinates (x10⁴) for $[Mn(H_2L2)(H_2O)_2](ClO_4)_2$

atom	x	y	z	atom	x	y	z
Mn	5000	7574(1)	7500	O1	4642(2)	9006(3)	8647(3)
N1	5000	5720(4)	7500	O2	6167(2)	7637(3)	8706(4)
C3	5000	3494(6)	7500	Cl	1883(1)	6180(1)	6910(1)
C4	4501(4)	4037(4)	8250(5)	O11	2298(7)	5174(7)	7185(7)
C5	4529(3)	5180(3)	8241(4)	O15	2666(13)	5988(16)	6741(18)
C6	4054(3)	5896(4)	9051(4)	O12	1869(6)	6146(8)	5652(6)
C7	3462(3)	5374(5)	9849(5)	O16	1261(15)	6510(18)	6064(19)
N2	4195(2)	6917(3)	8951(3)	O13	1098(5)	6021(7)	7295(10)
C8	3779(3)	7744(5)	9644(5)	O17	1656(13)	5369(17)	7713(18)
C9	4333(4)	8731(5)	9775(5)	O14	2187(5)	7093(7)	7514(8)

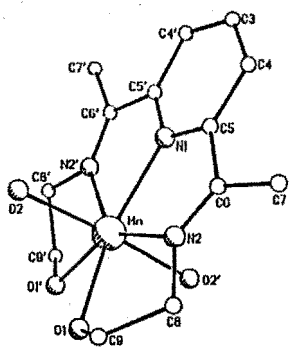

Table 45: Atomic coordinates (x10^4) for $Mn(H_2L2)(NCS)_2$

atom	x	y	z	atom	x	y	z
Mn	2500	7711(1)	0	N2	1288(2)	7036(2)	1040(1)
N1	2500	5886(2)	0	C8	707(3)	7815(2)	1580(2)
C3	2500	3703(3)	0	C9	401(3)	8823(2)	1035(2)
C4	1864(3)	4250(2)	588(2)	O1	1573(3)	9106(2)	679(2)
C5	1882(2)	5350(2)	569(1)	N20	4432(2)	7818(2)	1017(2)
C6	1214(2)	6040(2)	1169(1)	C21	5523(3)	8155(2)	1259(2)
C7	539(3)	5514(3)	1860(2)	S22	7074(1)	8611(1)	1601(1)

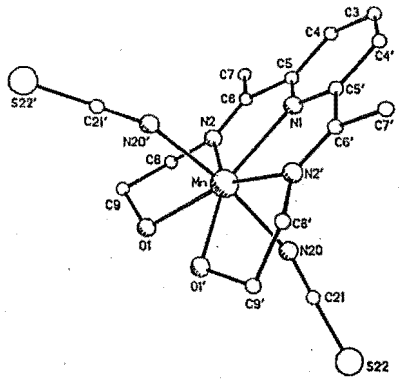

Table 46: Atomic coordinates (x10^4) for $Mn(H_2L2)(N_3)_2$

atom	x	y	z	atom	x	y	z
Mn	5000	1795(1)	2500	N2	3924(2)	2475(3)	1430(6)
N1	5000	3620(4)	2500	C8	3370(3)	1694(4)	1009(8)
C3	5000	5802(5)	2500	C9	3735(3)	748(4)	159(9)
C4	4385(3)	5254(4)	2016(7)	O1	4305(2)	424(2)	1381(5)
C5	4413(3)	4148(4)	2028(6)	N20	5540(2)	1688(3)	-273(6)
C6	3787(3)	3460(4)	1490(7)	N21	6064(3)	2183(3)	-673(7)
C7	3073(3)	3965(4)	1119(10)	N22	6577(2)	2660(4)	-1058(8)

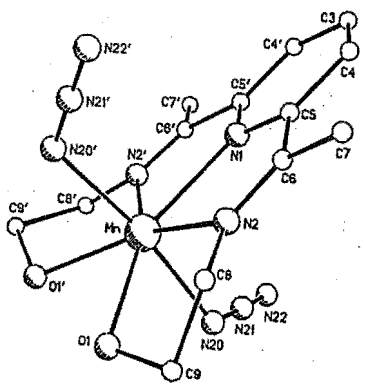

Table 47: Atomic coordinates (x10^4) for $[Ni(H_2L2)_2](ClO_4)_2.H_2O$

atom	x	y	z	atom	x	y	z
Ni	0	0	5000	C8	-2148(21)	-2194(22)	5360(11)
N1	0	0	3802(8)	C9	-1662(42)	-3404(32)	5534(15)
C3	0	0	2176(10	O1	-1907(25)	-4149(36)	5173(14)
C4	-968(20)	-775(17)	2575(8)	Cl	-5000	0	2050(4)
C5	-842(16)	-823(15)	3420(8)	O11	-5561(19)	892(22)	1578(11)
C6	-1716(11)	-1546(17)	3977(11)	O12	-5854(21)	-623(21)	2680(8)
C7	-2820(19)	-2371(18)	3569(11)	O20	0	0	0
N2	-1491(13)	-1393(11)	4711(6)				

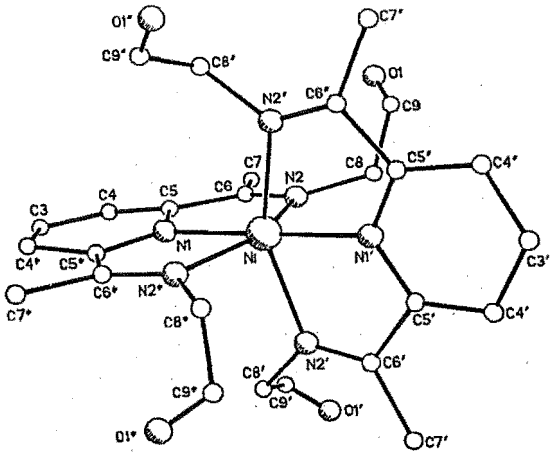

Table 48: Atomic coordinates (x10^4) for $[Ni(H_2L2)(NCS)_2]_2$

atom	x	y	z	atom	x	y	z
Ni	4436(1)	6814(1)	6259(1)	C10	6542(3)	4690(3)	5740(2)
N1	4027(2)	8010(2)	5144(2)	O2	6341(2)	4667(2)	4691(2)
C1	4755(3)	8259(3)	4644(2)	C11	6796(3)	6002(3)	6134(2)
C2	4510(3)	9120(3)	3883(2)	N3	5848(2)	6800(3)	5723(2)
C3	3507(3)	9725(3)	3659(3)	C12	5804(3)	7531(3)	4995(2)
C4	2760(3)	9448(3)	4172(3)	C13	6668(3)	7699(3)	4469(3)
C5	3035(3)	8578(3)	4918(2)	N70	4938(2)	5444(3)	7260(2)
C6	2324(3)	8181(3)	5542(3)	C71	5265(3)	4487(3)	7579(2)
C7	1204(3)	8757(4)	5328(3)	S72	5744(1)	3135(1)	8033(1)
N2	2744(2)	7367(3)	6208(2)	N60	5050(2)	8133(3)	7294(2)
C8	2102(3)	6940(4)	6865(3)	C61	5233(3)	8709(3)	8007(2)
C9	2361(3)	5607(4)	7167(3)	S62	5493(1)	9547(1)	9011(1)
O1	2157(2)	4791(2)	6344(2)				

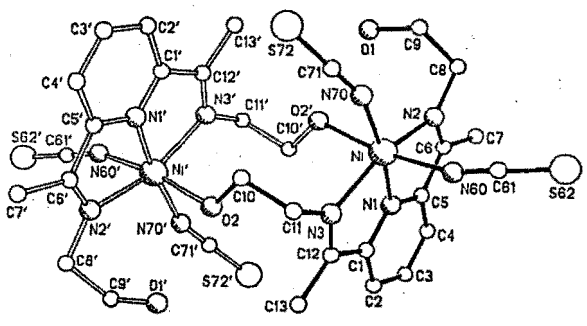

Table 49: Atomic coordinates (x10⁴) for $Mn(HL3)_2(NCS)_2$

atom	x	y	z	atom	x	y	z
Mn	7498(1)	9956(1)	11700	C13	8961(3)	13339(4)	10956(5)
N1	6721(2)	8529(3)	11400(4)	C14	8241(2)	13155(4)	10422(5)
C1	6063(2)	8325(3)	12030(5)	C15	7898(2)	12195(3)	10663(5)
C2	5656(3)	7407(3)	11791(5)	C16	7139(3)	11959(3)	10112(5)
C3	5929(3)	6690(4)	10880(5)	N12	6845(2)	11064(3)	10277(4)
C4	6611(3)	6885(4)	10236(5)	C17	6104(2)	10873(4)	9660(5)
C5	6982(2)	7812(3)	10510(4)	C18	6192(3)	10175(4)	8442(5)
C6	7694(3)	8074(3)	9817(5)	O10	6670(2)	10639(3)	7434(4)
N2	8030(2)	8937(3)	10047(4)	N10	6726(3)	10520(3)	13270(4)
C7	8721(3)	9156(4)	9282(5)	C10	6229(3)	10819(3)	13936(5)
C8	8542(3)	9890(4)	8105(6)	S10	5537(1)	11244(1)	14904(1)
O1	8008(2)	9442(3)	7188(4)	N20	8312(2)	9387(3)	13137(4)
N11	8236(2)	11425(3)	11386(3)	C20	8856(3)	9186(3)	13747(5)
C11	8929(2)	11620(3)	11887(5)	S20	9609(1)	8903(1)	14638(1)
C12	9308(2)	12558(3)	11698(5)				

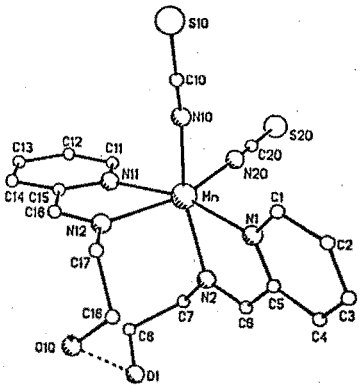

Table 50: Atomic coordinates (x10⁴) for $[Mn(HL3)(NCS)_2]_x$

atom	x	y	z	atom	x	y	z
Mn	4237(1)	558(1)	1274(1)	C7	3859(2)	4226(5)	383(1)
N1	2999(2)	1028(5)	1585(1)	C8	4351(2)	6366(5)	494(1)
C1	2717(2)	-51(8)	1964(2)	O1	3858(1)	8188(4)	666(1)
C2	1971(2)	468(8)	2146(2)	N11	4420(2)	-2598(5)	1662(1)
C3	1516(2)	2146(7)	1940(1)	C11	4582(2)	-4429(6)	1805(1)
C4	1792(2)	3290(7)	1547(1)	S11	4838(1)	-7005(1)	2013(1)
C5	2536(2)	2664(5)	1379(1)	N21	5330(2)	994(5)	896(1)
C6	2862(2)	3733(5)	949(1)	C21	5930(2)	877(5)	699(1)
N2	3563(2)	3205(4)	823(1)	S21	6783(1)	718(2)	422(1)

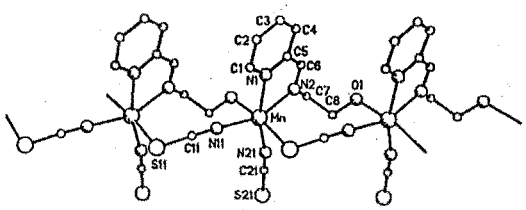

Table 51: Atomic coordinates (x10^4) for [Ni(HL3)$_2$](ClO$_4$)$_2$

atom	x	y	z	atom	x	y	z
Ni	1301(6)	951(8)	0	C15	200(21)	-1368(41)	658(22)
N1	2133(22)	-879(51)	152(34)	C16	404	-101	1402
C1	2268(22)	-1626(51)	-634(34)	N12	728	879	1117
C2	2756(22)	-3044(51)	-711(34)	C17	1238	2546	1804
C3	3110(22)	-3713(51)	-1(34)	C18	1576	3821	1323
C4	2975(22)	-2966(51)	785(34)	O2	1956	2882	447
C5	2486(22)	-1548(51)	861(34)	Cl1	1400(15)	7430(36)	3260(14)
C6	2120(31)	-386(71)	-1324(33)	O11	1792(34)	8511(79)	2878(34)
N2	1564(22)	1176(65)	-1191(25)	O12	641(54)	6769(119)	2651(56)
C7	1441(32)	2022(61)	-1752(33)	O13	601(82)	7973(173)	3815(93)
C8	1317(53)	3946(93)	-1128(32)	O14	1374(93)	6986(123)	3864(57)
O1	645(26)	2945(53)	-555(29)	Cl2	3663(29)	2421(48)	1882(16)
N11	464(21)	-1046(42)	-150(22)	O21	3829(33)	4201(69)	2039(26)
C11	265(21)	-2165(41)	-809(22)	O22	3391(28)	1978(66)	933(32)
C12	-198(21)	-3606(41)	-660(22)	O23	3131(46)	1940(104)	2316(50)
C13	-462(21)	-3929(41)	148(22)	O24	4029(27)	834(77)	2017(28)
C14	-263(21)	-2809(41)	807(22)				

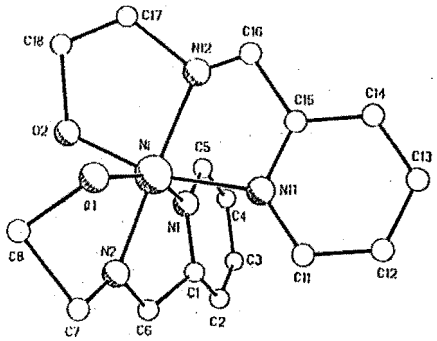

Table 52: Atomic coordinates (x10^4) for [Cu(HL3)(H$_2$O)$_2$(ClO$_4$)]$_2$(ClO$_4$)$_2$

atom	x	y	z	atom	x	y	z
Cu	7293(2)	6049(3)	-1095(1)	O2	7160(10)	3956(17)	-1327(6)
N1	6012(11)	6500(18)	-1435(7)	O3	8605(9)	5745(15)	-811(6)
C1	5293(13)	5594(22)	-1632(8)	Cl1	8400(4)	6895(6)	-2307(2)
C2	4442(15)	6178(25)	-1879(9)	O11	7615(11)	6290(21)	-2123(6)
C3	4306(17)	7723(27)	-1929(10)	O12	9173(10)	7000(17)	-1810(6)
C4	5024(14)	8498(24)	-1706(9)	O13	8645(12)	6074(22)	-2764(7)
C5	5879(14)	7984(24)	-1470(9)	O14	8119(12)	8365(19)	-2507(7)
C6	6680(13)	8890(26)	-1245(8)	Cl2	5933(4)	1907(6)	-345(2)
N2	7380(11)	8155(19)	-1033(7)	O21	6791(9)	2023(17)	-516(7)
C7	8219(14)	9056(26)	-800(8)	O22	5365(10)	3078(18)	-632(7)
C8	8485(13)	8975(25)	-129(8)	O23	6091(12)	1974(20)	268(6)
O1	7830(9)	9523(16)	152(6)	O24	5527(11)	576(17)	-536(9)

Table 53: Atomic coordinates (x10^4) for $[Zn(HL3)(H_2O)_2(ClO_4)]_2(ClO_4)_2$

atom	x	y	z	atom	x	y	z
Zn	7313(1)	5990(1)	-1062(1)	O2	7150(2)	3948(3)	-1348(1)
N1	5958(2)	6566(4)	-1410(2)	O3	8679(2)	5790(3)	-784(1)
C1	5246(3)	5729(5)	-1609(2)	Cl1	8306(1)	6919(1)	-2282(1)
C2	4413(3)	6279(5)	-1862(2)	O11	7604(2)	6204(3)	-2038(1)
C3	4302(3)	7730(5)	-1917(2)	O12	8020(2)	8350(3)	-2429(1)
C4	5037(3)	8612(5)	-1713(2)	O13	9128(2)	6961(4)	-1836(2)
C5	5845(3)	7980(4)	-1461(2)	O14	8447(3)	6204(4)	-2809(2)
C6	6665(3)	8832(4)	-1236(2)	Cl2	5947(1)	1997(1)	-329(1)
N2	7391(2)	8220(3)	-1007(1)	O21	6827(2)	1991(4)	-509(2)
C7	8193(3)	9091(4)	-801(2)	O22	5614(3)	598(4)	-385(2)
C8	8496(3)	8986(5)	-123(2)	O23	5372(2)	2980(4)	-681(2)
O1	7835(2)	9591(3)	189(1)	O24	6058(3)	23399(6)	270(2)

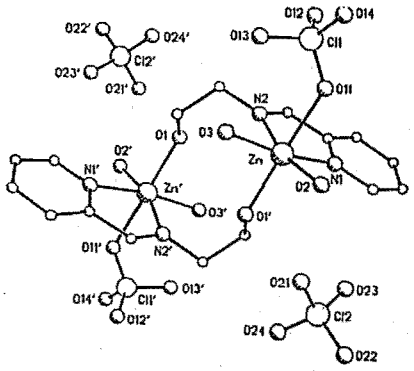

Table 54: Atomic coordinates (x10^4) for $[Mn(HL6)(L6')]_2(ClO_4)_4.2EtOH$

atom	x	y	z	atom	x	y	z
Mn1	902(1)	2341(2)	2656	N40	1442(5)	752(11)	4738(7)
N1	1349(5)	1290(11)	1941(7)	C41	1630(8)	447(15)	5353(10)
C1	1894(8)	1122(15)	1952(11)	C42	1542(7)	-494(13)	5650(10)
C2	2155(9)	285(16)	1523(11)	C43	1231(7)	-1153(14)	5353(9)
C3	1792(8)	-303(17)	1085(12)	C44	988(7)	-923(15)	4696(10)
C4	1259(8)	-147(16)	1093(11)	C45	1106(6)	43(13)	4418(9)
C5	1016(8)	753(16)	1524(11)	C46	812(7)	442(14)	3768(10)
C6	427(7)	846(12)	1530(9)	C47	189(7)	533(14)	3854(9)
C7	32(9)	373(18)	1074(13)	C48	-92(7)	-169(14)	3449(9)
N2	261(5)	1556(12)	2015(8)	C49	-666(8)	-360(16)	3419(11)
C8	-332(9)	1911(18)	2065(12)	C50	323(6)	-762(12)	3071(9)
C9	-404(9)	2501(17)	2798(13)	C51	262(9)	-1552(16)	2588(11)
O1	88(4)	2987(10)	2987(7)	C52	754(8)	-1977(17)	2284(12)
N10	1154(6)	3801(10)	2097(8)	C53	1269(9)	-1668(18)	2458(12)
C11	931(8)	4025(15)	1491(11)	C54	1322(7)	-774(14)	2991(10)
C12	1085(8)	5054(15)	1147(11)	N50	846(6)	-415(10)	3235(8)
C13	1456(7)	5681(13)	1445(9)	O40	1083(4)	1322(8)	3537(6)
C14	1648(6)	5411(13)	2052(9)	Cl1	295(2)	2913(4)	9794(3)
C15	1494(7)	4470(13)	2374(9)	O11	678(8)	2174(13)	9980(11)
C16	1750(9)	4011(18)	3024(13)	O12	541(7)	3891(11)	9674(8)
C17	2446(8)	3921(15)	2973(11)	O13	-96(8)	2975(13)	10329(9)

continued...

continued...

C18	2646(10)	4639(17)	3351(12)	O14	3(7)	2556(13)	9222(9)
C19	3266(10)	4881(22)	3471(16)	C12	942(2)	7417(4)	9876(3)
C20	2255(7)	5267(15)	3733(11)	O21	642(10)	6620(18)	9476(15)
C21	2352(12)	6044(19)	4224(16)	O22	1466(7)	7095(17)	9951(11)
C22	1822(9)	6457(18)	4507(12)	O23	677(9)	7457(15)	10552(10)
C23	1346(10)	6104(18)	4330(12)	O24	918(9)	8428(14)	9614(10)
C24	1312(7)	5345(14)	3797(10)	C13	3547(2)	1902(4)	1994(3)
N20	1754(7)	5017(16)	3553(12)	O31	3690(9)	2449(13)	2582(10)
O10	1517(4)	3177(8)	3279(5)	O32	3091(6)	2350(14)	1624(9)
Mn2	1678(1)	2168(2)	4127(2)	O33	3437(9)	916(15)	2128(10)
N31	1262(6)	3275(11)	4904(9)	O34	3992(7)	1926(18)	1599(14)
C31	684(8)	3425(16)	4872(12)	C14	2976(2)	7260(4)	1876(4)
C32	468(11)	4128(19)	5306(14)	O41	3260(8)	8231(16)	2107(10)
C33	776(12)	4703(22)	5687(16)	O42	2788(14)	6745(27)	2450(15)
C34	1368(13)	4666(23)	5734(16)	O43	2562(11)	7438(22)	1538(23)
C35	1612(8)	3768(15)	5313(10)	O44	3409(9)	6902(21)	1640(21)
C36	2159(10)	3514(19)	5257(13)	O60	2682(8)	-330(16)	3196(10)
C37	2614(13)	4028(23)	5753(18)	C60	2835(19)	-1210(33)	3633(17)
N32	2330(6)	2896(13)	4839(11)	C61	2600(17)	-1075(25)	4288(22)
C38	2867(13)	2433(25)	4766(18)	O70	-102(6)	4923(12)	3487(8)
C39	3010(13)	1821(27)	4168(18)	C70	-178(12)	5731(19)	3009(15)
O30	2501(6)	1509(10)	3809(9)	C71	-263(16)	5533(26)	2342(14)

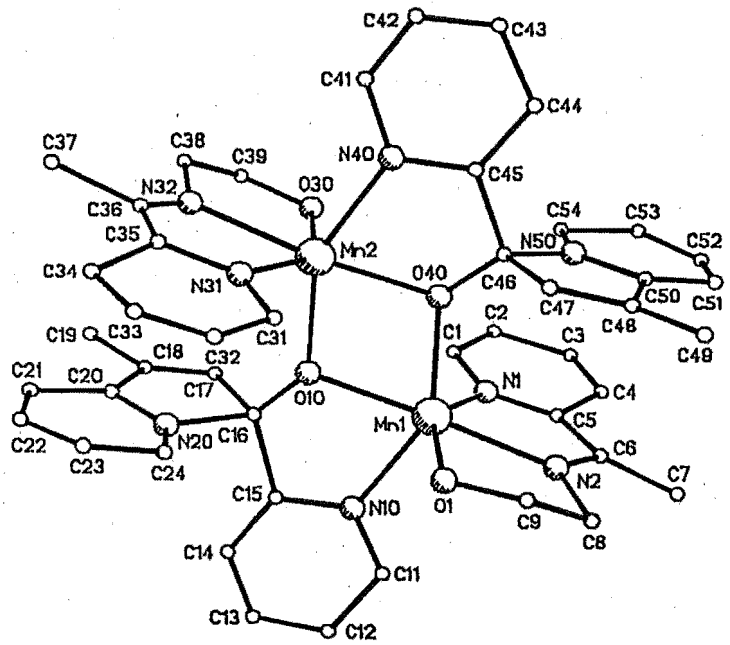

Table 55: Atomic coordinates (x10^4) for [Mn(HL6)(L6')]$_2$(ClO$_4$)$_4$.2MeCN

atom	x	y	z	atom	x	y	z
Mn	5647(4)	-534(2)	752(4)	N3	4020(25)	-997(11)	1200(23)
N1	6057(19)	1120(8)	1857(17)	C25	4244(27)	-1539(12)	1137(25)
C1	7212(23)	1107(10)	1605(21)	C26	5485(24)	-1764(10)	905(22)
C2	7860(25)	1630(9)	1556(21)	C27	5579(28)	-2393(11)	819(26)
C3	7170(23)	2091(10)	1735(21)	N4	6327(18)	-1411(8)	696(17)
C4	5852(23)	2064(10)	2063(21)	C28	7624(26)	-1536(12)	481(26)
C5	5314(20)	1530(8)	2142(18)	C29	8435(28)	-1012(11)	571(27)
C6	4065(24)	1355(10)	2381(22)	O2	7772(18)	-550(8)	289(17)
C7	3011(26)	1765(11)	2704(25)	Cl1	-236(6)	-295(3)	-2357(6)
C8	3963(21)	832(8)	2311(19)	O11	-296(21)	-845(8)	-2290(26)
C9	5260(18)	601(8)	2000(17)	O12	-1315(18)	-90(8)	-2883(20)
O1	5140(13)	321(6)	900(12)	O13	895(18)	-101(8)	-2806(21)
C10	5856(19)	222(8)	2902(18)	O14	-247(29)	-87(10)	-1220(19)
C11	6156(21)	427(9)	4021(20)	Cl2	498(9)	2897(4)	514(7)
C12	6641(19)	75(8)	4849(19)	O21	81(41)	2483(19)	-299(26)
C13	6838(24)	-460(11)	4581(24)	O22	1502(57)	2698(19)	1110(30)
C14	6533(24)	-632(12)	3431(24)	O23	-346(29)	2951(12)	1265(36)
N2	6013(16)	-294(7)	2610(16)	O24	800(42)	3341(17)	220(43)
C21	2837(26)	-765(11)	1480(24)	N90	868(24)	1591(10)	-3499(23)
C22	1947(34)	-1145(15)	1722(30)	C90	155(24)	1387(10)	-4133(22)
C23	1967(42)	-1660(19)	1684(35)	C91	-739(30)	1031(13)	-4830(28)
C24	3159(27)	-1905(12)	1277(26)				

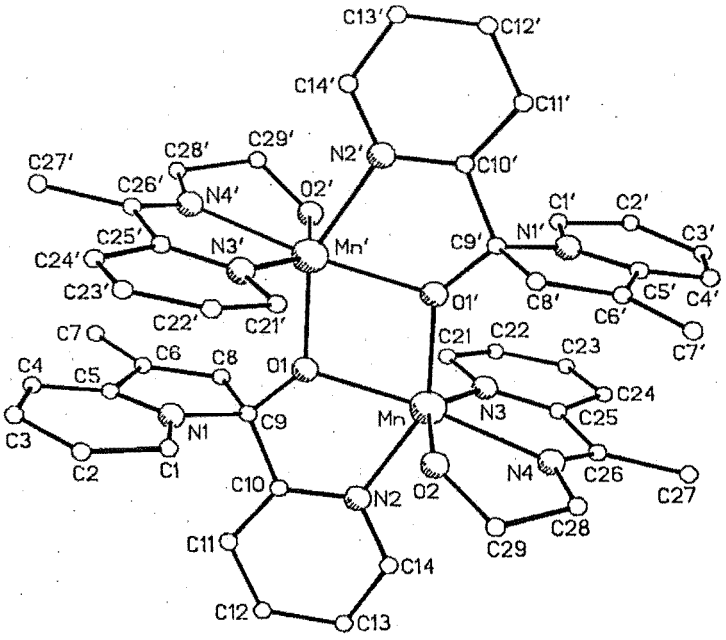

Table 56: Atomic coordinates (x10^4) for $[Mn(H_2L9)(NCS)_2]_x$

atom	x	y	z	atom	x	y	z
Mn	308(1)	5527(1)	7410(1)	O2	-3940(1)	5408(2)	4995(1)
N1	664(1)	4632(2)	8822(1)	C11	-3089(2)	5074(3)	4797(2)
C1	-23(1)	3838(2)	8930(1)	C12	-2108(2)	5215(2)	5704(2)
C2	190(2)	3219(2)	9798(1)	C13	-2070(2)	4236(2)	6456(1)
C3	1135(2)	3460(2)	10555(2)	N3	-1099(1)	4339(2)	7323(1)
C4	1842(2)	4274(2)	10429(1)	C14	-1020(1)	3700(2)	8066(1)
C5	1586(1)	4857(2)	9547(1)	C15	-1850(2)	2857(2)	8125(2)
C6	2263(2)	5791(2)	9318(1)	N21	388(2)	6197(2)	6142(1)
C7	3276(2)	6176(2)	10098(2)	C21	574(2)	6815(2)	5608(1)
N2	1901(1)	6203(2)	8459(1)	S21	835(1)	7727(1)	4862(1)
C8	2451(2)	7185(2)	8150(2)	N31	-319(1)	7401(2)	7613(1)
C9	3111(2)	6515(2)	7726(2)	C31	-432(2)	8538(2)	7654(1)
C10	3545(2)	7527(2)	7269(1)	S31	-626(1)	10129(1)	7707(1)
O1	4109(1)	8567(2)	7920(1)				

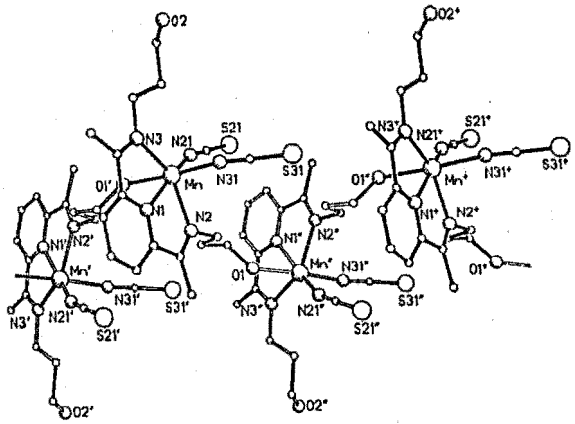

Table 57: Atomic coordinates (x104) for $Ni(H_2L9)_2](ClO_4)_2$

atom	x	y	z	atom	x	y	z
Ni	5000	7821(1)	7500	O1	6802(1)	11464(2)	10182(1)
N1	5710(1)	7804(2)	7107(1)	O2	3444(1)	3253(2)	5855(1)
C1	5505(2)	7060(3)	6518(2)	C11	3970(2)	3619(3)	6628(2)
C2	5990(2)	7056(3)	6223(2)	C12	3655(2)	4805(3)	6799(2)
C3	6679(2)	7840(3)	6560(2)	C13	3577(2)	5969(3)	6339(2)
C4	6877(2)	8603(3)	7166(2)	N3	4387(1)	6510(2)	6588(1)
C5	6367(2)	8572(3)	7430(2)	C14	4723(2)	6342(3)	6219(2)

continued...

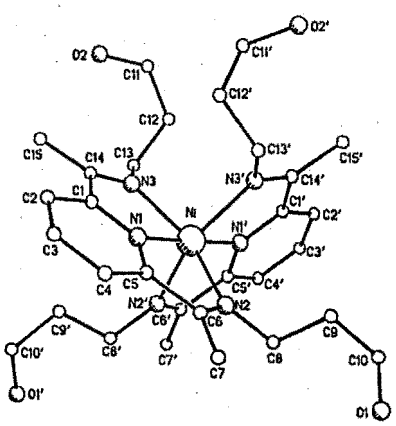

continued...

C6	6451(2)	9382(3)	8049(2)	C15	4398(2)	5560(3)	5517(2)
C7	7167(2)	10273(3)	8447(2)	Cl	3953(1)	12504(1)	8683(1)
N2	5875(1)	9240(2)	8162(1)	O11	3871(2)	13812(3)	8463(2)
C8	5837(2)	10045(3)	8709(2)	O12	4685(3)	12332(4)	9398(2)
C9	6298(2)	9445(3)	9493(2)	O13	3967(3)	11742(4)	8155(2)
C10	6316(2)	10346(3)	10061(2)	O14	3278(3)	12222(4)	8724(3)

Table 58: Atomic coordinates ($x10^4$) for $[Ni(H_2L9)(NCS)_2]_x$

atom	x	y	z	atom	x	y	z
Ni	8002(1)	333(1)	2079(1)	O2	11156(3)	3360(4)	2754(2)
N1	7007(3)	-469(5)	916(3)	C11	11246(4)	2160(7)	2219(4)
C1	7145(4)	-277(6)	152(4)	C12	10363(4)	1153(7)	1921(4)
C2	6469(4)	-827(6)	-671(4)	C13	9413(4)	1959(7)	1374(4)
C3	5670(4)	-1591(7)	-659(4)	N3	8551(3)	1001(5)	1119(3)
C4	5534(4)	-1781(7)	134(4)	C14	8055(4)	581(6)	304(4)
C5	6234(4)	-1187(6)	928(4)	C15	8281(4)	848(7)	-513(4)
C6	6238(4)	-1238(6)	1856(4)	N60	7252(3)	2252(5)	1922(3)
C7	5366(4)	-1868(7)	1968(4)	C61	6834(4)	3320(7)	1915(4)
N2	7006(3)	-715(5)	2498(3)	S62	6225(1)	4793(2)	1869(1)
C8	7118(4)	-725(6)	3446(4)	N70	9061(3)	988(5)	3275(3)
C9	6719(5)	625(7)	3686(4)	C71	9777(4)	1493(7)	3808(4)
C10	6958(5)	694(7)	4698(4)	S72	10781(1)	2259(2)	4535(1)
O1	6609(3)	2009(5)	4876(3)				

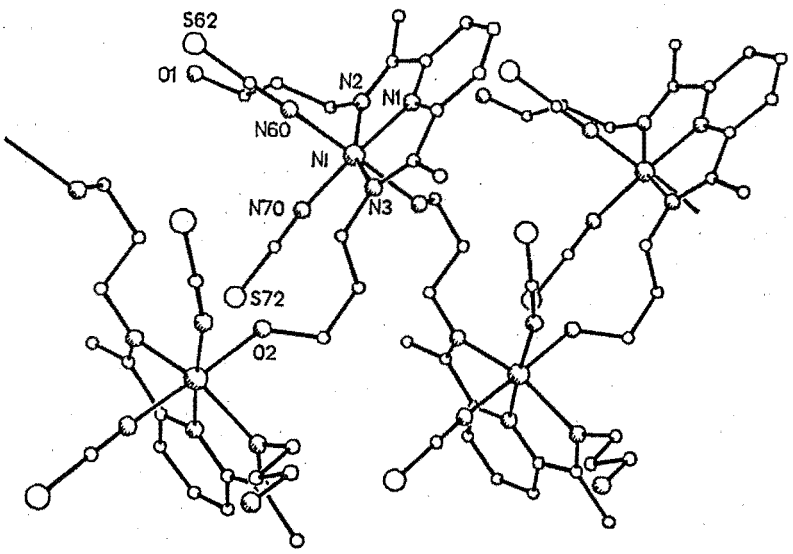

Appendix B

PHYSICAL MEASUREMENTS

Infrared spectra were recorded in the range 4000-200 cm^{-1} as KBr discs or liquid smears using a Pye-Unicam SP3-300 infrared spectrophotometer. All spectra were referenced to the 1601.4 cm^{-1} polystyrene absorbance.

A Varian DMS100 spectrophotometer was used in measurements of electronic spectra of solutions in the range 11,111-50,000 cm^{-1}. Spectra of solid samples were recorded using a Beckman DK-2A ratio recording spectrophotometer.

1H and 13C nmr spectra were usually obtained on a Varian XL300 Fourier transform spectrophotometer.

Microanalyses were determined by the Campbell Microanalytical Laboratory, University of Otago, Dunedin.

A conductivity cell of cell constant 0.251, constructed from platinum electrodes in conjunction with a resistance/capacitance bridge was used for measurements of electrical conductance.

Mass spectra were obtained by two methods: FAB (Fast Atom Bombardment) and ^{252}Cf PDMS (Plasma Desorption Mass Spectrometry). The low resolution FAB spectra were run on a Kratos MS80 RFA mass spectrometer using a magic bullet (1:3 dithioerythritol:dithiothreitol) matrix. The ^{252}Cf PDMS spectra were obtained by Dr. L.K. Pannell of NIDDK, National Institutes of Health, Bethesda, USA.

EXAFS (Extended X-ray Absorption Fine Structure) and XANES (X-ray Absorption Near Edge Spectroscopy) were obtained by Dr. S.P. Cramer of the National Synchrotron Light Source, Brookhaven National Laboratory, New York, USA.

Room temperature magnetic moment studies were carried out using a Newport Instruments Gouy balance. Detailed low temperature measurements were obtained by Dr. J-M. Latour and Dr. J-P. Tuchagues of CNRS at Grenoble and Toulouse respectively.

A Philips PW1729 X-ray powder diffractometer was used to record powder diffraction patterns.

REFERENCES

1. See for example: (a) E.E. Conn, P.K. Stumpf, G. Bruening and R.H. Doi, *"Outlines of Biochemistry"*, 5th Ed., John Wiley and Sons, Singapore, 1987, 487; (b) H. Curtis, *"Biology"*, 4th Ed., Worth Publishers, New York, 1983, 221.
2. Govindjee, T. Kambara and W. Coleman, *Photochem. Photobiol.*, 1985, **42**, 187.
3. G.C. Dismukes, *Photochem. Photobiol.*, 1986, **43**, 99.
4. G. Renger, *Angew. Chem. Int. Ed. Engl.*, 1987, **26**, 643.
5. V.L. Pecoraro, *Photochem. Photobiol.*, 1988, **48**, 249.
6. A.G. Volkov, *Bioelectrochem and Bioenerg.* (a section of *J. Electroanal. Chem.*, 1989, **275**), 1989, **21**, 3.
7. P. Joliot, G. Barbieri and R. Chabaud, *Photochem. Photobiol.*, 1969, **10**, 309.
8. B. Kok, B. Forbush and M. McGloin, *Photochem. Photobiol.*, 1970, **11**, 457.
9. B. Forbush, B. Kok and M. McGloin, *Photochem. Photobiol.*, 1971, **14**, 307.
10. J.M. Anderson and N.A. Pyliotis, *Biochim. Biophys. Acta*, 1969, **189**, 280.
11. V.V. Klimov, S.I. Allakhverdiev, V.A. Shuvalov and A.A. Krasnovsky, *F.E.B.S. Lett.*, 1982, **148**, 307.
12. G.C. Dismukes and Y. Siderer, *Proc. Natl. Acad. Sci. USA*, 1981, **78**, 274.
13. (a) C.F. Yocum, C.T. Yerkes, R.E. Blankenship, R.R. Sharp, and G.T. Babcock, *Proc. Natl. Acad. Sci. USA*, 1981, **78**, 7507. (b) N. Murata, M. Miyao, T. Omata, H. Matsunami and T. Kuwabara, *Biochim. Biophys. Acta*, 1984, **765**, 363. (c) N. Tamura and G. Cheniae, *Biochim. Biophys. Acta*, 1985, **809**, 245.
14. J.C. de Paula, W.F. Beck and G.W. Brudvig, *J. Am. Chem. Soc.*, 1986, **108**, 4002.
15. Ö. Hansson, R. Aasa and T. Vänngård, *Biophys. J.*, 1987, **51**, 825.
16. See for example: (a) N. Murata and M. Miyao, *T.I.B.S.*, 1985, 122. (b) J. Barber, *T.I.B.S.*, 1987, 321. (c) J-D. Rochaix and J. Erickson, *T.I.B.S.*, 1988, 56. (d) J. Deisenhofer, O. Epp, K. Miki, R. Huber and H. Michel, *Nature*, 1985, **318**, 618. (e) B. Ford, *Nature*, 1989, **337**, 510.

17. B-K. Teo, *Acc. Chem. Res.*, 1980, **13**, 412.

18. J.E. Penner-Hahn in *"Metal Clusters in Proteins"*,(L. Que Jr. editor), ACS Symposium Series **372**, American Chemical Society, Washington D.C., 1988, Chapter 2.

19. V.K. Yachandra, R.D. Guiles, A.E. McDermott, J.L. Cole, R.D. Britt, S.L. Dexheimer, K. Sauer and M.P. Klein, *Biochemistry*, 1987, **26**, 5974.

20. D.B. Goodin, V.K. Yachandra, R.D. Britt, K. Sauer and M.P. Klein, *Biochim. Biophys. Acta.*, 1984, **767**, 209.

21. G.N. George, R.C. Prince and S.P. Cramer, *Science*, 1989, **243**, 789.

22. G.W. Brudvig and R.H. Crabtree, *Proc. Natl. Acad. Sci. USA*, 1986, **83**, 4586.

23. G.W. Brudvig in *"Metal Clusters in Proteins"*,(L. Que Jr. editor), ACS Symposium Series **372**, American Chemical Society, Washington D.C., 1988, Chapter 11.

24. M. Sivaraja, J.S. Philo, J. Lary and G.C. Dismukes, *J. Am. Chem. Soc.* 1989, **111**, 3221.

25. (a) J.B. Vincent and G. Christou, *F.E.B.S. Lett.*, 1986, **207**, 250. (b) H. Kretschmann, J.P. Dekker, Ö. Saygin and H.T. Witt, *Biochim. Biophys. Acta*, 1988, **932**, 358.

26. (a) Ö. Saygin and H.T. Witt, *F.E.B.S. Lett.*, 1984, **176**, 83. (b) Ö. Saygin and H.T. Witt, *F.E.B.S. Lett.*, 1985, **187**, 224.

27. K. Brettel, E. Schlodder and H.T. Witt, *Biochim. Biophys. Acta*, 1984, **766**, 403.

28. V.K. Yachandra, R.D. Guiles, A. McDermott, R.D. Britt, S.L. Dexheimer, K. Sauer and M.P. Klein, *Biochim. Biophys. Acta*, 1986, **850**, 324.

29. (a) J.B. Vincent and G. Christou, *Inorg. Chim. Acta*, 1987, **136**, L41. (b) G. Christou and J.B. Vincent, *Biochim. Biophys. Acta.*, 1987, **895**, 259. (c) G. Christou and J.B. Vincent in *"Metal Clusters in Proteins"*,(L. Que Jr. editor), ACS Symposium Series **372**, American Chemical Society, Washington D.C., 1988, Chapter 12.

30. R.J. Kulawiec, R.H. Crabtree, G.W. Brudvig, G.K. Schulte, *Inorg. Chem.*, 1988, **27**, 1309.

31. C. Christmas, J.B. Vincent, H-R. Chang, J.C. Huffman, G. Christou and D.N. Hendrickson, *J. Am. Chem. Soc.*, 1988, **110**, 823.

32. S.P. Cramer, personal communication.

33. C. Critchley, *Biochim. Biophys. Acta*, 1985, **811**, 33

34. V.K. Yachandra, R.D. Guiles, K. Sauer and M.P. Klein, *Biochim. Biophys. Acta.,* 1986, **850**, 333.

35. R.J. Pace, personal communication.

36. W.F. Beck and G.W. Brudvig, *J. Am. Chem. Soc.,* 1988, **110**, 1517.

37. W.F. Beck, J.C. de Paula and G.W. Brudvig, *J. Am. Chem. Soc.,* 1986, **108**, 4018.

38. W.F. Beck and G.W. Brudvig, *Biochemistry,* 1987, **26**, 8285.

39. (a) P.O. Sandusky and C.F. Yocum, *Biochim. Biophys. Acta,* 1986, **849**, 85. (b) C. Preston and R.J. Pace, *Biochim. Biophys. Acta,* 1985, **810**, 388. (c) E.K. Pistorius and G.H. Schmid, *Biochim. Biophys. Acta,* 1987, **890**, 352.

40. (a) S. Saphon and A.R. Crofts, *Z. Naturforsch.,* 1977, **C32**, 617. (b) V. Förster and W. Junge, *Photochem., Photobiol.,* 1985, **41**, 183.

41. Ö. Hansson, L-E. Andréasson and T. Vänngård, *F.E.B.S. Lett,* 1986, **195**, 151.

42. R. Radmer and O. Ollinger, *F.E.B.S. Lett,* 1986, **195**, 285.

43. Ö. Saygin and H.T. Witt, *Biochim. Biophys. Acta,* 1987, **893**, 452.

44. C. Critchley and A.M. Sargeson, *F.E.B.S. Lett.,* 1984, **177**, 2.

45. See for example: (a) T.J. Meyer, *Acc. Chem. Res.,* 1989, **22**, 163. (b) D.W. Bruce, D.J. Cole-Hamilton and P. Pogorzelec, *J. Chem. Soc. Dalton Trans.,* 1987, 2941. (c) I. Willner, Y. Eichen and A.J. Frank, *J. Am. Chem. Soc.,* 1989, **111**, 1884.

46. (a) K. Wieghardt, U. Bossek, D. Ventur and J. Weiss, *J. Chem. Soc., Chem. Commun.,* 1985, 347. (b) K. Wieghardt, U. Bossek, L. Zsolnai, G. Huttner, G. Blondin, J-J. Girerd and F. Babonneau, *J. Chem. Soc., Chem. Commun.,* 1987, 651. (c) K. Wieghardt, U. Bossek, B. Nuber, J. Weiss, J. Bonvoisin, M. Corbella, S.E. Vitols and J.J. Girerd, *J. Am. Chem. Soc.,* 1988, **110**, 7398. (d) K. Wieghardt, U. Bossek, J. Bonvoisin, P. Beauvillain, J-J. Girerd, B. Nuber, J. Weiss and J. Heinze, *Angew. Chem. Int. Ed. Engl.,* 1986, **25**, 1030.

47. J. E. Sheats, R.S. Czernuszewicz, G.C. Dismukes, A.L. Rheingold, V. Petrouleas, J. Stubbe, W.H. Armstrong, R.H. Beer and S.J. Lippard, *J. Am. Chem. Soc.,* 1987, **109**, 1435.

48. S. Ménage, J-J. Girerd and A. Gleizes, *J. Chem. Soc., Chem. Commun.,*1988,431.

49. See for example: (a) M.A Collins, D.J. Hodgson, K. Michelsen and D.K. Towle, *J. Chem. Soc., Chem. Commun.*, 1987, 1659. (b) M. Stebler, A. Ludi and H-B. Bürgi, *Inorg. Chem.*, 1986, **25**, 4743. (c) P.M. Plaksin, R.C. Stoufer, M. Mathew and G.J. Palenik, *J. Am. Chem. Soc.*, 1972, **94**, 2121.

50. D.K. Towle, C.A. Botsford and D.J. Hodgson, *Inorg. Chim. Acta,* 1988, **141**, 167.

51. J.S. Bashkin, A.R. Schake, J.B. Vincent, H-R. Chang, Q. Li, J.C. Huffman, G. Christou and D.N. Hendrickson, *J. Chem. Soc., Chem. Commun.*, 1988, 700.

52. (a) H-R. Chang, S.K. Larsen, P.D.W. Boyd, C.G. Pierpont and D.N. Hendrickson, *J. Am. Chem. Soc.*, 1988, **110**, 4565. (b) H. Diril, H-R. Chang, X. Zhang, S.K. Larsen, J.A. Potenza, C.G. Pierpont, H.J. Schugar, S.S. Isied and D.N. Hendrickson, *J. Am. Chem. Soc.*, 1987, **109**, 6207.

53. S. Raghunathan, C. Stevenson, J. Nelson and V. McKee, *J. Chem. Soc., Chem. Commun.*, 1989, 5.

54. K. Wieghardt, U. Bossek, B. Nuber, J. Weiss, S. Gehring and W. Haase, *J. Chem. Soc., Chem. Commun.*, 1988, 1145.

55. J.B. Vincent, H-R. Chang, K. Folting, J.C. Huffman, G. Christou and D.N. Hendrickson, *J. Am. Chem. Soc.*, 1987, **109**, 5703.

56. R. Bhula, G.J. Gainsford and D.C. Weatherburn, *J. Am. Chem. Soc.*, 1988, **110**, 7550.

57. (a) X. Li, D.P. Kessissoglou, M.L. Kirk, C.J. Bender and V.L. Pecoraro, *Inorg. Chem.*, 1988, **27**, 1. (b) D.P. Kessissoglou, M.L. Kirk, C.A. Bender, M.S. Lah and V.L. Pecoraro, *J. Chem. Soc., Chem. Commun.*, 1989, 84.

58. J.S. Bashkin, H-R. Chang, W.E. Streib, J.C. Huffman, D.N. Hendrickson and G. Christou, *J. Am. Chem. Soc.*, 1987, **109**, 6502.

59. (a) G.C. Dismukes, J.E. Sheats and J.A. Smegal, *J. Am. Chem. Soc.*, 1987, **109**, 7202. (b) B. Mabad, J-P. Tuchagues, Y.T. Hwang and D.N. Hendrickson, *J. Am. Chem. Soc.*, 1985, **107**, 2081.

60. K. Wieghardt, U. Bossek and W. Gebert, *Angew. Chem. Int. Ed. Engl.*, 1983, **22**, 328.

61. K.S. Hagen, T.D. Westmoreland, M.J. Scott and W.H. Armstrong, *J. Am. Chem. Soc.*, 1989, **111**, 1907.

62. (a) V. McKee and W.B. Shepard, *J. Chem. Soc., Chem. Commun.*, 1985, 158. (b) S. Brooker, V. McKee, W.B. Shepard and L.K. Pannell, *J. Chem. Soc. Dalton Trans.*, 1987, 2555.

63. S. Brooker, S.P. Cramer and V. McKee, unpublished results.

64. J. Aussoleil, P. Cassoux, P. de Loth and J-P. Tuchagues, *J. Am. Chem. Soc.*, in the press.

65. Q. Li, J.B. Vincent, E. Libby, H-R. Chang, J.C. Huffman, P.D.W. Boyd, G.Christou and D.N. Hendrickson, *Angew. Chem. Int. Ed. Engl.*, 1988, **27**, 1731.

66. V. McKee and S.S. Tandon, *J. Chem. Soc., Chem. Commun.*, 1988, 1334.

67. (a) J.B. Vincent, C. Christmas, J.C. Huffman, G. Christou, H-R. Chang and D.N. Hendrickson, *J. Chem. Soc., Chem. Commun.*, 1987, 236. (b) J.B. Vincent, C. Christmas, H-R. Chang, Q. Li, P.D.W. Boyd, J.C. Huffman, D.N. Hendrickson and G. Christou, *J. Am. Chem. Soc.*, 1989, **111**, 2086.

68. (a) A.R.E. Baikie, A.J. Howes, M.B. Hursthouse, A.B. Quick and P. Thornton, *J. Chem. Soc., Chem. Commun.*, 1986, 1587. (b) A.R. Schake, J.B. Vincent, Q. Li, P.D.W. Boyd, K. Folting, J.C. Huffman, D.N. Hendrickson and G. Christou, *Inorg. Chem.*, 1989, **28**, 1915. (c).D. Luneau, J-M. Savariault and J-P. Tuchagues, *Inorg. Chem.*, 1988, **27**, 3912. (d) D. Luneau, J-M. Savariault, P. Cassoux and J-P. Tuchagues, *J. Chem. Soc. Dalton Trans.*, 1988, 1225. (e) K.S. Hagen, W.H. Armstrong and M.M. Olmstead, *J. Am. Chem. Soc.*, 1989, **111**, 774.

69. C. Christmas, J.B. Vincent, J.C. Huffman, G. Christou, H-R. Chang and D.N. Hendrickson, *Angew. Chem. Int. Ed. Engl.*, 1987, **26**, 915.

70. P.D.W. Boyd, Q. Li, J.B. Vincent, K. Folting, H-R. Chang, W.E. Streib, J.C. Huffman, G. Christou and D.N. Hendrickson, *J. Am. Chem. Soc.*, 1988, **110**, 8537.

71. T. Lis, *Acta Cryst.B*, 1980, **36**, 2042.

72. F.M. Ashmawy, C.A. McAuliffe, R.V. Parish and J. Tames, *J. Chem. Soc., Chem. Commun.*, 1984, 14. (b) F.M. Ashmawy, C.A. McAuliffe, R.V. Parish and J. Tames, *J. Chem. Soc. Dalton Trans.*, 1985, 1391.

73. R. Ramaraj, A. Kira and M. Kaneko, *Angew. Chem. Int. Ed. Engl.*, 1986, **25**, 825.

74. N.P. Luneva, E.I. Knerelman, V.Y. Shafirovich and A.E. Shilov, *J. Chem. Soc., Chem. Commun.*, 1987, 1504.

75. L.F. Lindoy, *"The Chemistry of Macrocyclic Ligand Complexes"*, Cambridge University Press, Cambridge, 1989.

76. (a) S.M. Nelson, *Pure and Appl. Chem.*,1980, **52**, 2461. (b) S.M. Nelson, *Inorg. Chim. Acta,* 1982, **62**, 39. (c) S.M. Nelson in "*Copper Coordination Chemistry; Biochemical and Inorganic Perspectives*" (K.D. Karlin and J. Zubieta editors), Adenine Press, New York, 1983, 331.

77. D.E. Fenton, *Pure and Appl. Chem.,* 1986, **58**, 1437.

78. (a) E. Weber and F. Vögtle, *Chem. Ber.* 1976, **109**, 1803. (b) J. Jazwinski, J-M. Lehn, D. Lilienbaum, R. Ziessel, J. Guilhem and C. Pascard, *J. Chem. Soc., Chem. Commun.,* 1987, 1691.

79. N.H. Pilkington and R. Robson, *Aust. J. Chem.,* 1970, **23**, 2225.

80. H. Adams, N.A. Bailey, D.E. Fenton, R.J. Good, R. Moody and C.O. Rodriguez de Barbarin, *J. Chem. Soc. Dalton Trans.,* 1987, 207.

81. K. Faulalo, M.Sc. thesis, University of Canterbury, 1988.

82. (a) E.B. Fleischer and S.W. Hawkinson, *Inorg. Chem.,* 1968, **7**, 2312. (b) M.G.B. Drew, S.G. McFall, S.M. Nelson and C.P. Waters, *J. Chem. Res.,* 1979, 16.

83. (a) D.E. Fenton, S.J. Kitchen, C.M. Spencer, P.A. Vigato and S. Tamburini, *Inorg. Chim. Acta,* 1987, **139**, 55. (b) D.E. Fenton, S.J. Kitchen, C.M. Spencer, P.A. Vigato and S. Tamburini, *J. Chem. Soc. Dalton Trans.,* 1988, 685.

84. M.G.B. Drew, J. Nelson and S.M. Nelson, *J. Chem. Soc. Dalton Trans.,* 1981, 1678.

85. N.A. Bailey, D.E. Fenton, I.T. Jackson, R. Moody and C.O. Rodriguez de Barbarin, *J. Chem. Soc., Chem. Commun.,* 1983, 1463.

86. V. McKee and J. Smith, *J. Chem. Soc., Chem. Commun.,* 1983, 1465.

87. N.A. Bailey, D.E. Fenton, R. Moody, C.O. Rodriguez de Barbarin, I.N. Sciambarella, J-M. Latour, D. Limosin and V. McKee, *J. Chem. Soc. Dalton Trans.,* 1987, 2519.

88. V. McKee and S.S. Tandon, *J. Chem. Soc., Chem. Commun.,* 1988, 385.

89. M. Bell, A.J. Edwards, B.F. Hoskins, E.H. Kachab and R. Robson, *J. Chem. Soc., Chem. Commun.,* 1987, 1852.

90. M.G.B. Drew, B.P. Murphy, J. Nelson and S.M. Nelson, *J. Chem. Soc. Dalton Trans.,* 1987, 873.

91. M.G.B. Drew, P.C. Yates, J. Trocha-Grimshaw, K.P. McKillop and S.M. Nelson, *J. Chem. Soc., Chem. Commun.,* 1985, 262.

92. (a) S.M. Nelson, M. McCann, C. Stevenson and M.G.B. Drew, *J. Chem. Soc. Dalton Trans.*, 1979, 1477. (b) M.G.B. Drew, M. McCann and S.M. Nelson, *J. Chem. Soc., Chem. Commun.*, 1979, 481. (c) M.G.B. Drew, M. McCann and S.M. Nelson, *Inorg. Chim. Acta,* 1980, **41**, 213. (d) M.G.B. Drew, M. McCann and S.M. Nelson, *J. Chem. Soc. Dalton Trans.*, 1981, 1868.

93. (a) S.M. Nelson, F. Esho, A. Lavery and M.G.B. Drew, *J. Am. Chem. Soc.*, 1983, **105**, 5693. (b) M.G.B. Drew, P.C. Yates, J. Trocha-Grimshaw, A. Lavery, K.P. McKillop, S.M. Nelson and J. Nelson, *J. Chem. Soc. Dalton Trans.*, 1988, 347. (c) M.G.B. Drew, P.C. Yates, F.S. Esho, J. Trocha-Grimshaw, A. Lavery, K.P. McKillop, S.M. Nelson and J. Nelson, *J. Chem. Soc. Dalton Trans.*, 1988, 2995.

94. (a) K.G. Strothkamp and S.J. Lippard, *Acc. Chem. Res.*, 1982, **15**, 318. (b) A.E. Martin and S.J. Lippard in "*Copper Coordination Chemistry; Biochemical and Inorganic Perspectives*", (K.D. Karlin and J. Zubieta editors), Adenine Press, New York, 1983, 395.

95. (a) P.K. Coughlin, J.C. Dewan, S.J. Lippard, E. Watanabe, J-M. Lehn, *J. Am. Chem. Soc.*, 1979, **101**, 265. (b) M.G.B. Drew, C. Cairns, A. Lavery and S.M. Nelson, *J. Chem. Soc., Chem. Commun.*, 1980, 1122. (c) P.K. Coughlin, S.J. Lippard, A.E. Martin and J.E. Bulkowski, *J. Am. Chem. Soc.*, 1980, **102**, 7616.

96. G. Black, E. Depp and B.B. Corson, *J. Org. Chem.*, 1949, **14**, 14.

97. M. Newcomb, J.M. Timko, D.M. Walba and D.J. Cram, *J. Am. Chem. Soc.*, 1977, **99**, 6392.

98. R. Lukes and M. Pergál, *Collection Czechoslov. Chem. Commun.*, 1959, **24**, 36.

99. R. Miller and K. Olsson, *Acta Chem. Scand. B,* 1981, **35**, 303.

100. "*Organic Syntheses*" *Collective Volume 4*, (N. Rabjohn editor), John Wiley and Sons, New York, 1967, 831.

101. K. Olsson and P. Pernemalm, *Acta Chem. Scand. B,* 1979, **33**, 125.

102. W.N. Haworth and W.G.M. Jones, *J. Chem. Soc. (C),* 1944, 667.

103. (a) E.P. Papadopoulos, A. Jarrar and C.H. Issidorides, *J. Org. Chem.*, 1966, **31**, 615. (b) V. McKee, Ph.D. thesis, The Queen's University of Belfast, 1979, 153.

104. O. Mancera, G. Rosenkranz and F. Sondheimer, *J. Chem. Soc.*, 1953, 2189.

105. G.R. Owen and C.B. Reese, *J. Chem. Soc. (C),* 1970, 2401.

106. I. Murase, M. Hatano, M. Tanaka, S. Ueno, H. Okawa and S. Kida, *Bull. Chem. Soc. Jpn.*, 1982, **55**, 2404.

107. M.G.B. Drew, J. Nelson, F. Esho, V. McKee and S.M. Nelson, *J. Chem. Soc. Dalton Trans.*, 1982, 1837.

108. G.M. Sheldrick, *SHELXTL User Manual,* Revison 4, Nicolet XRD Corporation, Madison, Wisconsin, 1984.

109. G.M. Sheldrick, *SHELXS-86; A Program for Crystal Structure Solution,* Göttingen University, 1986.

110. G.M. Sheldrick, *SHELX76, Program for Crystal Structure Determination,* Cambridge University, 1976.

111. (a) M.G.B. Drew, F. Esho, and S.M. Nelson, *Inorg. Chim. Acta,* 1983, **76**, L269. (b) M.G.B. Drew, F. Esho, A. Lavery and S.M. Nelson, *J. Chem. Soc. Dalton Trans.*, 1984, 545.

112. (a) H. Adams, N.A. Bailey, D.E. Fenton, S. Moss and G. Jones, *Inorg. Chim. Acta,* 1984, **83**, L79. (b) D.E. Fenton in *"Biological and Inorganic Copper Chemistry"*, Vol. II, (K.D. Karlin and J. Zubieta editors), Adenine Press, New York, 1986, 179.

113. D.E. Fenton and R. Moody, *J. Chem. Soc. Dalton Trans.*, 1987, 219.

114. S. Brooker and V. McKee, *J. Chem. Soc., Chem. Commun.*, 1989, 619.

115. (a) F.A. Cotton, A. Davison, W.H. Ilsley and H.S. Trop, *Inorg. Chem.*, 1979, **18**, 2719. (b) L.R. Groeneveld, G. Vos, G.C. Verschoor and J. Reedijk, *J. Chem. Soc., Chem. Commun.*, 1982, 620. (c) P.A. Harding, K. Hendrick, L.F. Lindoy, M. McPartlin and P.A. Tasker, *J. Chem. Soc., Chem. Commun.*, 1983, 1300. (d) G.A. van Albada, R.A.G. de Graaff, J.G. Haasnoot and J. Reedijk, *Inorg. Chem.*, 1984, **23**, 1404. (e) J.L. Mesa, T. Rojo, M.I. Arriortua, G. Villeneuve, J.V. Folgado, A. Beltrán-Porter and D. Beltrán-Porter, *J. Chem. Soc. Dalton Trans.*, 1989, 53.

116. B.P. Murphy, J. Nelson, S.M. Nelson, M.G.B. Drew and P.C. Yates, *J. Chem. Soc. Dalton Trans.*, 1987, 123.

117. I.F. Taylor, Jr. and E.L. Amma, *J. Cryst. Vol. Struct.*, 1975, **5**, 129.

118. C.O. Rodriguez de Barbarin, Ph.D. thesis, University of Sheffield, 1984.

119. W.J. Geary, *Coord. Chem. Rev.*, 1971, **7**, 81.

120. (a) R.G. Hayter, *J. Am. Chem. Soc.*, 1962, **84**, 3046. (b) R.G. Hayter and F.S. Humiec, *Inorg. Chem.*, 1963, **2**, 306. (c) R.D. Feltham and R.G. Hayter, *J. Chem. Soc.*, 1964, 4587.

121. R.M. Fuoss and L. Onsager, *J. Phys. Chem.,* 1957, **61**, 668.

122. J.E. Lind, Jr., J.J. Zwolenik and R.M. Fuoss, *J. Am. Chem. Soc.,* 1959, **81**, 1557.

123. J.F. Coetzee and G.P. Cunningham, *J. Am. Chem. Soc.,* 1965, **87**, 2529.

124. A.C. Harkness and H.M. Daggett, Jr., *Can. J. Chem.,* 1965, **43**, 1215.

125. (a) A. Davison, D.V. Howe and E.T. Shawl, *Inorg. Chem.,* 1967, **6**, 458. (b) M.S. Elder, G.M. Prinz, P. Thornton and D.H. Busch, *Inorg. Chem.,* 1968, **7**, 2426.

126. S. Brooker, J-M. Latour, V. McKee and J-P. Tuchagues, unpublished results.

127. S. Brooker, V. McKee and L.K. Pannell, unpublished results.

128. (a) E.F. Bertaut, D. Tranqui, P. Burlet, P. Burlet, M. Thomas and J.M. Moreau, *Acta Cryst.,* 1974, **B30**, 2234. (b) D. Tranqui, P. Burlet, A. Filhol and M. Thomas, *Acta Cryst.,* 1977, **B33**, 1357.

129. S. Brooker, S.P. Cramer and V. McKee, unpublished results.

130. D. Wester and G.J. Palenik, *J. Am. Chem. Soc.,* 1974, **96**, 7565.

131. T.J. Giordano, G.J. Palenik, R.C. Palenik,and D.A. Sullivan, *Inorg. Chem.,* 1979, **18**, 2445.

132. C. Pelizzi, G. Pelizzi, G. Predieri and S. Resola, *J. Chem. Soc. Dalton Trans.,* 1982, 1349.

133. M.V. Capparelli, P. de Meester, D.M.L. Goodgame, S.J. Gunn and A.C. Skapski, *Inorg. Chim. Acta,* 1985, **97**, L37.

134. M.G.B. Drew, A.H. bin Othman and S.M. Nelson, *J. Chem. Soc. Dalton Trans.,* 1976, 1394.

135. M.G.B. Drew, A.H. bin Othman, S.G. McFall, P.D.A. McIlroy and S.M. Nelson, *J. Chem. Soc. Dalton Trans.,* 1977, 438.

136. M.G.B. Drew, A.H. bin Othman, S.G. McFall, P.D.A. McIlroy and S.M. Nelson, *J. Chem. Soc. Dalton Trans.,* 1977, 1173.

137. (a) M.M. Bishop, J. Lewis, T.D. O'Donoghue, P.R. Raithby and J.N. Ramsden, *J. Chem. Soc., Chem. Commun.,* 1978, 828. (b) M.M. Bishop, J. Lewis, T.D. O'Donoghue, P.R. Raithby and J.N. Ramsden, *J. Chem. Soc. Dalton Trans.,* 1980, 1390.

138. (a) W. Micklitz and S.J. Lippard, *Inorg. Chem.,* 1988, **27**, 3067. (b) W. Micklitz, S.G. Bott, J.G. Bentsen and S.J. Lippard, *J. Am. Chem. Soc.,* in the press.

139. (a) J.E. Andrew, A.B. Blake and L.R. Fraser, *J. Chem. Soc. Dalton Trans.*, 1975, 800. (b) K. Neupert-Laves and M. Dobler, *Helv. Chim. Acta,* 1977, **60**, 1861. (c) B.B. Hughes, R.C. Haltiwanger, C.G. Pierpont, M. Hampton and G.L. Blackmer, *Inorg. Chem.,* 1980, **19**, 1801.

140. J. Drummond and J.S. Wood, *J. Chem. Soc.,* 1970, 226.

141. J. Nelson, B.P. Murphy, M.G.B. Drew, P.C. Yates and S.M. Nelson, *J. Chem. Soc. Dalton Trans.,* 1988, 1001.

142. (a) D.W. Johnson and H.K. Mayer, *Inorg. Chim. Acta,* 1987, **126**, L1. (b) D.W. Johnson, H.K. Mayer, J.P. Minard, J. Banaticla and C. Miller, *Inorg. Chim. Acta,* 1988, **144**, 167.

143. S. Brooker and V. McKee, *Acta. Cryst.,* 1988, **C44**, 350.

144. J.E. Huheey, *"Inorganic Chemistry: Principles of Structure and Reactivity"*, 3rd Ed., Harper and Row, New York, 1983, 73.

145. S. Patai, *"The Chemistry of Functional Groups: The Chemistry of the Carbonyl Group"*, (John Wiley and Sons, editor), 1966, 600.

146. R.L. Carlin, *"Magnetochemistry"*, Springer-Verlag, Berlin, 1986, 53.

147. (a) D.H. Busch and J.C. Bailar, Jr., *J. Am. Chem. Soc.,* 1956, **78**, 1137. (b) E. König and K. Madeja, *Spectrochim. Acta,* 1967, **23A**, 45. (c) J. Nelson, S.M. Nelson and W.D. Perry, *J. Chem. Soc. Dalton Trans.,* 1976, 1282.

148. C. Cairns, S.G. McFall, S.M. Nelson and M.G.B. Drew, *J. Chem. Soc. Dalton Trans.,* 1979, 446.

149. L. Walz, H. Paulus, W. Haase, H. Langhof and F. Nepveu, *J. Chem. Soc. Dalton Trans.,* 1983, 657.

150. (a) J-P. Laurent, J-J. Bonnet, F. Nepveu, H. Astheimer, L. Walz and W. Haase, *J. Chem. Soc. Dalton Trans.,* 1982, 2433. (b) H. Astheimer, F. Nepveu, L. Walz and W. Haase, *J. Chem. Soc. Dalton Trans.,* 1985, 315.

151. J.A. Bertrand and J.A. Kelly, *Inorg. Chim. Acta,* 1970, **4**, 204.

152. G. Cros and J-P. Laurent, *Inorg. Chim. Acta,* 1988, **142**, 113.

153. J.A. Davis and E. Sinn, *J. Chem. Soc. Dalton Trans.,* 1976, 165.

154. E. Sinn, *J. Chem. Soc., Chem. Commun.,* 1975, 665.

155. J.A. Bertrand and C.E. Kirkwood, *Inorg. Chim. Acta,* 1972, **6**, 248.

156. G.R. Clark and G.J. Palenik, *Cryst. Struct. Commun.,* 1980, **9**, 449.

157. J.A. Montgomery and J.A. Secrist, *"Comprehensive Heterocyclic Chemistry"*, Vol. 5, (K.T. Potts, editor), Pergamon Press, Oxford, 1984, 607.

158. M. Koikawa, H. Okawa and S. Kida, *J. Chem. Soc. Dalton Trans.*, 1988, 641.

159. (a) D.J. Barnes, R.L. Chapman, F.S. Stephens and R.S. Vagg, *Inorg. Chim. Acta,* 1981, **51**, 155. (b) R.L. Chapman, F.S. Stephens and R.S. Vagg, *Inorg. Chim. Acta,* 1981, **52**, 161.

160. S.P. Perlepes, T. Kabanos, V. Hondrellis and J.M. Tsangaris, *Inorg. Chim. Acta,* 1988, **150**, 13.